INTERFACE STRENGTHENED GRAPHENE OXIDE REINFORCED PVA NANOCOMPOSITES

Swarnima Kashyap

Department of Ceramic Engineering
National Institute of Technology Rourkela

INTERFACE STRENGTHENED GRAPHENE OXIDE REINFORCED PVA NANOCOMPOSITES

Dissertation submitted in partial fulfillment

of the requirements of the degree of

Doctor of Philosophy

in

Ceramic Engineering

by

Swarnima Kashyap

(Roll Number: 511CR102)

based on research carried out

under the supervision of

Prof. Shantanu K. Behera

&

Prof. Swadesh K. Pratihar

December, 2016

Department of Ceramic Engineering
National Institute of Technology Rourkela

Department of Ceramic Engineering
National Institute of Technology Rourkela

Date:

Certificate of Examination

Roll Number: *511CR102*
Name: *Swarnima Kashyap*
Title of Dissertation: *Interface strengthened graphene oxide reinforced PVA nanocomposites*

We the below signed, after checking the dissertation mentioned above and the official record book (s) of the student, hereby state our approval of the dissertation submitted in partial fulfillment of the requirements of the degree of Doctor of Philosophy in Department of Ceramic Engineering at National Institute of Technology Rourkela. We are satisfied with the volume, quality, correctness, and originality of the work.

Prof. S.K.Pratihar
Co- Supervisor

Shantanu K Behera
Principal Supervisor

Prof. R.Majumdar
Member, DSC

Prof. S.Paria
Member, DSC

Prof. P.Mahanandia
Member, DSC

Name
External Examiner

Prof. Ritwik Sarkar
Chairman, DSC

Bibhuti Bhusan Nayak
Head of the Department

Department of Ceramic Engineering
National Institute of Technology Rourkela

Dr. Shantanu K. Behera
Ph.D., Lehigh University (USA)
Assistant Professor

Date:

Supervisor's Certificate

This is to certify that the work presented in the dissertation entitled "*Interface strengthened graphene oxide reinforced PVA nanocomposites"* submitted by *Swarnima Kashyap*, Roll Number *511CR102*, is a record of original research carried out by her under my supervision and guidance in partial fulfillment of the requirements of the degree of *Doctor of Philosophy* in *Department of Ceramic Engineering*. Neither this dissertation nor any part of it has been submitted earlier for any degree or diploma to any institute or university in India or abroad.

Shantanu K Behera

Dedication

Dedicated to my maa-papa,
my husband and baby Yuvika

Declaration of Originality

I, *Swarnima Kashyap*, Roll Number: 511CR102 hereby declare that this dissertation entitled *Interface strengthened graphene oxide reinforced PVA nanocomposites* presents my original work carried out as a doctoral student of NIT Rourkela and, to the best of my knowledge, it contains no material previously published or written by another person, nor any material presented for the award of any degree or diploma of NIT Rourkela or any other institution. Any contribution made to this research by others, with whom I have worked at NIT Rourkela or elsewhere, is explicitly acknowledged in the dissertation. Works of other authors cited in this dissertation have been duly acknowledged under the section "Bibliography". I have also submitted my original research records to the scrutiny committee for evaluation of my dissertation. I am fully aware that in case of my non-compliance detected in the future, the Senate of NIT Rourkela may withdraw the degree awarded to me on the basis of the present dissertation.

Date:
NIT Rourkela   Swarnima Kashyap

Acknowledgments

With all the efforts and support received, I am thankful to the supreme power who energized me and gave me enough strength to undertake this work.

This compilation owes my first sincere thanks to my advisor, Prof. Shantanu K. Behera, who always inspired me, and ignited my imagination of thoughts into a meaningful scientific expression. His patient and extremely supportive attitude towards each phase of my career has influenced me as a thinker and a better person in life. His scientific expertise and vision of thoughts always inspired me to produce a better quality of work. His contribution as a role model for inculcating curiosity, knowledge, and wisdom in me would always help me produce the best in me. Additionally, I would like to extend sincere thanks to my co-advisor Prof. S. K. Prathihar for his interests and sharing of knowledge throughout the tenure of my research. His patience and friendly attitude as an advisor always gave an expanse to the horizon of my thoughts to produce better results.

Next, I would like to thank the members of my Doctoral Scrutiny Committee (DSC), Prof. R. Sarkar, Prof. R. Majumdar, Prof S. Paria and Prof. P. Mahanandia for providing me with their constructive criticism over the research area. I would also like to thank the Head of the Department, Prof B. B. Nayak and all the faculty members of the Department of Ceramic Engineering who provided me with inputs required for the research and motivated me to work in the right direction. I would also like to put on record my sincere thanks to Prof. P. M.G Nambissan (SINP, Kolkata) for his support in carrying out PALS experiments. Thanks are due to Prof. A. Tripathi (Sikkim Central University) for his assistance in Raman spectrometry.

I express my very special thanks to Ipsita Priyadarshini Swain who dedicated her valuable time in my research. Her expertise as a mechanical engineering student benefited me to develop a clear understanding of the problem. Her positive and patient attitude towards me, throughout my stay in the campus, has left me with lots of delighted moments to cherish. Extended support from my friends including Dr. Geetanjali Parida, Parinita Aggarwal, Ashely Thomas, Abhisek Choudhary, Jayarao Gorinta, Neera Singh and Soumini

Mondal in different ways possible deserve a special vote of thanks. I would also like to acknowledge the expertise of Mr. Subhabrata Chakrobarty in electron microscopy, who engaged his time in providing us with interesting morphologies that turned out as an important part of the thesis.

I wholeheartedly appreciate the immense love, support, and sacrifices made by my husband Mr. Akhilesh Prasad and my baby Yuvika. You always understood me and provided me with the best of your capabilities. I was able to complete the work only with the inspiration, drive and support you gave me. I thank both of you for being there always, on the sidelines patiently cheering me up.

My very special thanks to my motivators, my father and mother, who lived my dreams and contributed in achieving them with unconditional support in every way possible. I am so much of what I learned from you, and all your support shall be printed on my heart. I wholeheartedly thank my parents-in-law, who were great moral support for me in the toughest of times.

I owe this achievement to my mother's positive attitude that always encouraged me to believe in myself and prove my mettle. I am extremely thankful to my sister Dr. Anudeepika, brother Yashashvi, and my relatives who always added enthusiasm and charm to my journey.

Last but not the least, I would like to thank all the staff members of the Department of Ceramic Engineering and the Institute for providing me with such a supportive and positive ambiance for the successful completion my thesis.

Date:
NIT Rourkela

Swarnima Kashyap
Roll No: 511CR102

Abstract

Graphene, an atomic layer of sp^2 bonded carbon atoms in the hexagonal lattice, is the building block of many carbon forms, including carbon nanotubes, Buckminster Fullerenes, carbon onions, and graphite. Its exceptional properties, for example, Young's modulus of 1 TPa, breaking strength of 140 GPa, thermal conductivity of 5000 $Wm^{-1}K^{-1}$, and high specific theoretical surface area of 2650 m^2g^{-1}, have warranted use in many structural and functional applications. One of the most important uses of it lies as fillers in the fabrication of polymeric nanocomposites. Its special two-dimensional morphology featuring high available surface area with a nanometric thickness of the platelets can be exploited in load bearing, electrical, and barrier applications. However, the reinforcing agents and their types, considerably influence crystallinity, microstructure, and glass transition of the composites, which in turn affect materials properties. Therefore, underpinning the processing-microstructure-property relationship in these materials is of paramount importance.

The preferred route of graphene production is through the top-down approach, where graphene oxide (GO) is synthesized by chemical exfoliation method followed by suitable reduction of GO to graphene. GO possesses various oxygen-containing functional groups that make it easily dispersible in aprotic solvents. Subsequently, by various chemical treatments, some of those functional groups can be removed, and few others attached/created, and the filler-matrix interface can be engineered. The crux of the current work lies in the approaches to strengthen the matrix-reinforcement interface by various types of amines, resulting in unprecedented ultrastrong and ultra-tough PVA nanocomposites. Positron annihilation lifetime spectroscopy has been used to highlight the effect of interfaces. X-ray diffractometry and thermal analysis have been used to understand crystallinity in the samples. Raman and FTIR spectroscopy have been used to understand the disorder in carbon and the chemical functional groups, respectively. Microstructural analysis (using scanning and transmission electrons) of matrices and fractured surfaces have been performed to reveal the distribution of fillers, fracture process, formation of nematic crystals, and the *in-situ* formation of carbon nanoribbons for strengthening.

An order of magnitude increase has been found in Young's modulus and fracture strength of the composites. Such profound increase in strength can be ascribed to the nematic ordering of the functionalized GO flakes in the polymer matrix. In another variant, the formation of carbon nanoribbons from the wrinkled GO platelets and their interpenetrating distribution in the polymer matrix led to enhancement in strength and toughness.

Keywords: Graphene, Graphene Oxide, PVA nanocomposites, Interface strengthening, Electron microscopy, Mechanical properties.

TABLE OF CONTENTS

LIST OF FIGURES

LIST OF TABLES

CHAPTER 1

Introduction.

In this chapter, recent advances in understanding the interface-controlled properties as a function of graphene structure in a polymer nanocomposite are briefly discussed. The scope of the current investigations is then broadly defined.

Nanocomposites with carbon-based fillers have opened up material development and research areas, mostly utilizing graphite (to limited extents), carbon fibers, expanded graphite, carbon black, carbon nanofibers, as well as particulate nanostructured carbon. As a consequence, moderate improvements in the mechanical properties have been achieved. Utilizing carbon fibers have shown improvements in the macro properties of the polymer composites. However, primarily influenced by the development of a synergistic network of fillers, these fillers have a tendency to aggregate reducing the strength of composites [1]. Modifying graphite with strong acid treatment results in exfoliated graphite galleries which can accommodate functional groups as well as polymer chains. Improved mechanical properties of expanded graphite intercalated polymers composites were observed for the polymer such as poly(styrene-co-methyl methacrylate), PMMA blended with polyvinyl chloride (PVC), poly(lactide) or polystyrene (PS) [2-4], where the tensile strength of the composites improved as compared to the neat polymers. Subsequent improvements were obtained by utilizing carbon nanotubes as fillers [5]. However, their partial dispersion in the polymer matrix was found to affect the mechanical properties of the developed composites. Efforts to establish suitable conditions for load transfer have been observed by altering the processing techniques and surface functionalities in the fabrication of the composites. Examples of such kinds include electrospinning the polymer–CNT blend to enhance the alignment and interactions amongst the polymer and the filler leading to enhanced compressive strengths [6]. Similarly, functionalizing CNTs with styrene in the poly(vinyl chloride) polymer matrix, improved the alignment and tensile strengths of the polymer nanocomposites [7]. Despite the fact that CNTs as fillers produced high mechanical strengths than the other graphitic fillers, the unique combination of strength, highest Young modulus, two-dimensional morphology of graphene coupled with the ease of fabrication of the composites and that of processing of graphene have made graphene an ideal candidate as a reinforcement in high-performance polymer composites.

Graphene is defined as a single sheet of sp^2 hybridized carbon atoms arranged in a honeycomb lattice structure. It is the basic building block to different allotropes of carbon including graphite, carbon nanotubes, or Buckminsterfullerenes. Because of the high strength of the covalent bonds between the carbon atoms, graphene possess excellent tensile strength (~125 GPa), and Young's modulus (~1000 GPa) [8], making it the stiffest material known, and stronger than steel. Furthermore, being atomically thin in nature, these sheets of carbon atoms possess high thermal conductivity (5000 $Wm^{-1}K^{-1}$) [9] and high charge mobility (~200,000 $cm^2\ V^{-1}\ s^{-1}$) [10] assigning graphene as the best conductor of heat and electricity. Unlike carbon nanotube or buckyballs, graphene sheets bear all the carbon atoms on the surface of the sheets only, providing a large theoretical surface area (2630 m^2/g). Such attributes of the two-dimensional sheet compiled with high tensile strengths, encourage graphene for applications such as flexible electronics, quantum capacitors, hydrogen storage devices, chemical sensors and nanocomposites [11-13].

Graphene offers significant advantages over other fillers as it extends up to huge lengths and widths with a thickness of only 0.34 nm, (in the case of few-layered graphene, the thickness can be up to few nanometers). It cannot cleave, giving rise to maximum strength in the out of plane direction. Its large surface area provides strengthened interfaces with the matrix, thus enabling many opportunities to engineer interfaces. Graphene in the polymer matrix has properties that are distinct from the same filler on the micron scale. For example, exfoliated graphite flakes synthesized from the alkali metal-graphite intercalation compound (GIC) polymerization, as fillers in polyethylene or polypropylene could increase the stiffness of the finished product [14]. Additionally, graphene oxide derived fillers can exhibit stiffness, strength, and strain-to-failure that substantially exceed those of traditional micrometer diameter carbon fiber [15]. Micrometer-scale graphite flakes approach to the critical crack size, thus causing early failure, while graphene-based fillers are a few orders of magnitude thinner than the graphite flakes. This prevents the early breakdown of the composite promoting enhanced toughness and ductility. Thus graphene-based fillers have been used to fabricate novel robust and tough functionally distinct polymer composites. However, the fact that these nanostructured additives profoundly influence polymer structure morphology and microstructures, which result in the enhanced properties, more detailed investigations in the processing-structure-property relationship of these composites is fundamentally warranted.

Pristine graphene is devoid of any defects or functional groups, which makes its dispersion in aqueous systems difficult. This restricts complete utilization of graphene sheets of its excellent properties. Several routes have been used to exploit the exfoliation and stabilization of fillers before their addition *ex-situ* /or *in-situ* a polymer matrix, thereby controlling the macroscopic performance of the material. Alternative routes include tailoring of graphene oxide, which is an intermediate in the processing of graphene from graphite by chemical routes. Such a route is interesting as it provides an opportunity to achieve property enhancements in the aqueous processable aqueous polymer systems. Lerf-

Klinowski model shows that graphene oxide produced by Hummers or modified Hummers method, produce structures with hydroxyl and epoxy groups present, in higher concentrations in the basal plane and carboxylic acid groups at the edges of the sheets (Fig.1.1) [16]. Such solvent based exfoliation methods of graphene oxide produce sheets with large lateral dimensions which can be chemically functionalized and dispersed in polymer matrices, and further deoxygenated to yield novel composites.

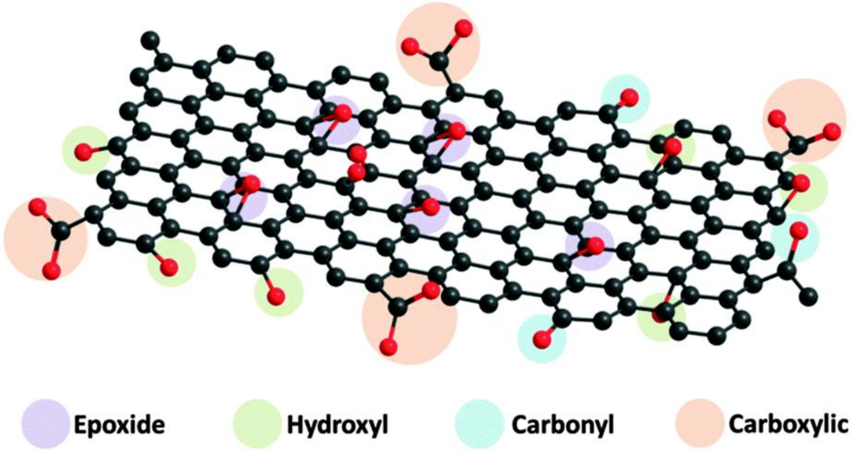

Figure 1.1 Lerf Klinowski model displaying functional groups on graphene oxide, containing epoxide, hydroxyl, carbonyl and carboxylic groups.

Exfoliated graphene oxide produced by thermal or sonication methods provides morphology with different lateral dimensions [17]. Thermally exfoliated graphene oxide (TEGO) sheets contain remnant oxygen groups and exhibit a crumpled accordion-like morphology with lateral dimensions ranging up to few hundreds of nanometers only [18]. Such crumpled nanosheets intercalated in the polymer matrices disperse well in polymer matrices, but produce property enhancements at higher weight fractions, of about 2 wt% [19, 20]. Similarly, sonication methods provide well-exfoliated sheets in the solvent, but the fragments of the sheets are again reduced down to few hundred of nanometers limiting the aspect ratio advantage of large area graphene sheets [21]. Mechanical stirring is an alternative route to exploit the graphene sheets with large lateral dimensions. However, relatively low yield and slow procedures of exfoliation suggest alternative routes be explored for GO exfoliation and dispersion. These variations in the lateral dimensions and microstructures of graphene oxide sheets enable different degrees of interfacial interlocking and adhesion with the polymer matrix which finally lead to varying levels of property enhancement.

Regarding dispersion of graphene in the polymer matrices, several routes have been used to exploit the exfoliation and stabilization of fillers before their addition (*ex-situ* or *in-situ*) in a polymer matrix, thereby controlling the macroscopic performance of the material For example isocyanate treated graphene oxide exfoliated as functionalized graphene oxide platelets exhibit stable dispersions in polar solvents [22]. Similarly, GO dispersed in acetone followed by multi-step functionalization of graphene in the epoxy matrix have successfully fabricated systems with enhanced mechanical performance [23]. Furthermore, polystyrene polymer intercalated with functionalized graphene sheets improved the elastic modulus and tensile strength by 58% and 70% of their neat polymer [24]. Epoxy intercalated with functionalised graphene improved the flexural strength by 48% and with additional improvements in their thermal stability and glass transition temperatures [25].

These studies suggest that the intrinsic filler properties strongly influence the structure-property relationship of a polymer nanocomposite. They play a major role in graphene-based polymer nanocomposites as they profoundly influence the chemical, thermodynamic, interfacial and morphological features of the segmented polymers [26-30]. Optimum composite performance is often achieved by tailoring fabrication conditions and or/ by functionalizing the fillers [22, 31, 32]. In most cases, functionalization enhances the mechanical performance of the graphene-based polymer systems. These elements preferentially form supramolecular complexes with enhanced interfacial adhesion and dispersion of the graphene in the polymer matrix. Many polymeric systems with various routes of dispersing graphene in the matrices with improved mechanical properties have been observed. Functionalized carbon-based fillers ranging from 0.1 to 5 wt. % show an improvement over 30-350% increase in the elastic modulus and about 50-200 % increase in the tensile strength for different polymers like Nylon-6, poly(methyl methacrylate) (PMMA), poly(vinylidene) (PVDF) and epoxy [33-35]. In summary, a wide variety of improved mechanical performance can be achieved by altering the interfaces of different polymeric systems with the incorporation of graphene fillers.

Poly (vinyl alcohol), (henceforth referred to as PVA) polymer exhibits mechanical properties sensitive to graphene filler incorporation with and without functionalization. For example, PVA polymer loaded with 0.7 wt% of graphene oxide improves the tensile strengths [36]. On the other hand, improvements in the tensile strengths were observed for a filler loading of 1.8% [37]. Functionalized graphene combined with polymer matrices have also shown to exhibit enhanced mechanical properties. In essence, with the use of some functionalities, the rate of tensile strength and elastic deformation of the composites can be varied by several degrees in the polymer matrix. For instance, PVP-stabilized reduced graphene sheets incorporated in the PVA matrix exhibited improved strengths for a loading of 0.7 wt. % filler loading [38]. Subsequently, the addition of sulfonated graphene sheets in the PVA matrix produced improved tensile performances by 117% at 3 wt.% of graphene filler [39].

Ideally, graphene sheets incorporated in a polymer matrix should exist as rigid disks or platelets in the polymer matrix. However, it is practically observed that graphene sheets follow a bent or crumpled platelet-type structure in the polymer matrix. These bend structures in the polymer, affect the crystallinity of the polymer matrix. It is shown that graphene sheets in the polymer matrix tend to scroll up when heated above its glass transition temperatures [40]. If there is strong compatibility between the polymer and the graphene sheets, the effect of scrolling is suppressed to high temperatures, producing a more extended conformation. However, if the affinity amongst the polymer and the graphene sheets is reduced, the sheets take up a more crumpled or scrolled morphology [41]. The retention or change of filler morphology can influence materials microstructures and properties and acquire the ability to control these microstructures can lead to tailoring of properties. Furthermore, a substantial part of the polymer crystallinity is also affected by the addition of fillers that act as nucleating sites affecting the rate of crystallization and crystal growth. However, the extent of its effect on crystallinity is a function of the filler morphology, its functional groups as well as the polymer matrix [36, 42].

Gradually an understanding has evolved that considers an additional volume element in addition to the two phases of matrix and filler in the nanocomposite. These are the interphase zones that exist at the periphery of the fillers and the matrix and can evolve to a volume element with few tens of nanometer thickness. Interfaces have been found to control many properties in the polycrystalline ceramics and metal systems. Similarly, the evidence is evolving for such regions to occur in the polymer nanocomposites as well. Quantitative evaluation of such interphase zone in polymer nanocomposites depends on the interaction between the polymer and the filler. The interface region of polymer extends entirely over the polymer chains in the matrix, with altered mobility over hundreds of nanometers away from the interface. Such an interface can have properties and structures that are different from that of the bulk polymer and can alter glass transition, crack propagation, electron transport, and load transfer properties.

These studies suggest that the difference in the mechanical properties can be attributed to several factors including filler morphology, their degree or homogeneity of dispersion, orientation, and interfacial adhesions. Thus the outstanding problems of the area with polymer/GO composites lie in understanding the properties of GO fillers regarding their dispersion state in the polymer matrix, interfacial interactions, change in the crystallinity of the segmented polymers, [27-30] and the influence of all of these parameters in the microstructures of the composites.

Therefore, the approach of the current work is first to synthesize graphene oxide by the top-down chemical approach, which offers advantages of a straightforward and fast process, over the mechanical exfoliation or epitaxial growth of methods are serendipitous and difficult to control the morphology of synthesized graphene. Chemical exfoliation methods of graphene oxide produce lateral sheets of large dimension, (of course this depends on the precursor graphite types), which can be chemically functionalized and dispersed in polymer matrices, and further deoxygenated to yield novel composites. However, deoxygenation of the GO sheets in the polymer matrix result in agglomeration or aggregation in the polymer matrix, which compromises mechanical properties of the composites. Therefore the optimum composite performance would be achieved by tailoring fabrication conditions and or/ by functionalizing the graphene oxide [31, 32, 43]. In most cases, non-covalent interactions like H-bonding, or covalently grafting the graphene oxide filler enhances the mechanical properties of the graphene-based polymer composites, through the formation of supramolecular complexes with enhanced interfacial adhesion and dispersion of the fillers in the polymer matrix.

With the above-said basics, the second part of the work has been carried out with the fabrication of a series of *in-situ* functionalized graphene-based PVA composites. This was done by functionalizing the GO sheets with different amines and *in-situ* reducing them to achieve some extent of graphene type character of the fillers as well as impart homogeneity of the filler in the polymer. This has been carried out by studying the aqueous colloidal stability of the amine treated graphene oxide fillers separately before incorporating them in the polymers. The structural, functional and chemical attributes of the composites would be explored to gain further insights into the nature of *in-situ* reduced graphene oxide intercalated polymer composites.

Electron microscopic techniques such as field emission scanning electron microscopy (FESEM), high-resolution transmission electron microscopy (HRTEM), and high angle annular dark field images (HAADF) in scanning transmission electron microscope (STEM) have provided valuable information regarding the interfacial chemistry.With distinct contrasts amongst the polymer chains and the graphene sheets, these techniques describe the orientation filler in the matrix affecting the composite deformation. HAADF-STEM imaging on thin electron transparent foils of materials (typically ceramic and metals) have provided the ability to image interfaces and bulk by discriminating between electron scattering from different atomic numbers.Therefore it is a preferred technique to detect extremely low quantities of high atomic number elements in a bulk/ interface of relatively low atomic number elements [44]. However, HAADF-STEM as a characterization tool for polymeric composites has not been as much of other materials. Only a few studies in careful study of PVA-graphene system have been reported through FESEM or HRTEM only [45-48]. Interpretations of such classic interfacial interactions have not been vividly reported by HAADF or STEM techniques so far.

In this work some efforts have been made to understand the microstructures and morphological features of the carbon-based reinforcements from amongst the polymeric phase, where the latter is a combination of carbon, hydrogen, and oxygen with considerably low atomic density (within a volume), leading to a clear difference between the electron scattering from a filler to that of the matrix. Also, conventional brightfield imaging has been used to observe the overall morphology. HRTEM methods have been used to understand the crystalline parts of the composites (the fillers) and quantitatively infer about their structural order.

Fourier transform infrared (FTIR) spectroscopy provides information on the functional group and specific chemical moieties with its polymer matrix. Coupled with Raman spectroscopy the changes in the filler structure and order can be assessed. X- ray diffraction (XRD) and differential scanning calorimetry (DSC) can provide information about crystallinity of the reinforced polymer system. Large deformations in the polymer matrix depend on the nature of the entangled polymer chains [49]. Composed as an interpenetrating network of amorphous and crystalline chains, the crystallinity of the polymers are largely affected by the presence of graphene fillers. Graphene fillers restrict the mobility of free chains in the matrix which in turn affects the free volume density of the polymeric chains, thus affecting the glass transition temperatures and the crystallinity of the matrix. Herein we have tried to disseminate the effect of interfacially bonded fillers in the polymer matrix on account of the glass transition behavior.

These complementary characterisation tools corroborated with the processing methods of the composites have been exploited in this thesis to understand the structural, thermal behavior, morphology, and microstructural aspects, influencing the mechanical properties of functionalised graphene reinforced PVA composites.

The thesis is organized as follows:-

Chapter 1 introduces the area of carbon nanostructured material reinforced polymer nanocomposites their specific developments and challenges in graphene based polymer composites.The current work is introduced in the overall context of the existing challenges and scientific gaps. Chapter 2 provides an extensive literature on polymer composites with reinforcements over macro to micro to nano scale. Various processing parameters, schemes, including toughening and strengthening mechanisms, physicochemical properties and their influence on engineering properties have been discussed, with special reference to graphene/PVA systems. Chapter 3 briefs about the material synthesis, composite fabrication, details of the characterization tools used and the methods of mechanical property evaluation. Chapter 4 describes the aqueous colloidal stability of graphene oxide with various reductants such as hydrazine and amines. Results of the mechanical properties, morphology, crystallinity and other characterization techniques have been discussed in chapter 5 for graphene oxide reinforced PVA composites and hydrazine reduced GO/PVA composites. The subsequent chapters are built on the effect of various amines. The use of triethanolamine (TEOA), as a reductant /functionalizing agent, has been discussed in chapter 6. In chapter 7, the application of triethylamine (TEA) as the functionalization agent has been discussed. An additional step of hydrazine reduction after TEA functionalization of the fillers in the polymer nanocomposite has been discussed in chapter 8. In the concluding part, chapter 9, relevant and most significant aspects of each of the chapters are assimilated in the broad context of the processing structure- property relationship in functionalized graphene reinforced polymer composites.

CHAPTER 2

Literature review.

This section embodies the background and developments in carbon reinforced polymer composites. Works on different graphene based polymer composites have been majorly reviewed with a focus on aqueous polymer systems exploited for enhanced mechanical properties. Different strengthening mechanisms, mathematical models, and the challenges in the prevailing systems have been discussed next. Scope and objectives of the thesis are then briefly outlined.

2.1 Polymer composites.

Humankind has been familiar with the art of composite fabrication since long. Composed of two or more constituent materials with distinct properties-namely matrix and reinforcement: composites are formed as a combination of these parts to produce a new material with a desired set of characteristic properties. Common of such kinds are straw-reinforced mud bricks, and concrete, which involve reinforcing straw or loose stones/ gravel with cement to enhance the strength of the composites. These materials were traditionally utilized for the construction of houses, buildings, roads and bridges. More advanced forms of composites include metal matrix composites, ceramic matrix composites, and polymer matrix composites. These are utilized in the fabrication of automobile bodies, swimming pools, storage tanks, household and electronic appliances. In modern engineering, polymer composites are classified as fiber reinforced polymer composites (FRPs) and glass reinforced polymer composites (GRPs). These are composed of a polymer matrix (which is either a thermoplastic or thermoset) embedded with different filler or reinforcement, like short or long fibers or laminates, or particles such as glass, carbon or aramid.

Polymers are attractive as they possess a host of beneficial properties including, low coefficient of friction, good corrosion resistance, good moldability, lower machining cost, and light-weightedness. Such characteristics of polymers combined with filler materials produce engineered structures in the field of construction, electronic, automobiles [50], medical science [51] sports [52], and energy industries [53]. Besides this, high-performance of the polymer composites are being used in military, marine and aerospace industries [54]. Furthermore, electrical and electronic areas including housing equipment, tool handles, insulation, storage tanks or fitting materials in plumbing involving materials like thermoplastics and thermosets have been an emergent field of application for everyday engineering applications [55].

Application based polymer composites largely depend on the nature of the filler employed. Examples of such kind include a large number of fillers such as clay [26], glass [56], carbon, aramid fibers [27], talc [28], calcium carbonate [57] or mica [29]. These fillers mixed with polymer matrices enhance load bearing or structural applications where the resultant polymer composites possess improved mechanical properties synergistically derived from both the filler and matrix components as compared to the pristine polymer.

Commercial progress of polymer composites dates back to their specific application in automobiles. The most well known field of polymer composites was an automotive application by Toyota for a timing belt cover. General Motors further utilized exfoliated clay reinforced in thermoplastic polyolefin (TPO) for an exterior step assist for automotive application [58]. Many different uses have seen identified for the polymer composites, the latest being wings and fuselage in Boeing 787 aircraft. [59] Besides this, a ground swimming pool was made in the year 2006 by using fiber reinforced composite, as a non-corrosive alternative to galvanized steel [60]. Carbon fiber reinforced with Du Pont Kevlar (five times stronger than steel) were used to make military transit cases creating 30% lighter cases with high strength in the year 2008 [61].

Composite systems were initially fabricated as particle-reinforced systems composed of large particle reinforced and dispersion strengthened composites and fibre reinforced composites comrising of glass or carbon fibres as fillers in a polymer matrix. In large particle composites, the filler is usually of a large size, meaning, they are left untreated at the atomic or molecular level. The matrix bears a major share of the load and transfers some of the applied stress to the filler, which bears a fraction of the load. Examples of such kind include concrete. Here, the matrix is the mortar, and the filler is the gravel which when evenly distributed in matrix results in better mechanical properties. In the case of dispersion-strengthened composites, the filler is usually of a smaller diameter between 0.01 and 0.1 µm. These leads to the strengthening on a much finer level. In this case, the matrix bears most of the applied load, and the small dispersed particles hinder or impede the motion of dislocations. Classic examples of such kind include thoria-dispersed (or TD) with 3vol % ThO_2 in Ni or Ni-based alloys for elevated temperature application and Al_2O_3-reinforced pure aluminum particles, also known as sintered aluminum particles (SAP) [62]. These classifications suggest that the mechanical property enhancement is attributed to the size of the filler in the polymer matrix.

Extensions of these principles to polymer composites involved embedding small glass fibers in a polymeric matrix classified as glass reinforced plastic (GRPs). The filler is defined as fiberglass because the glass is drawn into thin fibers, with diameters normally ranging between 3 to 20 µm. Moreover, such fibers are relatively robust and chemically inert in nature, making them feasible for applications in corrosive environments with high strength. These GRPs find applications in areas such as body parts of marine automotive, plastic pipes and transportation industries. However, development of such polymer composites requires a higher volume fraction of filler content for achieving required property improvement. Therefore, there arose a need to develop light-weight and sturdy composites for enhanced mechanical properties. A class of such composites was designed as carbon fiber reinforced polymer (FRPs) composites. Carbon fibers are superior to other fillers regarding strength, elastic modulus, and corrosion. Sports equipment is one area where carbon fiber reinforced composites are commercially available. An initial use of such fillers was done by a company, named Inmat LLC in the year 2011. They included the use of exfoliated clay for barrier applications, which involved a 20 µm coating on the interior of a tennis ball to prevent depressurization. Soon after the commercial availability of carbon nanotubes, it popularized as a reinforcement in the epoxy matrix to produce flexible and lightweight tennis rackets and hockey sticks [63]. Subsequently, a company of Austria, produced the first graphene-based commercial artifacts, like a tennis racket. State of the art in constructing such a racquet was to produce light weight, thin and extremely flexible racket as compared to the previous versions [64].

Carbon black is one of the oldest species in the carbon family. Having a high surface to volume ratio, albeit lower than that of activated carbon, carbon black has lower polycyclic aromatic hydrocarbon content. This has been employed in plastics, paints and inks as a color pigment, [65] or as a reinforcing filler in tires and other rubber products. Up to now, a large number of polymers have been studied using carbon black as a filler. Imoisili et al. (2013) made studies with natural rubber reinforced carbon black hybrid filler. These hybrid fillers showed improved mechanical property including tensile strength, modulus, abrasion resistance and hardness with the increase in the carbon black filler [66]. This was attributed to the effective load transfer from the matrix to the fillers. Senthivel et al. (2015) reported the improved mechanical response of carbon black/ Halloysite nanotube ($Al_2Si_2O_5(OH)_4.nH_2O$) in nitrile rubber composites [67]. Chatopadhya et al have reported an increase in strength of styrene-butadiene rubber (SBR)-carbon black/ organoclay hybrid systems (2010) [68]. Similarly, You-Ping et al. (2006) communicated the increased the flex fatigue life of carbon black filled with SBR with the addition of nano-dispersed clay [69].

Expanded graphite (EG) is another class of carbonaceous filler, which has been studied for mechanical property improvement in polymer matrices. Expanded graphite has shown substantial mechanical [70], electrical and thermomechanical response [71, 72]. Asma et al. (2005) revealed that EG reinforced epoxy matrices have higher elastic modulus than neat epoxy [73, 74]. Zheng et al. (2004) showed improved tensile and stiffness of polyethylene expanded graphite composites (10 and 17wt%) under uniaxial loading, at a given volume fractions as per composite theory [75]. Epoxy-expanded graphite studies made by Baptista et al. (2016) showed that at very high loadings of 11.5 wt. % of EG, the tensile properties, and ultimate stress values of the nanocomposites increases.

These results showed that the property enhancements made by expanded graphite were observed at a very high filler loading, inferring expanded graphite as a macro size filler. This results in less interfacial interaction for unit weight of the fillers and hence moderate enhancement in mechanical properties at lower loadings of the filler. This led to study another class of carbon-based filler called as carbon fiber. Eriksen, (1976) studied carbon fiber/epoxy composites for superior creep properties. Fitzer and Heym (1976) showed that carbon/polyimide composites bear high-temperature strength than most carbon fibers. Polyphenylene sulfide (PPS), polysulfones (PS), and polyether ketone (PEEK) were studied for high performance and strength of materials. PPS with continuous fiber prepregs were used in making composite laminates. PEEK, is a semi-crystalline polyether that combines excellent toughness with chemical inertness.

Waddon et al. (1987), showed that these carbon fiber composites were tougher than the epoxy/ carbon fibers based composites [76]. Satish et al. (2002) studied the improved modulus and compressive strength of polypropylene by 50 and 100 % at a low weight percentage of carbon nanofiber loading [77]. Subsequently, they also studied the enhanced thermal stability, enhanced modulus retention with improved compressive strengths [78]. Besides this, Xu et al. (2004) studied vinyl ester resins with carbon fibers. The Flexural modulus and strength was expected to increase with the fiber loading. However, their results featured decreased mechanical properties as the filler content was raised to 10% and remained almost same for higher filler content of about 25% [79]. This failure was attributed to fiber orientation, poor fiber microdispersion, adhesion and increase in the void content with increasing filler loading. Epoxy matrix with carbon fibers was studied by Koo et al. (2004) to show enhanced mechanical properties by reinforcing carbon fiber in the matrix before curing [80]. Soon improvements by utilizing carbon nanofibers were studied by Sadeghian et al. (2006) sufficing resistance to delaminating glass-fibre reinforced polyester composite [81]. Vivekananda et al. (2012) showed that addition of 30 wt.% of carbon fibers into poly trimethylene terephthalate (PTT) showed significant improvement in tensile and flexural strength as compared to neat PTT. Their results confirm enhancement of properties with increasing fiber content, satisfying good compatibility between the polymers and the fillers [82]. Lately, Chen et al. (2012) studied 2D carbon fiber reinforced epoxy laminated composite as engineering structures for aerospace applications. They studied the tensile properties of the composites through the thickness of the composites which showed that a material deforms in a linear elastic mode before fracture. However, as the strain rate is increased, the tensile strength increases significantly and the breakage mode changes [83].

Jo et al. (2008) incorporated nano clay to strengthen a resin concrete (11% polyester resin and 89% of mineral fillers (sand and limestone) [84]. Bauer et al. (2008) strengthened polyester resins by montmorillonite treated nanofillers by grafting silane functional groups resulting in increased mechanical properties [85]. 4% nano clay in a vinyl ester resin increased the modulus of the nanocomposite as seen by Chen et al. (2007) but decreased the elongation at break as compared to the virgin resin [86]. Further Karger-Kocsis et al. (2003) studied hybrid resins modified vinyl ester/ epoxy with two different types of clay fillers showing that the fracture energy of the nanocomposites containing 0.5wt.% nano clay was doubled compared to the pure resins [87]. The breaking strength and elasticity modulus in compression of epoxy resins increased by nano clay on surface treatment. Kasgoz et al. (2014) showed the effect of different types of carbon fillers on cyclic olefin copolymers (COC) composites based on the geometrical and structural parameters of different carbon nanofillers [88]. They showed that carbon black, carbon fillers, graphene and expanded graphite, all showed no significant difference in the hardness due to the filler type and the rigid structure of polymeric phase. Nevertheless, the melt rheology of carbon black and expanded graphite showed an increase in melt viscosity much higher than graphene and carbon filler due to their high surface area and agglomerated structure.

These examples of macroscopic fillers suggest that the mechanical properties of composites largely depend on the interfacial area and the intensity of intermolecular interactions between the matrix and the filler [89]. Therefore, there arises a need to replace the traditional composites with a new class of fillers for enhanced interfacial interaction, and hence better properties. This can be resolved by employing fillers at the nanometric level, which result in a higher surface to volume ratio and a higher aspect ratio. While nanofillers are usually below 100 nm in size, their higher specific surface area than the larger particles allows to substantially reduced filler loading. Shifting over to the nanoscale filler alongside optimization of synthesis parameters helps not only to reduce the consumption of the filler but also remarkably improves the properties of the composite materials.

2.2 Polymer nanocomposites.

Studies on metallic, ceramic, and polymer nanocomposite systems have been carried out extensively since the 1990s. While metals and to a lower degree, ceramic matrices are used for nanocomposite applications, polymer matrix nanocomposites have been a prominent area of research. With parameters of processability, fiber reinforced property, structure, and morphological aspects [90, 91] polymer based nanocomposites [92, 93] have opened up new areas of high performance applications.

Nanostructured fillers including exfoliated clay or montmorillonite, nano-oxides including TiO_2 [94-97], SnO_2 [98-100], Al_2O_3 [101-103], ZnO [104, 105] or nano silica [106-108], have been used in the processing of polymer nanocomposites. Additionally, graphite nanoplatelets, carbon nanotubes, carbon nanofibers, graphene, carbon black and a host of additional nanoscale inorganic fillers have added interesting enhancement in material properties. Although the nanostructured fillers differ from each other regarding shape, structure, the property enhancement in these fillers owes to their high aspect ratio and effective volume fraction utilization. This means that if the size of the filler is reduced, the interfacial area is improved, resulting in properties different from bulk materials even at low filler loading. Therefore, it becomes interesting to observe the effect of these fillers affecting the overall properties of different polymer matrices.

Nanocomposites are considered as multiphase materials where one of the phases has one, two or three dimensions less than 100 nm dispersed in a bulk matrix [109]. In other words, we can consider these as structures with nanoscale repeat distances between different phases composing the material. These materials possess design uniqueness and property combinations those are not present in the conventional polymer composites. These unique properties attribute to the change in particle properties, which suggests that when the particle size is less than a particular level, called as ‘critical size,' it results in enhanced properties [110].

Thus, according to standards defined in ISO/TS27687 (2008), the nanocomposites are distributed as:-

1) One-dimensional (1D) nanofiller: nanotubes and nanofibers with diameter lower that 100nm;

2) Two-dimensional (2D) nanofiller: in the form of plates, laminates or shells with a thickness less than 100 nm.

3) Three-dimensional (3D) nanofiller: iso-dimensional nanoparticles such as nanometric silica beads with all dimensions less than 100 nm.

To fabricate nanocomposites with better mechanical properties, a system with lower filler content is desired to provide better interfacial interaction. While the technology for the incorporation of 3D nanofillers (in the form of particulates) in different polymeric systems have matured and industrialised, there remains great prospects for further improvement in composite properties by the use of 1D and 2D nanofillers. This is achieved by utilizing nanostructured fillers like carbon nanotubes, or graphene in modern trends.

2.3 Carbon nanotubes (CNTs) as fillers.

Discovered by Ijima (1991), CNTs have gained tremendous interests towards the development of their applications owing to their unique set of electronic, mechanical and structural properties and extremely large aspect ratios [111]. These members of fullerene family are classified as a tube-shaped material made up of carbon, with a diameter on the nanoscale. These are hollow structures with the walls formed by one atom thick sheets called graphene. These sheets roll at specific and unique (chiral) angles, and the combination of these rolling angles and radius decide the properties of the nanotubes regarding their metallic or semiconductor nature. Depending on the number of rolls the sheet of carbon atoms require to make CNTs, we categorize them as single-walled nanotubes (SWNTs) or multi-walled nanotubes (MWNTs). SWNTs have a diameter close to 1nm and have lengths of a million times [112], whereas MWNTs have diameters between 2 to 25 nm [113]. Natural alignment of the nanotubes also occurs in the form of ropes held together by van der Waals forces or pi stacking [113].

CNTs are the strongest and stiffest materials discovered regarding strength and elastic modulus respectively. The strength arises from the covalent sp^2 bonds between the individual carbon atoms. Yu et al. (2000) showed a tensile strength of about 63 GPa for MWNTs [114], whereas Peng et al. (2008) showed individual CNTs with the strength of around 100 GPa [115]. Its specific strength of up to 48,000 $kN.m.kg^{-1}$ suggests CNTs as the best-known materials, compared to high carbon steels with the strength of 154 $kN.m.kg^{-1}$ [116]. These enhanced properties in bulk nanotubes are utilized as composite fibers to improve the yield strengths of the bulk composites. Current areas of applications include fabricating tips for atomic force microscope, scaffolds for tissue engineering [117], storage devices and polymer nanostructure applications [114].

Although the strength of individual CNTs is extremely high, MWNTs have reduced strengths up to a few GPa, due to the weak shear interactions between the adjacent sheets. Moreover, because of their hollow structures, they undergo buckling when placed under compressive torsional stress [118]. Therefore, the enhanced properties are achieved by utilizing bulk nanotubes as composite fibers to improve the yield strengths of the bulk composites.

2.4 CNT-based polymer composites.

Use of carbon-based fillers has led to the development of high-performance polymer nanocomposites. The distribution of the fillers (eg. CNT) plays an important role in composite properties. The composites in which CNTs are agglomerated, bundled or entangled together leads to defects in the composites and limits the efficiency of the reinforcement effects. Composites with well-dispersed or aligned nanotubes in the polymer matrix generally exhibit better mechanical and functional properties. Jin et al. (1998) reported the alignment of nanotubes and orientation of nanotubes in polyhydroxy amino ether (PHAE) polymer [119]. Similar studies made by Ajayan et al. (1994) on CNTs randomly dispersed in an epoxy matrix found that slicing the composite caused partial alignment of the CNTs on the cut surface [120]. Heer et al. (1995) fabricated aligned nanotube films by drawing a nanotube suspension through a micropore filter [121]. Feng et al. (2003) attempted to prepare well aligned polyaniline-MWNT composite films by in situ polymerization [122]. Similarly, Raravikar et al. (2005) prepared polymethyl methacrylate (PMMA)-MWNT composite films by infiltrating pre-aligned MWNT arrays on the quartz substrate via CVD method [123].

Qian et al. reported enhanced mechanical properties, (2004) which showed that MWCNTs in a polystyrene matrix increase the elastic modulus and tensile strength by 42% and 25% as compared to the neat polystyrene [124]. Gorga and Cohen, (2004) investigated the effect of nanotube orientation on the mechanical properties of PMMA-MWNT nanocomposites, which showed that addition of just 1% MWNT to PMMA leads to a very large increase in tensile toughness [125]. Liu and Wagner, (2005) investigated the mechanical behavior of rubbery and glassy epoxy resins reinforced with MWNTs. They reported a 28% increase in Young’s modulus in the rubbery system and 50% increase in improved toughness for glass epoxy resin composites. Manchado et al. (2005) reported that the addition of 0.25-0.75 wt % of SWCNTs to polypropylene matrix increases the tensile strength, stiffness, and the storage modulus considerably [126]. Subsequently, modifications were made in the processing parameters to produce better CNT-based polymer composites. Wang et al. (2008) showed that adding sodium dodecyl sulfate (SDS) to CNTs resulted in an increase in the Youngs modulus reaching the theoretically predicted values. Their results show that CNTs are effective reinforcement for improving the mechanical properties of electrospun PVA fibers [127]. Later on Fritzsche et al. (2009) studied the incorporation of CNT in silica fused natural rubber to improve the tensile strengths with a very low amount of CNT [128]. Khan et al. (2013) showed that only 0.3wt% of CNTs in the epoxy composites can improve the elastic and fracture toughness of the epoxy composite by 40% and 50% [129]. Gupta et al. (2014) show that only 1% of MWNTs added to epoxy matrix increases the tensile strength and strain at failure values [130]. Recent studies made by Liu et al. (2016) showed that incorporating only 1wt.% of MWNTs in the polyvinyl alcohol (PVA) polymer, the tensile modulus, and tensile strength improved greatly by 115 and 120 % as compared to the neat polymer [131]. The unusual properties of high tensile modulus of 1TPa, tensile strength in the range of 50 –150 GPa and failure strains more than 5% CNTs have resulted in the property improvement of the composites [132, 133].

.

2.5 Graphene as fillers.

Prior studies with 3D and 1D graphitic fillers on a macro or nanoscale have been reported since long [134, 135] but the 2D filler, graphene gained a fresh look since 2004, after the discovery made by Novoselov et al. [136]. Graphene is the youngest member of the carbon family. It is an allotrope of carbon in two dimensions (2D) with carbon atoms arranged in a honeycomb lattice. Structurally, it is responsible for building all the graphitic structures. Layers of graphene stack on top of each other to form graphite with an interlayer spacing of 0.334 nm. Besides this the extended honeycomb structure rolls to form 1D nanotubes and wraps to form 0D fullerene type structures (Fig.2.1) [137].

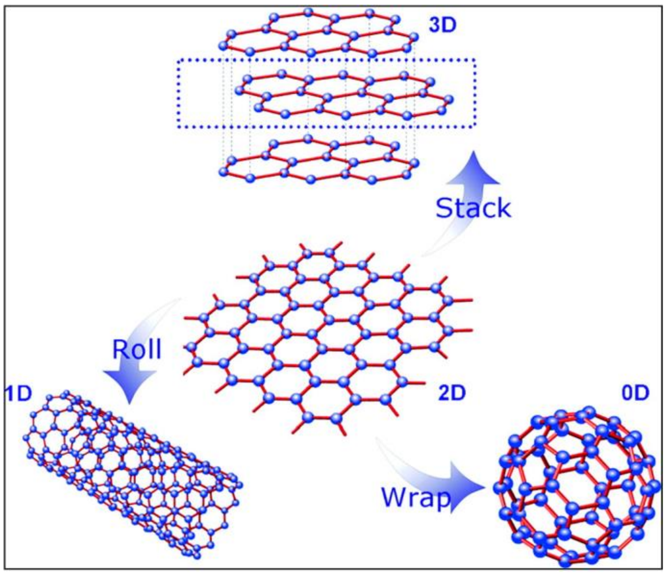

Figure 2.1. The building block of all graphitic structures [138].

Graphene has excellent properties in terms of strength (~100 GPa), stiffness (~1 TPa) [8] thermal conductivity (5000 $Wm^{-1}K^{-1}$) [9] buckling resistance, and high fatigue strength [139, 140]. Its high specific area (2630 m^2g^{-1}) and intrinsic mobility (200 000 $cm^2 v^{-1} s^{-1}$) [141, 142], and optical transparency marks its importance for application such as flexible electronics, solar cells, photovoltaics, capacitors and hydrogen storage devices [143, 144]. Such versatile features and projected applications, suggest several production techniques ranging from the mechanical exfoliation of high-quality graphene to the direct growth on carbides or metal substrates, or the chemical routes using graphene oxide to the newly developed approach at the molecular level.

First attempts were made by Geim’s group in 2004 [145] to produce single sheet graphene by a simple method of cleaving a graphite crystal with an adhesive tape to its limit. The remarkably simple yet efficient method statistically brought a 1μm thick graphite flake to a monolayer thin sample. Soon, supported growth type methods were developed on solid substrates by exploiting two different mechanisms; the thermal decomposition of carbon-rich faces of carbides [146, 147] or the epitaxial growth of graphene on metallic or metal carbide substrates by chemical vapor deposition of hydrocarbons [148, 149]. Despite the fact that this growth method produced wafer scale graphene, the drawback of lower yield made it limited to electrical applications only. Gradually, large scale production of graphene became a necessity, and chemical routes were revisited [150] with a new challenge of converting graphene oxide to graphene by versatile reduction methods.

Extensive works made by Staudenmeir, Brodie's and Hummers produced large polyaromatic hydrocarbons (PAH) as sub-nanometer fragments of graphite. This atomically precise structure of graphene fragments offered an absolute precision of the edge structure of nanoscale graphene domains. Brodie's work of oxidative intercalation of potassium chlorate in concentrated sulphuric and nitric acid produced modified graphite flakes composed of highly re-hybridized carbon sheets bearing hydroxyl and carboxyl moieties. This suspension was initially named graphitic acid but soon were more commonly known as graphite oxide (GO). Following his work, Hummers soon reported a faster and safer route to graphite oxide [151] where graphite was dispersed into a mixture of concentrated sulphuric acid, sodium nitrate and potassium permanganate (replacing the potassium chlorate) at 45°C for a couple of hours. The X-ray diffraction investigation of graphite oxide showed the total disappearance of the typical graphite inter-layer diffraction peak (0.334 nm) and the appearance of a new one indicating a larger interlayer spacing (0.65-0.75 nm) [147]. Graphite intercalation compounds obtained by the intercalation of sulphuric acid between the graphite layers were commonly used in chemical, electrochemical, and industrial applications. After the intercalation of graphite by one of these methods, few or even single-sheet materials were obtained by decomposing the intercalated reactant to produce a large amount of gas in the van der Waals space by chemical or thermal means. Thus, their routes turned out to be a versatile approach for producing graphene at large scale and making it useful for various applications.

Since graphene oxide platelets are readily obtainable in large quantities, it is relatively easier to exfoliate and disperse them in an aqueous processable polymer matrix. By virtue of its built-in functional groups available, these sheets form a strong interface with a polymer matrix. However, earlier studies have shown that individual nanoplatelets of graphene oxide are often wrinkled and have inferior mechanical properties to graphene. Therefore, it gets important to study the filler morphology and its incorporation in reduced or unreduced form influencing the mechanical properties of the developed nanocomposites.

Interface-controlled properties are a function of the structure of graphene oxide. The primary contributors to the structure include the precursor material (including sample-to-sample variability), berthollide character (i.e. no stoichiometric atomic composition), and the different methods of production. For example, mechanical peeling produces single layer graphene oxide of much larger dimensions and aspect ratio, but the yield is very low [147]. Similarly, graphene produced by Hummers or modified Hummers method possess structures with hydroxyl, and epoxy groups present in higher concentrations on the basal plane, with carboxylic acid groups around the periphery of the sheets. SEM analysis shows that the presence of carboxylic groups on the outer limits of sheets produces a crumpled morphology of large lateral dimensions. Such fillers in the polymer matrix may have a strong interlocking character that affects the mechanical behavior. On the other hand, exfoliation of graphene oxide produced by thermal or sonication methods provides morphology with different lateral dimensions. Suspensions produced by sonication have been found to reduce the lateral dimensions by order of magnitude of few hundred nanometers [17]. Such sheets of varied lateral dimensions provide opportunities to incorporate these fillers in polymer matrices and tailor material microstructure with associated properties.

2.6 Reduction of graphene oxide.

Physical properties of graphene oxide are very much different from graphene. Graphene oxide is decorated with oxygen-containing groups on its surface making it highly soluble in water or polar solvents and chemically insulating. Notably, graphene bears a restored conjugated structure of the π-network, making it soluble only in non-polar solvents and is electrically conductive. The restored conjugated structure is an important aspect of the application of graphene making it majorly responsible for improved electrical conductivity [152-154], high mechanical strength [140, 155], optical or thermal behavior [9, 156-159]. This suggests that the reduction process is one of the most important conversion processes.

Reduction can be achieved via chemical [160], thermal [161] or electrochemical processing routes [162]. Considering the ease, viability, and large scale production by chemical routes, typical strong reducing agents like hydrazine hydrate [163-167], hydroalcoholic acid [168], sodium borohydride [169] or sodium hydride [170] are commonly used to reduce graphene oxide to graphene. However, despite several advantages of chemically reduced graphene, the persistent challenge over these methodologies involve great extent or defects, crumpling, residual functional groups or tendency to agglomerate due to attractive van der Waals forces [171].

For example, using hydrazine as a reductant, accumulation of N-charges occur, and formation of hydrocarbons arise from the carboxyl group reaction [172]. Secondly, hydrazine is highly toxic and results in very high agglomeration of the reduced product [173, 174]. Therefore, the choice of an appropriate reductant becomes an important parameter for reduction. Few results of reduction using different reductants such hydrazine hydrate, HI, and $NaBH_4$ were confirmed by Song et al. (2012). Their results show that HI reduction produces less agglomerated GO films, good flexibility, and improved tensile strength, whereas $NaBH_4$ and hydrazine produce reduced GO films that are rolled up and broken into pieces [164] (Fig.2.2). Siegfried et al. (2013) made another group of studies utilizing different reducing agents like hydrazine, Vitamin C and hydriodic acid (HI). In one group, they used a stream of hydrazine vapor in nitrogen to reduce graphene oxide deposited on the surface. In the second group, a drop of vitamin C was dropped on the film, and in the third group, hydroiodic acid was dropped to reduce GO. Raman analysis made on these three samples showed that the number of defects present on the HI reduced samples were comparatively low. Henceforth HI was considered as an efficient reductant to reduce GO over hydrazine and Vitamin C which are relatively strong and weak reducing agents [175].

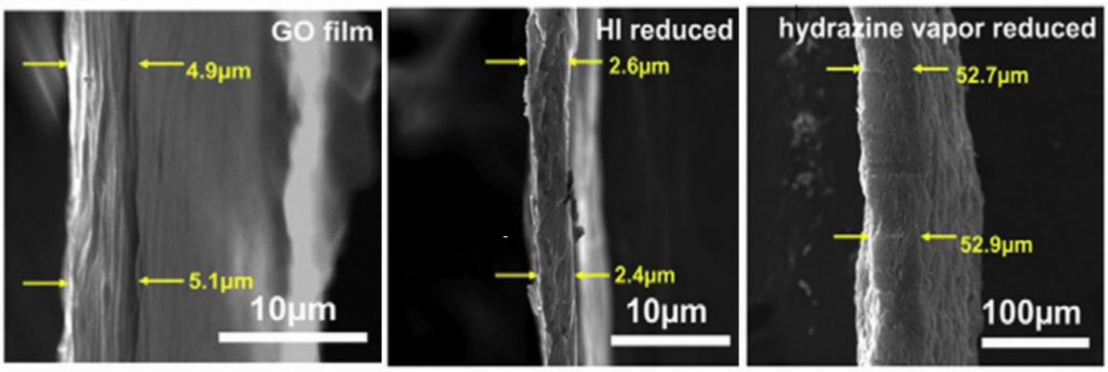

Figure 2.2. Different types of graphene obtained by using different reductants.

Similar reduction studies by Alimard et al. (2012) showed that graphene oxide reduced by hydrazine could not effectively remove the carboxylic groups. Further stabilizing it with ammonia for a higher pH enabled well-dispersed reduced GO colloids in water without any stabilizers. Unless stabilized, the reduced powder immediately agglomerated, attributing to its hydrophobic nature. However, when the reduction was made by sodium borohydride in aqueous media, all the parent oxygen-containing functional groups were removed resulting in an IR inactive solid called graphene [176]. Also, sodium borohydride reduction produces a few impurities in the final product [169] and lower sheet resistance. Besides this, $NaBH_4$ has been employed as a reagent to reduce aldehydes and ketones to alcohols [177]. Similarly, the majority of carboxyl and epoxy groups can be changed to hydroxyl groups in the reduction of GO by $NaBH_4$ [178] . These reports conclude that the most straightforward goal of any reduction process is to produce a graphene-like material similar to pristine graphene obtained from conventional scotch tape method. However, the realization of pristine graphene from chemically derived GO is still a challenge.

Further, these reducing agents, which are capable of converting graphene oxide to graphene, importantly require an understanding of different changes when reduced *in-situ* with the polymers. Majorly, these reductants tend to agglomerate the reduced filler in the matrix material, resulting in weak interfacial bonding and weak mechanical properties. Thus, a careful choice of the reductant is important to for the fabrication of polymer composites. Different researchers have used several names in the literature thus processed reduced graphene oxide, as reduced graphene oxide (RGO), chemically converted graphene (CCG) or graphene (G) on the basis and extent of reduction, We have referred graphene oxide as (GO) and reduced graphene oxide as (CCG).

2.7 Graphene-based polymer composites.

Graphene-based polymer composites have evolved as one of the most significant and interesting research areas in the past few years. Incorporating graphene in polymers shows extravagant properties of the nanocomposites [32, 136, 179, 180]. Such nanocomposites have opened large areas of applications ranging from energy [181], thermal transport [32] to biology [182]. Their superior electrical [183, 184] and mechanical response [185, 186] have heralded graphene as a radical alternative to conventional filler in the fabrication of polymer nanocomposites. For instance, graphene combined with polystyrene [187] display high electrical conductivity and enhanced thermal behavior. Incorporating it in PMMA, significantly improves the mechanical behavior at very low filler loadings [188-191]. Graphene reinforced with ultra-high molecular weight polyethylene results in improved tensile strength and creep resistance [192]. Polyethylene-graphene films have been used to improve the friction and wear properties under the lubrication of normal or saline water [193]. Cai et al. (2009) showed a significant increase in the young’s modulus and hardness value by ~900% and 327% respectively with the incorporation of 4.4 wt. % of graphene oxide nanoplatelets in polyurethane. Their results show that due to the formation of chemical bonding, there is a strong interaction between the graphene sheets and the polyurethane (PU) polymer, allowing effective load transfer [194].

Improved mechanical properties were observed via covalent bonding between the filler and the matrix for increased interfacial stress transfer [195]. Zhen et al. (2010) showed that grafting caprolactum over graphene sheets added to a nylon-6 polymer unprecedentedly doubled the tensile strength of the nanocomposite for a loading of only 0.1 wt% (56 to 123 MPa) [196]. Also, Miller et al. (2010), showed the covalent bonding between GO and epoxy polymer with the help of coupling agent exhibits strength improvement by 30% and young's modulus by 50%, without compromising the resin toughness [35]. In another approach of atom transfer radical polymerization (ATRP), initiators attach covalently via esterification with alcohol present on the filler GO surface. Such studies showed increased mechanical and thermal property improvement in the neat polymer matrices [24, 197]. Some polymers develop a covalent bond between the matrix and the filler without the need for additional grafting. Such behavior has been observed in polymers like epoxy, which on curing with an amine hardener, gets directly incorporated with GO platelets [198], while for polyurethanes, thermally reduced graphene oxide functioned as a chain extender by reacting with the isocyanate groups of the monomer or prepolymer [47, 199]. Variants of typical *in situ* polymerization and solution mixing methods provide useful methods of dispersing graphene in polymer matrices like aqueous suspensions of GO platelets with latex based polymers [200]. Besides this developing aerogel structures with polymers produces nanocomposites with defined morphologies and improved mechanical properties [201].

The polymer chain mobility, chain conformations, degree of chain ordering or crystallinity all can vary significantly with the formation of the graphene/polymer interface. This suggests that understanding the relationship between processing, microstructures and property is key to the fabrication of high performance polymer nanocomposite.

2.8. Graphene-based PVA composites.

As different works investigate a variety of polymers as matrices for nanocomposites, it is very important to determine the nature of the polymer matrix employed, i.e. hydrophobic or hydrophilic. Depending on the nature of the matrix, there would be an interfacial interaction and resultant enhancement in mechanical properties. This is a vital parameter to understand because poor adhesion between the reinforcement and the matrix would result in ineffective load transfer. Since hydrophobic matrix limits their usage due to poor compatibility with the fillers, recent studies are carried out on hydrophilic polymers.

Hydrophilic polymers advance over hydrophobic polymers due to their ease of gelation, thickening or emulsification and minimized interaction problems with the fillers.

Application of hydrophilic polymers include materials like the development of superabsorbent polymer composites, drug delivery systems, pharmaceuticals, humectants, binders, lubricants, and film-formers [202-204]. Examples of aqueous based polymers include polyethylene glycol (PEG) suitable for drug delivery applications, polyvinyl pyrrolidone (PVP) is suitable for pharmaceutical applications as a binder in tablet formulations, adhesives, suspensions in syrups or toxicity reducers in injectable or oral preparations [205]. Simultaneously, hydrophilic polymers bear the capacity to hold a large amount of water, enrolling them to be highly flexible as compared to natural tissues. Structurally, these polymer chains bear hydrophilic groups that reside on the backbone. These groups can be non-ionic, cationic or amphoteric [206]. This allows good interfacial interaction of the polymer with the fillers. Polyacrylic acid (PAA), a biodegradable water soluble polymer used for industrial applications including super adsorbent in disposable nappies, water treatment [207] modified with copolymer makes it suitable for a wide range of medicinal applications safely [208]. Polyacrylamides are another class of synthetic polymers widely employed for drug delivery, microanalysis of proteins, toxin removal, and other biomedical applications [209, 210].

Another group of the hydrophilic polymer is polyvinyl alcohol (PVA). Synthesized by the polymerization of vinyl acetate monomer to polyvinyl acetate (PVAc), it subsequently hydrolyses to get PVA polymer. The extent of hydrolysis and content of acetate groups in the PVA affects the crystallization and solubility of PVA. Furthermore, the solubility of PVA depends on the degree of polymerization (DP), hydrolysis and the solution temperature. Varying these factors, affect the degree of hydrogen bonding in the aqueous solution and the solubility of PVA. Moreover, PVA shows a high degree of swelling in water and bears a rubbery nature. This utilizes PVA for varied applications including lubricant for contact lenses, the lining of artificial hearts, drug delivery applications and biosensors.

Literature studies by Pavia et al. (2004) show that 5 wt% CNT reinforced PVA matrix exhibits higher film strength for the nanocomposite film as compared to pristine PVA films [211]. Wejing et al. (2006) discussed the improvement in the tensile modulus by more than 130% on a 2 wt% nanotube loading [212]. Surawut et al. (2007) made similar studies on electrospun PVA- nanofibre mats with carbon black nanoparticle. The films became more rigid with the addition and increasing the amount of CNTs [213]. Sergio et al. (2015) show that 0.5wt.% CNTs functionalized with PVA polymer by chemical stabilization, result in maximum elastic modulus due to proper alignment of the CNTs in the PVA matrix [212].

Hou et al. (2009) obtained interesting results for enhanced mechanical properties by using few-walled carbon nanotubes (FWNTs) in the PVA matrix. They observed a relative Youngs modulus value (dY/dV_f) of 1648 GPa, with only 0.2 wt% functionalized filler in the PVA matrix [214]. This value is 400 GPa higher than the reported value of (dY/dV_f = 1244 GPa) by Cadek et al. (2004) [215]. They indicate that FWNTs are practically the optimum reinforcing filler for the next generation CNT based composite materials. Another set of studies made by Zhang et al. (2015) showed MWCNTs grafted with PVA through Freidel-Crafts alkylation exhibit tensile strength and modulus of 926 MPa and 59 MPa, respectively. These values were high enough for a filler content of 3 wt.%, an increase of 280.6% and 421% of pure PVA fibers [216]. Wu et al. (2016), studied the subsequent performance of CNTs–PVA nanocomposites via layer-by-layer deposition method. Their results show a remarkable increase in strength from 50 MPa for pristine PVA polymer to 1255 MPa for 63.3 vol% CNTs in the composites [131].

One of the important objectives of the current work is to explore reinforcing behaviour of graphene and its derivative forms in aqueous colloidal processing of polymer matrices [37, 217]. Polyvinyl alcohol (PVA) is a water soluble polymer, made by the hydrolysis of polyvinyl acetate. It contains a large number of OH groups on its surface. This increases the polar nature of the polymer as compared to the discussed polymers discussed so far and is a suitable matrix for the intercalation of the filler. Therefore, PVA was selected as a model system for a polymer matrix for aqueous processing of graphene based polymer nanocomposite fabrication.

PVA is a commodity polymer with excellent film forming, emulsifying and adhesive properties, enhanced with good strength and elongation properties. It has high flexibility as well as oxygen or aroma barrier properties [218]. This makes it applicable in areas such as energy devices [219], medicine [220], pharmaceuticals [221], textile, gas barriers, fiber reinforcement in cement based composites [222] or food packaging material [223]. However, the ductility of the polymer is humidity dependent [224, 225]. The water that acts a plasticizer reduces the tensile strength but increases the elongation and tear strength. This restricts the utilization of graphene-based PVA films for their flexible behavior. Thus, there arises a need to study this polymer with ways to enhance the flexible behavior and develop structures that can bend, twist and can stretch to user needs.

Early reports on PVA-GO systems were made by Liang et al. (2009). They reported 82% increase in tensile strength (49 MPa to 89.6 MPa) and a 57% improvement of Young’s modulus (2.13 GPa to 3.35 GPa) by the addition of only 0.7 wt % graphene oxide [36]. These experimental studies were in agreement with the theoretical simulations by the Halpin-Tsai model for almost single layer exfoliated sheets. Xu et al. (2009) followed this work and reported that Young’s modulus and the tensile yield containing 3 wt.% graphene oxide was 4.8 GPa (128% improvement) and 110 MPa (69% improvement) respectively, [217] against 65 MPa and 2.1 GPa for pristine PVA. Morimune et al. followed the PVA-GO composite fabrication to produce effective improvements in Young modulus at a low wt% of 0.1. Their results showed that at lower wt% of GO, PVA-GO composites exhibit rigid sheet-like structures responsible for the increased elastic modulus values as compared to pristine PVA films [226]. Jiang and Shen (2010) complimented the previous works to reveal the behavior of graphene/PVA composites. They communicated the improvement in tensile strength behavior of the pristine PVA films from 23 to 49.5 MPa, for the nanocomposite film with 3.25% *ex-situ* reduced graphene loading [227].

Yuan reported *ex-situ* reduced filler loading, (2011) with 116% (69 MPa) increase in the tensile strength as compared to neat PVA (32 MPa) by the addition of only 0.8 wt.% graphene. The graphene employed here was partially reduced so as to develop better interlocking of the reduced graphene sheets with the matrix [228]. Hydrogels of *ex-situ* reduced GO in PVA polymer composites were prepared by utilizing a very low content of the filler by Surudzic et al. (2016). Their results displayed the tensile strength of 177 from 114 MPa and Young modulus values of 0.56 to 0.68 GPa respectively. These values suggested improvement of 56 % in tensile strength and 21.4% in Young's modulus for filler content as low as 0.01 wt % GO in a matrix of 10 wt% PVA polymer [229]. Nevertheless, *ex-situ* reduced methods are not preferred because of difficulties in dispersion in aqueous media.

Due to their mechanical property enhancements, *in situ* methodologies are the center of much consideration and applications. Such advancements were reported by Zhao et al. (2010) for *in situ* reduction of graphene oxide sheets in the PVA matrix functionalized by sodium dodecyl benzyl sulphonic acid [37]. Their results report that the functionalised graphene/PVA films had an improved tensile behavior up to 42 MPa from PVA against 17

MPa for pristine PVA film with a loading of only 1.8% graphene. Also, an improvement in the Youngs modulus by 940% (0.10 GPa to 1.04 GPa) was observed with a loading of only 1.8% graphene. Their results concluded that there exists a mechanical percolation limit of 1.8% below which the graphene nanosheets can be well dispersed in the polymer matrix, increasing will affect the mechanical behavior and further loading will cause nanosheet stacking together finally decreasing the efficiency of the mechanical properties.

The *in situ* behavior of the graphene-PVA composites was justified by Wang et al. (2011) for enhanced mechanical and water resistance properties. Their studies revealed that 0.5 wt% of graphene oxide reinforced PVA composite films had an increase up to 34% (23 to 31 MPa) in tensile strength and 34% in elongation at break. On the other hand, the tensile strength and elongation at break improved by 212% (23 to 72 MPa) and 16% for the same loading of *in situ* reduced graphene-based PVA films [230].

Bao et al. reported comparative investigations on PVA-GO and in situ reduced PVA-GO composites with lower filler loadings (2011). The mechanical properties significantly increased as compared to the neat PVA matrix. It was concluded that introducing 0.8 wt% of GO, the tensile modulus increases by 54% (4.8 to 7.4 GPa) and tensile strength by 52% (95 to 144 MPa) in a PVA-GO 0.8% composite system. Subsequent reduction of graphene oxide achieves a maximum increase of 66% (4.8 to 8 GPa) in tensile modulus and 66% increase in tensile strength (95 to 158 MPa) for (PVA-G 0.8%) composites [231]. Their results showed no significant difference in the mechanical properties on the reduction of graphene oxide. Similar results obtained by Bian et al. (2015) showed a 25% increase in the tensile strength increased from 47 to 59 MPa and 900% enhancement in Young's modulus for the composites with a 4 wt% of the GO filler [232]. From these results it is important to note that the state of the filler in the form of graphene oxide or reduced graphene oxide makes a huge difference in the mechanical properties of the composites. Furthermore, such reduction effects are sometimes not as discernible as can be seen from the work of Bao et al.

It is indeed a paradox that needs resolution. GO is expected to form homogenous dispersion is an aqueous polymeric system due to the presence of functional group on its basal plane and edges that can bind with the polymer matrix through hydrogen bonding. However, due to the defective nature of GO, its intrinsic tensile modulus itself is quite low as compared to that of graphene. On the other hand, graphene which has excellent strength and modulus is difficult to be dispersed in an aqueous polymer colloid, thus causing inhomogeneous distribution of the fillers. Moreover, for the lack of functional groups the filler/matrix linkages are also limited, leading to ineffective load transfer.

Therefore it is necessary to increase the amount of functional groups on the surface of graphene sheets to enhance the interfacial interaction. One of the best approach is to develop chemical bonds between the filler and the matrix. Salavagione et al. (2009) first documented [233] covalent functionalization of graphene oxide to PVA polymer via esterification reaction of carboxylic groups followed by a comprehensive study of isolation and characterisation of PVA-functionalised graphene oxide. Besides, they also demonstrated that the esterification reaction depends on the tacticity of the polymer, and the covalent linkages are responsible for remarkably altering the crystallinity and thermal stability of the composites. Their strategies to control the interfacial interactions between the filler and the polymer suggested designing of new high strength nanocomposites.

The behaviour of functionalized graphene polyvinyl alcohol nanocomposites was studied by Liu et al. (2011) where graphene sheets were functionalised non-covalently with aromatic amino acids and prepared reduced graphene oxide through hydrazine hydrate. Though these works were mainly dependent on the water, disperse ability, 23% improvement in tensile strength from 38.4 to 47.2 MPa, and a moderate increase in Young's modulus from 1.48 to 1.56 GPa was achieved by 0.2 wt.% graphene sheets [234]. To understand the fact that functionalization of graphene sheets improve the mechanical behaviour, Cheng et al. (2012) grafted PVA with graphene oxide (PVA-g-GO) films and then filled them in the PVA polymer for strong interfacial adhesion. 1wt % graphene oxide in the PVA-g-GO added to the PVA matrix significantly improved the tensile strength from 22 to 47 MPa and Young modulus from 0.16 to 0.53 GPa. These values represent an increment of almost 113% and 230% respectively. They claimed that the PVA functionalised PVA-graphene films were not only stronger but also tougher [235].

Cano et al. (2012) studied the improvements in the mechanical properties of the graphene oxide based materials by covalent attachments of esterified GO to the polymer chains. The mechanical properties of the esterified GO-PVA composites were obtained by adding the esterified GO to different molecular weights of the PVA polymer. They showed that the modulus and strength are increased by 60% and 400% for PVA polymer of weight 50 and 150 kg/mol about the pure polymer for functionalised-PVA-GO loadings even below 0.3% [236]. This is an important report to look at the section in the mechanical properties data of composites in the context of the molecular weight and other pristine polymer matrix characteristics. Layek et al. (2012) alleviated the in situ approach by utilizing the surface of GO sheets. Graphene oxide contains various oxygen-containing functional groups on their basal planes and edges. This makes it hydrophilic and easily dispersible as individual sheets in polar solvents, subsequently resulting stable suspension to produce graphene/polymer nanocomposites. Their route of modifying graphene oxide in the PVA matrix suggests anchoring the reduced graphene to sulfur (-SO_3H) followed by the incorporation in the PVA matrix. Their results showed the highest increase of strength 48 to 130 MPa (170%), strain at break 187 to 256 (37%) and elastic modulus of 5.5 from 2.9 GPa (90%) increase for a 3 wt% graphene filler over PVA [39]. This suggests that increasing the amount of functional groups on the surface of graphene sheets via chemical bonding enhances the interfacial interaction between the filler and the matrix resulting in enhanced mechanical properties.

The recent developments in the fabrication include works done by Ma et al. (2013). They report that glucose reduced graphene oxide with an aqueous solution of polyvinyl pyrrolidone (PVP) has tensile strength improvement from 105 to 154 MPa and Young modulus increase from 3.3 to 4.3 GPa (30%) for 0.7 wt. % of PVP- stabilized reduced graphene oxide (PVA-rGO) films [38]. The substantial improvements correspond to the functionalization by PVP to the PVA-GO film. Shenbin et al. (2015) reported structural enhancements in tensile strengths. Their results showed that tensile strength and modulus of the 50 wt.% PVA-GO composites were high as 280 MPa and 13.5 GPa. Further modifying the PVA-GO composites with sulfur, the tensile strength, and modulus modified from 50 MPa and 2.3 GPa for the PVA polymer to 252 MPa and 8.5 GPa respectively [237]. Another structure dependent studies were made by Jie Chen et al. (2015), which showed an improved tensile strength from 23 to 88.5 MPa (284%) by crosslinking PVA with 5% of boric acid, on a graphene oxide loading of 0.2 wt.% against the neat PVA- GO composite films [238].

Improvements in the composites are latest reported by Shao et al. (2016). They propose simultaneous reduction and functionalization of graphene oxide using polyethyleneimine (PEI). Such composites exhibited great strength and toughness with a filler content of 0.5 wt.%. The tensile strength and Young’s modulus increased up to 117 MPa (53.9%) and 4.8 GPa (52%) from pure PVA values of 76 MPa and 3.16 GPa respectively [239].

Author & Year	Wt. %	Improvement Elastic Modulus (%)	Improvement Tensile strength (%)	Journal , Ref
		PVA-GO system		
Liang et al, 2009	0.7	57	82	Advanced functional materials [36]
Xu et al, 2009	3	128	69	Carbon [217]
Wang et al, 2011	0.5		34	Polymer international[230]
C.Bao, 2011	0.8	54	52	Material chemistry [231]
S. Morimune, 2011	0.1	76		Conference proceeding [226]
Sunil Rathod, 2014	5	230	67	AIP conference proceeding [320]
Qibo et al, 2015	4	900	25	Polymer science , series A, [232]
Shenbin et al, 2015	50	486	460	RSC Advances [237]
		***Ex situ* reduced PVA- G system**		
Jiang Shen, 2010	3.25	-	115	Journal of applied polymer science [227]
Yuan et al, 2011	0.8		116	Polymer bulletin [228]
Surudiz et al, 2016	1	21.4	56	Journal of industrial and engg. Chemistry [229]
		***In situ* reduced PVA- G system**		
Zhao et al, 2010	1.8	94	150	ACS, applied material interface [235]
Wang et al, 2011	0.5		212	Polymer international, [230]
C.Bao, 2011	0.8	66	66	Material chemistry [231]
		Functionalized PVA- GO/G system		
Salavagione et al, 2009	1			macromolecules [233]
Liu et al, 2011	0.2	5.4	23	Polymer science [234]
HK Cheng et al, 2012	1	113	230	ACS applied material Science, [235]
M. Cano et al, 2012	0.3	400	60	carbon [236]
Layek et al, 2012	3	90	170	carbon [39]
H-Ma et al, 2013	0.7	30	46	Material letters [38]
Shenbin et al, 2015	50	269	404	RSC advances [237]
Jie Chen et al, 2015	0.2		284	[238]
Shao et al, 2016	0.5	52	53.9	Material and design [239]

Table 2.1. Property matrix for PVA based GO/G different systems.

These studies as displayed in table 2.1 present an overview of research endeavors addressing the mechanical properties of PVA graphene nanocomposites. Particular emphasis has been given in these work on the enhancement of tensile strength, Young's modulus, and the methods of reduction employed. These data sets suggest that there are certain key factors that influence the role of graphene nanosheets in the mechanical behavior of the PVA-graphene nanocomposites.

2.9 Strengthening mechanism.

Primarily the strength of a nanocomposite depends on the combined effect of the reinforcing filler, the matrix, and the interface. The interface can be defined as a bounding surface between the matrix and the filler, by taking advantage of which a unique combination of properties can be achieved. This suggests that interfacial interactions significantly influence the properties of polymer nanocomposites. Interfacial interactions are strongly affected by two types of forces, intermolecular and intramolecular. Intramolecular forces of adhesion appear amongst the polymer chains, while intermolecular forces of interaction appear between the polymer chains and the GO sheets. The chemically exfoliated GO sheets bear abundant oxygen-containing functional groups that endow it to attach with hydrophilic PVA. Due to this matrix filler interaction, an interphase forms spontaneously in the composites with properties different from those of the matrix or the filler.

Thermodynamically, the strength of adhesion between GO and the polymer can be characterized by the interaction energy of the filler and the matrix. This means that the interaction occurs at the interphase only when the surface energy of the neat polymer (γ_P) is less than the surface energy of GO filler (γ_{GO}) or the thermodynamic parameter $\chi_S > 0$ [240] ($\gamma_P < \gamma_{GO}$). Results from Chaoying Wan and Biqiong Chen (2012) show preferable interfacial interactions in polystyrene polymer due to the attachment of the aromatic ring in styrene to GO, via non-covalent electrostatic and van der Waals interactions [240, 241]. Similar works done by Hu et al. (2014) studied that graphene oxide derivatives and poly (vinyl chloride) grafted with PMMA nanocomposites. They had an increased storage modulus at 0.2 wt% GO as a result of the facilitated dispersion in the polymer matrix by the polar groups of GO [242]. These results show that along with the dependence on the surface energy parameter, the reinforcement effects further enhance via covalent or non-covalent interactions between the matrix and the fillers. This was accomplished successfully via hydrogen bonding between the polymer hosts and GO filler, respectively.

Xiaoming et al. (2010) showed effective load transfer between chitosan and GO filler due to strong hydrogen bonding and enhanced tensile strength 40 to 89 Mpa, Young modulus 1.32 to 2.7 GPa which are about 122% and 64% increment respectively [243]. Jiang et al. (2010), showed a significant change in the tensile strength to 49 MPa from 23 MPa for a 3.25 wt.% of the graphene filler in the PVA polymer. This significant improvement is attributed to the strong interfacial interaction between PVA and graphene sheets, due to hydrogen bonding [227]. May et al. (2012) produced nanocomposites with two types of graphene inclusion, namely, short and long graphene flakes characterized by typical aspect ratios of ~ 1000 and 2000. Short flakes had mean dimensions of length, width, and thickness as 1.1 µm, 0.5 µm, and 1 nm respectively. Whereas the long flake dispersed in the PVA matrix had the mean dimensions as 2.3µm, 1.3µm, and 1.2nm thickness. They found that short graphene flakes moderately enhanced the strength, in which case the effective Young modulus (dY/dV) was around 170 GPa. In contrast, the large flakes significantly enhanced Young's modulus by 680 GPa (dY/dV), with V as the volume fraction of graphene flakes. Based on their experimental data, they concluded that 0.4 wt% of graphene inclusions with a higher aspect ratio enhanced the mechanical properties of PVA attributed to the geometry, dispersion state and aspect ratio of the inclusions [244].

Mahendran et al. (2016) describe another methodology suggesting that large aspect ratio and molecular level dispersion of GO in the polymer matrix is important for favorable property improvements. They showed that PVA/poly-2-acrylamido-2-methyl-1-propane sulfonic acid (PAMPS)/GO composites enhanced Young's modulus up to 4 times for a 0.5 wt% of the filler content [45]. Another set of studies by Cano et al. (2012) showed that graphene oxide with lateral flake size of about 1 to 7 microns, functionalised with PVA, showed better compatibility and interfacial stress transfer from the polymer to graphene. They reported an increase in Young's modulus and strength of 40% as compared to the pristine polymer only at a weight fraction. of 0.3% [236]. Wang et al. (2016) studied the effect of graphene/glass fiber/ epoxy composites on the mechanical properties with two different lateral dimensions. They used 3 wt% and 5 wt% of graphene sheets with specific surface area of 750 m^2/g and 150 m^2/g embedded in a matrix of epoxy and glass fiber. Results showed 26.3% improvement in the flexural modulus of the composites with the addition of 5 wt% graphene nanosheets with surface area of 150 m^2/g [48].

These studies conclude that a larger aspect ratio of the filler is an important parameter to influence the mechanical property of the composite. However, these properties also depend on studying the role of dispersion and morphology of the filler. Zhao et al. (2010) examined the mechanical enhancements because of filler dispersion, which is a function of the volume fraction (V)/weight fraction (w) of the graphene filler. They discussed that as the graphene loading increases from 0% (corresponding to the neat PVA polymer) to 1.8%, the tensile strength increases monotonically from 17 to 43 MPa. Further increment in the filler loading to 3%, increases the tensile strength but decreases the elongation at break value from 212% for the neat PVA to 98% for the composite. Following their discussion, the non-monotonous character relates to the progression from the homogenous dispersion of graphene inclusion to spatially inhomogeneous dispersion during an increase in the filler content. At a lower filler content, graphene nanosheets are homogeneously dispersed in the matrix, thus provide a linear and fast change in its mechanical character. However, as soon as the filler content exceeds its critical value, small distances between the neighboring graphene sheets forces them to join due to the van der Waals interaction between the sheets (Fig.2.3). This is accompanied by end-to-end interaction, overlapping in the parts or even restack by planes. Because of which the dispersion of PVA-graphene becomes inhomogeneous, and the mechanical properties change [37]. This aspect is imperative to understand the strengthening mechanisms of the polymer composites.

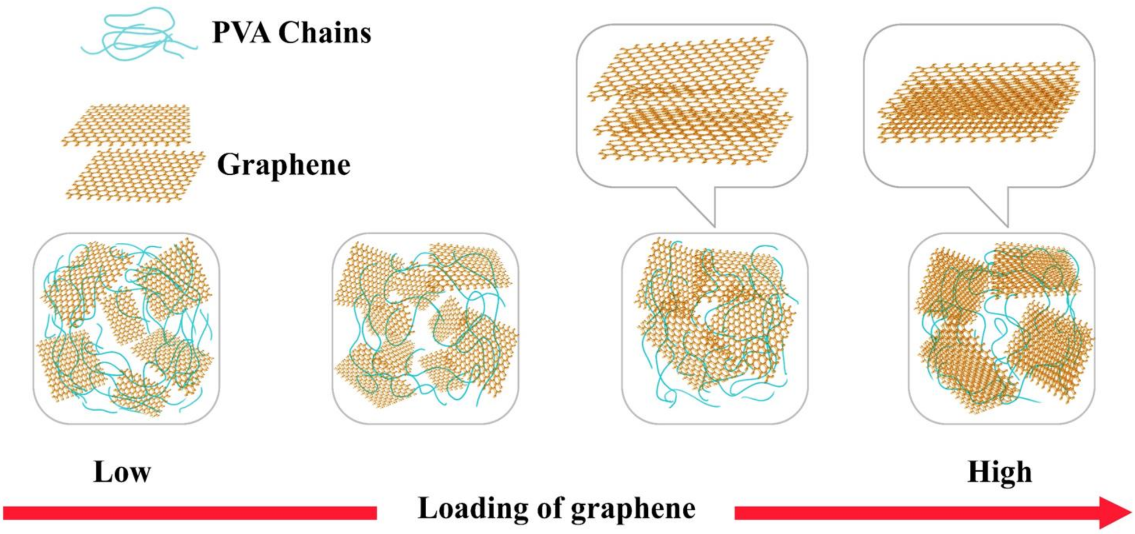

Figure 2.3. Nature of dispersion of graphene filler loading in a polymer matrix.

It is difficult to tell the form of graphene that has been used just from the title of the published literature. Since the word ‘‘*graphene*’’ is often used to describe work containing graphene oxide, thus the careful reading of the original papers is often necessary to determine exactly the type of graphene that was employed. To simplify the text, Bao et al. (2011) reported a comparative work where both kinds of reinforcements GO and graphene were employed to quantify the mechanical properties by the effect of both fillers differently. In particular, they reported that graphene nanosheets were stronger than GO since they had higher aspect ratio than that of GO sheets. However, GO had much more functionalities on its surface than graphene. This suggests that GO fillers are better dispersed and have stronger binding with the polymer matrix. This should indicate that GO-polymer composites should have better mechanical properties, which is not validated always. Okvid (2013) explained this with reasons being the high mechanical characteristics of strength and Young’s modulus of the reinforcing inclusions graphene. Secondly, higher aspect ratio and surface area of graphene as compared to graphene oxide [245]. Although, uniform dispersion following the prevention of agglomeration and strong binding between the matrix and the polymer are important factors determining the strength. Nevertheless, the crucial parameter in determining the mechanical property enhancement lies in the inherent features of high aspect ratio, surface area and young’s modulus of graphene filler [231, 246].

Further review works from Okvid (2013) suggest that graphene inclusions were more effective in enhancement of the mechanical properties of graphene based polymer composites owing to the filler strength and Young modulus. However, parameters of high strength, filler aspect ratio, dispersibility, and bonding can be regulated, controlled or modified to improve the mechanical characteristics of the developed composites [245]. Graphene-based fillers with high aspect ratio feature crumpled morphology of the sheets [247]. This results in irreversible agglomerates, making it difficult to utilize it as a propriety material [43, 248]. Moreover, the propensity of graphene sheets to fold stably–i.e. bending or crumpling to acquire a minimum energy state [138, 249, 250] confines their availability for larger aspect ratio films.

Thus, there arises a requirement to produce almost flat, less wrinkled and long-range order graphene sheets with less crumpling. To achieve these researchers have developed ways to produce almost flat sheets via substrate bonding [251], electrostatic stabilization [252], epoxy bonding [253] or microwave exfoliation [254]. However, the fact remains that these sheets suit well for soft matter physics or electrical property evaluation. Also, for use as filler for flexible property enhancement, the developed graphene sheets lag roll-to-roll production and smooth texture of the produced sheets.

Young et al. (2012) demonstrated that monolayer or bilayer graphene has better load transfer than tri-layer or multi-layer [255]. Without compromising an even dispersion, higher filler loading is easy to achieve with multilayer graphene. Therefore, there is a balance in the design of graphene-polymer nanocomposites between a higher filler loading and decreased load transfer as the number of layers in graphene filler increases. Regarding loading mode, it is interesting to note that the graphene fillers went into compression under tensile loading and vice versa. With this evaluation, they concluded that the interfacial load transfer, mechanical interlocking caused by wrinkled surface and defects in graphene are the main factor in controlling the reinforcement mechanisms.

Reasons for crumpling of the graphene sheets can be attributed to the reducing method employed during chemical reduction. Particularly when graphene oxide is reduced *ex-situ* via hydrazine, it results in extremely agglomerated and crumpled sheets [160]. Moreover, it remains a challenge to reduce with reductant like lithium aluminum hydride (LAH) in a colloidal dispersion. This is due to excess side reactions with solvents commonly used for dispersing graphene oxide (i.e. water) resulting in aggregation. Similarly, alkaline solutions such as NaOH, or KOH [256] produce restacked or aggregated graphene sheets whereas phenols like gallic acid, tannin acid, dopamine, tea polyphenol [257-259] produce weakly reduced graphene oxide sheets. With few functionalities reduced, these *ex-situ* reduced aggregated graphene sheets often result in inferior mechanical properties. Thus to sufficiently utilize graphene for mechanical behavior, dispersion of graphene oxide sheets is done in a matrix via *in situ* reduction technique [260-262]. This proves to be an alternative in producing well-dispersed filler in the matrix and almost flat, less wrinkled sheets to develop polymer nanocomposites.

Another aspect to which the mechanical properties of a semi-crystalline polymer and their composites rely on is on polymer crystallinity and glass transition temperature. Polymers comprise of entangled molecular chains resulting in the formation of crystalline and certain amorphous regions (Fig.2.4). Adding of a nanofiller to a semi-crystalline polymer induces a change in the degree of crystallization, crystallite size, glass transition temperature and their structure, which in turn affects the mechanical strength of the composites. Also, strong hydrogen bonding interactions due to the addition of graphene filler to polymers affect the mobility of the polymer chains, subsequently altering the glass transition T_g of the nanocomposites formed.

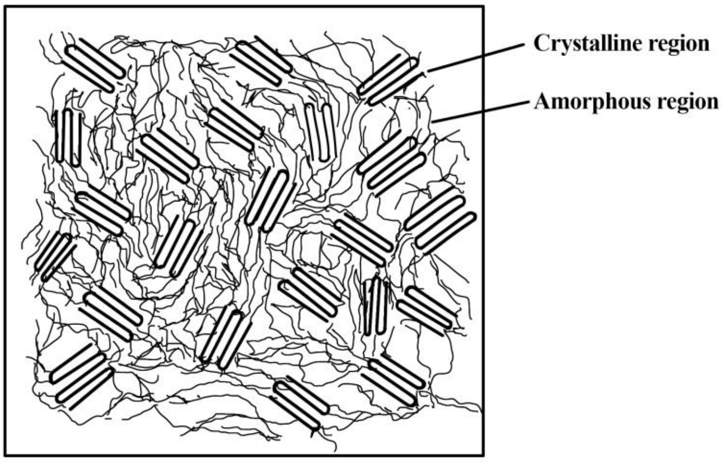

Figure 2.4 Mixed amorphous and crystalline structure of the polymer.

Liu et al. (2005) have reported results for PVA /SWNT composites. They propose that H-bonding interaction may occur between the hydroxyl groups attached to the surface of carbon nanotubes and hydroxyl groups grafted onto PVA backbone. These interactions supposedly affect the mobility of the PVA polymer chains [263]. Similar effects were observed by Jhang et al. (2010) who showed that the constraining of the polymer chains by graphene fillers resulted in increased crystallinity and hence improved mechanical properties [227]. In one study, Salavagione et al. (2011) studied the organic group modified PVA-rGO structure for crystallinity behavior. They reported that modifying the PVA surface in the presence of hexyl carbodiimide (DCC) and 4-dimethylaminopyridine (DMAP) catalyst, followed by hydrazine reduction, elevates the glass transition temperature of the hybrid PVA-rGO composites. It is due to the restricted segmental mobility of the PVA chains attached to bulky organic molecules. The crystallinity is transformed, and the melting temperature increases by 100℃ [264].

Interestingly, there are opposing views in the literature with regards to the effect of graphene based fillers on the crystallinity of the composites. Pujari et al. (2015) discussed a reduction in crystallinity with the GO loading primarily due to the restricted dynamic motion of the bonded PVA molecules. They further suggested that the strong interaction between PVA and the GO reduced the original hydrogen bonding between the PVA molecules, resulting in a lower free volume fraction of the polymer chains. The net effect of these variations was a reduction in Young's modulus and T_g properties. Comparison with other literature they reveal that crystallinity is the only deterministic parameter for the evolution of mechanical properties [265].

However, certain records from Mahendran et al. (2016) show no significant change in the crystallinity on reinforcing graphene in PVA matrix. They suggest that the increase in Young's modulus occurs by increasing the interfacial interaction between the GO and the polymer matrix, the large aspect ratio of the filler and molecular level dispersion of the filler in the matrix as favorable effects for the enhanced mechanical properties [45, 266].

Nevertheless, most of the published literature suggest a positive change in crystallinity of the composite upon filler addition. Besides this Jyongsi et al. (2012) suggested that graphene plays an important role in increasing the crystallinity and hence mechanical properties by acting as an effective nucleating agent during the crystallization process, accelerating the degree and rate of crystallinity. They further suggested that graphene acts at nucleating agent only at low concentrations of filler contest at low concentrations (<1wt%) and above that (>1wt%), it enhances mechanical properties by acting as nanofiller [267]. These studies suggest that depending on the polymer and the incorporation of graphene-based filler, shows an increase, decrease or no change in the degree of crystallinity of a semicrystalline polymer and corresponding mechanical properties.

2.10 Mechanical models for nanocomposite properties.

Different experimental data sets show that interfacial interaction between filler and matrix influences the properties of graphene based polymer composites. Depending on the size (area) of the interface and the strength of interaction, the adhesion between the polymer and the filler leads to effective load transfer properties. However, the extent of this interaction is influenced by various other parameters including size of the interface, filler anisotropy and orientation, and aggregation/ homogeniety of the fillers. In addition, there also is a chemical aspect of these interfaces that could define the degree of strengthening, for example, low energy dispersive forces, or high energy covalent type interactions. Nevertheless, the strength of adhesion or interfacial interaction is difficult to be determined experimentally. There have been a few experiments to quantify interfacial interactions mainly employing Raman spectroscopy (by measuring the shift of D and G bands of the Raman spectra), and by AFM-based peel strength measurements. An alternative approach is to introduce an interfacial interaction term to the existing micromechanical models, thereby acquiring a first-hand knowledge of such interactions [268].

For the prediction of the elastic modulus of composites, Halpin-Tsai model is one of the most widely accepted and used expression [269]. It relates the composite moduli to the volume fraction of the filler phase, the relative moduli of the constituents and the reinforcement geometry (e.g. the aspect ratio) in a straightforward method. It relates the longitudinal and transverse moduli of a composite as:-

$$\frac{E_C}{E_m} = \frac{1 + \eta\xi\varphi_g}{1 - \eta\varphi_g} \dots\dots\dots\dots\dots\dots\dots\dots\dots\dots\dots\dots\dots\dots\dots\dots\dots\dots\dots (i)$$

$$\eta = \frac{\left(\frac{E_g}{E_m}\right) - 1}{\left(\frac{E_g}{E_m}\right) + \xi} \dots\dots\dots\dots\dots\dots\dots\dots\dots\dots\dots\dots\dots\dots\dots\dots\dots\dots\dots (ii)$$

Where E_c E_m and E_g are Young's moduli of the composite, polymer matrix and the filler respectively. This equation is based on two assumptions: First, the particle and the matrix are linearly elastic, isotropic and bonded to each other. Secondly, the intramolecular interactions (interactions between the filler) are not considered. This is purely a mechanical model which is suitable for composites, where the interfacial strengthening/aspects are neglected [36, 270]. Properties of composites with similar filler/matrix microstructures, and with different degrees of interfacial interaction, cannot be reconciled with Halpin-Tsai model.

Interface dependent studies were validated by a set of equations modeled by Pukanzsky et al. (1990) who applied a parameter B, which is a measure of the strength of interaction to the existing interface created by the polymer and the filler. He showed that the size of the interface and the strength of interaction significantly influence the nanocomposite properties [271]. His model describes the composition dependence of tensile yield stress or tensile strength of particulate filled polymer composites. The expression for yield stress is defined as:-

$$\sigma_y = \sigma_{y_0} \frac{1 - \varphi_f}{1 + 2.5\varphi_f} \exp(B\sigma_y\ \varphi_f) \dots\dots\dots\dots\dots\dots\dots\dots\dots\dots\dots (iii)$$

Where σ_y and σ_{yo} corresponds to the yield stresses of the composite, and that of the polymer matrix respectively, φ_f the volume fraction of the filler in the composite and B $_{\sigma y}$ the parameter characterizing interaction. The term $\frac{1-\varphi_f}{1+2.5\varphi_f}$ takes into account the decrease of the effective load bearing cross section owing to the introduction of the filler into the polymer matrix. Since the effect of various filler type is different on the tensile properties, Pukanszky classified the fillers as reactive, non-reactive or inactive. He suggested that treating the fillers with certain functionalities result in producing reactive fillers which produce higher interfacial interaction, corresponding to increase in the yield stress and strength of the composite. In another case, if the surface of the filler is not modified with any functionalities, the filler results in a non-reactive interfacial interaction with the polymer. In this case, the mechanical properties of the composites decrease as compared to those of the composites with reactive interfaces. Lastly, for an inactive filler, the mechanical properties remain unchanged and unaffected owing to no interaction at the filler/matrix interface. Another advantage of the model is that a proper evaluation of the experimental results can reveal structural irregularities in the composite (void formation, dewetting, and aggregation) and the sensitivity of the polymer matrix to these irregularities. However, the model had certain limitations. This equation was not valid where the matrix continuity was disrupted. Such composites were characterized by a high defect concentration and brittle fracture. Secondly, this model does not explicitly take into account the effect of filler anisotropy, unlike the Halpen-Tsai model which has an expression for random as well as aligned fillers in a composite [272, 273].

Comparing different models with experimental data, we surmise that the mechanical strength of a nanocomposite majorly depends on the native properties of the filler. Bearing the fact that interphase plays a major role in the mechanical properties owing to a large interface contact. Some results have shown mechanical property improvements on a lower filler content too. Regardless, the discrepancy between these results and theory highlights that there is a need to develop further understanding of the relative contributions of the native filler properties and the change in the polymer matrix regarding the reinforcement in the composite systems.

2.11 Scope and objective of the work.

Despite the immensely successful application of graphene and graphene derivatives as fillers; there still exists many scopes to understand the fundamentals of filler-matrix interface, the reasons for strength and toughness improvement, and the mechanism of load transfer. Moreover, as discussed earlier, the nanocomposites perhaps cannot be appropriately modeled based simply on the micromechanical methods involving the properties and geometry of the matrix and the filler [274-276]. The importance of interface, as has been pointed out in a graphene/PMMA system, cannot be overlooked. Estimation of the interfacial shear stresses agreed with van der Waals type interactions between the matrix and filler [277], suggesting that weak dispersive forces also mediated the interaction between the matrix and graphene platelets. The weak dispersive forces at the interfaces indicate that they can be tailored by esterification and/or amidation to impart covalent or other stronger type of interactions thereby increasing the interfacial shear stresses.

Due to the complex interactions between the polymer and graphene attached with functional groups, the load transfer mechanism can be suitably enhanced. Another interesting and important aspect is the morphology and microstructure of the nanocomposites. The homogeneity of filler dispersion, its type, coupled with the chemical interactions can influence interface controlled properties, such as load transfer, crack propagation, and electronic transport. Unfortunately, literature on the morphology and microstructures of graphene/polymer composites exist only on a few systems. Therefore, there is a need to address the said characteristics in a parametric evaluation. Furthermore, there is a limited agreement on the glass transition behavior and polymer crystallinity of the composites upon graphene (oxide) reinforcements, with often contradicting reports in the literature. In turn, some of these behaviors also need to be reconciled along with other observations from the microstructures and morphology finally leading to property enhancements.

With the above said objectives in mind, the present work is carried out with large natural graphite crystal derived graphene oxide and its functionalized forms as the fillers and polyvinyl alcohol as the matrix. PVA is selected as much for its technological importance as a model system for aqueous processable polymers. The filler content has been purposefully chosen in the low to moderate range of (0.4 to 1 wt%), to observe the transition of various properties.These mass fractions correspond to even further lower range of volume fraction of the fillers in the composites. The effect of a few amines on the aqueous colloidal stability of graphene oxide, dispersing them in the polymer system and the fabrication of the composites have been studied. Physico-chemical, structural, and morphological characterization techniques have been applied to understand the features. The composite films have been evaluated through uniaxial tensile deformation mode and the results have been discussed in the overall context of the physicochemical properties of the composites.

CHAPTER 3

Materials and methods.

This part of the thesis embodies information on the various synthesis, sample fabrication methods, array of analytical techniques used as well as the property evaluation procedures.

3.1 Synthesis of graphene oxide.

Graphene oxide synthesis was carried out by the modified Hummers method with large crystal sized natural graphite as the precursor [278]. In a typical experiment, 2 g of natural graphite flakes were mixed with 46 ml of concentrated H_2SO_4 (Merck, India) in a three-necked round bottom flask kept in an ice bath. The temperature of the ice bath was well controlled and not allowed to rise above 10 °C. This cooled mixture was stirred for 30 minutes following which 6 g of the oxidant, $KMnO_4$ (Merck, India) was gradually added to it. This mixture was further allowed to stir for 30 minutes. Subsequently, the ice bath was removed, and the mixture was heated to bring the temperature up to 35 °C and was kept at this temperature for the next 1 hour with vigorous stirring. Subsequently, a large amount of deionized (DI) water (92 ml) was added to the mixture which increased the reaction temperature to around 98 °C. Controlled addition of water is a major step here to prevent an explosion of the reactants. The mixture was further stirred for about an hour, with the temperature of the reaction maintained at 98 °C, following which additional DI water (280 ml) was added to the mixture. Then the reaction was terminated by adding 50 ml of 30% H_2O_2 (Merck, India) to oxidize the unreacted graphite, which turned the slurry bright yellow in color. Thus obtained GO suspension was washed with 1:10 HCl solution (500 ml) to remove the metal ions. The paste collected from the filter paper was dried at 60 °C. The agglomerated powder was re-dispersed in deionized water and washed rigorously 5-7 times with more deionized water until the pH was nearly 7. The paste collected on the filter paper was dispersed into water by ultrasonication, and centrifuged for 30 minutes at 4000 rpm to remove any unexfoliated GO. The GO platelets were obtained by drying the filtrate at 60 °C in air. The process of making GO is depicted in Fig.3.1.

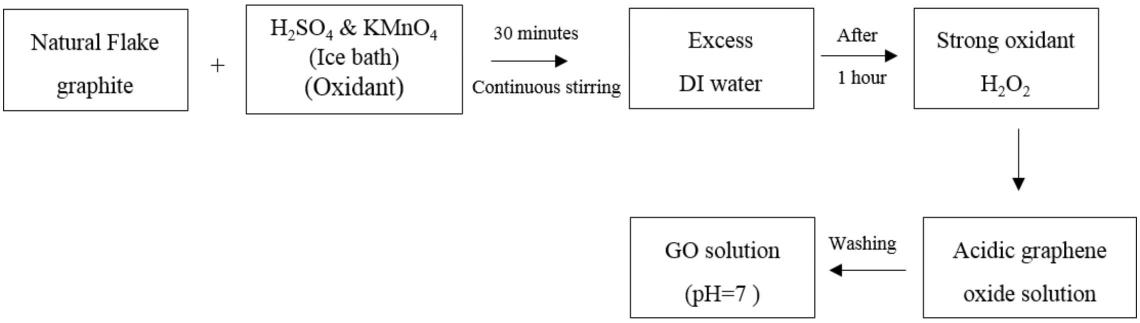

Figure 3.1. The method of preparation of graphene oxide by modified Hummers method.

3.2 Reduction of graphene oxide.

The prepared GO powder was dispersed in the aqueous media and reduced with different reductants to obtain stable colloids of chemically converted graphene oxide (CCG), which was subsequently dried to obtain the CCG powders.

3.2.1 Reduction with hydrazine.

20 mg of graphene oxide flakes were sonicated in 20 ml distilled water to make a deep brown colored colloid (Fig.3.2). The colloid was added to a round bottom flask and stirred at 80 °C under reflux. Subsequently, 1 ml of 80% hydrazine hydrate (Merck, India) solution was added to the flask and refluxed for 24 hrs. The color of the solution changed from deep brown to deep black indicating the reduction of graphene oxide to graphene. Chemically converted graphene with hydrazine (CCG_H) powder was subsequently obtained by washing the reduced GO colloid solution with water and drying it in an oven at 80°C. To eliminate the effect of refluxing on the GO colloid (without any reductant), the light brown colored GO colloid was refluxed at 80°C for 24 hours, which resulted in no change in the color of the batch. This confirmed the effect of hydrazine on the color change of GO colloid.

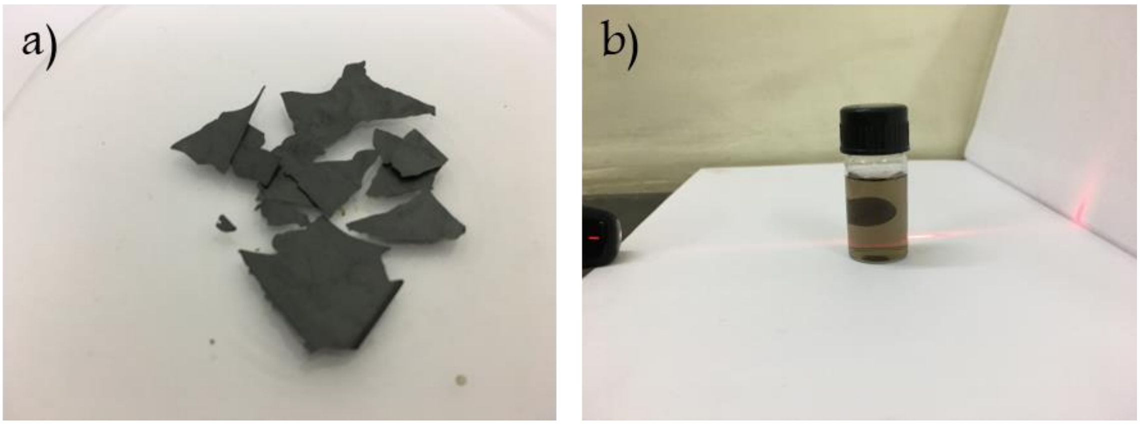

Figure 3.2. (a) Digital images of GO flakes prepared by modified Hummer's method, (b) Colloidal dispersion of GO in water; the Tyndal effect of the path of the light beam can be observed within the GO colloid in the vial.

3.2.2 Reduction with triethanolamine (TEOA).

20 mg of graphene oxide (GO) powder were sonicated in 20 ml DI water to obtain a uniform GO colloid (1% w/v). The colloidal solution was transferred to a round bottom flask and refluxed in an oil bath at 80°C. 0.5 ml of TEOA (Loba Chemie) was added to the flask and

stirred for 24 hours resulting in a color change of the solution from brown to completely black. The obtained solution was dried at 80^{o} C in an oven to obtain a glassy gray colored powdered (CCG_{TO}) and was used for further characterizations. In order to confirm the successful reduction of GO by TEOA, this system was optimized by varying the quantity and time of reduction process.

3.2.3 Reduction with triethylamine (TEA).

Similar reduction procedure as TEOA was followed with (triethylamine) TEA. 20 mg of GO powder was sonicated in 20 ml water to obtain uniform GO colloidal solution. The colloidal solution was transferred to a round bottom flask and refluxed at 80°C. The color of the solution remained brown until 0.5 ml of TEA (Loba Chemie) was added to the above solution. The TEA added sample was refluxed in an oil bath for 24 hours at 80 ^{o}C to observe the color change and ensure complete reduction of the GO colloid. The reduced (CCG_{T}) sample was washed with water and dried in oven overnight resulting in a blackish gray colored graphene powder. The obtained powder was utilized for further characterizations.

3.3 Fabrication of graphene oxide reinforced PVA nanocomposites.

Various sets of PVA composites with a filler loading of 0.4 wt. %, 0.8 wt. % and 1.0 wt. % of GO or treated GO were fabricated by a conventional solvent casting method (Fig.3.3). The first was a series of PVA-graphene oxide (PGO) composite films with varying weight % of GO without any treatment of the fillers. Subsequently, nanocomposite films of PVA with various reductants, including hydrazine, TEOA, TEA, and a combination of TEA and hydrazine. A typical process of fabricating the composites is depicted in Fig.3.3.

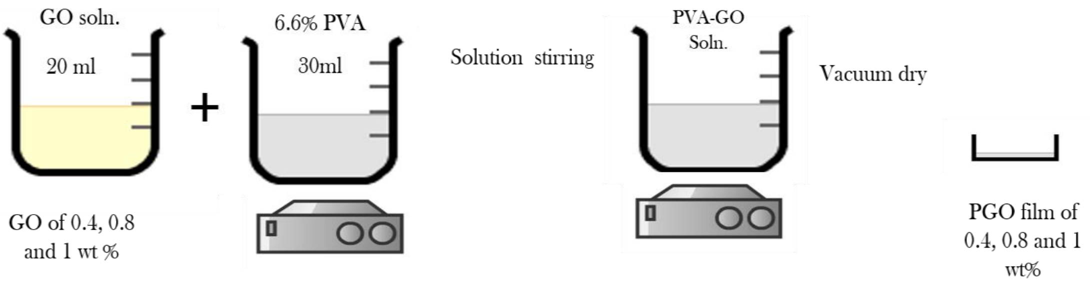

Figure 3.3 Method of fabrication of PVA-GO films.

3.3.1 Fabrication of PVA-GO films.

2g of PVA was dissolved in 30 ml deionized water at 95°C under reflux to form an aqueous solution. Separate solutions of GO with varying wt% (0.4 to 1%) powders were sonicated in 20 ml DI water to form a yellowish-brown colloidal solution. The obtained GO solutions were mixed with PVA under vigorous stirring for about 2 hours at 60 °C to form PVA-GO (50 ml) colloids. The PVA colloid is comparatively thicker than the GO colloid, which makes the mixing of the two components difficult and does not mix instantly. Therefore, vigorous stirring of the aqueous GO mixed PVA colloid is required to ensure complete and uniform mixing. Finally, 10 ml of the as prepared homogeneous PVA-GO colloids with different concentrations were poured onto glass petri dishes and kept in a vacuum at 40 °C for 48 hours to form GO reinforced PVA composite films. The films were then peeled off the substrate for further characterizations. The prepared films typically had 70-80μ thickness. Hereafter, these composites have been termed as PGO series of films.

3.3.2 Fabrication of hydrazine reduced PVA-GO (PGH) series.

The fabrication of PVA nanocomposites films with GO and hydrazine as the reductant was carried out by adding 1 ml of hydrazine hydrate (80% wt) to the PVA-GO blends (50 ml). This blend was then refluxed for 24 hours at a temperature of 80 °C, during which the brown polymer blend gradually turned black. 10 ml of the obtained blends were individually cast onto glass petri dishes and dried under vacuum at 40 °C until weight equilibrium. The cast and dried films were peeled off the petri dish for further characterization. Sets of thick film with 0.4, 0.8 and 1.0 wt. % of graphene oxide (to PVA) were prepared by this method. These films have been named as PGT series of composites.

3.3.3 Fabrication of TEOA reduced PVA-GO (PGTO) series.

50 μl TEOA was added to the PVA-GO blend and refluxed for 24 hours to obtain a uniform TEOA reduced PVA-GO colloid. The black colored colloid was similarly cast onto glass petridish and dried at 40°C until weight equilibrium. The films were peeled off the glass and used for further characterizations. These films were termed as PGTO series.

3.3.4 Fabrication of TEA reduced PVA-GO (PGT) series.

Similarily, 50ml of the PVA-GO blend along with 0.5 ml of TEA was refluxed for 24 hours to obtain a uniform TEA reduced PVA-GO colloid. Castings of the blend were made by dropping 10 ml of the colloid on glass petridish and kept for drying at 40°C until weight equilibrium. The cast films were peeled off the petri dish for further characterization.These films have been named as PGT series of composites.

Critical parameters considered for the drying of the colloid were the drying temperature and the type of substrate used for casting the solution. It was observed that when the colloids were dried in an oven at temperatures of 60 ^{O}C or 80 ^{O}C, it resulted in shrinking, cracking, and wrinkling of the films in all types of composites. Besides, when the colloids were cast onto a plastic petri dish, the drying was not so uniform.It had occasional pinholes in the films, and the film was highly wrinkled and delaminated from the sides of the petri dish. Representative images of the defective composites are given in Fig.3.4.

Figure 3.4. Digital images of improperly dried defective composites.

However, drying the colloids at nominal temperatures of 40 ^{O}C in an oven for 24 hours, eliminated the physical issues of the films related to shrinking, cracking and wrinkling. Utilizing glass petri dishes for drying the films, produced uniformly dried films without delamination or any other defect (Fig.3.5).

This suggests that the drying temperature and the type of substrates utilized for the drying of the colloids are important parameters to consider in the fabrication of the films.

Figure 3.5 Digital images of properly dried defect free GO-based PVA composites.

3.4 Material characterization and property evaluation.

Ultraviolet and visible spectroscopy (UV) of the colloids was done using a UV-Vis spectrophotometer (Perkin Elmer USA). All the samples were well dispersed in the aqueous medium before analysis. Zeta potential measurements of the GO colloids was made by Zeta sizer (Malvern Nano Zeta sizer, UK). The study was made at room temperature using water as the reference.

Crystallography and phase assemblage of the materials were evaluated by X-Ray diffraction (XRD). The diffractometer (Rigaku, Ultima IV, Japan) had a Cu-Kα radiation (λ= 1.5416Å) fitted with a Ni filter. The scanning range was 5 to 50° 2Ө with a scan speed of 20°/min and 40 KV and 25A conditions.The said conditions had enough signal intensity for qualitative evaluation.

Thermal behavior of the samples was studied with a (Mettler Toledo, DSC-822e) differential scanning calorimeter (DSC). The composite samples were sliced into small pieces, placed in an aluminum pan holder and scanned in a temperature range of 25° C to 300 °C at a heating rate of 10℃/min. The % crystallinity was calculated using the equation:-

$$\chi_c = \frac{\Delta H_f}{\Delta H_f^{\circ}} * 100 \ldots\ldots\ldots\ldots\ldots\ldots\ldots\ldots\ldots\ldots\ldots\ldots . (i)$$

Where χ_c is the percent crystallinity, ΔH_f is the enthalpy of fusion at the melting point and ΔH_f° is the enthalpy of fusion of the totally crystalline polymer measured at equilibrium melting point. The term ΔH_f° is a reference value and represents the heat of melting if the polymer were 100% crystalline. The established reference value of enthalpy used for PVA polymer was taken as 138.6 Jg^{-1} [279]. The % crystallinity was calculated by calculating the area under the thermogram in the melting region normalized by the standard value of 138.6 J g^{-1} using the software provided with the DSC instrument.

Fourier transform infrared spectroscopy (FTIR) was recorded on an Alpha-E (Bruker, Germany) instrument with a scan resolution of 2 cm^{-1} and a wavenumber range from 4000 to 500 cm^{-1}. Spectra of GO and the fabricated films were collected using the attenuated total reflectance (ATR) technique with air as the background for the sample spectra.

Raman spectroscopy was carried out in the GO powders, and the various types of GO reinforced PVA composites with a spectrometer (Horiba, Jobin Yvon), with 756 nm Laser over the range of 1000 cm^{-1} to 2000 cm^{-1}.The objective was to observe the positions and associated shifts of the G and D bands from the carbon structure.

Positron annihilation lifetime spectroscopy (PALS) experiments were carried out to understand the distribution of nanovoids in the composites. The sample films were cut into the required number of pieces of approximate dimensions 10 mm × 10 mm and stacked together in equal pieces on both sides of the positron source. The positron source, in this case, is a radioactive ^{22}Na isotope (in the form of NaCl taken within a thin ~ 2 mg cm^{-2} Ni foil envelope), which emits positrons with energies up to a maximum of 545 keV. These positrons, having their end point energies, will penetrate into a material of density ρ (gm cm^{-3}) up to a distance (or depth) $1.86/\rho$ millimeters. Therefore the sample should cover the positron source on both sides over a thickness larger than these penetration depths so that all of the positrons are strictly captured and annihilated within the sample material itself. In this case, the density of PVA being 1.25 gm cm^{-3}, the minimum thickness required is $1.86/1.25 \approx 1.5$ mm. Multiple layers of the fabricated composites were placed on top of each other to get a stack measuring 1. 5 mm thickness (typically 10-15 foils).

The mechanical properties of the fabricated films were tested on a universal testing machine (Tinius Olsen, UK) at room temperature. A load cell of 1KN was used with a tensile loading rate of 5 mm min^{-1} according to D638 ASTM standards [280]. All of the samples were cut with a razor blade into dog bone shapes of 5 mm width and 20 mm gage length, and fixed into regular cardboard windows of (30 mm x 30 mm dimension) to hold the films in the tensile tester teeth and to ensure uniform stretching. Five samples were tested for each film type, and their mean value and standard deviation were recorded. From the stress-strain curves, the elastic modulus (E), yield strength (σ_y), tensile strength (σ) values were calculated.

The tensile properties were measured using the standard formulas for stress and strain by converting the obtained force and extension data as:-

$$\varepsilon = \frac{\delta l}{L} \ldots\ldots\ldots\ldots\ldots\ldots\ldots\ldots\ldots\ldots (ii)$$

Where δl is the extension of the gage length of the film, L is the original length of the film and ε is the strain. The value of the ε at the point of failure of the film is taken as the strain at failure (ε_f). The strength was calculated by normalizing the load with the cross section of the film as per the following formula :-

$$\sigma = \frac{F}{A} \ldots\ldots\ldots\ldots\ldots\ldots\ldots\ldots\ldots\ldots\ldots\ldots. (iii)$$

The thickness of the films measured by SEM was used to calculate the area of cross section (A) and subsequently the strength.

Elastic modulus was calculated from the linear position of the stress-strain diagram from the slope. The toughness of the films was calculated by finding out the area under the stress-strain diagram. At least five samples of each type of the films were tested, and the mechanical property values were averaged.

Morphological investigation of GO fillers and the fractured surfaces of the samples were investigated by field-emission scanning electron microscopy (FESEM, FEI Nova, NanoSEM, Eindhoven, NL) in secondary electron mode. The powdered samples of (GO or CCG) were drop cast on the conductive carbon tape and directly mounted on the stub to view the morphology. The composite films, on the other hand, were sheared or fractured and stuck between a specially designed aluminum mount.

Macroscopic wrinkling and distribution of GO platelets in the polymer/GO nanocomposites were characterized by transmission electron microscope (TEM) (Technai G^2, FEI, Eindhoven, NL). The GO and the composites were prepared by depositing diluted dispersions of the colloid on carbon-coated grids and dried at ambient temperature in vacuum before analysis. The microscope was operated at 300 kV accelerating voltage with a field emission gun. Furthermore, some samples were analyzed by high angle annular dark field (HAADF) technique using the scanning transmission electron microscopy (STEM) mode.

CHAPTER 4

Aqueous colloidal stability of graphene oxide and reduced graphene oxide.

This chapter outlines the stability of aqueous colloids of graphene oxide and chemically converted graphene oxide (CCG) with hydrazine, triethanolamine, and triethylamine as reductants. Structure, morphology, and zeta potential measurements have been performed to infer the results.

4.1 Characterization of Graphene oxide (GO).

The X-ray diffractogram of graphite flakes exhibited characteristic features of flaky graphite such as a sharp diffraction peak at 26.6°, corresponding to the (002) reflections (Fig.4.1). This indicated the interlayer spacing of 0.334 nm between the single graphene sheets in the graphite crystal. In the diffractogram of the graphene oxide powders, the (002) peak at 26° was completely absent, indicating destruction of the parent interlayer spacing of the graphite structure. However, a peak at 2θ of 10.9° appeared with considerably reduced intensity. This indicates two important aspects with regards to the structure of graphene oxide. First, the interlayer spacing between the carbon layers has increased substantially (appearance of the peak at lower 2θ). And, secondly, the crystal size has considerably reduced (not the lateral size, but the stack thickness) as indicated by the reduced peak intensity. The peak in the GO material corresponds to an interlayer distance of 0.78 nm.

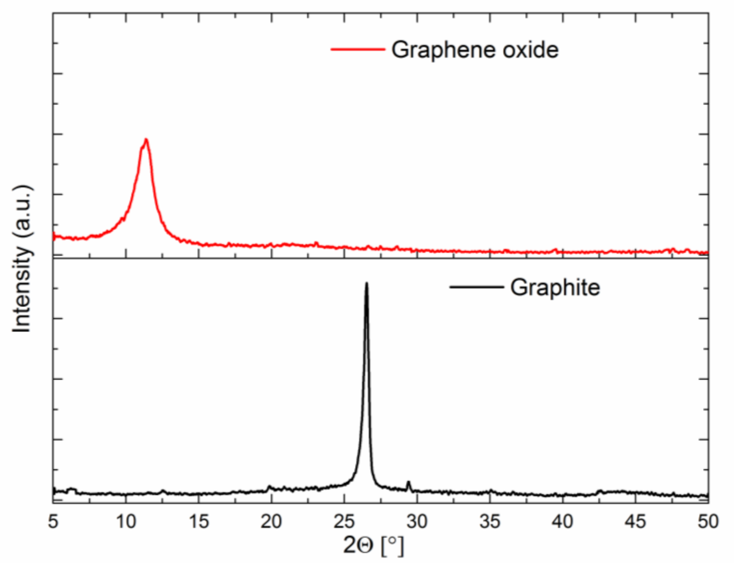

Figure 4.1. XRD diffractograms of graphite and graphene oxide.

Such a change in the interlayer spacing is attributed to the formation of oxygen-containing functional groups in graphite sheets during the strong acid treatment [281]. These oxygen-containing functional groups intercalate the spaces between graphene oxide sheets, resulting in the appearance of the sp^3 character to the GO sheets, which is different from the purely sp^2 character of graphite [147].

Morphological characteristics of graphite and graphene oxide were observed by scanning electron microscopy (SEM) methods (Fig.4.2). A drop of the as-prepared GO colloid (at pH ~7) was casted on metallic stubs, and the images were recorded in secondary electron mode. Representative images of natural graphite show a highly agglomerated layered structure (Fig.4.2 (a)). However, the graphene oxide sheets were observed as a semi-transparent wrinkled two-dimensional sheet of carbon atoms (Fig.4.2 (b)). To observe the features of GO with better clarity, SEM imaging with a field electron source was carried out. Even on a much finer scale also it was found that the GO sheets exhibited clear wrinkling and folding of the carbon sheets. Due to the highly energetic and unstable reaction condition and high surface tension of the solvent during the exfoliation procedures, carbon layers with the wide lateral area, but much reduced thickness become unstable in the layered structure [282]. This leads to local wrinkling of the graphene sheets (Fig.4.3.(a)). These features, as explained in later chapters, have a profound influence on the usage of GO as fillers. High-resolution imaging of these wrinkles can additionally enable us to make approximations on the thickness of the few layered graphene oxide, as the smallest fold would typically indicate (twice the size) of the layer thickness (Fig.4.3 (b)).

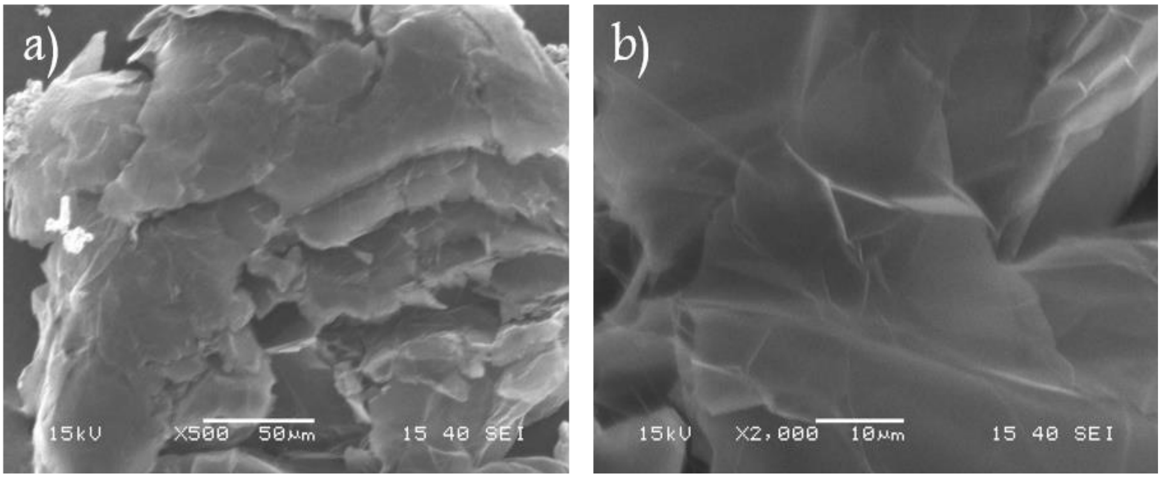

Figure 4.2. Scanning electron micrographs of (a) natural graphite crystals (b) graphene oxide.

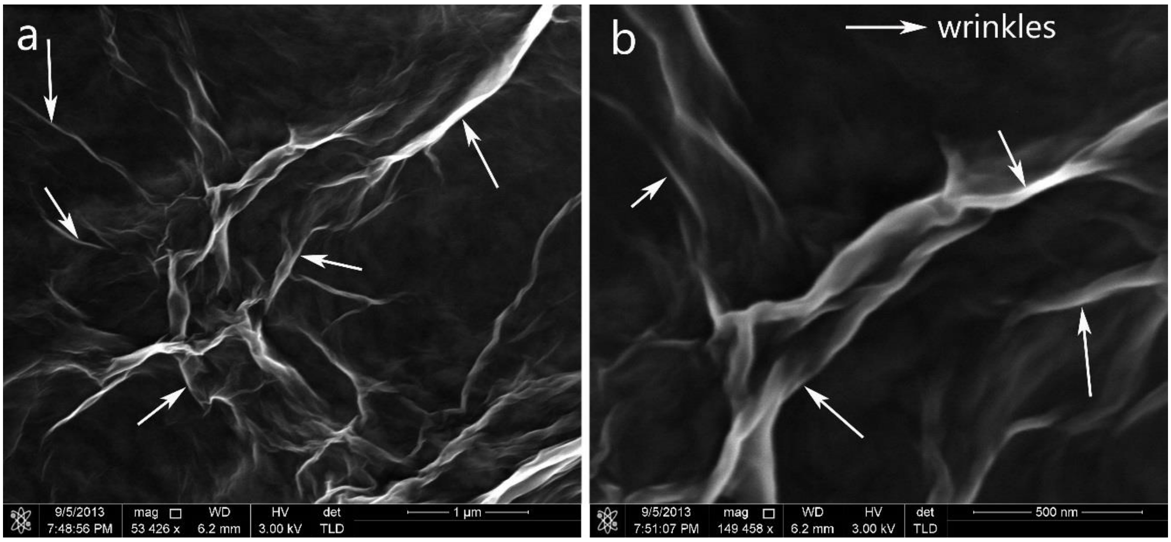

Figure 4.3. Field emission scanning electron micrographs of graphene oxide; (a).multiple folding and wrinkling of the graphene oxide foils, (b) the wrinkles at a higher magnification.

A highly electron transparent two-dimensional sheet of graphene oxide was observed by field emission transmission electron microscopy. High magnification image (Fig. 4.4(a)) enables us to see the fine contrast difference (electron transparency) between the bare grid and the areas covered with GO layers. The fine wrinkles on the plane (marked 1), folds on the plane (marked 2) and folds at the GO edge (marked 3) can be clearly observed. Corrugations on the surface are attributed to the various defects and functional groups which emerge during the oxidation process. High surface tension amongst the GO nanosheets tends to agglomerate the sheets with each other. However, the imaging reveals well dispersion of GO sheets in water. Selected area electron diffraction (SAED) pattern for GO was recorded in the areas of the layered GO. A clear set of diffraction spots with hexagonal symmetry was characteristic of a crystalline order in the basal plane of graphene oxide. This observation is in contrast to some of the early reports where it was claimed that graphene oxide produced from Hummers method is amorphous [260, 283]. However, completely crystalline, as well as nanostructured graphene oxide, was synthesized in this case. It also indicates that the number of layers in the GO material is negligible (possibly less than 5) due to the lack of a diffraction pattern (spot) with regards to the interlayer spacing of 0.778 nm as observed from XRD. An additional possibility is that during the ultrasonication of GO colloids, the graphene layers in the GO structure may also break down leading to the formation of GO with only one or two layers [284].

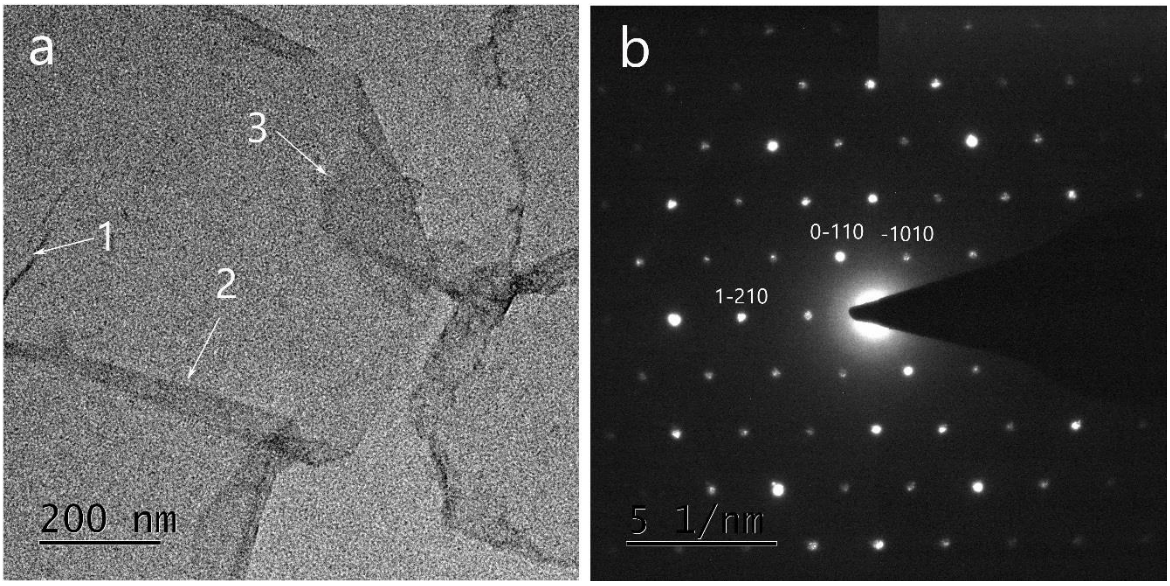

Figure 4.4. Transmission electron microscopy of graphene oxide; (a) high-resolution image of GO indicating excellent electron transparent, with wrinkles on the surface (1), and folds on surface (2), and edge (3) are marked, (b) selected area diffraction pattern of GO indicating hexagonal –like symmetry of the carbon atoms.

Energy dispersive X-ray spectrometry was performed on the GO layers by switching the scanning transmission microscopy mode, where a very fine electron beam is rastered over the sample area, and the emanating X-ray signals were recorded. The mapped area clearly indicated a higher concentration of Carbon over the sample area. Interestingly a very small portion of the signals constitutes of oxygen, indicating the presence of oxygen-containing functional groups in GO, and also that the concentration of oxygen is very small in the synthesized graphene oxide. The elemental mapping of carbon, oxygen, and the combined signals are presented in Fig.4.5.

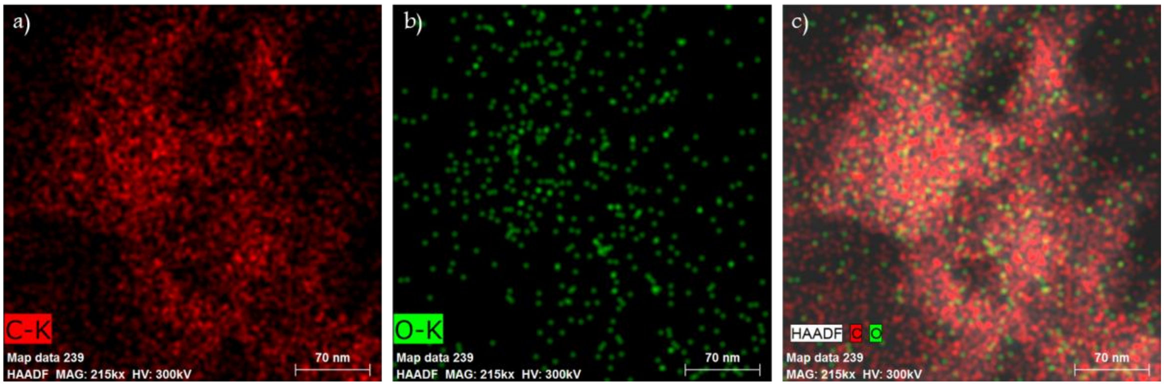

Figure 4.5. Energy dispersive X-ray spectroscopy of graphene oxide; (a) elemental map of carbon, (b) elemental map of oxygen, (c) combined signal of carbon and oxygen.

Exfoliation of graphene oxide results in the formation of oxygen-containing functional groups on the basal planes and the edges of graphene oxide. A qualitative analysis of these moieties is obtained from the FTIR spectrum (Fig.4.6). Pristine graphite sheets display few peaks at 1600cm^{-1} assigned to the C=C stretching in the parent sp^3 hybridized structure. On exfoliation of graphite to graphene oxide, GO comprises of strong peaks at 3384 cm^{-1} associated with the skeletal vibrations from COOH and OH stretch present on the graphene oxide edges. Besides C=C, C=O, and C-O-C stretch is observed at peaks corresponding to, 1646, 1720 and 1021 cm^{-1} (Table 4.1). C=O and C-O-C peaks are assigned to the formation of carboxylic groups at the edges and epoxy groups at the basal planes of graphene oxide, respectively. These moieties allow GO to be dispersed in water and to use it for waterborne formulations.

Peaks υ (cm^{-1})	Graphite	Graphene oxide
3384		O-H bonded water molecule
2980,2930, 1600	C=C	C=C
1720		C=O
1021		C-O-C

Table 4.1. A correlation chart of various functional groups presents in graphite and graphene oxide.

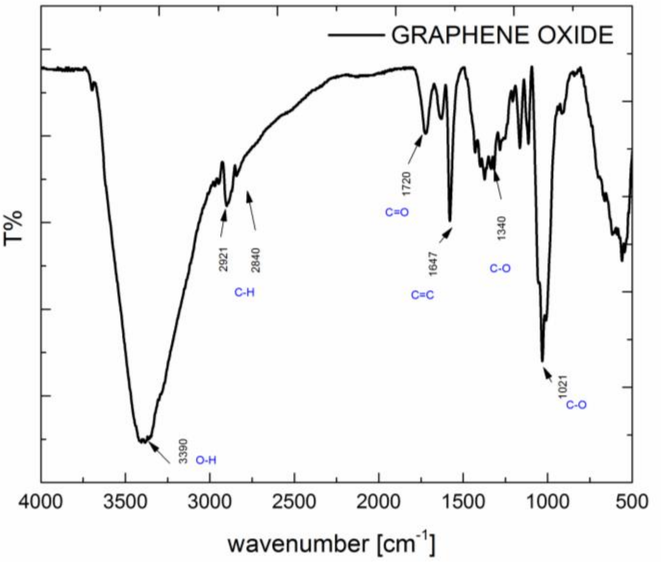

Figure 4.6. FTIR spectra for graphene oxide.

The Raman spectrum of graphene oxide (Fig.4.7) produced two peaks, one at (1594 cm^{-1}) and another at 1316 cm^{-1}. The materials were kept on a Si substrate and excited with a 785 nm laser. Literature suggests that G peak in the GO sample is observed at around 1578 cm^{-1} and a distinct D’ peak at around 1604 cm^{-1} [285]. The presence of the D’ peak is a measure of the quality of defects in GO. However, the absence of any D’ mode accompanied with a high G band value, is attributed to the superimposition of the G and D’ modes. This gives rise to an apparent G peak also called as G_{app}. This G_{app} peak suggests that the sheets have a high defect density producing a D’ peak whose energy was low enough to be superimposed by the G peak [286].

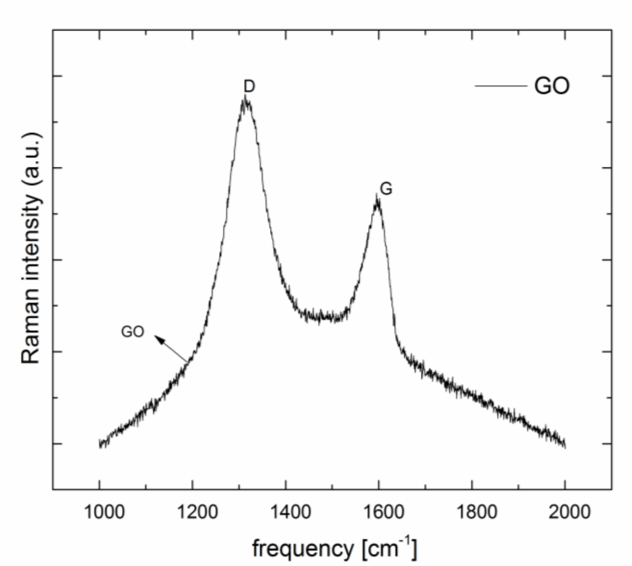

Figure 4.7. Raman spectrum of graphene oxide.

Theoretically, the D peak positioned at 1350 cm^{-1} is related to the size of the in-plane sp^2 domains due to the C-C stretching in all carbon structures [287]. Since oxidation process generates many structural defects, a shift in the intensity of the D peak from 1350 cm^{-1} to 1313 cm^{-1}. This can be attributed to the presence of a large amount of disorders present in the graphene oxide powder [288] primarily on the edges of the carbon structure.

Utilizing the ratio of the peak intensities I_D/I_G, one can use the Raman spectra to characterize the level of disorder/defects in graphene oxide. This ratio is inversely proportional to the average size of the sp^2 clusters [289]. The D band is a result of the vibration of the sp^2 bonded carbon atoms whereas the G band is due to the in-plane stretching vibrations of the sp^2 bonds. Here the GO powder obtained an intensity ratio of 1.42. This value is comparable to the values reported in the literature. The ratio in this work (1.42) indicated the presence of defects but is relatively a decent quality of GO.

4.2 Reduction of graphene oxide by hydrazine.

In this section, the synthesis and aqueous stability of hydrazine reduced graphene oxide are elaborated. The resulting form is termed as chemically converted graphene (CCG).

Furthermore, to denote hydrazine, the said term was called as CCG_H. The synthesis procedure has been outlined in the section 3.2.1.

4.2.1 Physico-chemical aspects.

Diffractograms of graphite and graphene oxide have spelled out the exfoliation of graphene oxide from graphite (Fig.4.1). Reduction of graphene oxide to graphene by hydrazine completely diminishes the graphene oxide peak. This indicates that the graphene oxide layers are fully expanded and completely exfoliated. Also, the CCG powders, after filtration and drying, also do not seem to restack; evident by the absence of any peaks for CCG in the X-ray diffractogram (Fig.4.8).

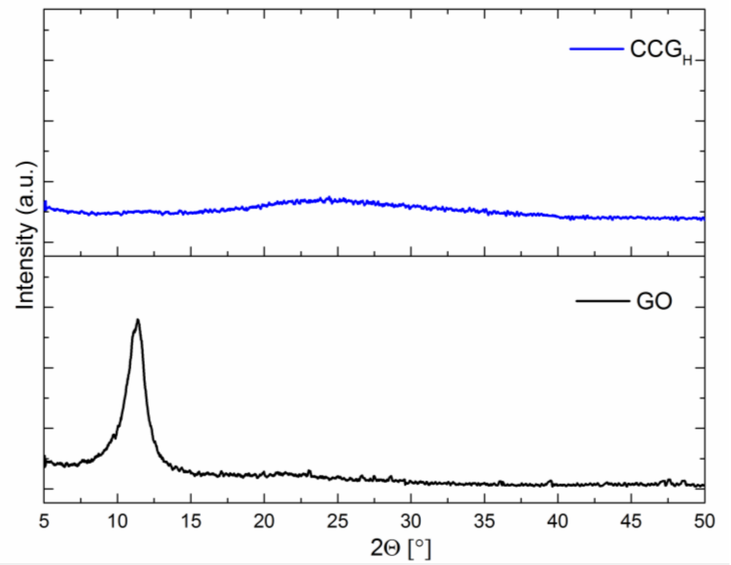

Figure 4.8 X-ray diffractogram of graphene oxide and hydrazine reduced graphene oxide (CCG_H).

Exfoliation of graphene oxide resulted from the breaking down of graphite sheets due to oxidation. Peripheral hydroxyl groups on the edges of the GO sheets increase the affinity of graphene oxide in water, allowing easy dispersion of these sheets in water. However, to obtain better exfoliation of graphene oxide, the sheets are dispersed in deionized water and further ultrasonicated in a horn type sonicator. Reduction of graphene oxide to chemically converted graphene (CCG_H) also indicated stable dispersion, although the color of the dispersion changed from brown to absorbing black.

UV-vis spectroscopy was performed to observe the plasmon transitions for the aqueous colloids of GO and CCG_H. Graphene-based colloids can exhibit interesting absorption patterns at the wavelength regions of ~230 nm, ~260 nm, and ~300 nm, corresponding to transitions involving π, σ, and n electrons of different bond energies [290]. The GO colloids produce a characteristic peak at ∼230 nm, which is attributed to the π-$\pi*$ plasmon of the C=C bond. The UV-Vis spectra for the CCG_H colloids (Fig.4.9), on the other hand, displayed the plasmon peak at 260 nm, which is a considerable peak shift to a higher wavelength. This is due to the reduction of the epoxy groups and restoration of conjugation in the graphene sheets which lowers the energy required, and thus increases the wavelength of the π-π* transitions. This also predicts that CCG_H possesses substantially decreased oxygen content and higher sheet size for which the value of λ_{max} shifts to a higher wavelength. With the restoration of the conjugation in the hexagonal carbon sheets, the material is more graphene-like, and is expected to show high thermal conductivity and electrical conductivity (also evident from the absorbing black colour of the colloid). For the graphene oxide colloids we also observed a shoulder peak at 300 nm (Fig.4.9). Literature suggests that there exists a bond excitation value at ~300 nm corresponding to the n-π* transition of the C=O chromophores for aldehyde and ketone molecule [291]. On the other hand, this peak almost vanishes for the CCG_H colloids indicating the absence of the C=O chromophores in the colloid. The obtained colloid has been studied for its aqueous colloidal stability by titrating it with a base and acid, which shall be a later part of the chapter.

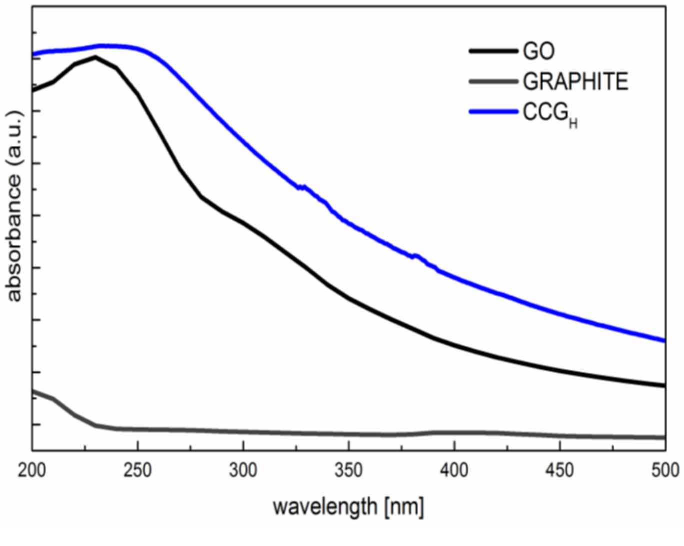

Figure 4.9. UV-Visible spectra of graphite, graphene oxide and chemically converted graphene (CCG_H).

Restoration of the conjugate bonds in CCG_H are confirmed by the FTIR spectrum with the disappearance of almost all of the functional groups as compared to the GO spectrum. This curve is similar to that of graphite with few bonds displayed only at 1600 cm^{-1} along with 2900 cm^{-1} corresponding to the alkene stretch present in the parent graphitic structure. This confirms that graphene oxide is successfully reduced to graphene.

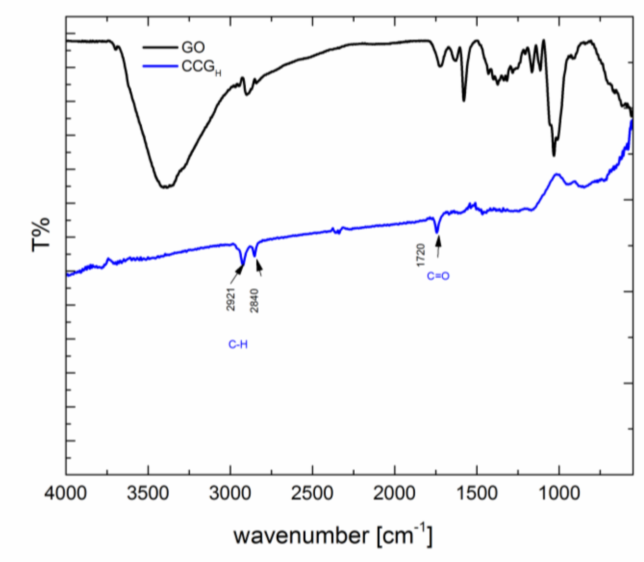

Figure 4.10. FTIR spectra of graphite, graphene oxide and chemically converted graphene by hydrazine (CCG$_H$).

SEM images of the CCG$_H$ powders, dropped on to the stubs from aqueous dispersions, showed wrinkled and crumpled morphology similar to the parent GO structure (Fig.4.11). The exfoliation procedure weakens the van der Waals forces between the graphitic planes, causing the sheets to exfoliate. The interesting part was that the reduced sheets did not appear to stack up to form graphitic structures, as corroborated by the XRD analysis.

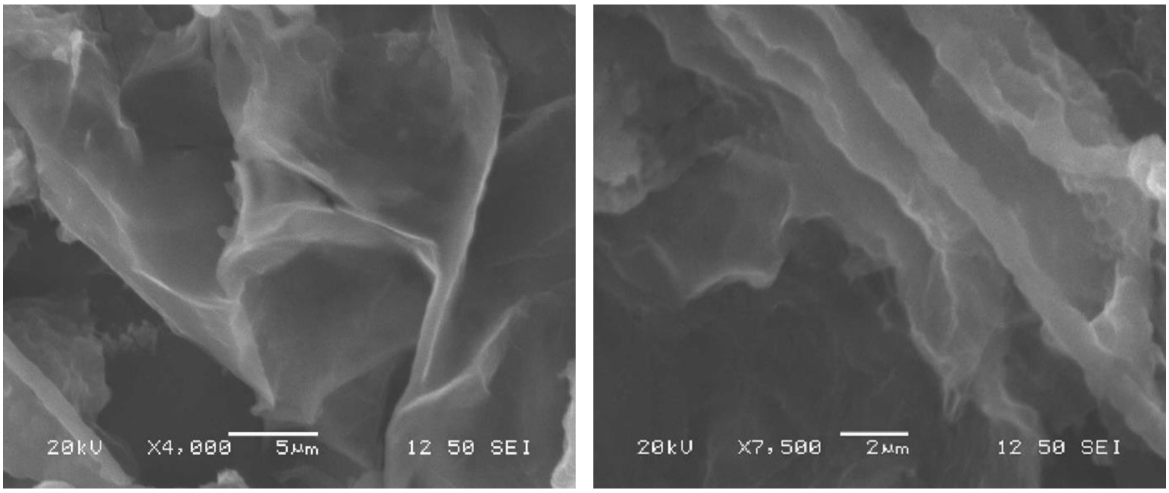

Figure 4.11. Morphology of the chemically reduced graphene sheets (CCG$_H$).

Transmission electron microscopy of the hydrazine reduced graphene oxide (CCG_H) samples was done by dropping aqueous colloids on the sample stub. The images (Fig.4.12 a & b) exhibit highly transparent sheets with usual wrinkled folded structure. The sheets had some extent of defects (nanoholes) which may have formed during the reduction process. The morphology was typically equivalent to that of graphene oxide. Generally, it is shown that after hydrazine reduction, a large amount of restacking of the sheets occur leading to thicker graphene layers. High-resolution imaging of one of the edges indicated stacking of 5 layers (Fig.4.12c). By measuring the contrast variation, (Fig.4.12d), it was found out that the interlayer separation was ~3.3Å. This indicates conversion to graphitic interlayer distance (which is lower that the interlayer distance in graphene oxide), and thus confirms the restoration of double bonds following the reduction of epoxy groups on the basal planes.

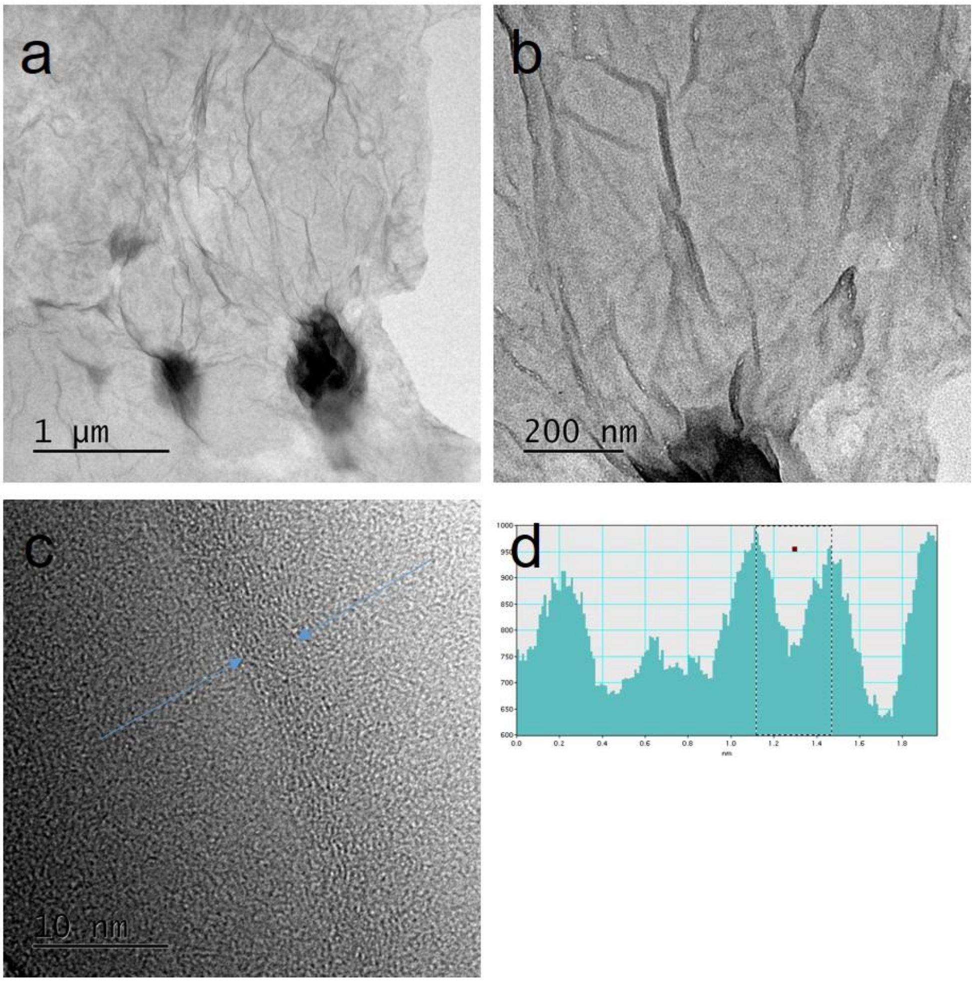

Figure 4.12. Highly electron transparent sheets of (a & b) chemically reduced graphene oxide (CCG_H), some defects (holes) can be seen on the sheets,(c) high-resolution image of a sheet indicating 5 layers of graphene, (d) contrast variation exhibiting the interlayer separation to ~3.3Å, analogous to the graphitic plane spacing.

4.2.2 Restoration of conjugation and aqueous colloidal stability.

The behavior of graphene oxide colloids is influenced by various parameters, including pH, particle size, and zeta potential. An understanding of these parameters and their influence on the stability of the colloids is key to exploiting aqueous synthesis routes for the fabrication of graphene-based hybrids and composites. In this part, the change in zeta potential, light absorption, and equivalent particle size of graphene oxide and chemically converted graphene colloids over a range of pH are reported.

Both CCG_H and GO sheets are negatively charged colloidal particles carrying varying concentration of functional groups. Oxygen-containing functional groups present on the GO sheets make it highly hydrophilic. On the other hand, in CCG_H, the remnant oxygen-containing groups impart stability of the mildly oxidized graphene oxide sheets in aqueous media. As the colloid is titrated with NaOH/HCl, the ensuing change in the pH of the colloid leads to agglomeration of the graphene-based colloidal particles.

Zeta potential (ζ) is an important factor for characterizing the stability of colloidal dispersions. It is a measure of the negative charge on the double layer associated with the colloidal particle as a consequence of the ionization of different functional groups. Generally, GO particles with zeta potential in the range −30 mV to +30 mV are considered stable due to electrostatic repulsion [292]. Our measurements show that zeta potential for the GO colloids is pH sensitive, and effective dispersion of the colloids occurred within the pH range of 4–12 (Fig.4.13). Experimentally, we observed that and the highest magnitude of is obtained at pH 10 (−48.6 mV), although the pH range of 7–11 showed the highest (negative) charge.

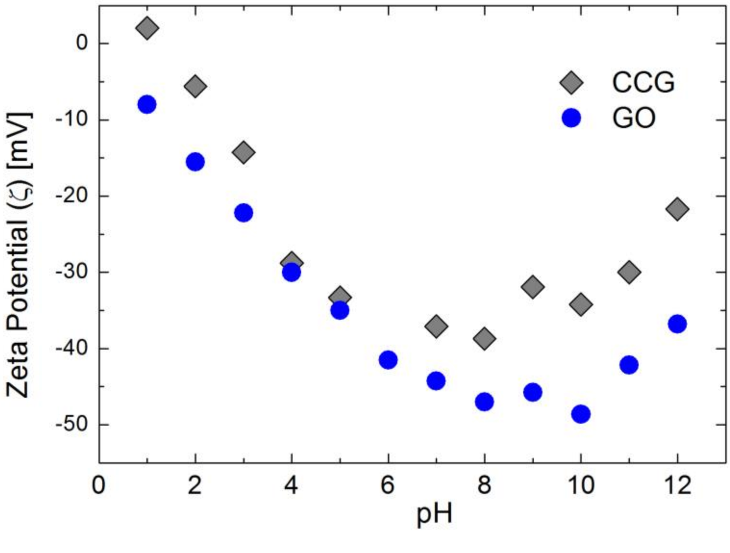

Figure 4.13. Zeta potential of aqueous colloids of GO and CCG_H at different pH.

Dynamic light scattering (DLS) results for both GO and CCG_H colloids showed similar trends with subtle differences. It must be mentioned here that the attempt is not to estimate the average particle size of GO and CCG_H. DLS is a technique that is well suited for estimating the size of spherical particles. GO and CCG_H particles, on the contrary, are particulate systems that possess extremely large ratios of length or breadth (few microns) to the thickness (few nanometers). Therefore, the DLS pattern of such a system could provide a convoluted result, which is expected to be close to the lateral dimensions of the GO and CCG_H platelets. However, the objective here is to compare the relative change in the platelet size as a function of pH. For the graphene oxide sample at pH 7, the size distribution varied in the range of 250 nm to 570 nm (Fig.4.14). However, as the sample was titrated with NaOH to a higher pH, the population lay in the range of approximately 300 nm to 500 nm. The stability of the GO colloid improves as NaOH acts as a hydrogenating agent for graphene oxide [293]. Moreover, it has also been reported that NaOH has an ability to successfully remove the oxygen functionalities from the surface of GO to form activated graphene sheets [294, 295]. These activated sheets begin to stabilize themselves in the solution by reducing their effective cluster size. Thus, the change in color and stability of the NaOH titrated samples could be due to the development of small-sized activated graphene sheets. GO colloids, on the contrary, when titrated with HCl result in very large sheet size and poor stability. This can be attributed to the increase in H^+ ions in the solution, which gradually increases the sheet size and reduces the stability.

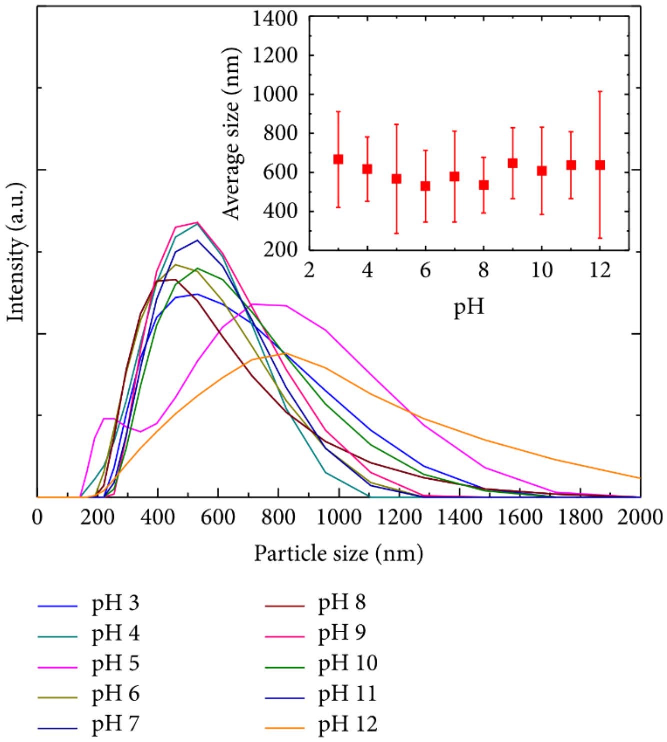

Figure 4.14. Particle size distribution of GO colloids at different pH; inset shows the average particle size.

These observations reiterate our findings from the zeta potential measurements that GO colloids are more stable in the 3–11 pH range. The thickness of the GO sheets is normally expected to increase with a decrease in pH due to increasing protonation of acidic groups (C–OH, COOH) present on the sheets. Protonation decreases the negative charge on the sheets, thereby decreasing electrostatic repulsion between them, leading to agglomeration of the sheets and reduced colloidal stability. However, it was observed that, in the pH range of 6–9, the particle size distribution remains almost the same, and the distributions for colloids of pH 10 and 11 exhibit tails towards higher size. The reason for a slightly higher size distribution in pH 10 and pH 11 could be ascribed to the salting out effect of the NaOH additives.

The CCG_H colloids, on the other hand, displayed sheet size in the range of 200 nm to 700 nm at pH 7 (Fig.4.15). On titrating them with NaOH, the CCG_H sheets in the pH range from 7 to 10 stabilize uniformly and lie in the range of 200 nm to 400 nm. However, above pH 10, the sheets agglomerate, and their size sharply increases over 1 micron, with very few sheets in the nanometric range (not included in Fig.4.14). This dramatic shift is supported by Fan et al. [256], who comment that the stability of the CCG_H sheets is attributed to a strengthened electrostatic stabilization under alkaline conditions, as the repulsion between the negatively charged sheets should increase at higher pH values. Thus, as the repulsion lies within their threshold limits, the CCG_H colloid is stable, and above a threshold limit, the sheets begin to agglomerate and destabilize themselves.

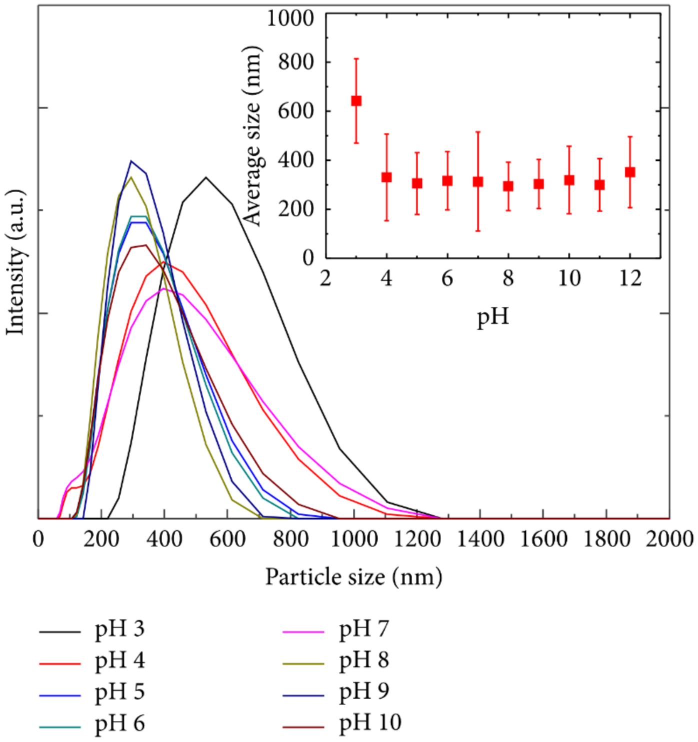

Figure 4.15. Particle size distribution of CCG_H colloids at different pH; inset shows the average particle size.

Overall, the DLS spectra of GO and CCG_H colloids exhibited size in the range of 200 nm to 1000 nm, with the distribution tailing off at higher sizes for the pH range of 3–10. The distributions for colloids of pH 1-2 and pH 10-11 were completely different from the distributions in the pH range of 3–9, the average being observed beyond 1 micron at the pH extremes.

This result closely matches with our common observation of a highly agglomerated GO colloid that is not transparent yellow but showed a muddy appearance. This suggested that the neutral pH range was found to be processing of GO colloids.

UV-vis spectroscopy was employed to observe the plasmon transitions for the titrated GO and CCG_H colloids. The characteristic peak of GO colloids at ~230 nm attributed to the π- π^* of the C=C bonds is similar for samples in the pH range of 2 to 11 (Fig.4.16). However, at pH 1 and pH 12, the absorption pattern appeared completely different, roughly indicating a continual decay of absorption with wavelength. At pH 1, this arises as a result of high amount of sedimentation that takes place due to the aggregation and low repulsion within the sheets.

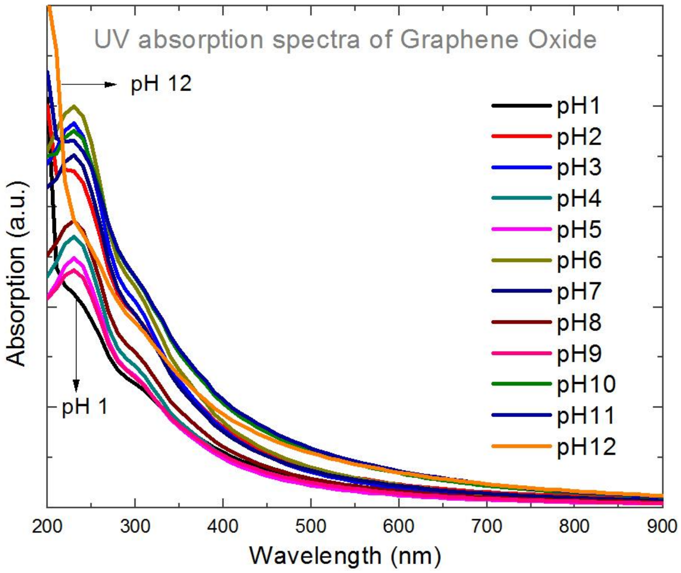

Figure 4.16. UV-Vis spectroscopy of GO colloids from acidic to basic conditions.

As for pH 12, the sedimentation occurs due to the salting out of the excess sodium ions. The UV-Vis spectra for the CCG_H colloids, displayed the plasmon peak at 260 nm, (Fig.4.17). Due to the reduction of the C=O groups and restoration of conjugation in the graphene sheets that lowers the energy required, as mentioned in section 4.2.1. The shoulder peak at 300 nm for the GO colloid (Fig.4.9), corresponding to the n-π^* transition of the C=O chromophores for aldehyde and ketone molecule [256], shift slightly due to the increased solvent polarity of graphene oxide as it is titrated with NaOH/HCl. On the other hand, this peak almost vanishes for the titrated CCG_H colloids indicating the absence of the C=O chromophores in the reduced form.

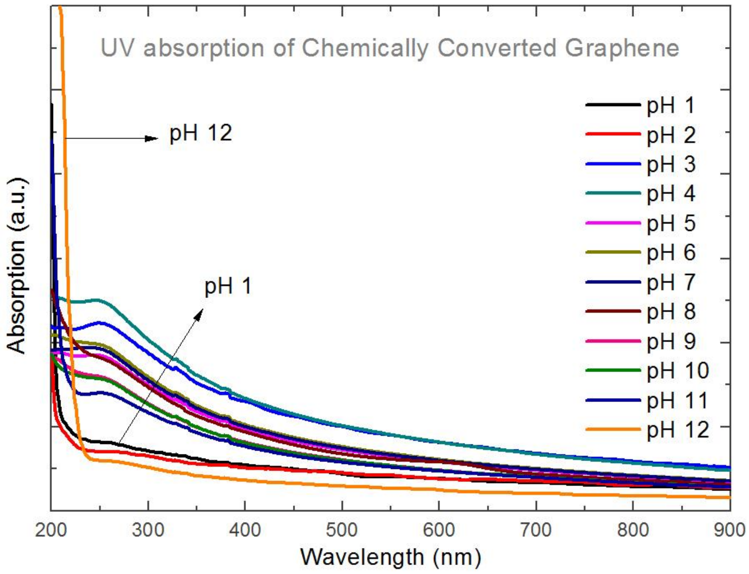

Figure 4.17. UV-Vis spectroscopy of CCG_H colloids from acidic to basic conditions.

In summary, aqueous dispersions of graphene oxide were found to be stable in the pH range of 4–12, with excellent dispersibility in the range of 7–11, as evidenced by highly negative zeta potential. The colloidal stability of chemically converted graphene in aqueous media was also found to be similar to that of graphene oxide colloids. UV-Vis spectroscopy of the chemically converted graphene colloids indicated the restoration of electronic conjugation in the graphene sheets. These findings are useful in the fabrication of graphene-based composites and hybrids from aqueous processing methods.

4.3 Reduction of graphene oxide by triethanolamine.

4.3.1 Physico-chemical properties.

X-ray diffractograms of reduced graphene oxide by triethanolamine (TEOA), produce a broad spectrum over the range from 5° tailing off to about 30° of 2Θ, (Fig.4.18). This was clearly different from the typical XRD pattern of GO (also shown in Fig.4.18), where a low-intensity peak was observed at~ 11°. The peak for CCG_{TEOA} can be thought of as a combination of two peaks. A small broad peak at ~12° in the CCG_{TEOA} powders corresponds to graphene oxide. A broad spectrum at around 22.5° was peculiar in that the intensity was very low, and the peak was highly broadened. Based on these features it can be surmised that TEOA reduced graphene oxide possess two different kinds of carbon structures. A portion of the powders is similar to graphene oxide with functional groups intercalated between the layers (interplanar spacing of 8Å) and with an extremely small stack size of the individual crystallites [169]. The other portion is more graphite-like, characterized by an interplanar spacing similar to graphite, as evident by the peak position. However, the extremely broadened nature of the peak indicates that the size of the graphite stacks is low, and it can be called either graphite nanoplatelets or few layer graphene [296].

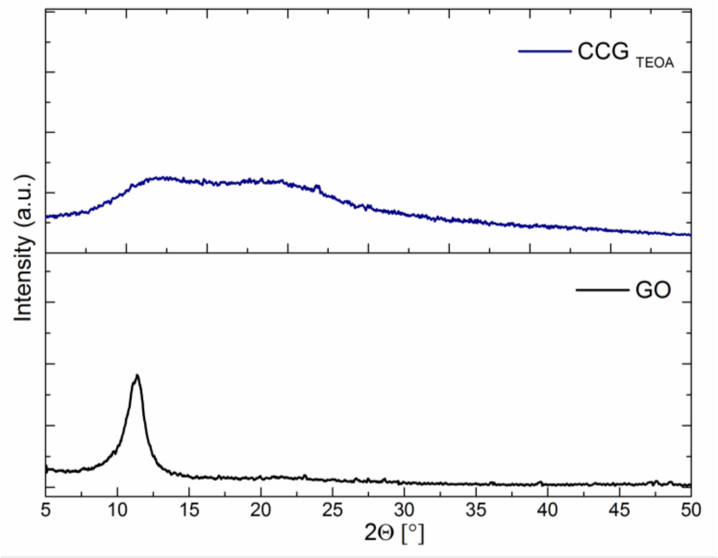

Figure 4.18. XRD spectra of graphite, graphene oxide and chemically converted graphene (CCG_{TEOA}).

TEOA is both a tertiary amine and a triol. Therefore TEOA reduces the epoxy groups on the graphene oxide sheets as well as functionalizes it. This is confirmed by the FTIR spectra of CCG_{TEOA}, which displays reduced intensity peaks for (C-O-C) groups and (C=O) groups at 1021 cm^{-1} and 1720 cm^{-1} as compared to the signals from GO powder. The spectrum also displays a medium intensity peak at 1650 cm^{-1}. This peak corresponds to C=C alkene stretch signifying the inherent doubly bonded carbon atomic structure of graphene oxide, coupled with a doublet peaks at 2980 and 2930 cm^{-1} (symmetric and asymmetric stretching vibration of–CH_2) group suggesting the restoration of carbon basal plane in GO (Fig.4.19) [297]. The reaction of TEOA molecule on graphene oxide is observed by the presence of few NO bonds (nitroso groups) at 1378 cm^{-1}. Additionally, a broad spectrum was observed at 3360 cm^{-1}, corresponding to the increased -OH groups in the reduced sol as a result of strong intermolecular hydrogen bonds from the alcoholic groups from TEOA. Decrease in the intensity of the C-O peaks at 1041 cm^{-1} and CH_2 peaks at 1455 cm^{-1} confirm the reduction of GO colloid by TEOA molecules [298].

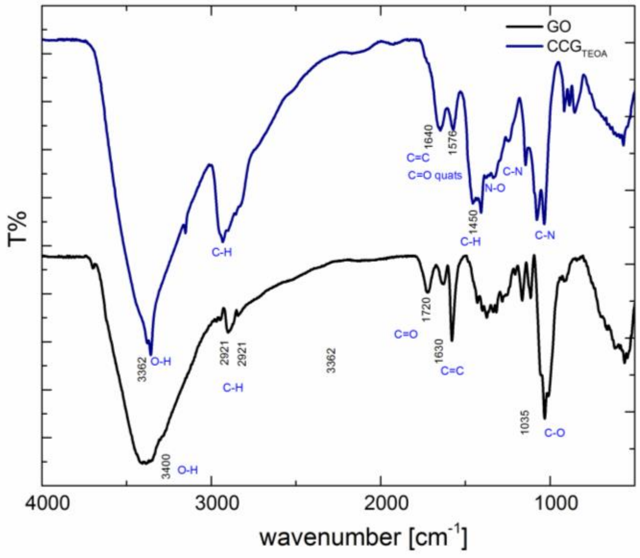

Figure 4.19. FTIR spectra of graphite, graphene oxide and chemically converted graphene by TEOA (CCG_{TEOA}).

TEOA, which is a strong base, comprises of three ($-CH_2OH$) molecules acting as the reducing agents. Under such condition, TEOA first dissociates to produce N^+ radicals by hydrolysis generating OH- groups (as depicted in the schematic, step A, Fig.4.20), with an initial of pH 9.5 [299]. Carbon in the epoxide groups of graphene oxide is very reactive electrophile. Therefore substantial ring relieves upon a nucleophilic attack on the least substituted position [300], by the transfer of a proton (oxidation) of the $-CH_2CH_2OH$ group in TEOA to $-CH_2CHO$. The reaction is accelerated in the presence of N^+ ions, which react with the oxygen atom on the ring-opened epoxy to reduce graphene oxide to its restored conjugated structure (seen at 1640 cm^{-1}), with some residual nitrous oxide (NO) gas (step B, Fig.4.20). Additionally, electrostatic interactions between the dissociated N^+ radical in TEOA and the carboxylic groups at the edges result in the formation of salts of carboxylic acids as quaternary ammonium cations (1556 cm^{-1}), also abbreviated as quats, (step C, Fig.4.19). This confirms that TEOA acts to reduce the epoxy groups at the basal planes of GO, and resides as quaternary ammonium salts at the edges of the reduced colloid. The increased number of hydroxyl molecules, due to the formation of quaternary salts improve the stability of the reduced colloid making it suitable for use in polar solvents [301].

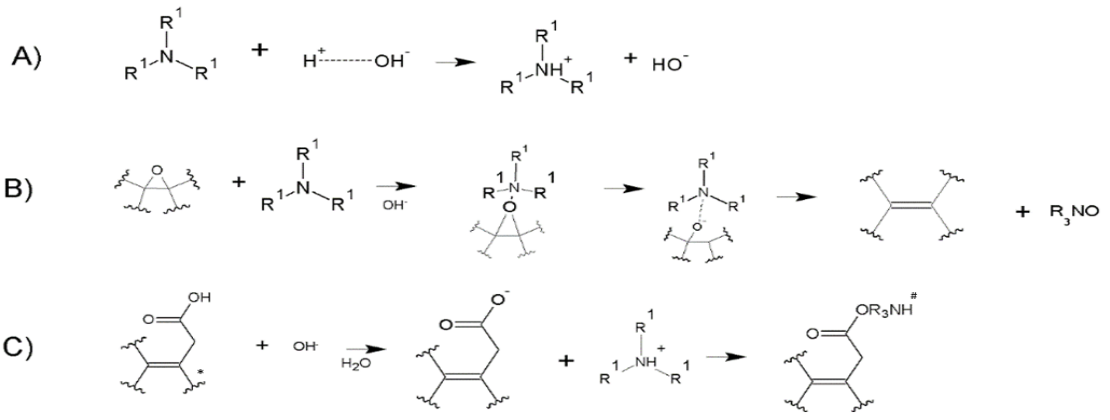

Figure 4.20. Possible reaction mechanism of GO reduced by TEOA, R_1=C_2H_5 OH, * refers to the OH and carboxylic groups on graphene oxide; # refers to the formed quaternary hydroxylammonium salts.

4.3.2 Restoration of conjugation and colloidal stability.

TEOA reduction produces prominent functional changes in the UV-visible absorption spectra of the GO colloids. The C=C chromophores at 230 nm reflect a shift towards a higher wavelength to 256 nm respectively (Fig.4.21). At the end of 24 hours, the π-π* plasmon shift to a higher energy, relating to the restoration of the C=C graphitic structure. However, substitution of the C=O group on the GO sheets occurs by an auxochrome with a lone pair, (which here is the triethanolamine), results in a shift of the absorption peak at 230 nm to a shorter wavelength, also referred to as a hypsochromic shift [297]. This shift is corroborated with the FTIR spectra showing the presence of hydroxylated quaternary salts of ammonium (quats), formed as a result of result of resonance interactions between the carboxyl groups and the lone pair of ammonium ions in the solutions. The tendency of the nitrogen atom in TEOA to withdraw electron from the carbonyl cation allows it to be held firmly than they would be in the absence of the resonating effects, thus shifting the position of the peak to a shorter wavelength.

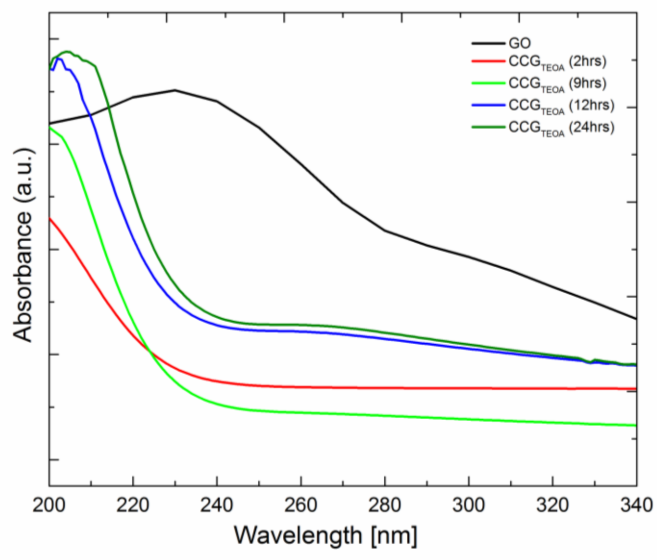

Figure 4.21. UV spectra of, graphene oxide and time-dependent chemically converted graphene (CCG_{TEOA}).

Lyophilic colloids of reduced graphene oxide sheets in an aqueous media can be produced by forming strong forces of interaction amongst the particles and the media. However, the graphene sheets tend to aggregate and increase in size, if these interactions exceed the cohesion frequency and the probable hindrance produced by the ions in the media. In the case of the CCG colloids reduced by TEOA, we observe that there is no distinct change in the size of the sheets (450 nm to 400 nm) and the reduced sol appears as a stable black colloid. While on one hand, the quaternary ammonium ions in the solution strongly bind with the reduced GO sheets resulting in sufficient steric hindrance to prevent aggregation, TEOA reduction perhaps enhances the stacking of the sheets in another portion of the reduced GO sheets.

The effect of steric hindrance provided by the quaternary ammonium ions is studied by the potentiometric studies of the CCG_{TEOA} colloid, (Fig.4.22). It is observed that for a given strength of TEOA ions, the stability of the CCG_{TEOA} improves with an increase in reaction time. However, again there is no major difference in the values of zeta potential at different time intervals (-31 mV to-28 mV). This suggests that TEOA does not enhance the colloidal stability. Rather, in this process, along with the reduction of the GO sheets, some amount of stacking of the graphene sheets occur, as evidenced by a moderate increase in the zeta potential. This also is congruent with the XRD results of the CCG_{TEOA} powders, where extremely small domains of stacked graphene sheets could be observed. Nevertheless, the zeta potential of the CCG$_{TEOA}$ colloids still had negative values, and that these colloids could be used for further processing.

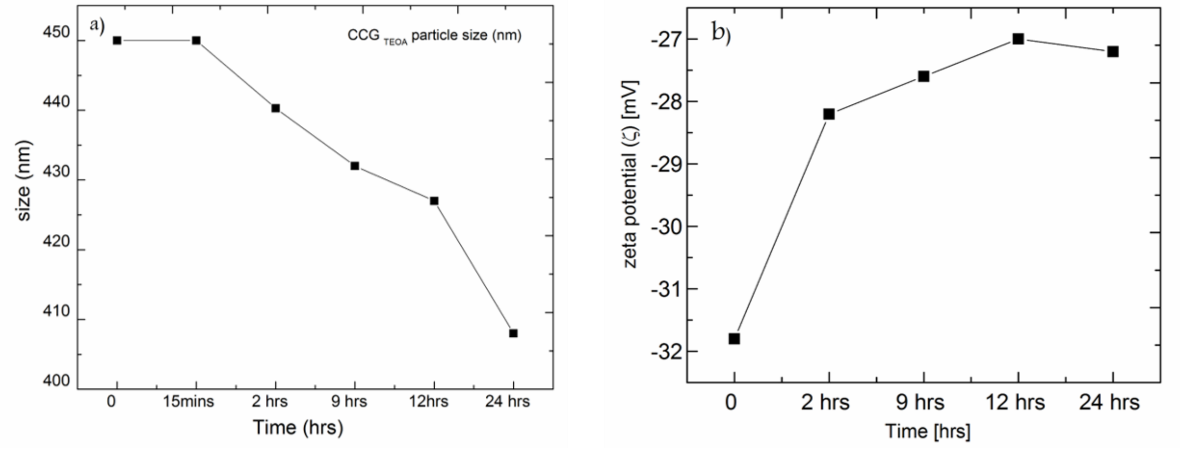

Figure 4.22. (a) The particle size of CCG$_{TEOA}$ with a time of reduction, (b) zeta potential of the colloid with time.

4.4 Reduction of graphene oxide by triethylamine.

4.4.1 Physico-chemical properties.

X-ray diffraction pattern for graphene oxide treated with triethylamine indicated virtually no feature, other than an extremely small hump in the 2Θ range centering around 20° (Fig.4.23). This clearly indicates complete exfoliation of graphene oxide sheets into single sheets of carbon atoms without restacking. This observation was qualitatively similar to the diffraction pattern of CCG formed by hydrazine reduction and was clearly different from CCG$_{TEOA}$.

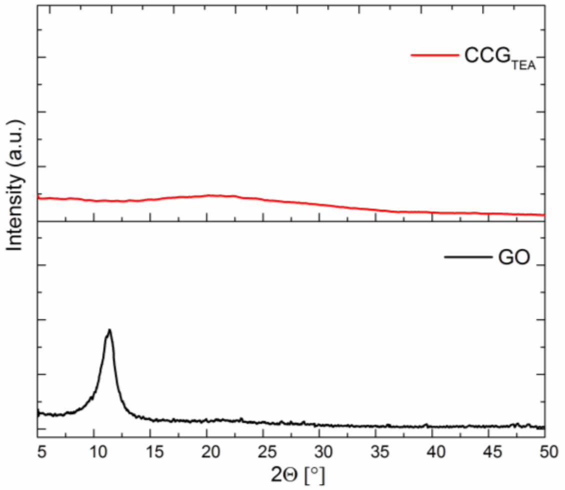

Figure 4.23. Diffractogram of graphite, graphene oxide and chemically converted graphene by TEA reduction (CCG$_{TEA}$).

A qualitative analysis of reduced colloids is obtained from the FTIR spectrum (Fig.4.24). Primarily, GO comprises of strong peaks at 3384 cm^{-1} associated with the skeletal vibrations from COOH and OH functional groups respectively. Along with C=C, C=O, and C-O-C stretch is observed at peaks corresponding to 1635, 1720 and 1021cm^{-1} respectively. The C=C peaks seen as a result of the inherent doubly bonded carbon atomic structure of graphene oxide conjugate with a pair of peaks at 2980 and 2930 cm^{-1} associated with the (symmetric and asymmetric stretching vibration of –CH_2 group) in the parent graphene oxide structure.

On reduction with TEA, it was observed that epoxy peak at 1021 cm^{-1} diminishes and the inherent C=C peak for GO at 1635 cm^{-1} shifts to 1600 cm^{-1} but with an increased intensity. The peak shift suggests the restoration of the carbon basal planes accompanied with the conjugation effects produced by the –C_2H_5 groups present on the TEA molecule. Likewise, we find some N-O vibrations at 1389 cm^{-1} due to the TEA reduction. Few carboxylic bonds are also observed at 1720 cm^{-1} peak in the reduced graphene spectra. This peak is attributed to the resonating effects induced by the unpaired electrons on the nitrogen atom. During reduction, the COOH groups attached to the GO sheets tend to draw in the electrons between the carbon and oxygen atoms through its electron withdrawing effect with TEA, so that the C=O bond becomes stronger resulting in a frequency absorption at 1720 cm^{-1} [297].

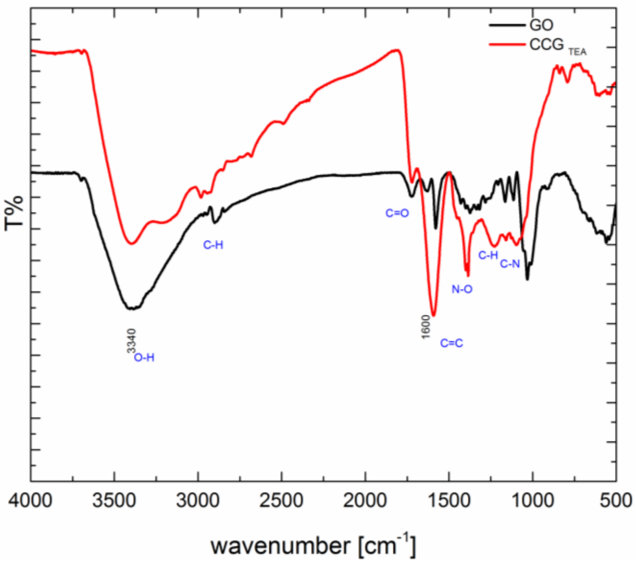

Figure 4.24. FTIR spectra of GO and TEA reduced graphene (CCG$_{TEA}$).

TEA is a tertiary aliphatic amine which reduces GO via nucleophilic substitution reaction by eliminating epoxy groups and forming quaternary ammonium salts [302]. When

TEA is added to the aqueous colloidal solution, it initially dissociates to produce OH ions in the solution increasing the basicity (step A, Fig.4.25). Part the basic effect of TEA and the high reactivity of the epoxide group in graphene oxide, TEA is capable of releasing a radical by oxidizing the $–C_2H_5$ groups to epoxy. The radical results in the ring opening of the epoxy species through the cleavage of C-O bonds, which converts back the C-O-C structure back to C=C faster than it can dissociate (step B, Fig.4.25). Additionally, the singlet oxygen ion released interacts with the N^+ radical on the TEA molecule to form stable nitro-molecules (NO). On the other hand, the dissociated quaternary ammonium ions produced in step A forms conjugated structures with the carboxylic ions on the edges of graphene oxide during reduction. Due to the electrostatic interactions between the N^+ groups in TEA and the carboxylic groups at the edges, TEA attaches itself to the edges in esterified carbonyl amide form and resides there as a bulky group in a resonating structure (step D, Fig.4.25). This confirms that TEA is efficient to reduce the epoxy groups at the basal planes of GO, and facilitates to sit as a bulky group to the edges, producing a conjugated stable structure as observed by the increase in the C=C character.

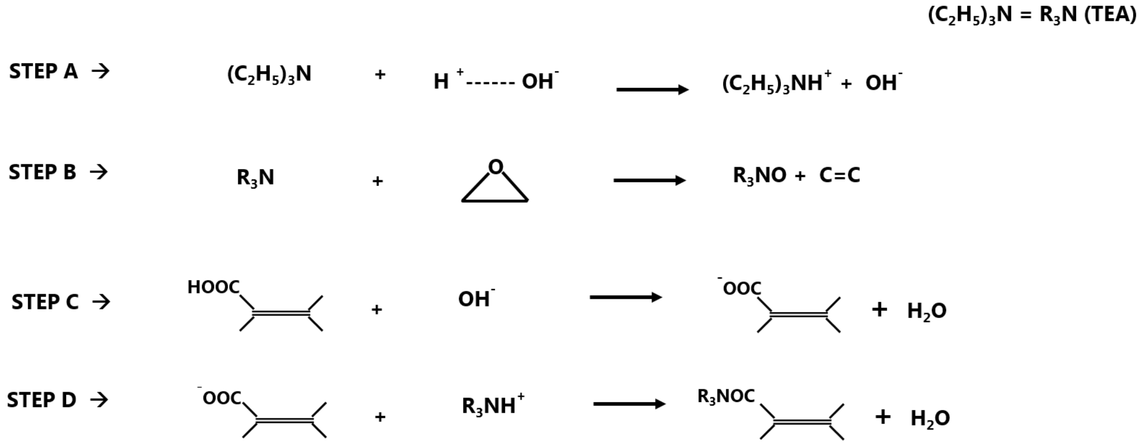

Figure 4.25. Possible reaction mechanisms of GO reduced by TEA, displaying the restoration of carbon bonds and formation of quaternary ammonium salts.

It is well known that as GO sheets reduce to graphene, they tend to restack due to the strong electrostatic force of attraction of the π-π bonds [290, 303, 304]. To minimize the restacking, we need to stabilize the sheets via some positively charged groups, which done by the quaternary ammonium salts formed by TEA. Additionally, it is important to quantify the amount of reductant utilized for effective reduction of GO.

4.4.2 Restoration of conjugation and aqueous colloidal stability.

The UV-vis absorption signal of GO and graphene colloids is the most simplistic and straight forward analysis to predict the transitions. GO colloids produce a characteristic peak at 230 nm attributed to the π-π* plasmon of the C=C bonds [290]. The UV-vis test was performed for the GO colloid for every 1 hour of refluxing time of the colloid in the presence of TEA. This peak remains uninterrupted during the reaction of GO with TEA for the initial 2 hours. Interestingly, it begins to shift gradually to a higher wavelength as the reaction time increases from 2 hours to 24 hours (Fig.4.26), indicating the reduction of C=O groups and restoration of conjugated C=C bonds in the graphene sheets. The restoration of the bonds due to the substantially decreased oxygen content shifts the value of λ_{max} shifts to a higher wavelength. With the restored bonds in the hexagonal carbon sheets, the material is more graphene-like.

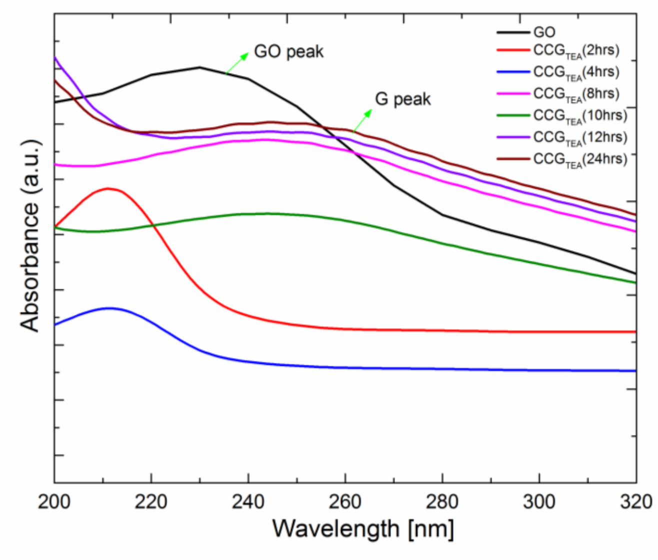

Figure 4.26. UV-visible spectroscopy of GO and CCG_{TEA} exhibiting the gradual transition of GO to the graphene-like character.

These observations can also be realized from a visual standpoint. The color of the GO colloid is essentially brown (seen in Fig.4.27, far right). The figure shows the digital photographs of the vials with the GO colloids refluxed from 0 to 24 hours in the presence of TEA. One can observe that the color of the colloid gradually turns black with an increase in the refluxing time, saturating between 12 to 24 hours.

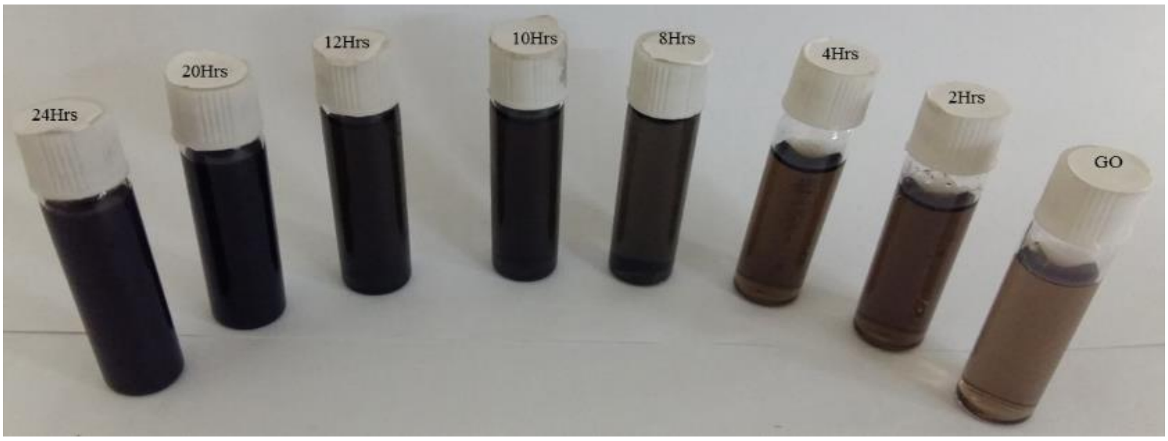

Figure 4.27. Vials with samples showing color change from graphene oxide (far right) to graphene (far left).

Zeta potential and dynamic light scattering studies interestingly show that a small amount of TEA effectively reduces and stabilizes the GO sheets. On increasing the quantity of the reductant the size and stability of the sheets increased up to 1ml of TEA, following which increases in the reductant quantity led to sudden increase in the equivalent particle size. Likewise, with 0.5 ml of TEA, the zeta potential of the colloid remained almost unchanged in the range of -36 to -38 mV. Further increase in the reductant amount led the colloid to show zeta potential in the range of -28 to-32 mV, indicating slightly reduced colloidal stability. Subsequently, only 0.5 ml of the TEA reductant was used for the GO colloid and the time of reduction was optimized (Fig.4.28).

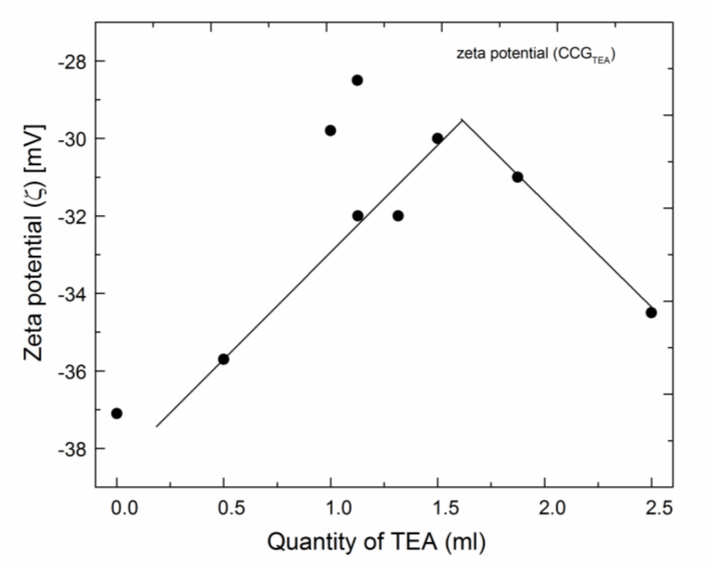

Figure 4.28. Variation of zeta potential with the amount of reductant used.

Zeta potential of the CCG_{TEA} colloids at different time intervals of reduction was measured. The results indicated persistent colloidal stability over the reaction time. Only. in the range of 4-10 hours, the zeta potential slightly reduced to the range of -32 mV to -38 mV (Fig.4.29). However, 12 hours or more reaction time imparted stability as good as that of unreacted pure GO-based colloids. This was optimized for strengthened electrostatic stabilization of the CCG_{TEA} colloids. Accordingly, DLS measurements also indicated the distribution of equivalent particle size for the 12-24 hours treated CCG_{TEA} samples similar to the pure GO colloids. The observed stability of the reduced colloids is a feature of the electrostatic stabilization of the reduced sheets induced by the quaternary ammonium ions. Compared to the stability of the graphene oxide colloid in aqueous media, increase in the ionic nature of the aqueous media, produces well stabilized and reduced CCG_{TEA} for a lower volume content of 0.5ml [305].

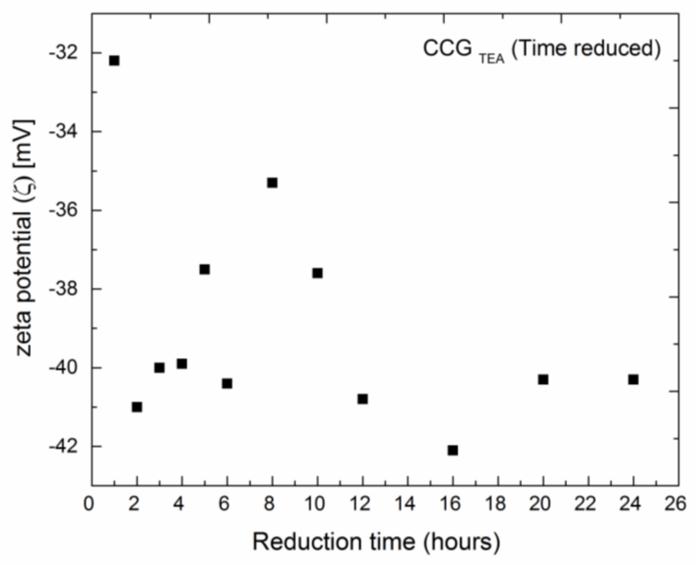

Figure 4.29. Variation of zeta potential with reaction time.

4.5 Chapter Summary.

In this chapter, the structure, and aqueous colloidal stability of graphene oxide, as well as graphene oxide reduced by various reductants have been discussed. The salient features can be summarized as follows.

- Good quality graphene oxide with large aspect ratio and few layers of stacking was synthesized by modified Hummers method. The morphology indicated wrinkles and folds, but with excellent crystallinity as evidenced by electron diffraction.

- Hydrazine reduced GO sheets indicated excellent colloidal stability at a neutral pH range, as confirmed by surface charge measurements. The CCG_H powders exhibited almost no features in the XRD spectrum indicating complete exfoliation of the layers, and no restacking.
- Triethanolamine reduced GO appeared to be partially exfoliated (like GO) and partially stacked. Its aqueous colloid was reasonably stable, but not as good as the CCG_H colloids.
- Triethylamine reduced GO colloid showed excellent colloidal stability in water, matching the dispersibility of GO in water. The CCG_{TEA} powders showed complete exfoliation with no feature in the XRD spectrum.

All of the reduced graphene oxide types exhibited the conjugation of the C=C bonds as evidenced by the UV-Vis spectroscopy. Based on this information, PVA-based composites with different types of fillers and functionalizations can be prepared by aqueous processing methods.

.

CHAPTER 5

Graphene oxide and reduced graphene oxide reinforced PVA nanocomposites.

In this chapter, physical, chemical, structural, and thermal properties of two different types of PVA nanocomposites, one with graphene oxide reinforcement, and other with *in-situ* hydrazine reduction, have been discussed.

Polymer films of PVA were fabricated as per procedures outlined in chapter 3. Graphene oxide was used as reinforcement (filler) at wt% of 0.4, 0.8 and 1.0 (% of PVA), and the complete films were prepared as per the section 3.3.1. These composites were called the PGO series. Likewise, in a similar procedure and loading of fillers, the *in-situ* reduction was carried out using hydrazine (Chapter 3, section 3.3.2), and films were fabricated by solution casting method. These films were called the PGH series. The fabricated pristine PVA films were transparent in appearance (Fig.5.1). The addition of graphene oxide filler in the polymer with increasing filler content of 0.4, 0.8 and 1 wt%, rendered the transparent films to appear as brown, dark brown and brownish-black (Fig.5.1). However *in situ* reduction of the polymer blend with hydrazine, produced completely black films on different filler loading of 0.4, 0.8 and 1 wt%. The change in color of the films can be attributed to the added fillers which contribute to chemical changes on the transparent PVA film. Amongst all the composites, (both PGO and PGH), only the PGO films with 0.4 wt% of GO loading had a decent level of transparency.Rest of the films were typically black. However, no speckled contrast was observed from the nanocomposites which is a qualitative indication of the excellent homogeneity of the fillers in the composite. The homogeneity was also presented even for the 1% loaded GO or CCG films that did not show any aggregation of the fillers on any part of the composite.

Figure 5.1. Physical forms of PVA, PGO-0.4, PGO-0.8 and PGO-1 films.

5.1.Structural and thermal behavior.

Structural and functional properties of polymeric materials are dependent on the crystallinity of the polymer and its glass transition temperature. The XRD analysis of pristine PVA films as can be seen in Fig.5.2, shows a peak at 19.6° 2θ, followed by weak signal at ~22^{O}. These features are indicative of a semi-crystalline polymer.

The graphene oxide filler intercalated PVA (PGO) composites exhibited similar features displaying only one major peak corresponding to PVA (Fig.5.2). No peak corresponding to graphene or graphitic carbon layers was discernible. This observation clearly demonstrates that the regular periodic structure of graphene oxide disappears as it fully exfoliates into individual sheets in the polymer matrix. One might also argue that the overall volume fraction of the filler is too low to get any appreciable signal from the filler phase. Nevertheless, the PGO-1 composite films displayed an increase in the intensity of the PVA peak, with features identical to those of pristine PVA film. The peak at 19.6^{O} was considerably more intense along with the appearance of faint signals at 27^{O} that correspond to PVA only. Increase in the intensity of the diffraction peak corresponds to more number of PVA chains packing together resulting in increased crystalline domains of PVA [306]. This is indicative of the increased number of small crystalline domains of PVA, rather than an increase in its size. An increase in the crystallite size evolves with a clear sharpening of the peak. In the current set of results, the intensity increases, but the width of the peaks remain similar to the pristine PVA signal. It may thus be inferred that incorporation of GO in the PVA matrix with lower concentrations of 0.4 and 0.8% does not appreciably influence the crystallinity of PVA. However, 1% GO loading, improves polymer crystallinity.

The diffractogram for the hydrazine reduced PGO composites namely, PGH-0.4, PGH-0.8, and PGH-1 composite, had phase evolution almost similar to that of the PGO composites. The crystallinity of the PGH-0.4 and PGH-0.8 was almost similar to pure PVA composites. The crystallinity for the PGH-1 was the highest amongst the PGH series of samples. However, the XRD intensity of PGH-1 was slightly lower than that of the PGO-1 composites. One can reconcile two observations from the XRD data of the two different types of composites. Literature suggests contradictory views on the crystallinity of polymers in general and for PVA in particular. While some reports indicate that GO improves crystallinity of PVA a few other reports have disputed.

Firstly, the crystallinity of the polymer composites starts to change only after a minimum level of loading of fillers. Secondly, the GO-based fillers induce better crystallization as compared to the reduced fillers. This can be explained by the fact that at these loading levels, the functional groups attached to the graphene oxide sheets start to bind to the polymer matrix inducing crystallization at the interfaces. The PGH samples, owing to the comparatively lower number of functional groups (as compared to that of the PGO-1 samples), are not able to induce many nucleation points. This can be ascribed to the reduction of the epoxy based functional groups and restoration of C=C bonds at the GO interface. This presumably decreases the number of heterogeneous nucleation points, thus reducing crystallinity.

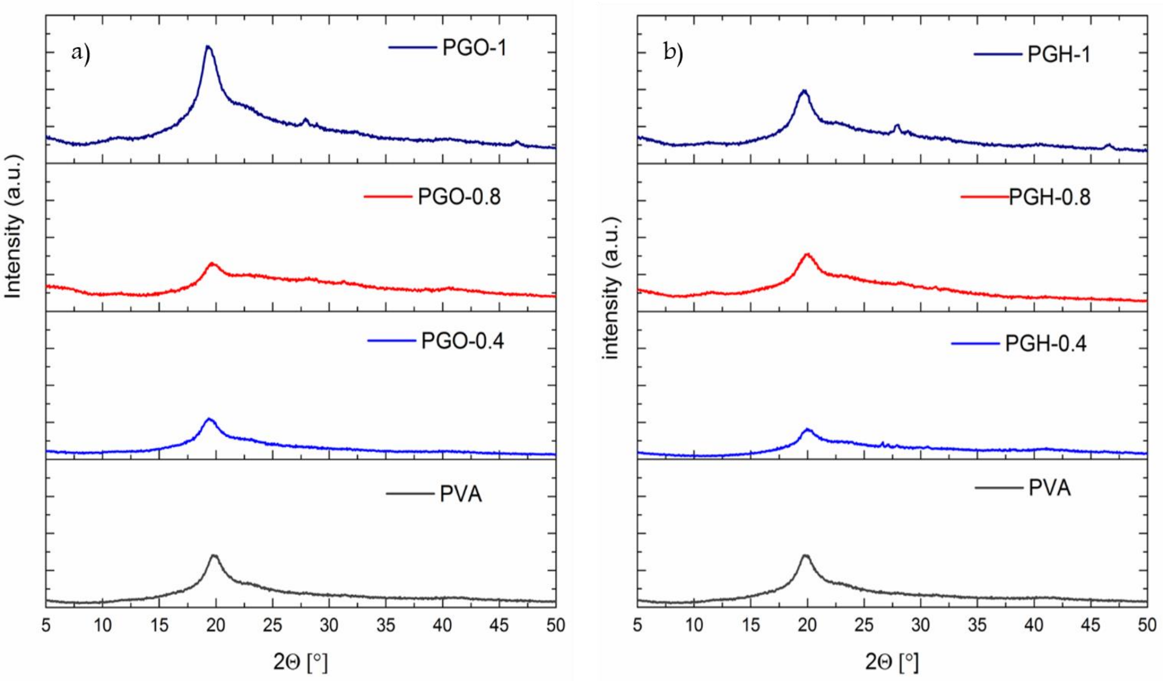

Figure 5.2. XRD diffractograms for (a) PGO series of composites (b) PGH series of composites; PVA is added in both figures for comparison. The scaling is same for all of the 8 patterns.

Differential scanning calorimetry (DSC) of the pure and GO reinforced composites was conducted to understand the thermal evolution and its relationship with the composite structure. The inflection point in the DSC traces was found out by drawing tangents and finding its intersection. This was termed as the glass transition temperature (T_g). The subsequent deep endotherm at higher temperature was marked as the melting temperature (T_m). On a gross approximation, the T_g can be used to understand the changes in the amorphous regions of the polymer and its transition to a rubbery state. The T_m, on the other hand, indicates melting of the crystalline domains in the polymer.

The results of glass transition (T_g) and melting temperatures (T_m) from DSC analysis of the films are listed in Table.5.1. The PGO and PGH films showed moderate variation in the glass transition temperature (Fig.5.3). PVA films displayed a T_g value of 105 °C. This value increases for the PGO-0.8 and PGO-1 composites to 114 °C and 117 °C. Such an increase in the T_g is attributed to the change in the polymer chemistry at the molecular level. PVA being a semi-crystalline polymer is composed of ordered chains and a few which are not ordered but are randomly strewn around. Intercalation of graphene oxide in these disordered chains (amorphous regions of the polymer), affects the polymer structure. Oxygen-containing groups on the graphene oxide sheets interact with the hydroxyl groups grafted on the PVA backbone [307]. This confines the movement of the random polymer chains in the matrix and affects the translational motion of these chains. Placing polymer chains in such a confined state by the fillers involves additional energy for the chains to wiggle and slither. This effectively occurs at a higher temperature than the pristine polymer, followed by the transformation from the rigid glassy state to a rubbery state. A similar increase in T_g for the PGH series was observed (Table 5.1), indicating incorporation of the fillers in the amorphous regions of the polymer.

Thermal behavior of the composites as analyzed from the DSC thermograms corroborate more or less with the findings from XRD analysis. The results suggest that there is no significant change in the melting point of the composites (the differences could be contained well within the error limits). However, clear differences in the T_g have been observed. This again underscores the fact that the polymer system is semi-crystalline. From the melting endotherm, the percent crystallinity was calculated, (Table 5.1).The increase in % crystallinity (χ_c) of the PGO-1 composite films corroborates the results from the XRD experiments. The ease of movements of the polymeric chains with an increase in temperature indicate the changes in T_g One can clearly observe the increase in the loading of fillers, the composite T_g moves to higher temperatures. This indicates that the filler constrains the movement of the polymer chains in the amorphous regions. Thus it can be inferred that the fillers (both GO and CCG) are uniformly and homogeneously dispersed within the amorphous regions of the polymer matrix even after drying of the films. The interpenetrating distribution of the fillers within the amorphous domains of the polymer is helped by the formation of hydrogen bonds between the polymer–OH groups and that of the filler. Such case also happens even in the CCG fillers as they also retain some of the carboxylic groups that are not affected by the hydrazine reduction. These bonds prevent the polymer chain mobility, thus increasing the T_g. In addition, the fillers also act as structural impediments to polymer chain mobility. Thus the glassy to rubbery transition is effectively delayed [191].

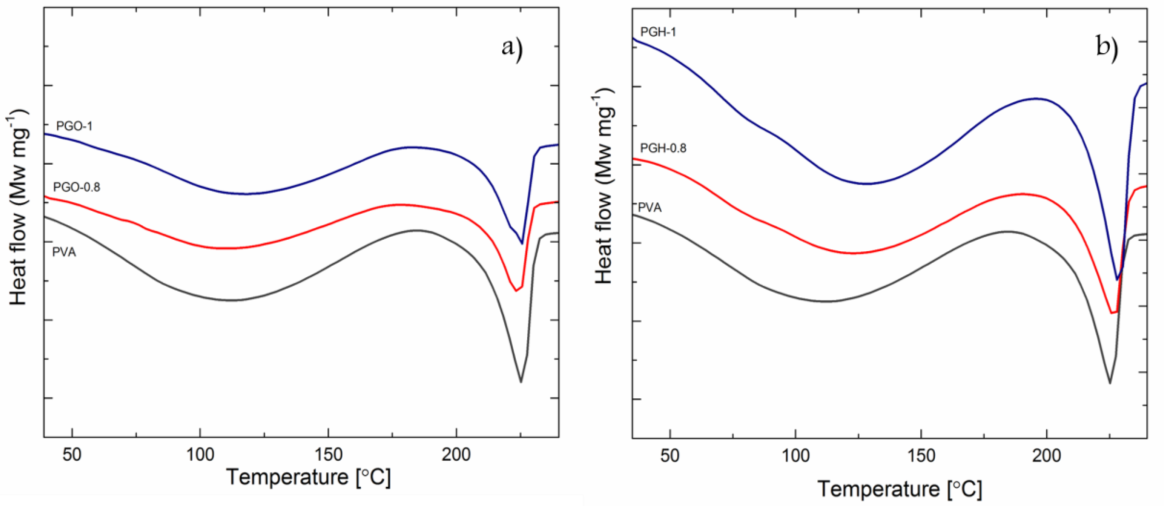

Figure 5.3. DSC thermograms of (a) PGO composites, (b) PGH composites.

Sample name	**T_g (°C)**	**T_m (°C)**	χ_c (%)
PVA	105	225	30
PGO-0.8	114	224	32.1
PGO-1	117	225	33.18
PGH-0.8	116	225	30.12
PGH-1	125	228	32

Table 5.1. Thermal properties of the PGO and PGH composites.

5.2 Infrared and Raman spectroscopy.

FTIR spectroscopy of the polymer composites (Fig.5.4) exhibited standard absorption peaks for the neat PVA polymer. Mainly composed of 1, 3-diol linkages $[-CH_2-CH (OH)-CH_2-CH (OH)-]$, a reflection of the –OH stretch is observed at 3200 cm^{-1}, and the CH_2 alkane stretch at 2947 and 2895 cm^{-1}. Along with, the C-H bend in the PVA molecule is observed at 1456 cm^{-1} and 1331 cm^{-1}. Peaks at 1140 and 1096 cm^{-1} are reflections of the crystalline and amorphous regions in the semi-crystalline polymer [308].

The PGO films are resultants of the dispersed graphene oxide sheets in the PVA polymer. Hence, these films exhibited similar functional features as that of the parent PVA. With skeletal peaks of OH, CH_2 and CH moieties, the composite films show additional bands at 1709 cm^{-1} (H-bonded C=O groups), 1734 (free C=O groups), 1595 cm^{-1} and 1556 cm^{-1} (stretching vibration of C=C and COO^- groups) respectively. Interestingly the PGO films display improvements in the crystallinity of the PVA polymer. The intensity ratio of (I_{1140}/I_{1096}) bands increases suggesting increased crystallinity as a function of the pristine polymer. PGH films on the other hand also present improvement in the crystallinity with an increase in the filler loading, but slightly lower than the PGO-1 films. Such relative changes are attributed to the reduced functional groups on the graphene sheets which do not sufficiently induce nucleation to enhance crystalline behavior as compared to the PGO -1 films.

On reducing the PGO films by hydrazine, the intensity of the C=C bonds increases signifying a reduction of the epoxy bonds on graphene oxide to graphene sheets in the PVA matrix, thus resulting in a small decrease in the mechanical properties of the PGH composites as compared to PGO.

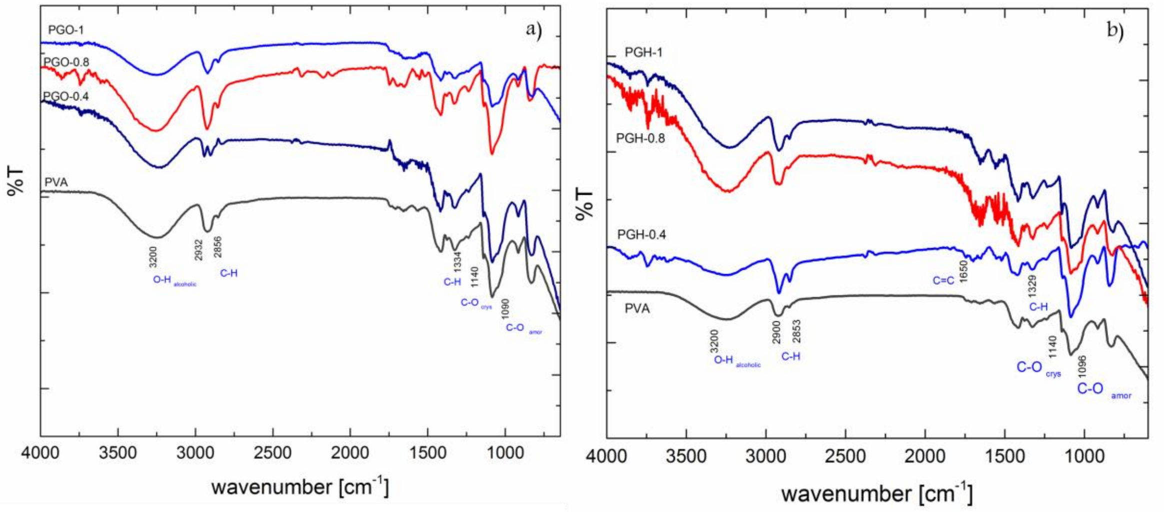

Figure 5.4. FTIR spectra for the PGO and PGH composite films.

Based on these results, we surmise that all of the functional groups of graphene oxide are not reduced in the *in-situ* reduced composites. The CCG_H fillers are not the ideal graphene sheets. Some of the functional groups, in particular, the epoxy groups on the basal plane of GO sheets, are reduced in the hydrazine reduction process. However, the groups on the edge of the sheets (according to the Lerf-Klinowski model) are –COOH and –OH groups that tend to remain even after hydrazine treatment as seen in (step B, Fig.5.5) [160]. The absence of functional groups on the basal plane may have facilitated orientation of the CCG_H sheets in the plane of the film. The groups at the edge of the sheets can still form hydrogen bonds with the polymer matrix.

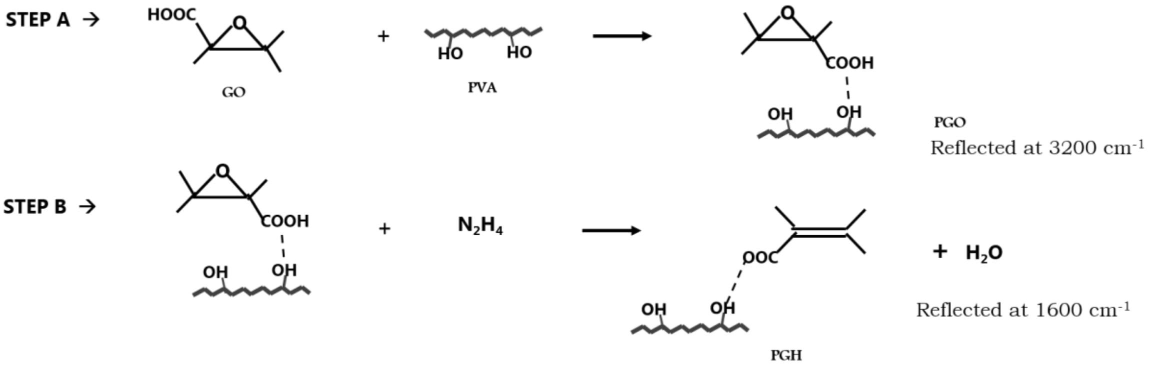

Figure 5.5. Reaction scheme for the formation of PGO and hydrazine reduced PGH composites.

The Raman spectra for the PGO composites (for example PGO-1) produced the D band at 1314 cm^{-1} and the G band at 1598 cm^{-1}(Fig.5.6). The G position is interestingly similar to that of GO powders. This indicates that the extent of defects in the in-plane graphitic layers remain almost the same. This is consistent with our approach that in the PGO series of composites, GO fillers are simply better dispersed in the matrix without any chemical modification. Likewise, the D band of the PGO-1 composites stayed fairly close to that of graphene oxide (1316 cm^{-1}). The I_D/I_G ratio, which is indicative of the inherent disorder in the carbon structure, also stayed similar (1.53 for GO vs. 1.57 for PGO-1). The subtle increase in the can be ascribed to better and homogeneous dispersion of the fillers with all the edges of the fillers contributing to the disorder.

On the other hand, the PGH series of composites (PGH-1), exhibited the G peak at 1595 cm^{-1}, and the D peak at 1321 cm^{-1}. The shift of the G peak to a lower wavenumber clearly indicates restoration of the conjugated carbon bonds in the in-plane structure. This is presumably due to the reduction of the epoxy groups by hydrazine. The shift of the G peak thus results from the disappearance (or decrease) of the D′ peak at 1620 cm^{-1} which influence the position of the G peak. Additionally, the I_D/I_G ratio was 1.27 (against 1.53 for the GO powders), indicating improvement in structural order. Therefore, Raman spectrometry clearly demonstrates the difference between the structural order of the fillers in the PGO and PGH series of composites.

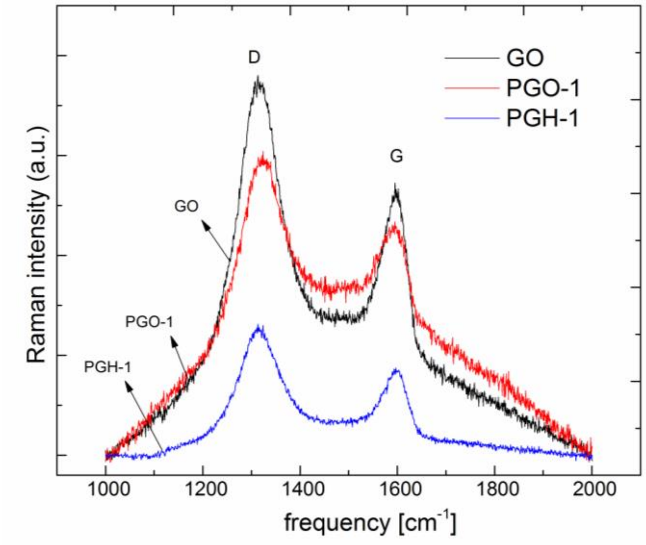

Figure 5.6. Raman spectra for the PGO and PGH composite films.

5.3 Positron annihilation lifetime spectroscopy.

Positron annihilation lifetime spectroscopy was conducted on select samples from the PGO and PGH series. To see the effect of the extent of filler loading, and also the reduction of the fillers, samples with 0.4 and 1 wt% loading of PGO and PGH series were used, along with the pure PVA samples for normalization. The positron lifetime spectra were recorded using a slow, fast coincidence spectrometer having a time resolution of ~ 190 ps. The peak-normalized raw data of the samples are as shown below.

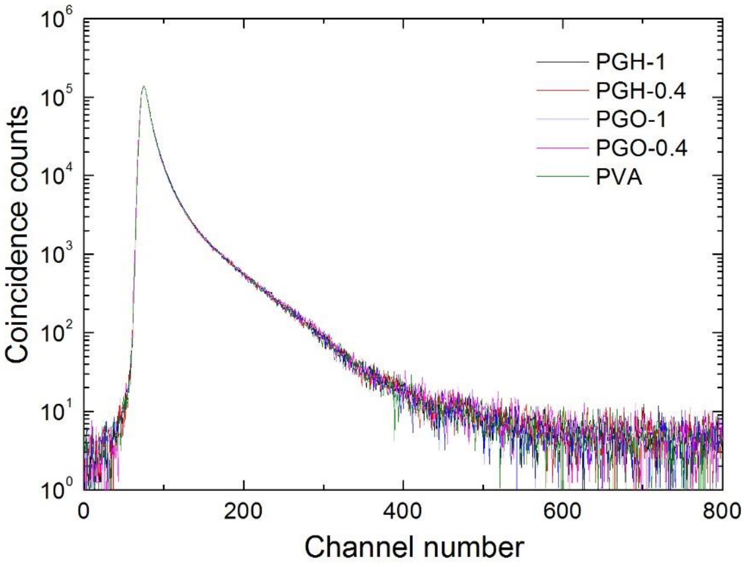

Figure 5.7.Peak normalized positron lifetime spectra of all of the samples indicating multi-exponential nature of the curves.

Figure 5.7 indicates a multi-exponential nature of the positron lifetime spectra with basically three exponential terms. Each spectrum can be described as

$$I(t) = I_1 e^{\frac{-t}{\tau_1}} + I_2 e^{\frac{-t}{\tau_2}} + I_3 e^{\frac{-t}{\tau_3}} \ldots\ldots\ldots\ldots Eq\ (i)$$

Where τ_1, τ_2, and τ_3 are the positron/positronium lifetimes, and I_1, I_2, and I_3 are the corresponding intensities. The data were further analyzed using the PALSfit program.

The analysis confirmed that the positron lifetime spectra of all the samples essentially had three components; as τ_1, τ_2 and τ_3 in the ascending order of their magnitudes (Table 5.2). The largest lifetime τ_3 arises out of annihilation of orthopositronium (o-Ps) atoms. These are metastable bound states of an electron and positron in each and with the spin of both aligned in the same direction. (If the spins are aligned in opposite directions, it is called parapositronium (p-Ps)). o-Ps atoms are supposed to have a fairly large lifetime of 140 ns in a vacuum but, in a material medium, it is cut short to only a few nanoseconds by an electron with an opposite spin from the surroundings. This is called the “pick-off” process.

SAMPLES	**LIFETIMES (ns)**			**INTENSITIES (%)**			**τ_f (ns)**	**τ_m(ns)**
	τ_1 (ns)	τ_2(ns)	τ_3(ns)	I_1 (%)	I_2 (%)	I_3 (%)		
PVA	0.1315	0.3232	1.2950	37.3142	43.6871	18.9987	0.1328	0.4363
PGO3	0.1353	0.3272	1.3299	37.6298	43.8840	18.4862	0.1373	0.4403
PGH3	0.1329	0.3289	1.3215	37.3997	44.3400	18.2603	0.1344	0.4368
PGO1	0.1395	0.3364	1.3052	38.0349	43.4863	18.4788	0.1423	0.4405
PGH1	0.1436	0.3362	1.2978	37.7181	43.6028	18.6791	0.1472	0.4432

Table 5.2 Peak normalized data of the multi exponential nature of the films fitted by the program PALSfit.

The o-Ps lifetime is a useful tool for the estimation of free volume sizes in the polymer sample. This comes from the Tao-Eldrup equation

$$\tau_3 = 0.5\left[1 - \frac{R}{R_0} + \frac{1}{2\pi}\sin\left(\frac{2\pi R}{R_0}\right)\right]^{-1} \ldots\ldots\ldots Eq\ (ii)$$

Where τ_3 is expressed in ns and the radius R in Å. Also, $R_0 = R + \Delta R$ where ΔR is the empirical electron layer thickness set equal to 1.66 Å.

Also often calculated is the free volume fraction f, which is expressed as $f = AV_fI_3$ where $V_f = (4/3)\pi R^3$ is the size of the free volumes in $Å^3$ and A is a constant, which is taken as 1/400 when the intensity I_3 is taken in %. The average radius of the free volume defects present in the samples is 2.10 Å and there are little variations in size or concentrations with GO reinforcement or reduction. The fractional free volume f is obtained as 1.75%.

There are changes however in the shorter lifetimes, τ_1 and τ_2, which are as follows. Both of the positron lifetimes increase with increase in the concentration of GO in the polymer. Note that τ_3 and its intensity I_3 do not change significantly, and hence the free volume defect size or their concentrations are unaffected by the GO inclusion. Not only I_3, even the other two intensities I_1 and I_2 are not affected by the GO inclusion or reduction. This means the overall defects concentration within the samples are also practically unaffected.

Thus the only change visible is a change in the defect present at the filler-polymer interface. If GO is dispersed in the polymer matrix in the form of nanostructured fillers/particles, there is the possibility that positrons are trapped at the GO-polymer interface. The interface is a physical region between the GO nanoparticle surface (edges) and the surrounding polymer. It can act as an extended positron trapping defect. τ_2 is the lifetime of the positrons getting trapped and annihilated in this defect. Since it increases with GO concentration, it implies that the size of this defect increases with GO concentration. This indicates that the interfacial area (region) pertaining to filler and the matrix increases with the increase in GO loading.

The shortest lifetime τ_1 comes from two reasons. There can be free annihilation of positrons in the polymer. This means a fraction of positrons can get annihilated with free electrons, without getting trapped into any kind of defects. The second contribution to τ_1 comes from the residential time of positrons getting trapped into the defects. It is difficult to point out how much fraction of the positrons are getting annihilated within the GO/CCG nanoparticles or within the polymer. The intensity I_2 is only a qualitative indication.

The bulk positron lifetime τ_f calculated from the analyzed results using the equation:

$$\frac{1}{\tau_f} = \frac{I_1}{\tau_1} + \frac{I_2}{\tau_2} + \frac{I_3}{\tau_3} \ldots\ldots\ldots. Eq\ (iii)$$

Eq. 3 shows the same kind of variation as the shorter lifetime τ_1. This follows from the relations:

$$\frac{1}{\tau_1} = \frac{1}{\tau_f} + \kappa_d \ldots\ldots\ldots\ldots.. Eq\ (iv)$$

Where the positron trapping rate

$$\kappa_d = \frac{I_2}{I_1}\left[\frac{1}{\tau_f} - \frac{1}{\tau_1}\right] \ldots\ldots\ldots. Eq\ (v)$$

Since the intensities, I_1 and I_2 did not change significantly in this case and the change in τ_2 is rather small, the trapping rate κd did not change significantly and τ_f simply followed the trend of τ_1. The positron trapping rate is also related to the defect concentration C through the relation κ_d=μC, where μ is called the specific trapping rate, the above observation will imply that the defect concentration within the samples did not change appreciably. Thus the only change we could observe was a small increase in size of the GO nanoparticles. That the defect concentration did not change appreciably means the nanoparticles could not agglomerate through the polymer matrix. In other words, their mobility was severely restricted. Heat treatment at different temperatures may give more information on this aspect.

The average positron lifetime τ_m defined as

$$\tau_m = \frac{\tau_1 I_1 + \tau_2 I_2 + \tau_3 I_3}{I_1 + I_2 + I_3} \dots\dots\dots\dots\dots\; Eq\ (vi)$$

Also did not change significantly, as shown in table 5.2. The results of analysis of the coincidence. Doppler broadened spectra are given below. The analysis is done as follows. The annihilation gamma rays going in opposite directions are recorded using two high pure germanium detectors. The background is significantly reduced by using the coincidence output as a mastergate. A two-parameter spectrum is then generated with the sum of the energies and their difference as the two coplanar perpendicular axes and the counts in the third axis.

A one-dimensional projection of the counts channel wise in the energy range 1022 ± 2.4 keV parallel to the energy difference axis was then made. The above curve was then divided by an identical curve obtained for a reference sample (PVA chosen in this case). The ratio thus generated is plotted against the electron momentum on the x-axis. The results of the above analysis are shown in figure 5.8, from which the following conclusions can be obtained.

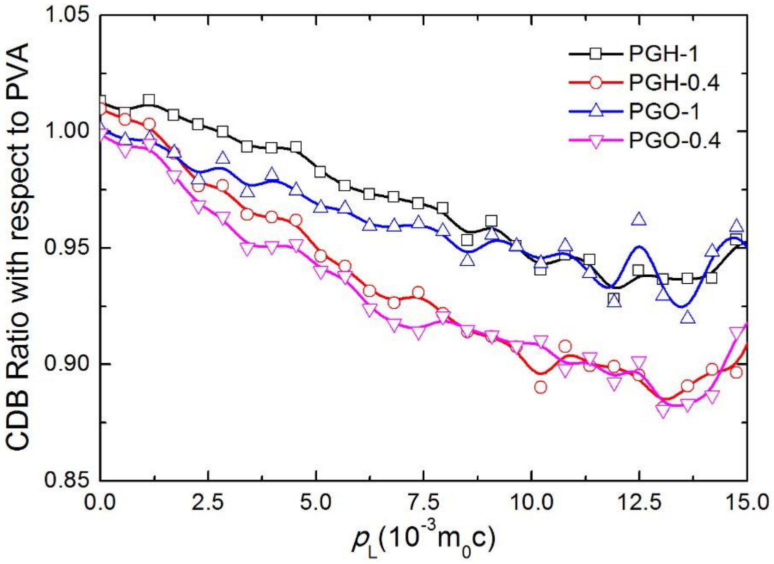

Figure 5.8. Coincidence Doppler broadening spectra of the composites area normalized with respect to that of pure PVA.

The overall electron momentum within the samples is not significantly altered due to the reduction treatment. The PGO and PGH curves of a given GO concentration appear within the error bars (not shown in the figure).

There is, however, a notable difference between the curves of PGO-0.4 and PGO-1. With increasing GO concentration, the curves are vertically shifted implying increased annihilation of positrons within the GO environment. Similar behavior was also seen for the PGH series of composites, where the CDB spectra of PGH-1 sample was vertically shifted with regards to that of PGH-0.4 samples. This can be explained by the fact that in the higher loaded samples, the extent of new interfaces created are much higher. As observed by microscopy, the fillers found homogeneously distributed in the composites. Thus the highly enlarged polymer/filler interface in the higher GO/CCG loaded samples are responsible for the annihilation of the o-Ps. This is consistent with the variation in τ_2 for all of the samples.

In summary, it can be said that the reinforcement with graphene oxide based fillers basically induced no considerable changes to the free volume defects. Furthermore, the concentration of the nanovoids or their distribution was also not affected. These are new information and are surprising because of heterogeneous environments, such as free volume defects when introduced, have been found in many material systems as effective sites for the segregation of impurities or foreign elements. On the contrary, the free volume defects are neither unaffected by the GO reinforcement, nor by their reduction to CCG. However, the bulk polymer is getting affected by the presence of GO, as indicated by the change in τ_f

and it is a significant observation. For, it emphasizes the extremely high reactivity of GO and its ability to form complexes with polymers and radicals. The fact that these complexes form and exist as defect sites at the matrix/filler interfaces, as evidenced by increased annihilation of the o-Ps, indicate that the influence of the interfaces can be modified or tailored to enhance mechanical properties.

5.4 Mechanical behavior.

The uniaxial tensile properties of the pristine as well as reinforced PVA composite films with a filler content of 0.4%, 0.8%, and 1% were evaluated, and the values were provided in Table 5.2.

The pristine PVA films showed average stiffness of 0.34 GPa and tensile strength of 23 MPa, which are typical values for PVA (although the same polymer with a different molecular weight can have different tensile properties). The reinforced composites, on the other hand, showed considerably improved tensile strength values as the filler loading was increased from 0.4, 0.8 to 1 wt. %. For the PGO-0.4 composites, the elastic modulus and tensile strength were 1.03 GPa and 77 MPa. Likewise, the PGO-0.8 films exhibited improved elastic modulus and tensile strength values of 84 MPa and 1.6 GPa. However, loading the polymer with a higher percentage of filler of 1%, the PGO-1 films produced higher tensile strength but a lower elastic modulus of 2 GPa and 130 MPa respectively. These values are exceptional in the sense that without any functionalization, the simple incorporation of GO in the PVA matrix at the level of 0.4, 0.8 and 1% resulted in improved mechanical properties. Representative stress-strain traces and their histograms are provided in the Fig.5.9 & Fig.5.10.

The *in situ* hydrazine reduced graphene oxide PVA composites (PGH-series) showed slightly different mechanical properties. At 0.4 wt.% filler loading (PGH-0.4), the composites showed 0.34 GPa elastic modulus, which is similar to that of neat PVA. However, there was a considerable improvement in the tensile strength (51.8 MPa). The ductility was largely unchanged with 110% strain at failure against 125% for the PVA films. However, at 0.8% and 1% loading of the fillers (PGH-0.8 and PGH-1), the elastic modulus found was 1.5 and 1.6 GPa respectively. These values are highly encouraging indicating values in the range of 400- 500% of the neat PVA properties. Additionally, what is more, interesting is the retention of ductility in these materials despite significant improvement in the elastic modulus. The composites failed on an average strain at failure of 150 and 165% for the PGH-0.8 and PGH-1 composites.

The ultimate strength at these loadings (0.8-1%) appears comparable in the range of 97-99 MPa, which of course are much higher as compared to that of neat PVA. The yield strength of the composites followed a trend similar to that of tensile strength. Representative stress-strain traces and histograms of the PGH composites are provided in Fig 5.9.

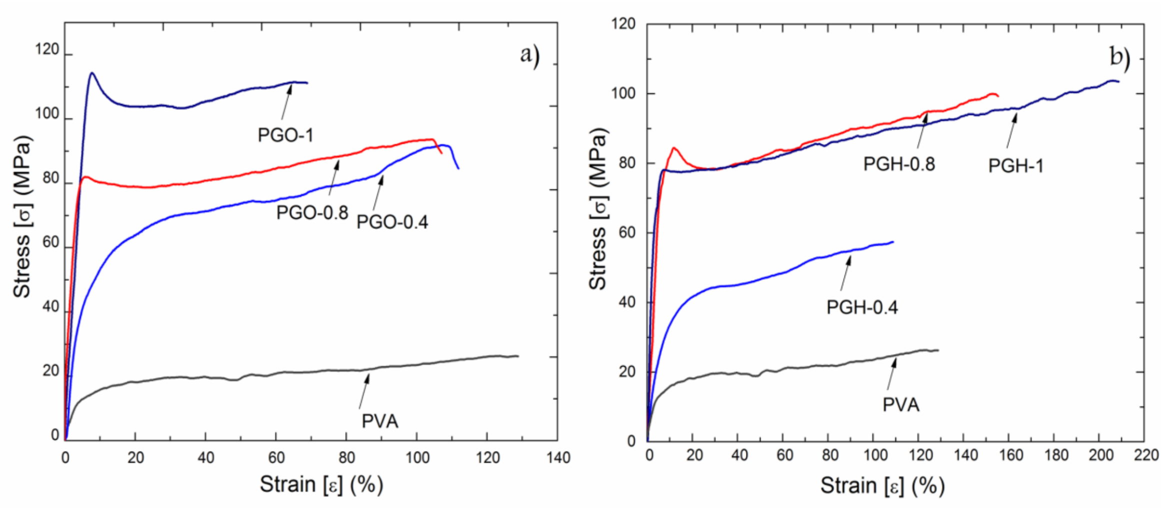

Figure 5.9. The representative stress- strain curve for PGO and PGH films.

Sample name	Youngs modulus (GPa)	Ultimate strength (MPa)	Elongation at break (%)	Yield strength (MPa)
PVA film	0.34 ± 0.04	22.47 ±3.6	125	15.76±3.0
PGO-0.4	1.03 ±0.38	77.36 ±25.3	110	60.35±17.5
PGO- 0.8	1.66 ±0.27	84.65±9.87	105	75.09±5.3
PGO-1	2.08 ±0.43	130.31±13.7	75	129.28±14.4

Table 5.3. Mechanical property evaluation of PGO curves.

Sample name	Youngs modulus (GPa)	Ultimate strength (MPa)	Elongation at break (%)	Yield strength (MPa)
PVA film	0.34± 0.04	22.45 ±3.6	125	15.37±3.0
PGH-0.4	0.46±0.07	51.83± 3.96	110	42.29±6.1
PGH-0.8	1.56±0.43	99.76±9.82	150	98.67±15.0
PGH- 1	1.68±0.53	97.64±26.87	165	76.64±17.9

Table 5.4. Mechanical property evaluation of PGH curves.

Some interesting features stand out from the data set. Generally, an increase in elasticity is observed with a decrease in the failure strain [309]. However, the current results from PGO composites exhibit improved elastic modulus, tensile strength, as well as high ductility, which is a desired combination of properties. Also, PGH composites exhibited improved tensile strength with a profound increase in ductility.

To summarize at a loading of 1 wt.% graphene oxide in PVA, we observed more than 5 times increment in elastic modulus and tensile strength (Fig.5.10). The property enhancement was attributed to the homogeneous distribution of fillers, and strong interfacial interactions (hydrogen bonds) between the fillers and the matrix. Composites fabricated after *in-situ* reduction of GO fillers did not alter the elastic modulus, but increased the strength ~350%. The failure strain of CCG based composites was much higher than that of both pure PVA and GO reinforced PVA composites, thus showing enhanced ductility.

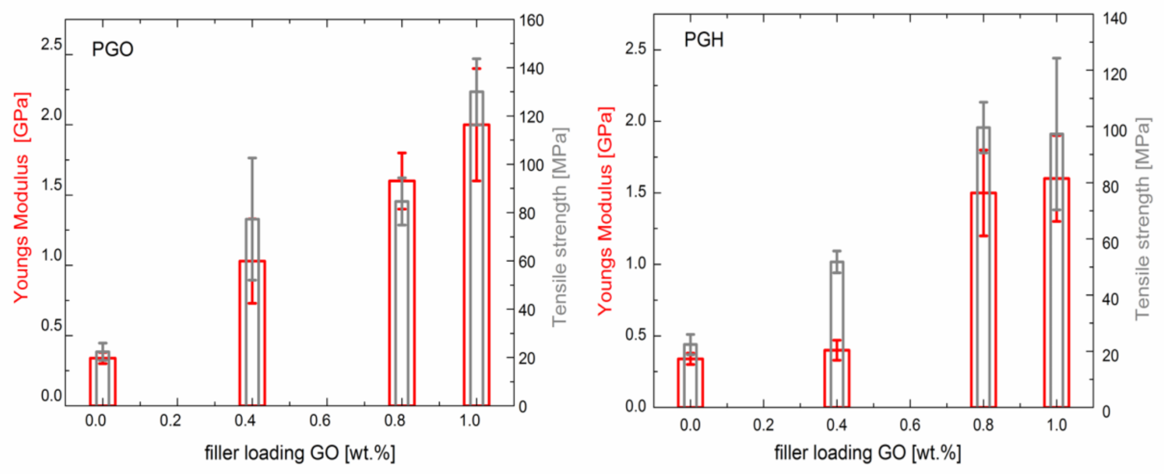

Figure 5.10. Results of mechanical properties of the PGO and the PGH composites.

Another interesting feature was the exhibition of strain softening in the reinforced composites (both PGO and PGH). The composites stay stable in the elastic regime with excellent load transfer from the matrix to the fillers. Further application of load, beyond the elastic limit, the slippage of the polymeric chains in the matrix is facilitated; thus relieving the stress with further yielding of the matrix. Additionally, the large extent of ductility (large strain before failure) also indicates a significant amount of load transfer during plastic deformation also. This indicates that the fillers remain strongly bonded to the matrix even at this stage. The comparatively large failure at strain of the PGH composites indicates some contribution from morphology, which is discussed in the next section.

5.5 Interfacial interactions.

Load transfer depends on interfacial interactions of the reinforcement with the matrix. GO bears oxygen-containing functional groups that are capable of forming strong bonds at the polymer interface, resulting in efficient load transfer. Strong interactions at the interface tend to restrict molecular chain movement resulting in higher tensile strength. This suggests that formation of such interfaces between the matrix and the reinforcement influence the mechanical properties of the heterogeneous polymer systems including filler intercalated polymer matrices.

Evaluation of such interfaces was quantitatively characterized for each type of the nanocomposite film with the help of Pukanszky equation [271]. This model describes the influence of surface treated filler (regarding the presence of functional groups) on the tensile strength of a polymer composite. It comprises of an interfacial interaction factor $B_{\sigma y}$ and the equation for tensile strength takes the form

$$\sigma_y = \sigma_{yo} \frac{1-\varphi_f}{1+2.5\varphi_f} \exp\left(B_{\sigma y}\varphi_f\right) \dots\dots\dots \mathrm{Eq}(vii)$$

Where φ_f is the volume fraction for the composites, σ_y and σ_{yo} is the tensile strength of the neat polymer film and the composite film respectively and $B_{\sigma y}$ is the interaction factor. The volume fraction of the filler is calculated by the using the density of the constituents:

$$V_f = \frac{\rho_C}{\rho_f} W_f \ ; \ \rho_C = \rho_f V_f + \rho_M V_M \ \dots\dots\dots\dots\dots\dots Eq(viii)$$

Where V_f and W_f are the volume and weight fractions of the graphene filler, V_f and V_M are the volume fractions of the filler and polymer matrix respectively. ρ_f and ρ_M are the densities of the graphene filler and matrix with values as 2.25 g/cm^3 for GO and 1.3 g/cm^3 for the PVA polymer. Utilizing the values of different weight fraction of the filler, their corresponding volume fractions are obtained as 0.24, 0.47 and 0.59 volume fraction of the GO.

Pukanszky model describes a relationship of functionalized graphene at the polymer interface. This model suggests that surface treatment/functionalities present on graphene oxide surface embedded in the polymer matrix are responsible for the increased interfacial interaction. Furthermore, factors such as the size of the interface, aggregation of filler at the interface are also responsible for the increased or decreased interfacial interactions, and hence the mechanical properties of the composites.

The empirical value of $B_{\sigma y}$, for each system can be determined from the experimental results. Assigning a physical meaning to this parameter improves the theoretical and practical approach to this model.

Evaluating the $B_{\sigma y}$ values for the PGO system (Fig.5.11a), the interaction factor for tensile strength increased from 1.2, 1.33 to 1.77 for a filler loading of 0.24, 0.47 and 0.59 volume fraction of the filler, corresponding to PGO-0.4, PGO-0.8 and PGO-1 films. Such an increase in the values of the interaction factor and the experimental values for tensile strength, suggest strong adhesion/interaction of the filler to the polymer matrix. This interfacial interaction results in adherence of the polymer to the filler surface, and an increase in the tensile strength.

In the case of hydrazine reduced PGO films, with a volume fraction of 0.24, 0.47 and 0.59 of CCG$_{H}$ filler, the interaction parameter displayed values of 0.85, 1.49 and 1.51 for PGH-0.4, PGH-0.8, and PGH-1 films respectively (Fig.5.11b). These values increased, with the increase in volume fraction of the *in-situ* reduced composite films. The values of the interaction parameter, however, clearly suggested that the PGO system had comparatively higher interactions at the interfaces as compared to the PGH composites at similar filler loading. This is consistent with our observed fact that in the composites with reduced form of the fillers, the interface interactions are comparatively lower due to the disappearance of various functional groups, especially the epoxy groups. Therefore, the interface interactions in the PGH composites are presumably edge- to edge interactions through remnant carboxylic and hydroxyl groups.

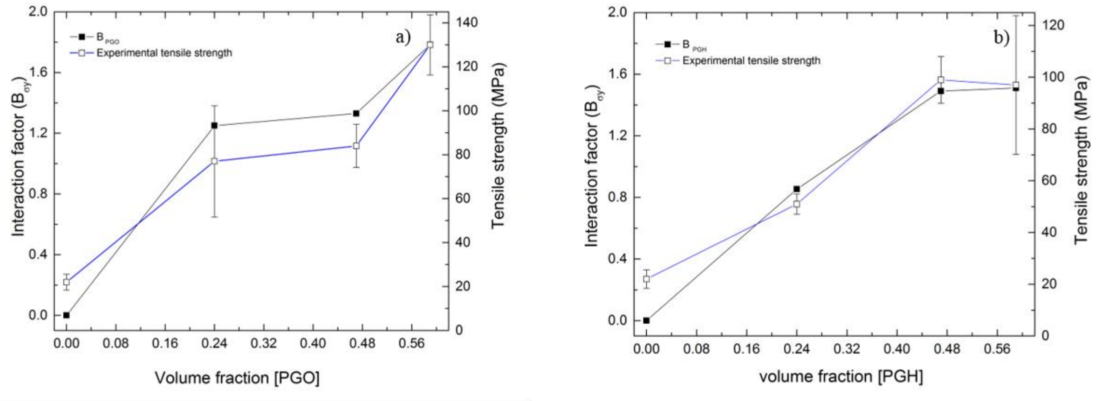

Figure 5.11. Dependence of interaction factor B on the tensile strength of (a) PGO-composite and (b) PGH composites for their corresponding volume fractions.

5.6 Morphological and microstructural aspects.

The morphological studies of the nanocomposites reveal some interesting information about the composites. The cross section of the PVA film (Fig.5.12) indicated features typical of a glassy polymeric system with no appreciable contrast. In the PGO films, however, outlines of the filler can easily be observed. In addition, in the PGO-0.4 composites, the GO layers were found to be randomly oriented, with no preferred direction of alignment. While strong interfacial bonding explains the enhanced tensile strength and modulus of the PGO composites, the ductility of these films can be attributed to the random alignment of the fillers. It is possible that on the application of stress, the randomly oriented GO fillers progressively align themselves parallel to the stress axis, thus increasing the strain. The basal plane of the GO structure contains the epoxy groups that get reduced by hydrazine. The filler density in the higher loaded samples was apparent from the micrographs. The randomly oriented fillers (as in PGO-0.4) were found to be comparatively better aligned for the PGO-0.8 samples, with the fillers showing pull-out from the matrix. The PGO-1 samples showed distinct kind of microstructures with clearly pulled out and recoiled fillers. This kind of microstructures has never been observed in a GO-reinforced PVA system to the best of author’s knowledge.

These images indicate extensively deformed samples where the sheet-like fillers have been rolled into a (presumably) tubular form or scrolls. The strong interfacial bonding between the polymers and fillers effectively transfers the load to the fillers. After failures, the fillers tend to recoil back to thermodynamically stable wavy structures. This enables improvement in tensile strength and elastic modulus by multiple factors, along with the retention of considerable ductility, a combination of properties rarely reported in the literature.

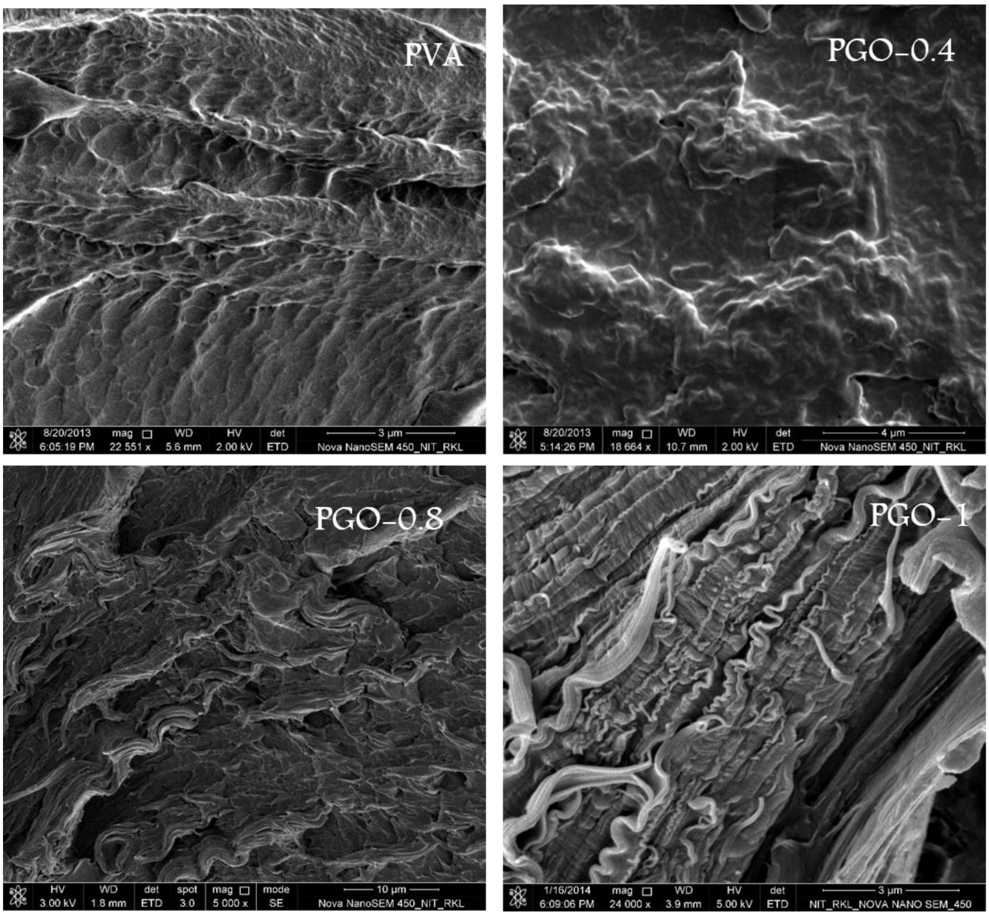

Figure 5.12. Microstructures of pristine PVA, PGO-0.4, PGO-0.8 and PGO-1 composites.

The cross-sectional morphology of the *in-situ* reduced PGH composites (Fig.5.13) exhibited preferred alignment of the fillers parallel to the film plane even at a filler content of only 0.4 wt%. Reducing the filler in the matrix, the randomly arranged structure orients itself to a “brick and mortar” structure. This lamellar arrangement for the reduced graphene oxide-PVA films arises due to the lack of interfacial bonding between the basal planes of the fillers. Additionally, such beneficial mechanical properties have been achieved at an extremely moderate level of the fillers. As discussed earlier, the PGH-0.4 samples showed the aligned orientation of the fillers. Interestingly, upon higher loading of the fillers (e.g., PGH-0.8 samples) similar microstructural features were observed with the layered arrangement of the fillers. Even for the PGH-1 samples, the distribution clearly showed outlines of the graphene reinforcement aligned parallel to the plane of the polymer composite.

Slippage of the CCG_H fillers can occur upon loading in the PGH composites, due to the lack of interfacial interactions between the basal planes of CCG_H and the PVA matrix. Such a process can lead to a high strain of the film. Moreover, platelet restacking or incomplete exfoliation results in a lowered effective modulus values due to decreased aspect ratio [310]. However, the fact that higher loading of filler does not decrease the mechanical properties indicate excellent homogeneity of the samples as seen by the electron microscopy.

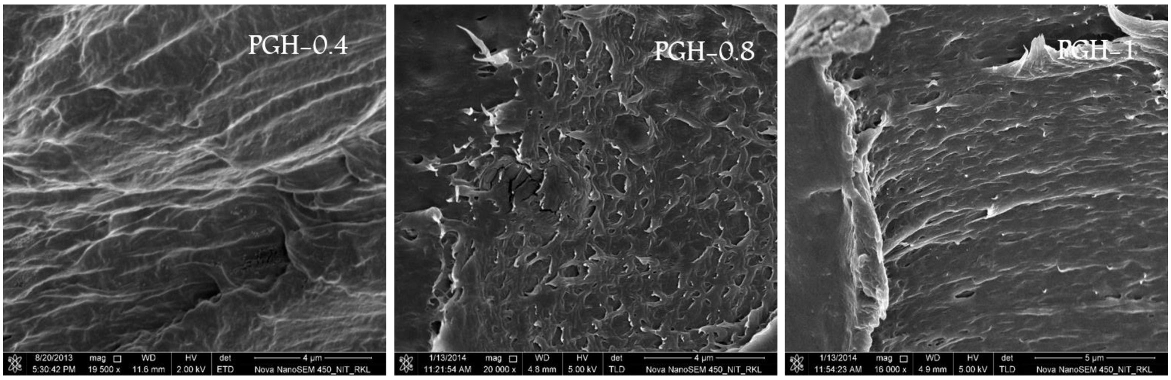

Figure 5.13. Microstructures of PGH-0.4, PGH-0.8 and PGH-1 composite films.

5.7 Chapter Summary.

The salient features of the chapter can be summarized as follows:

- GO loaded PVA nanocomposites with a filler loading of 0.4, 0.8 and 1 wt% exhibited considerably improved crystallinity of the composites at the highest filler loading. The *in-situ* reduced composites with hydrazine also exhibited similar features although the percent crystallinity was lower than the corresponding unreduced composites.
- Significant improvement in mechanical properties was observed (unreduced and reduced), especially in elastic modulus and tensile strength. While the *in-situ* reduced composites (PGH) showed strength and elasticity slightly inferior to the PGO composites, their failure strains were higher, indicating improved ductility.
- The results of Positron annihilation lifetime spectroscopy underscored the importance of interface regions that act as positron trapping sites. The level of trapping increased with filler loading. No apparent discrepancy between the positron trapping rates of PGO-1 and PGH-1 composites indicate equivalent levels of microstructural homogeneity and interface area density. Additionally, it was found that no additional nanoholes and voids were produced in the matrix due to the reinforcements.

- At a lower loading of GO fillers, the composites had microstructures which were random, while *in-situ* reduction indicated aligned morphology. At higher loadings, however, both of the unreduced and hydrazine reduced composites showed mostly aligned morphology.
- Strong interfacial bondings at the edges and planes for the PGO series indicating the homogeneous distribution of fillers in the PVA matrix, was ascribed to the substantial improvement in mechanical properties. The *in-situ* reduced composites had similar interfacial bonds, presumably only at the edges of the sheets and not in the in-plane regions.

CHAPTER 6

TEOA functionalized reduced graphene oxide reinforced PVA nanocomposites.

In this chapter, the fabrication and properties of triethanolamine functionalised graphene oxide based PVA composites have been discussed.

The TEOA functionalized GO reinforced PVA composites have been named as PGTO-0.4, PGTO-0.8, and PGTO-1, corresponding to graphene oxide loading of 0.4, 0.8 and 1wt%, respectively (Fig.6.1). Visibly these films appeared blackish brown to dark black in color on reduction with increasing wt % of filler in the PVA polymer. Overall, the distribution of the fillers appeared to be uniform without any speckled contrast from the films.

Figure 6.1. Digital images of the fabricated PGTO films at 0.4, 0.8 and 1wt% filler loading.

6.1 Structural and thermal behavior.

The diffractograms of the PGTO series of samples showed slightly improved crystallinity as compared to both PVA and PGO composites. Even at the level of 0.4%, the composites showed clearer and more intense signals ~ 19.6° 2Θ (Fig.6.2). The intensity progressively increased with higher loading of the fillers. One can argue that since the TEOA reduction step does not completely exfoliate the graphene layers in the GO, as it forms a combination of very thin graphitic crystallites and few-layered graphene oxide domains (Fig.4.18), crystallization of the polymer colloid may have been favored in these domains. This would technically result in a phase separated polymer matrix where the crystalline regions of the polymers are generally in the vicinity of the fillers, and the amorphous regions are elsewhere. Moreover, due to the formation of relatively large sized filler regions as an effect of TEOA reduction, the homogeneity in the distribution of the fillers in the composite is comparatively poor. This however is a hypothesis.

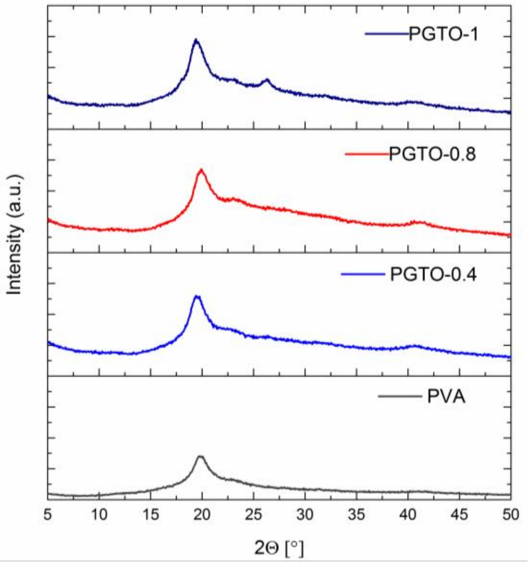

Figure 6.2. X-ray diffractograms of triethanolamine treated GO reinforced PVA composites. Pure PVA is included for comparison.

The XRD diffractograms can be correlated with the thermal behavior of the composites. The PGTO films displayed T_g values of 109 and 110°C for the PGTO-0.8 and PGTO-1 composites, respectively (Fig.6.3). Thus there is a consistent change of T_g by 4-5°C with a subtle change in the filler concentration. This clearly indicates that the mobility of the amorphous domains in the PGTO composites is hindered with respect to that of pure PVA. However, the changes in the T_g for the PGTO composites were not much as it is in the case of PGO or PGH composites. As suggested earlier, that the fillers are distributed uniformly throughout the amorphous regions in the PGO composites. In a similar argument, one can say that the distribution of the fillers in the amorphous regions in the PGTO composites may not be as uniform. It is also corroborated by the fact that TEOA functionalization effectively reduces the volume of graphene oxide by increasing the stacking of the reduced graphene oxide phase as well as the exfoliated graphite phase.

The DSC thermograms, on the other hand, did not show any considerable increase in the melting temperature. However, from the melting endotherm, percent crystallinity (χ_c) was calculated that exhibited slightly higher crystallinity for the PGTO composites. These observations are in agreement with the XRD results.

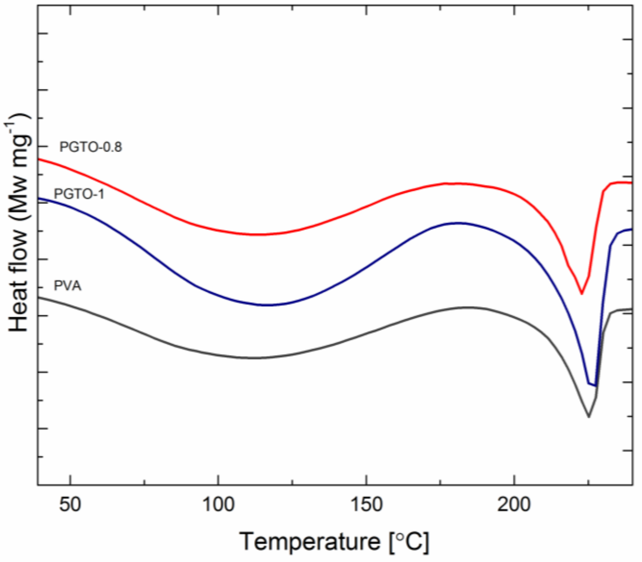

Figure 6.3. DSC thermograms of PGO and PGTO curves.

Sample name	**T_g (°C)**	**T_m (°C)**	**χ_c (%)**
PVA	105	220	30
PGTO-0.8	109	223	30.8
PGTO-1	110	223	32.3

Table 6.1. Thermal properties of the PGTO composites.

6.2 Infrared and Raman spectroscopy.

FTIR spectroscopy was utilized to understand the effect of reductant on the fabricated PGTO composites. Reduction of graphene oxide by TEOA in the PGTO films is confirmed by the presence of new absorption peaks of C=C bonds at 1650 cm^{-1} and C-N bonds at 1248 cm^{-1} (Fig.6.4).

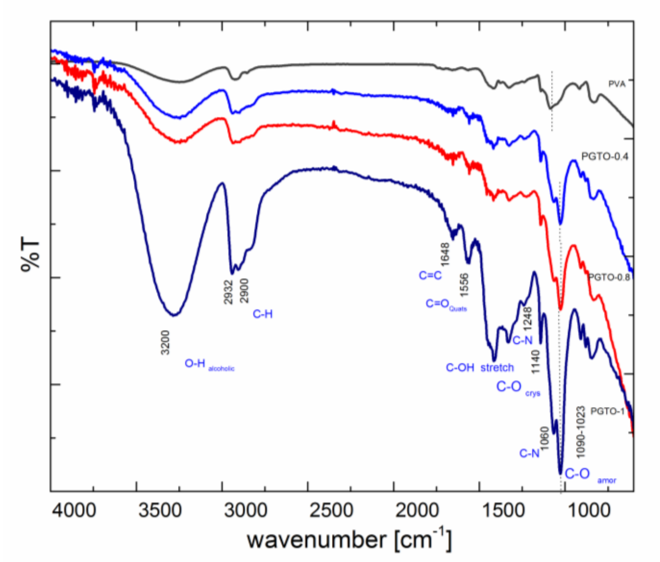

Figure 6.4. FTIR spectra for the PGTO composite films.

GO is comprised of a set of uncharged polar groups on the basal planes as epoxy and hydroxyl, few charged hydrophilic peripheral groups as COOH and few hydrophobic π-bonds domains [311]. Triethanolamine (TEOA), which is a combination of an amine and alcohol, reduces the epoxy bonds of GO to conjugated C=C structures in the PVA matrix in a similar manner as discussed in chapter 4. Simultaneously, it attacks the hydrophilic peripheral groups i.e. carboxylic group to produce conjugated carboxylate salts of quaternary amines, via hydrogen bonding, as reflected at 1566 cm^{-1}, (Fig.6.5, step B). Vis-a-Vis, the alcoholic groups, present in the TEOA moieties interact with the uncharged polar groups, (sp^2 networks, where present) on basal planes (-OH), via non-covalent interactions (π-π stacking). These bindings occur on moieties that do not involve in oxidation (remnant groups on GO) [312, 313]. These non-covalent functionalizations induce strong cohesive forces amongst the basal planes of the sheets, which result in the stacking of the sheets to some extent, which is also observed in the XRD spectra of the CCG$_{\text{TEOA}}$ powders.

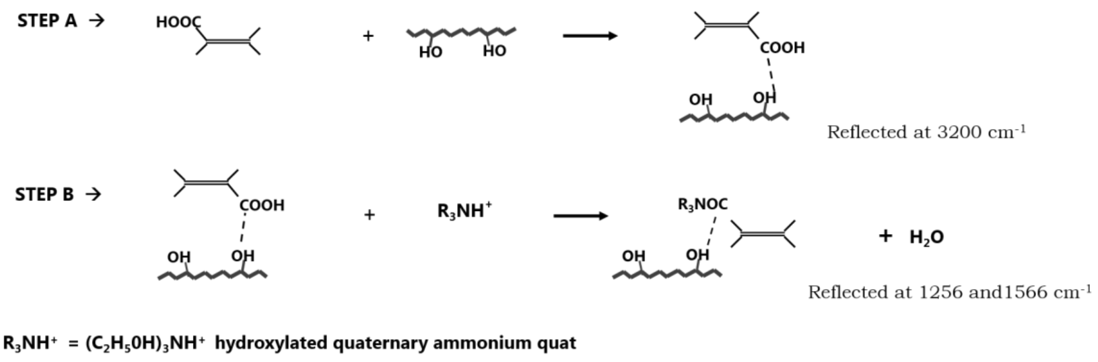

Figure 6.5. Reaction mechanism of TEOA in the fabrication of PGTO composites.

Further, a very distinct shift is observed in the C-O unbonded amorphous domains of the polymer chains. PVA polymer which reflects their amorphous domains at 1090 cm^{-1} significantly shift to 1028 cm^{-1} for the PGTO films. The shift in the peak position and wavenumber of the amorphous peak appears as a result of the non-homogeneity of the fillers in the amorphous regions of the PVA matrix.

Wavenumber	Functional groups	PVA	PGO	PGTO
3280-3257	-OH alcoholic	✓	✓	✓
2900-2930	CH_2 stretch	✓	✓	✓
1650-1600	C=C stretch		✓	✓
1566	Carboxylate salts			✓
1428	Aliphatic CH_2	✓	✓	✓
1325	CH bend	✓	✓	✓
1248,1060	C-N , aliphatic amines			✓
1140	Bounded C-O crystalline zone	✓	✓	✓
1090	Unbounded C-O amorphous zones	✓	✓	✓ (shifts to 1028)
825	Liberation peaks of PVA and water	✓	✓	✓

Table 6.2. Various energy absorption regions as reflected from the FTIR spectra.

Raman signals of carbon in the PGTO composites showed the G peak at 1595 cm^{-1} and the D peak at 1314 cm^{-1} (Fig.6.6). The G peak position was similar to that of the PGH-1 composites, indicating better ordering and reduced defects in the in-plane structure of the fillers. The D-peak however, indicate the existence of other functional groups at the filler edges that bond with the polymer matrix.

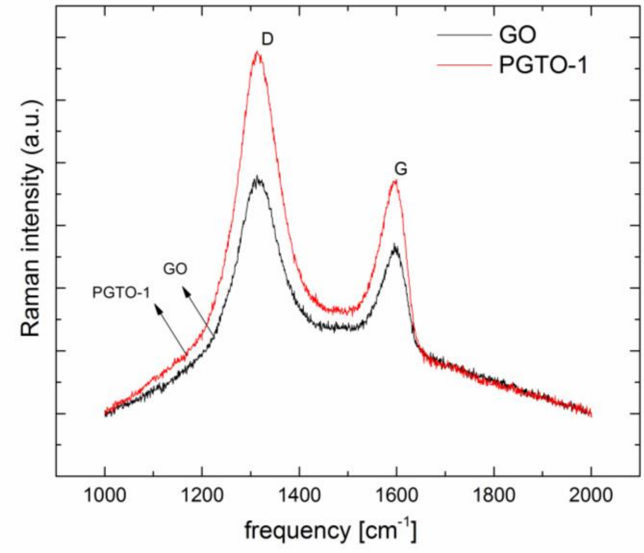

Figure 6.6. Raman spectra for the PGTO composite film.

6.3 Mechanical behavior.

The uniaxial tensile properties of the pristine as well as reinforced PVA composite films were carried out, and the values are provided in Table 6.3. The uniaxial tensile stress-strain plots (Fig.6.7), present properties that are similar to the PGO composites. The composites exhibited 65.8, 80.6 and 96.4 MPa tensile strength for 0.4, 0.8 and 1% TEOA reinforced PVA-GO composites. These values are slightly lower than their corresponding PGO composites. This behavior is congruent with the enhancement of strength by incorporation of carbon-based fillers. However, the effect of the TEOA functionalized GO fillers on the elastic modulus of the composites was not clearly noticeable. The modulus found were 0.6, 0.7, 0.9 GPa for the PGTO-0.4, PGTO-0.8, and PGTO-1 samples respectively. Although, these values are better that the elastic modulus of PVA, are clearly not so exciting as was the case with PGO or PGH.

One of the most important outcomes from this set of composites was that significantly large strain at failure values was observed for the PGTO films. These values are correspondingly higher as compared to their PGO counterparts. The improvement in ductility was very high for the PGTO-0.8 and PGTO-1 composites to the extent of 200% strain at failure. To investigate, if the *in situ* functionalization by TEOA changes the polymer matrix, in addition to the changes in the graphene oxide fillers, the neat polymer was treated with TEOA and films were fabricated. The films named PTO did not have any fillers. Mechanical property evaluation of these films (PTO) exhibited a tensile strength of 22 MPa, similar to the pure PVA values and the elastic modulus of 0.2 GPa which is considerably lower than that of pure PVA. Therefore, it follows that TEOA reduction step profoundly influences the elastic modulus of the polymer matrix itself.

Therefore, it may be concluded that TEOA mostly acts as a plasticizer for the composites. Although there has been an improvement of elastic modulus in the composites, the TEOA effect on the polymer matrix greatly offsets the effect of the fillers on elastic modulus. As a result, the overall improvement in the elastic modulus appears only moderate.

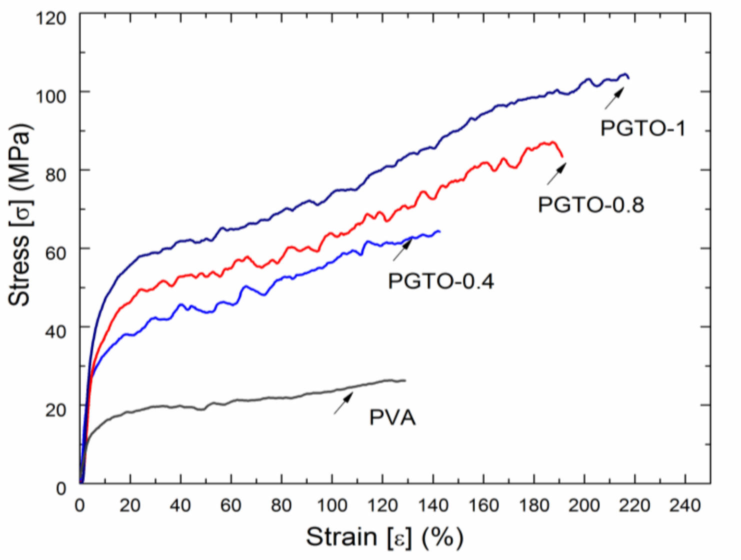

Figure 6.7. Representative stress-strain curve for the PGTO films.

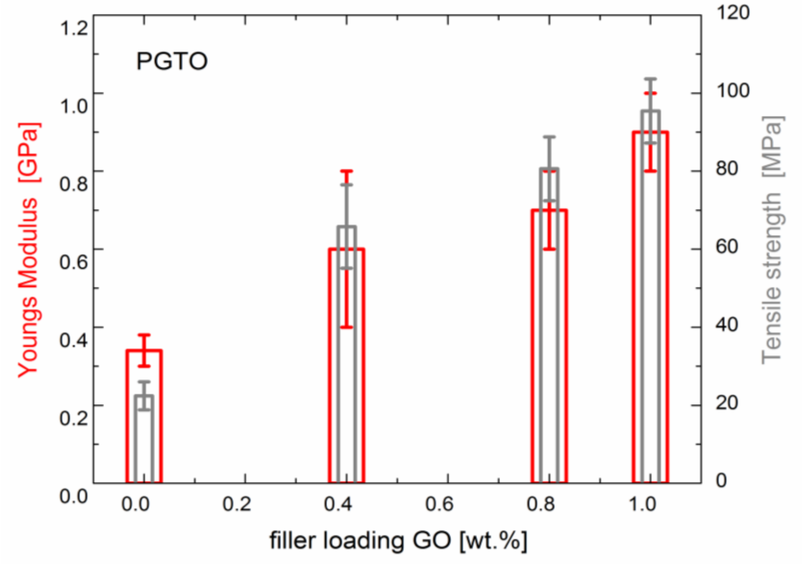

Figure 6.8. Results of mechanical properties of the PGTO films.

Sample name	Youngs modulus (GPa)	Ultimate strength (MPa)	Elongation at break (%)	Yield strength (MPa)
PVA film	0.34± 0.04	22.4 ±3.6	125	15.7±3.0
PGTO-0.4	0.65±0.42	65.58±10.67	152	44±15.20
PGTO-0.8	0.76±0.14	80.67±8.23	180	46.62±4.43
PGTO- 1	0.98±0.15	95.48±8.24	200	53.22±3.74
PTO	0.25±0.01	22.44±7.88	287	21.65±4.27

Table 6.3. Mechanical property evaluation of PGTO curves.

6.4 Interfacial interactions.

Interaction factor $B_{\sigma y}$ for the PGTO composites display emperical values of 1.22, 1.29 and 1.46 for the composites at filler loading of 0.24, 0.47 and 0.59 % volume fraction of GO in the PVA matrix. These values are low as compared to the PGO films with same volume fraction of GO, suggesting decreased interfacial interaction of the PGO films on reduction with TEOA. Ideally, surface treatment of the GO filller in the PVA matrix, produces increased interfacial interactions. However, incase of PGTO films treating the GO fillers with functional groups from TEOA results in the reduction of surface tension of GO filler, producing a non–reactive interface. These reduced interfaces are resultants of two factors, stacking of the reduced fillers in the matrix and the random orientation of the stacked fillers in the matrix.

Moreover, the presence of stacked structures in the matrix does not allow a preferred orientation or alignment to occur. This further hinders the homogeneous adherence of the filler to the polymer surface and hence a suitable interface is not obtained.

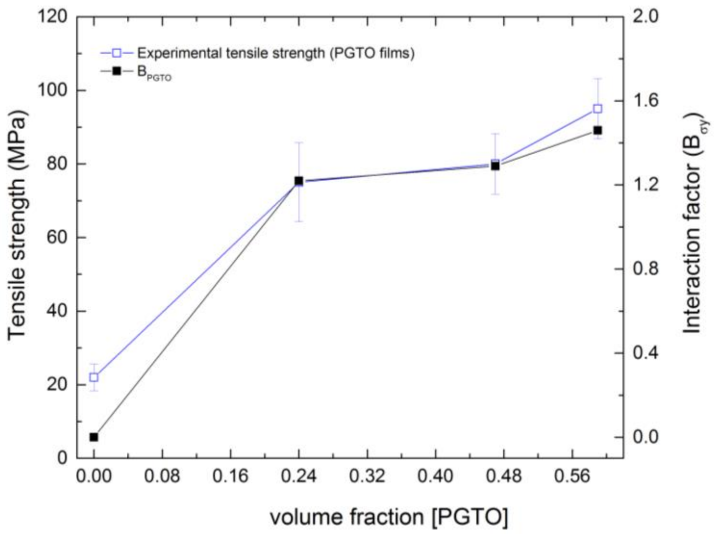

Figure 6.9. Dependence of Interaction parameter B on the tensile strength of the PGTO composites for their corresponding volume fractions.

6.5 Morphological and microstructural aspects.

The morphological features of the nanocomposites are correlated with the information acquired from the tensile tests. The pristine PVA film indicates features typical of a glassy polymeric system with no appreciable contrast as was seen in the earlier chapters. In the PGTO films, the random orientation of the filler becomes dominant with the increasing filler content. The images display fine contrast of the filler against the polymer (Fig.6.10).

Surprisingly, the cross section of the TEOA reduced PGO composite films also revealed a randomly arranged and aggregated morphology. These films did not any produce distinct features in the morphology as compared to their PGO counterparts. These obtained features describe the stacking of the reduced sheets in the PVA matrix to reduce the interfacial interactions with the matrix (Fig.6.10). The little increase in the mechanical properties of the reduced films arises as a result of the interfacial bonding between the filler and the matrix. With increasing filler concentration, these sheets induce interfacial debonding with the PVA polymer resulting in reduced strength as compared to the PVA-GO films but are considerably more ductile.

Based on these results, we surmise that in the *in-situ* reduction of the GO fillers with TEOA as a reductant reduces the epoxy groups of the graphene sheets, but attaches to the edge of the sheets connecting to the PVA chains via non-covalent linkage. Additional linkages at the basal planes due to the hydrogen bonding between the OH of TEOA and OH on the basal planes of GO, increase the cohesive energy amongst the sheets and finally stack over each other, resulting in weak bonding of these sheets with the polymers. These weak linkages induce slippage amongst the sheets resulting in increased ductility but reduced strength. The absence of functional groups on the basal plane may have facilitated orientation of the CCG_{TO} sheets in the plane of the film, but the aggregation of the films reduces the passivity of orientation.

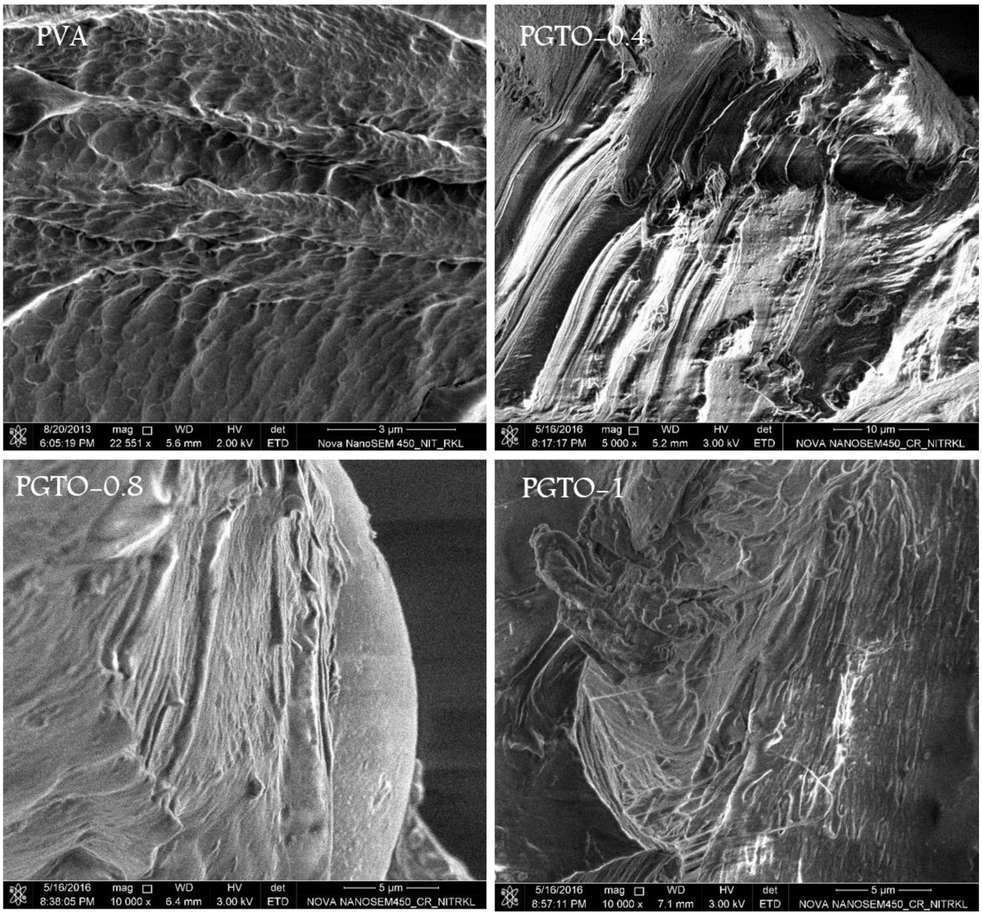

Figure 6.10. Microstructures of the TEOA reduced GO reinforced PVA nanocomposite.

Based on these findings, the microstructure of the PGTO composites can be suggested as per Fig.6.11. Here two types of fillers, such as few layered graphene oxide (with expanded interplanar carbon structure), and few layered graphite (with an interplanar distance similar to that of graphite) are shown. This is deduced from the XRD results of the CCG_{TEOA} fillers, as depicted in Chapter.4. These fillers are presumably well distributed within the polymer matrix with a considerable amount of crystalline domains contiguous to the fillers. The fact that the fillers are somewhat more clustered in the PGTO systems as compared to the PGO, the extent of polymer/filler interfaces formed are significantly reduced. For the lack of interfacial strength, these composites exhibit comparatively inferior load transfer, thus the results of mechanical properties.

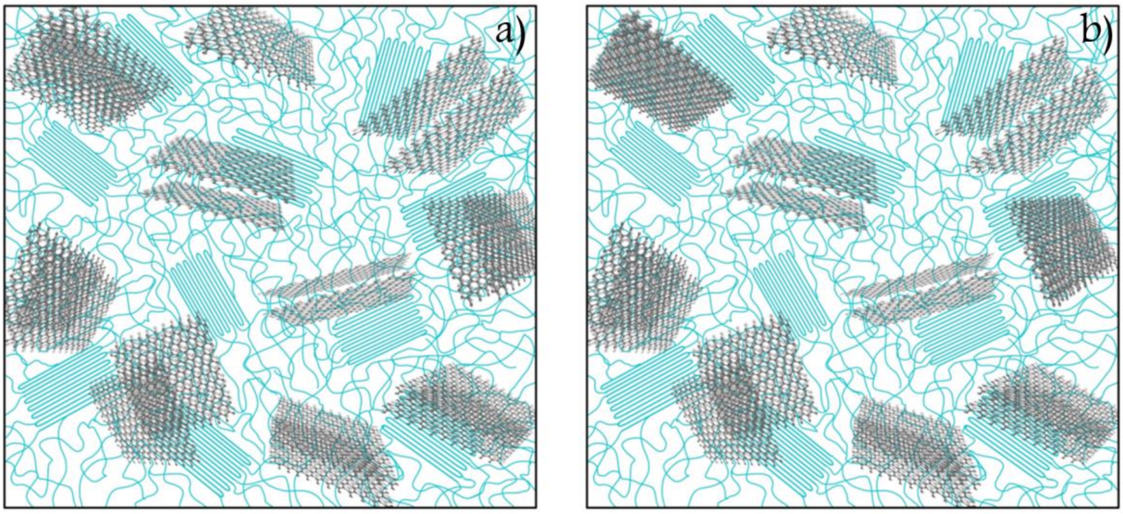

Figure 6.11. State of dispersion of GO in PVA polymer in (a) PGO composites (b) PGTO composites films.

6.6 Chapter summary.

- Dark brown to absorbing black colored PVA film were fabricated by functionalizing graphene oxide with triethanolamine.
- Graphene oxide sheets with restored C=C structures from epoxy groups are accompanied with strong non-covalent interactions between the OH groups on the basal planes of fillers and the alcoholic groups of the TEOA molecule.
- The microstructure can be thought of as a combination of few layered GO fillers and few layered stacked graphene sheets, which rendered relatively lower extent of polymer/filler interface.
- The mechanical properties were better than pure PVA, yet were not as good as the PGO or PGH composites, which can be ascribed to the reduced interfacial interactions between the fillers and the matrix.
- Triethanolamine possibly may have reacted as a plasticizer which was evident from the large failure strain values of these composites.

CHAPTER 7

Interface strengthened triethylamine functionalized graphene oxide reinforced PVA nanocomposites.

A novel fabrication route for the polymer nanocomposite was followed in this section. GO fillers (at various wt% level) were loaded with PVA aqueous blends along with in situ functionalization with triethylamine (TEA). Fabrication, microstructure, and properties of these composites are discussed in this chapter.

In the previous chapters, it was clearly evident that the formation of maximized interface area between the polymer and the fillers is an important aspect for the enhancement of mechanical properties. *In-situ* treated GO with or without hydrazine in the PVA composite led to the excellent dispersion of the fillers, which led to an appropriate increase in the mechanical properties. Along with dispersion of the fillers, it was also important to create bonding interactions between the fillers and the matrix. The PGO composites, due to their intrinsic oxygen-containing functional groups, the GO fillers created strong hydrogen bonds with the matrix, leading to efficient load transfer. In the PGH composites, due to the reduction of the fillers, the extent of interfacial interactions was slightly reduced. However, the well-aligned morphology helped improve the mechanical properties. The objective here is to create a homogeneous distribution of the fillers and enable strong interfacial bonds at the matrix/filler interface. Triethanolamine functionalization clearly did not work as well as simple GO reinforcements, due to the aggregation of the fillers that led to a drastic reduction in the interfacial contact area. Therefore, in this chapter, a different kind of amine namely, triethylamine, was used as the *in-situ* reductant in the processing of the composites. It was shown in chapter 4 that TEA reduction eliminates some of the oxygen-containing functional groups and restores the carbon double bonds imparting sp^2 character in the carbon sheets. The same reduction procedure was followed in the fabrication of polymer composites. Thus desired composites are termed as PGT series, with the wt% of fillers tagged with it.

The composite films physically appeared very smooth and uniform with clear black colouration. These films were clearly different from the brownish-dark color of the GO reinforced PGO films. Additionally, the films indicated higher black intensity as the filler quantity progressively increased from 0.4, 0.8 to 1% (Fig.7.1).

Figure 7.1 Digital images of the PGT series of nanocomposites films.

7.1 Structural and thermal behavior.

The X-ray diffractograms of the TEA functionalized GO reinforced PVA nanocomposite films (PGT-series) showed interesting trends in crystallinity. Even at the filler level of 0.4 wt%, the composites exhibited enhanced peak intensity at 19.6° 2Θ as compared to the signals of pure PVA. This particular intensity increased progressively with the addition of a higher amount of filler, as can be seen in the XRD plots for the PGT-0.8 and PGT-1 composites. The fact that the signal intensity increased without a change in the FWHM values of the peaks indicates that the crystallite sizes of the PVA remain almost the same. Only the number of such crystallites got increased with higher loading of the fillers. A direct observation of the structural nature of the fillers could not be commented upon from the XRD plots of the composites because the volume fraction of the fillers is extremely low for any meaningful signal. However, if we consider the XRD spectrum of the CCG_T presented as Fig.4.23, it is clear that the expanded interlayer distance of GO disappears and the CCG_T powders exhibit no peak at all. Only very weak signals observed at 26° 2Θ, indicating the formation of an extremely fine stack of the graphene sheets. It is expected that similar reduction and structural evolution would occur in the *in-situ* TEA functionalized GO reinforced PVA composites. This essentially indicates that the composites have homogeneously distributed graphene fillers and that the stacking of the graphene layers is extremely small.

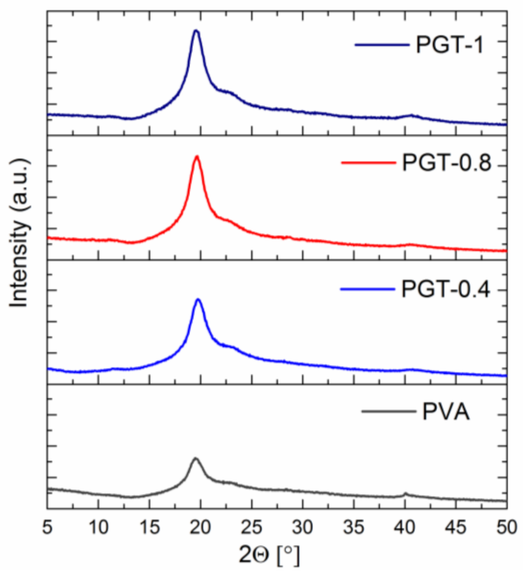

Figure 7.2. X-ray diffractograms of the PGT series of films. PVA is added for comparison.

The changes in the crystallinity of the PGT samples from the XRD diffractograms are corroborated with their glass transition temperatures obtained from the DSC thermograms (Fig.7.3). The PGT films displayed T_g values of 106 °C and 107 °C at filler loadings of 0.8 and 1% respectively. These values were lower than the T_g values of the PGO films (114°C, 117°C) with the same filler loading, but resembled more to the T_g values of the PVA values (105°C).

Changes in the T_g values of a polymer composite are attributed to the orientation of the graphene sheets in the polymer matrix [30]. Generally, graphene sheets intercalated in the amorphous domains of the polymer matrix affect the mobility of the amorphous chains thus increasing T_g of the composites. This was clearly observed in the PGO-series of the composites. However, it was seen that the T_g of the PGT composites were not greatly affected by the presence of the graphene fillers. Considering the enhanced crystallization of the composites, it can be argued that most of the crystallization of the polymers occur at the fillers (the GO sheets acting as the heterogeneous sites for nucleation), and there was less intercalation of the amorphous regions in and around the fillers. In other words, it can be said that the amorphous regions of the PGT-composite films were more or less like the amorphous regions of the pure PVA films. However, the crystalline domains in the PGT composites were different in that the regions formed contiguous to the graphene oxide reinforcements as seen in the (Figure 7.3). Since T_g is a representation of the polymeric chain mobility primarily in the amorphous regions, we observe no change in the T_g of the PGT composites as compared to pure PVA.

The PGT samples exhibit increased crystallinity with an increase in the filler loading. Well-dispersed fillers produce higher number and active interfaces that act as heterogeneous nucleating sites allowing the formation of ordered crystalline domains. These molecular chains away from such an interface require higher energy to form polymer crystallites. This accelerates the growth of the already formed crystallites at the filler-matrix interface, resulting in higher crystallization of the composites. Thus, it can be said that the composite has many regions of better crystalline order with GO reinforcements, and the volume of the amorphous domains are uniformly distributed withing the composite.

Interestingly new features were observed in the melting regions of the PGT composites. There was a small peak at 227°C, followed by a larger endotherm at 230°C. Both of these peaks were at comparatively higher temperatures than that of pure PVA (224°C). The first peak at 227°C is attributed to the melting of imperfect crystals formed due to annealing. Crystals formed at low crystallization temperature suggest a low degree of imperfection. These crystals partially melt and then recrystallize to give thicker crystals during the DSC scans. The second endotherm is the conventional melting of all the crystals in the polymer composite [314]. The slightly enhanced melting temperature may be attributed to the strong interaction of the crystalline domains with functionalised graphene (oxide) fillers.

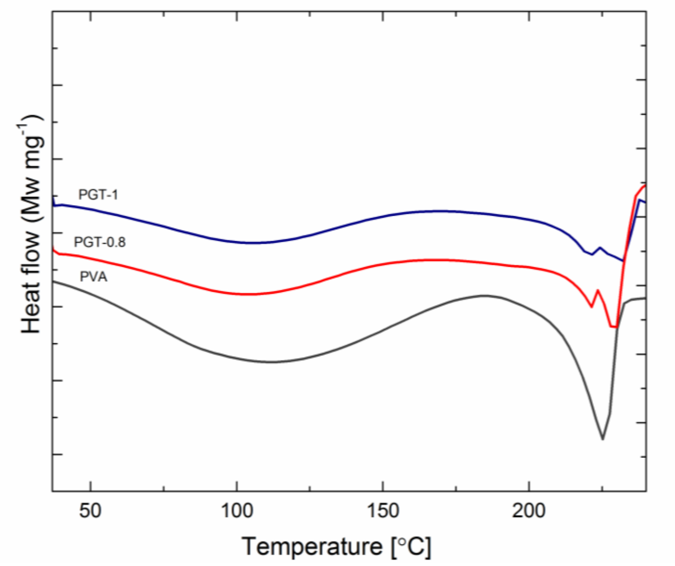

Figure 7.3. DSC thermograms of the PGT composites.

Sample name	T_g (°C)	T_m (°C)	χ_c (%)
PVA	105	220	30
PGT-0.8	106	230	36.8
PGT-1	107	230	38.6

Table 7.1. Thermal properties of the PGT composites.

7.2 Infrared and Raman spectroscopy.

FTIR spectra of the PGT-composites provide further evidence of the chemical interactions between the matrix and the fillers. Characteristic peaks of different functional groups present in the pristine PVA film, and PGO composites are identified in the (Fig.5.4). Herein, we present the chemical changes achieved on the TEA functionalization in the PGT composite films at varying filler load of 0.4, 0.8 and 1 wt%.

TEA is a tertiary amine that does not produce any absorption in the spectra. This makes its distinguishable from primary and secondary amines. Therefore, the spectra of PGT films show new peaks only at 1250 cm^{-1} (C-N stretch), and 1560 cm^{-1} (C=O salts). Along with a broad peak at 3200 cm^{-1} (OH, alcoholic peak), which appears due to the inhibition of the NH bonds of TEA with GO confirms the bonding of PVA with GO via hydrogen bonding (Fig. 7.4).

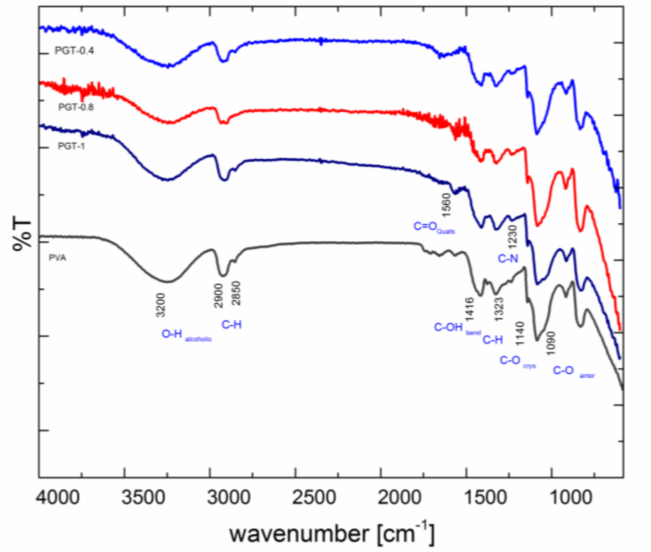

Figure 7.4. FTIR spectra of the PGT composite film.

Utilizing TEA as a reductant for graphene oxide sheets in the polymer matrix reduces the oxygen-containing functional groups (specifically epoxy) at the basal planes in a similar fashion as observed in Figure 7.5. GO forms hydrogen bonds with the –OH of the PVA chains, (Fig.7.5, step A). The addition of TEA in the PGO composite reduces both the epoxy and carboxylic groups of GO. In the case of *in-situ* reduction, TEA restores the C=C structure of graphene by reducing the epoxy molecules on the GO basal planes and functionalizes via increased H-bonding. This increase is reflected from the shift of peak from 1325 to 1332 cm^{-1} for the CH bonds. This intensity is sharper and clearer in the PGT composites as compared to the same in the PGO series. The increase in the number density of hydrogen bonds reflects the high strength and affinity of the tertiary amine with the polymer.

The carbonyl groups of the partially reduced GO sheets interact with TEA, resulting in the formation of stable carboxylate quaternary amines at the edges, as reflected at 1556 cm^{-1}, (Fig.7.4). These amine groups present in the reductant effectively stabilizes the reduce sheets in the matrix and aid in increased strength of the overall composite developed, (Fig.7.5, step B). The resultant carboxylate cations are composed of $(C_2H_5)_3N^+$ groups attached to the C=O of the carboxylate groups of reduced graphene oxide. Confirmation of these bonds is seen by the formation of additional peaks at 1250 cm^{-1}, corresponding to C-N bonds. These peaks are produced by the conjugation of TEA with graphene sheets and the polymer chains, resulting in the development of amino hydroxylated PGT complexes, (Fig.7.5, step B).

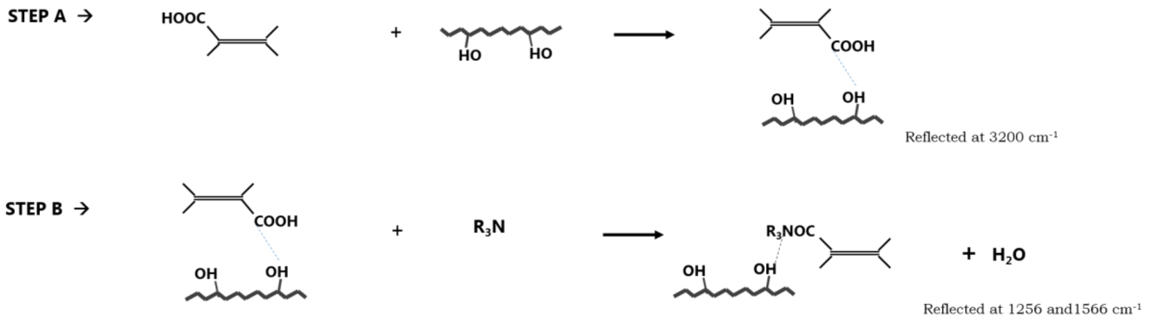

Figure 7.5. Reaction steps for the functionalization of PGO films by TEA on the edges (carboxylic group), $R_3N = (C_2H_5)_3N$.

The conjugation allows TEA molecule to graft at the graphene-PVA interface and strongly bind to the polymer matrix. The strong bond of the TEA molecules at the edges restricts the movement of the polymeric chains upon the application of load and effectively transfers the stress to the graphene fillers which is responsible for the substantial improvement in the elastic modulus.

To elucidate the effect of TEA on pristine PVA films, a blend of PVA and TEA solution without any graphene oxide filler was made and cast into a film. Inclusive of the skeletal peaks reflected from the PVA backbone; the TEA treated PVA films displayed a peak only at 2355 cm^{-1}. This peak arises by the reaction between TEA and PVA, resulting in the formation of an ammonium carboxylate complex in the form of zwitterions (internal salts) [315] with no additional peaks (Fig.7.6). Moreover, this peak is not reflected in the PGT samples. This suggests that TEA molecule has an affinity for both PVA and GO as independent systems. Where on the one hand, its addition to PVA results in the formation of zwitterions, its incorporation in a composite system of PVA and graphene oxide, results in formation of strong hydrogen bonds, conjugating between the matrix and the carbon reinforcements, with no signs of zwitterions.

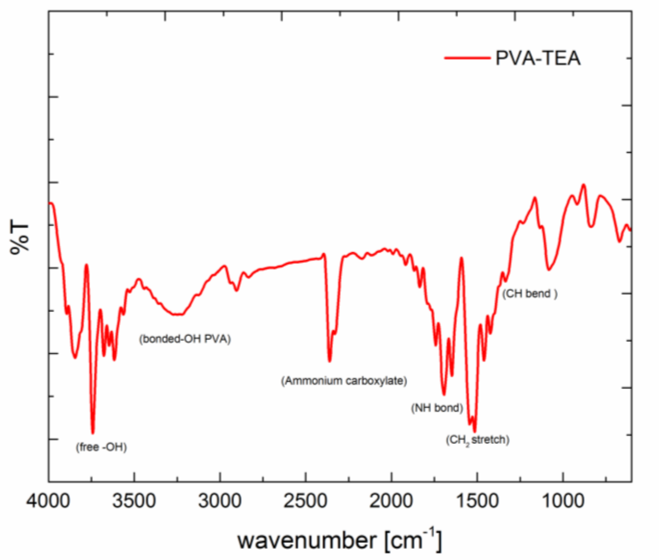

Figure 7.6. FTIR spectra of TEA treated PVA film.

The intensities of absorption corresponding to specific peaks in the FTIR spectra clearly reflect the influence of the fillers and reductant on the polymer matrix. The addition of filler in varying compositions produces absorptions at similar wavenumber, but with a progressive increase in their intensity with filler increment.

Wavenumber	**Functional groups**	**PVA**	**PGO**	**PGT**
3200	-OH alcoholic	✓	✓	✓
2900-2930	CH_2 stretch	✓	✓	✓
1560	Carboxylate quats			✓
1428	Aliphatic CH_2	✓	✓	✓
1400	C-OH stretch	✓	✓	✓
1325-1378	CH bend	✓	✓	✓
1250	C-N , aliphatic amines			✓
1140	Bounded C-O crystalline zone	✓	✓	✓
1090	Unbounded C-O amorphous zones	✓	✓	✓
825	Liberation peaks of PVA and water	✓	✓	✓

Table 7.2. Approximate regions of various types of bonds present in the PGO and PGT films of all compositions.

The PGT series of composites (PGT-1) exhibited the G peak at 1595 cm^{-1}, which was at a slightly lower wavenumber of 1598 cm^{-1} for the GO powders (Fig.7.7), indicating restoration of the in-plane order in the fillers. This can be ascribed to the disappearance of epoxy groups and restoration of the carbon double bonds of the GO filler in the PVA polymer, as was the case for the PGH composites. The D band was observed at 1318 cm^{-1}, slightly higher than that of GO (1314 cm^{-1}), indicating some interaction of the edges with the matrix. Importantly, the I_D/I_G ratio was 1.51, which was similar to that of GO, and lower than that of PGH-1 composites. The fact that the in-plane structures of the fillers become defect free, yet a comparatively similar I_D/I_G ratio to GO powders, indicate the homogeneous dispersion and an exfoliated type structure of the fillers. This will be discussed in more details in the microstructural section.

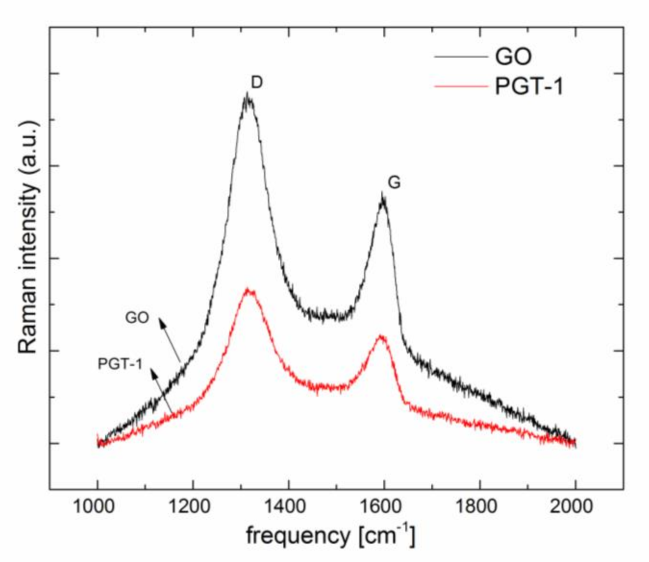

Figure 7.7. Raman spectra for the PGT film.

7.3 Mechanical behavior.

As was done in the previous chapters, a straightforward method to quantify the interfacial interactions between the polymer and the fillers is an evaluation of its mechanical properties. The PGT films exhibited exceptional mechanical properties as can be deduced from the representative stress-strain curves in the Fig.7.8.

The PGT-0.4 films exhibited distinct improvement in the elastic modulus as compared to the pristine (unmodified) PVA films (1.4 GPa vs. 0.34 GPa). Additionally, even at this level of fillers, the PGT-0.4 films had about 40% higher elastic modulus as compared to the PGO-0.4 films, indicating that the load transfer mechanism worked more efficiently in the PGT series films as compared to the PGO- films. Loading level at 1 wt.% of fillers also indicated a significant improvement in elastic modulus as much as 40% improvement as compared to the PGO series films at similar filler loading (2.8 GPa vs. 2.0

GPa). As compared to the pure PVA film, the PGT-1 composites had more than 8 times of its Young's modulus.

Much like the elastic modulus values, the yield strength of the PGT- series of composites showed excellent results. These values were much higher than those of the PGO series of composites with similar filler loading. While the nature of the stress- strain plots for the composites at lower loading (PGH-0.4 and PGO-0.4) were similar, a marked difference in the higher loading samples can be observed. In the PGO-0.8 and PGO-1samples, after the yield point the deformation region is accompanied by a decrease in the stress. This is more pronounced for the PGO-1 samples. This region is ascribed to strain softening behavior of the amorphous (semi-crystalline) ductile polymers (Fig.5.9). Interestingly, in the PGT composites, this behavior was totally absent beyond the yield point region, irrespective of the filler loading volume fraction. On the contrary, the stress was found to increase considerably with the increase in the strain of the composites (Fig.7.8). These are typical characteristics of strain hardening in composites. However, if one closely looks at the stress- strain traces, extremely small regions of strain softening can be observed. These small dips in strength with increase in strain was found from time to time in the progressively strain hardened material. This could indicate possible deformation of some soft/pliable domains in the polymer composites. Overall, the stress-strain traces indicate a milder form of strain hardening followed by mild softening throughout the loading regime.

The films exhibit an exceptional increase in the tensile strengths to 130, 137 and 212 MPa for the PGT films at varying filler loading of 0.4, 0.8 and 1% respectively (Fig.7.9). Such enhancement with an increase in the reinforcement, are attributed to the strong interfacial bonding of the functionalized graphene sheets strengthened by mechanical interlocking with the matrix. With strong dependence of the tensile strengths on the interfacial bonding, the mechanical properties majorly depend on the orientation of the fillers as they are increased in the matrix [37]. This analogy suggests that possibly the fillers remain uniformly dispersed throughout the microstructure even when the filler loading is higher.

The obtained mechanical properties (tensile strength, elastic modulus) warrant comparison with the published results in the literature. The exhibition of 8 times improvement in elastic modulus, and almost an order of magnitude increase in tensile strength, (22 MPa for the pure PVA and 212 MPa for the PGT-1 composites), have never been reported in the literature, for the polymer film strips with such low volume fraction

(0.69 vol%) of such carbon nanostructured based fillers. The fact that such high strength could be achieved for a moderately low specific gravity material, its specific strength (strength/density) which is in the range of 169 KN.m.Kg^{-1}, can be compared with magnesium alloys (158 KN.m.Kg^{-1}) and aluminum alloys (214 KN.m.Kg^{-1}) [316]. It also must be noted that these values are for the 1wt% filler loaded composites. A higher loading of the fillers might result in higher level of tensile strength and toughness which is beyond the scope of the current investigation.

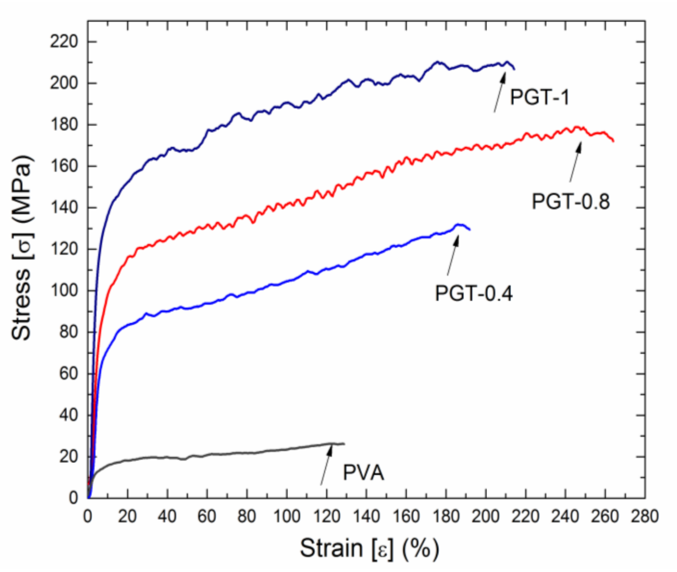

Figure 7.8. Representative stress-strain curves for PVA, PGT-0.4, PGT-0.8 and PGT-1 composites.

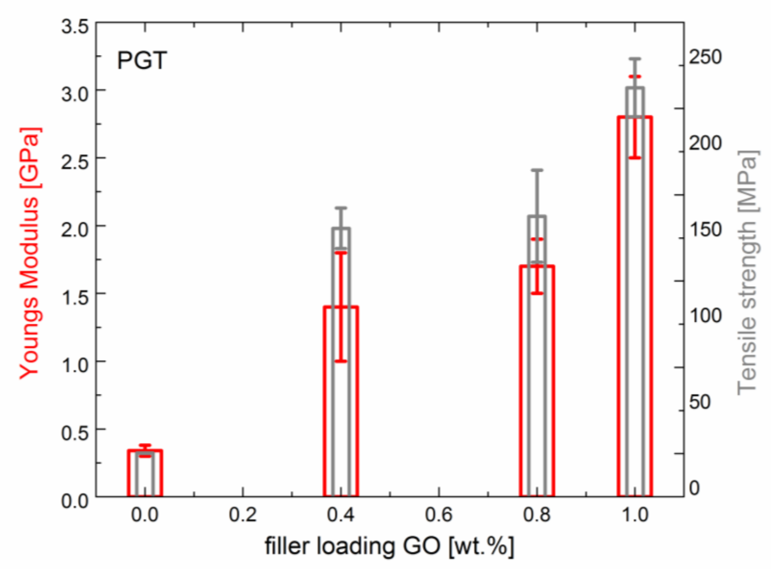

Figure 7.9. Results of mechanical properties of the PGT composites.

Another exciting aspect of the PGT- series films is their large strain at failure values, typically in the range of 190%, 260% and 200% (Table.7.3). These results clearly indicate that functionalization of the GO fillers with TEA results in excellent ductile films. Strain-at-failure values decrease with increase in the elastic modulus of the material (as can be seen with the PGO-series films). The strain of 200% before failure imparts an enormous level of toughness in the films.

Sample name	Youngs modulus (GPa)	Ultimate strength (MPa)	Elongation at break (%)	Yield strength (MPa)
PVA film	0.34± 0.04	22.43 ±3.6	125	15.73±3.05
PGT-0.4	1.46±0.4	130.67±11.7	190	82.25±6.24
PGT-0.8	1.77±0.26	137.56±26.7	226	100.27±9.79
PGT- 1	2.87±0.34	212.66±16.84	200	154.43±18.92

Table 7.3. Tensile values corresponding the representative tensile graph.

7.4 Interfacial interactions.

Evaluation of calculated tensile strength for PGT-0.4, PGT-0.8, and PGT-1 films show values of 1.6, 1.8 and 2.25 for 0.24, 0.47 and 0.59 volume fraction of the graphene oxide (Fig.7.10). Such increase in the tensile values for the interaction factor $B_{\sigma y}$ of the PGT films, suggest creation of a strong interactions at the polymer-matrix interface.

Strong interfaces are resultants of the high surface energy of the graphene reinforcement. Graphene oxide sheets are decorated with functional groups, which can be tailored with specific amines such as TEA. This is a typical case of reactive surface treatment of the GO fillers by Pukanzsky, where the polymers adhere more strongly at the filler-matrix interface. FTIR spectra show that TEA molecules mostly attach at the edge groups of the GO sheets, restricting the mobility of the interphase regions at the edges. The exceptional ductility along with high strengthened elastic modulus can be attributed to homogeneous nucleation of voids on extensive deformation, followed by growth of the voids. Such generation of microvoids makes the nearby regions resistant to hydrostatic pressure, which can also explain the strain hardening effects. The strong filler-matrix interface eventually leads to a fracture at much higher strains. However, mechanical data set shows an improvement in the ductility values also. Independent of the surface treatment, or the strong interfacial bindings, increased ductility are attributed to the sliding of the GO sheets coated with PVA polymer in the composite. Ductility here is an independent factor of the surface treatment.

The model also validates the increase in tensile strength to the morphology of the PGT composites. Alignment of the fillers in the matrix, produce strong binding or a reactive interface of the polymer to the fillers and hence high tensile strength in a composite.

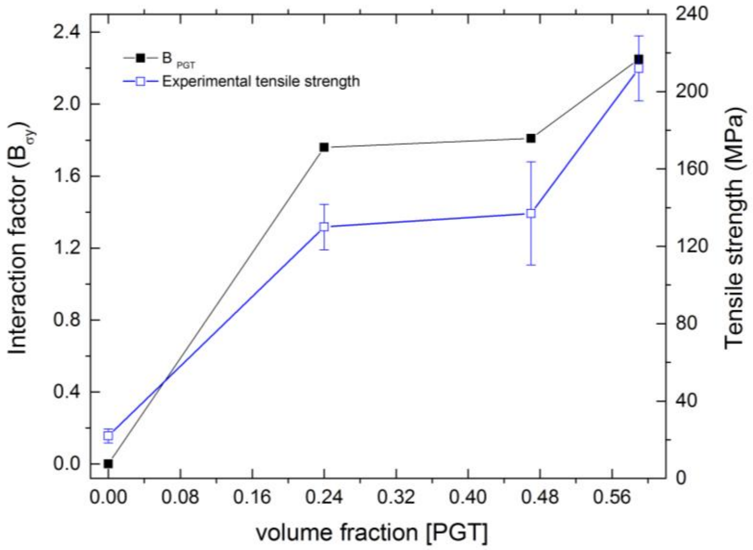

Figure 7.10. Interface interaction parameter in the PGT system of composites.

7.5 Morphological and microstructural aspects.

Transmission electron microscopy was performed by casting a drop of the polymer composite blend on carbon coated stubs, following by drying. A sharp contrast of the homogeneously dispersed web like reduced graphene sheets is observed against the polymer matrix. Even at a level of 0.7 vol % of the fillers, one can observe the homogeneous and continuous network of the two-dimensional fillers (Fig.7.11a). A higher magnification of the bright field TEM image indicates dark lines of contrast (Fig.7.11b). These lines are the imperfections in the fabricated GO sheets, generally termed as the wrinkles of the basal planes. A fair idea about the thickness of the GO fillers can be obtained by measuring the wrinkles in the micrographs (the thickness of the films should be less than half of the width). From these micrographs, it can be calculated that the GO sheets are of less than 10 nm size. Overall, it is clear that the fillers are homogeneously distributed in the polymer matrix. Selected area electron diffraction pattern (SAED) of the composite films indicated semi-crystalline nature of the films as observed from one set of a broad diffused ring that can be attributed to the (110) planes of PVA (Fig.7.11c).

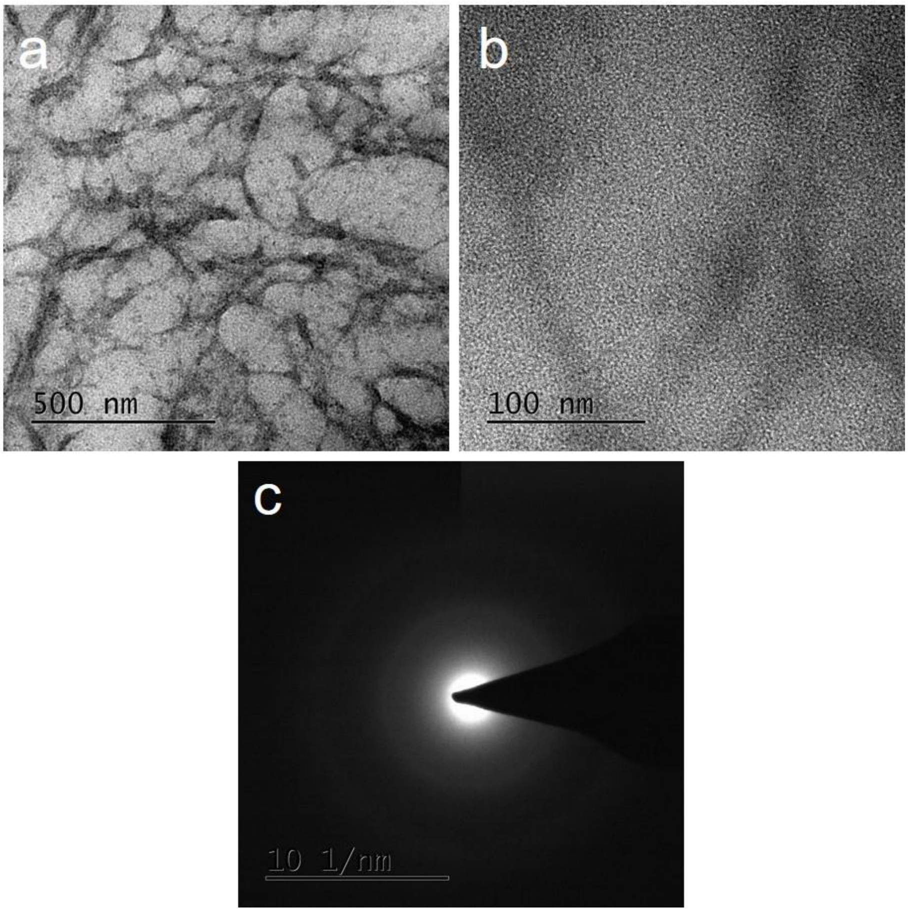

Figure 7.11. Transmission electron microscopy of the PGT-1 composite; (a) bright field image showing continuous.web-like fillers, (b) HRTEM imaging of a region showing graphene dispersion, (c) SAED pattern of the composite indicating semi-crystalline nature.

While Fig.11 depicted the general features of the composites from a relatively thicker region, a much finer and more electron transparent region exhibited the PGT-1 composite microstructure with remarkable clarity (Fig.12). Over a broad region the distribution of what appeared to be clearly exfoliated graphene sheets was very homogeneous. Moreover, the distributions had small domains of ordered alignment of the fillers, (Fig.12a), resembling the typical nematic liquid crystalline order in materials with anisotropy (high aspect ratio). Magnified imaging of a smaller region exhibited ordering of the fillers (Fig.12b). The features with dark contrast exhibited dimensions in the range of 5-8 nm, indicating that the filler thickness should be in the range of 4nm only. The speckled contrast in the background presumably has resulted from the signals of the underneath amorphous carbon layer of the sample grid on which the composite was solution cast.

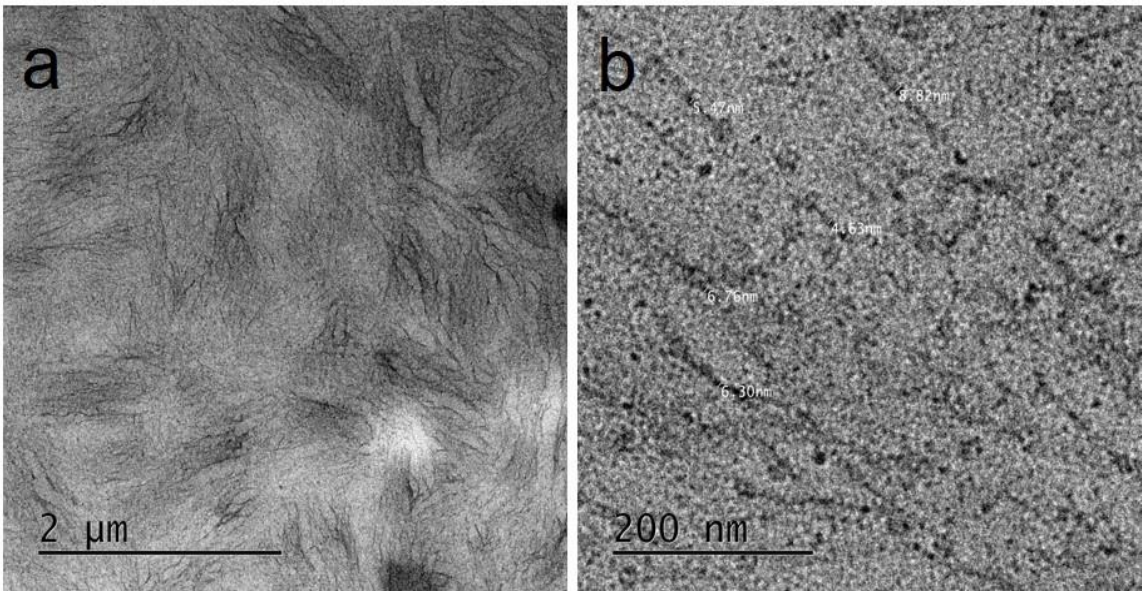

Figure 7.12. (a) Bright-field TEM image of a thin region of the PGT-1 composite; liquid crystalline type nematic ordering of the graphene oxide fillers can be clearly observed, (b) high-resolution micrographs of PGT-1 composites exhibiting local ordering of the fillers, and indicating filler thickness in the range of 5nm.

The advent of field emission sources for transmission electron sources for transmission electron microscopy has led to improvement in resolution and analysis of nanostructured features. While such studies are limited in polymeric systems, previous works have reported staining of the microtomed polymer composites with ruthenium bearing compounds for better clarity in the bright field imaging mode. Scanning transmission electron microscopy (STEM) of an electron transparent specimen can be conducted, and the recorded signals from an annular dark field detector can enhance resolution and contrast in the microstructure bearing two dissimilar phases differing in atomic number. Further improvement in detection of the transmitted electrons by a high angle annular dark field (HAADF) detector can clearly distinguish between materials/phases of different atomic numbers.

The graphene reinforced polymer composite in this work is a combination of a carbon-containing phase in a matrix of a polymer containing C, H, and O. However, with the typical platy two-dimensional morphological features of reduced graphene oxide, the distribution of the fillers can be understood well in the composite microstructure. The STEM–HAADF image (Fig.7.13a) exhibits a rather low magnification micrograph of the composite. The grayish region is representative of the polymer matrix, whereas the brighter regions represent the graphene fillers. A higher magnification HAADF-STEM (Fig.7.13b) exhibits fairly similar structure even inside a much reduced field of view. Interestingly, these micrographs are clearly similar to the ordered patterns observed in Fig.12a. However, the same local order was found to be maintained even at a much smaller (nanometric scale). The images interestingly mimic the classic nematic liquid crystalline microstructure with ordered domains where particulate materials of specific geometries are distributed. The formation of locally ordered nematic structures of graphene oxide films dried from aqueous colloids has been reported in the literature [317, 318]. This generally occurs for particulate systems with large aspect ratios (rods or platelets). At a lower loading of these fillers, the dried structures exhibit random orientation. However, upon an increase in the concentration of the fillers, the dispersion exhibits a phase transition from isotropic to nematic liquid crystalline phases. The Schlieren textures of the colloids have been observed by the cross-polarized optical microscopy. Nevertheless, observation of these structures in graphene reinforced polymer composites has not been reported in the literature.

These structural patterns form due to controlled and equilibrated drying conditions. Flow instability during drying leads to irregular structures. Therefore, liquid crystal type ordering of the fillers in the polymer can result from a well-controlled evaporation of the aqueous polymer blend.

Another important parameter is the stability of the aqueous colloid. The filler particulate materials need to the well dispersed in the solvent. Onsager’s theory states that above a critical concentration of anisotropic moieties (such as plates, rods), spontaneous entropy driven liquid crystalline nematic order occurs as a consequence of simply excluded volume interaction [319]. The term liquid crystalline order comes from the fact that the extent of order in the nematic phases are between that of a crystalline compound and a liquid. Therefore, during drying of the colloids, (polymer blends) radial spoke type patterns are observed, which cause the wrinkling of the graphene oxide sheets.

While on a macro scale, the PGT composites may appear as isotropic, on a microstructural level the liquid crystal type nematic order is clearly visible. Additionally, at the nanometric level also, such type of local ordering was observed from HAADF-STEM images (Fig.7.13b). Additional bright speckles /spots are also observed, which are mostly distributed in the polymer matrix region (the darker region), (Fig.13b). These white spots are from the extremely fine sized graphene fragments that remain in the colloidal solution from the GO fabrication stage itself. While, on the other hand, these features do not add much to the overall strengthening of the composites, due to their lack of high aspect ratio, they certainly add to the strengthening effect by simply strongly binding to the matrix. These features are also expected to act as impediments in the deformation of the polymer chains (on heating or loading), thus causing improvement in mechanical properties.

Further zooming on to the regions of higher bright contrast, clearly identifiable bright lines (appearing as veins in Fig.13b) could be observed. These lines are representative of the single layer and few layer graphene reinforcements. Also, then microstructure indicate clearly intercalated composites where the PVA polymeric phase is found between the graphene layers. As evident by the XRD spectra, the increased crystallinity of the composites would have resulted from heterogeneous nucleation sites at the edges of the graphene sheet. The excellent level of exfoliation of the graphene sheets creates many such sites for nucleation in the polymer matrix, which is corroborated by the increase in percentage crystallinity in the composite with increased filler content.

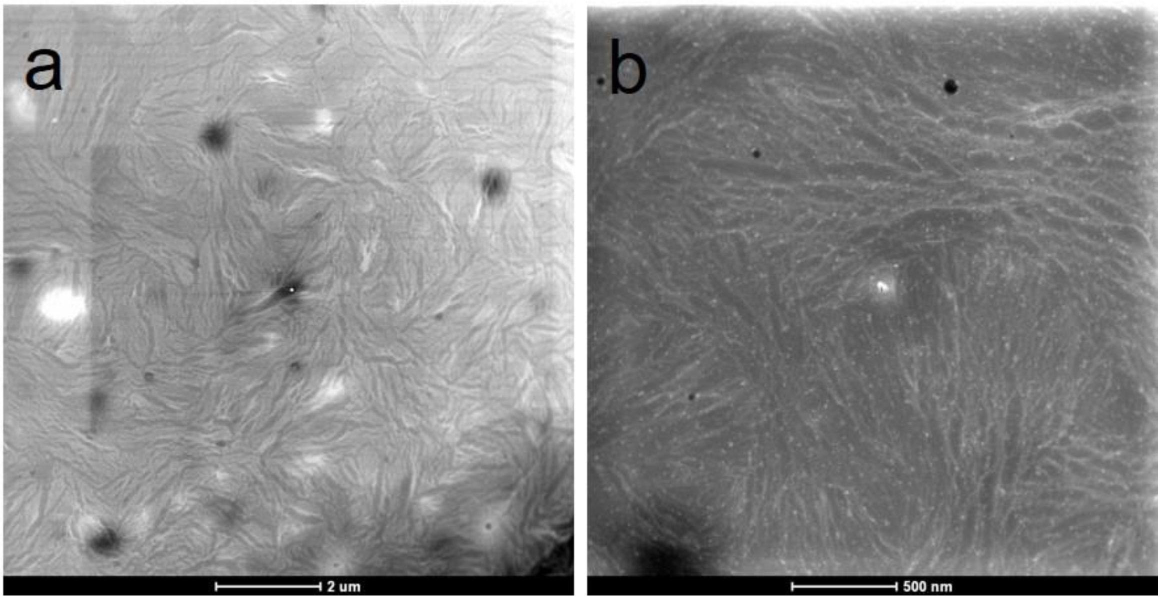

Figure 7.13. HAADF-STEM images of distributed graphene sheets in the polymer matrix for the PGT composite films indicating the liquid crystalline order in the film.

To observe the morphology of the PGT composites in the unstressed or unstrained conditions, the polymer films were cryogenically fractured by dipping the film in liquid nitrogen. The composites became extremely brittle and simple snapping of the films caused a fracture. The fractured specimens were coated with Au/Pd, and the cross-sectional regions were observed by scanning electron microscopy. The fractography was similar to that of pure PVA but layered morphology of the composites was clearly observable. The graphene oxide reinforcements (CCG_T) were not seen in isolation, but its outlines could be observed on the cross section of the fractured polymer (Fig.7.14a &b). The cryo-fractured cross-sectional images of the PGT samples indicated extensive perturbations in the crack propagation path in a non-planar mode. Therefore, the surface roughness of the fractured PGT composites was much higher than the pure PVA polymer, or the other composites discussed here. Thus the step-wise propagation of a crack in a highly brittle fracture environment can be concluded. Fractured surface roughness at much finer details can also be observed (Fig.14c &d).

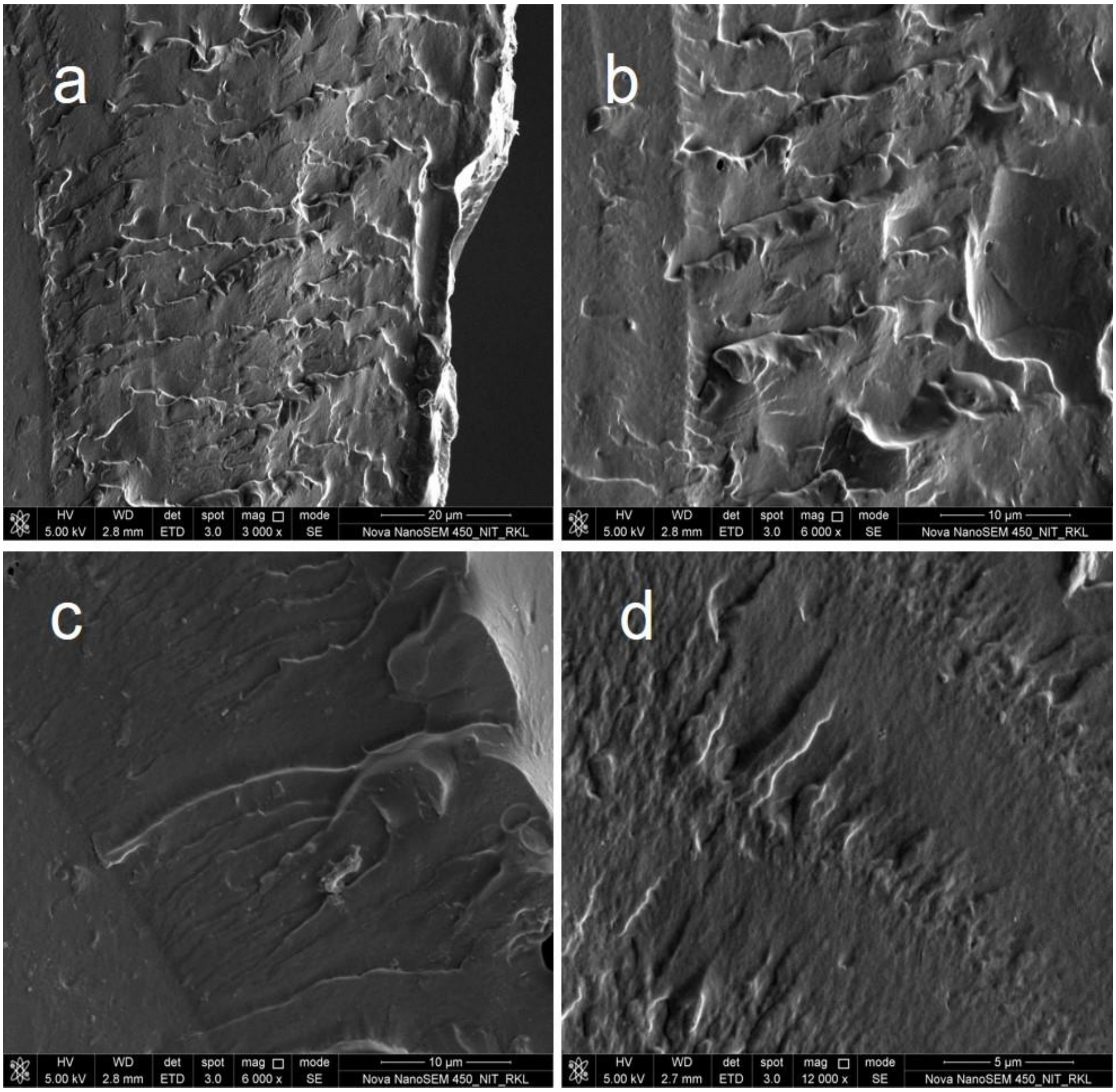

Figure 7.14. Scanning electron micrographs of the cryo-fractured PGT composites; (a & b) macroscopic roughness of the fractured cross-section, (c & d) roughness at a much finer scale.

The fractured regions of the stressed films (after tensile testing) were also observed in secondary electron mode. The cross section of the films (Fig.7.15) with extensive plastic deformation reveals homogeneously distributed microvoids that are precursors to crazing process, as was seen for the PGO- series of the composites (Fig.7.16). It is evidence for the classical process that is operative in the failure of these materials. The microvoids were generally observed in between the regions of the fillers and within the domains of the pure polymer matrix. Areas with larger voids exhibit the fibrillar structures being the functionalized graphene oxide fillers. The cracked fractured regions show extensively pulled out planar (two- dimensional) moieties that are graphene oxide still bonded to few (thus the thickness of the pullout appearing as very thick).

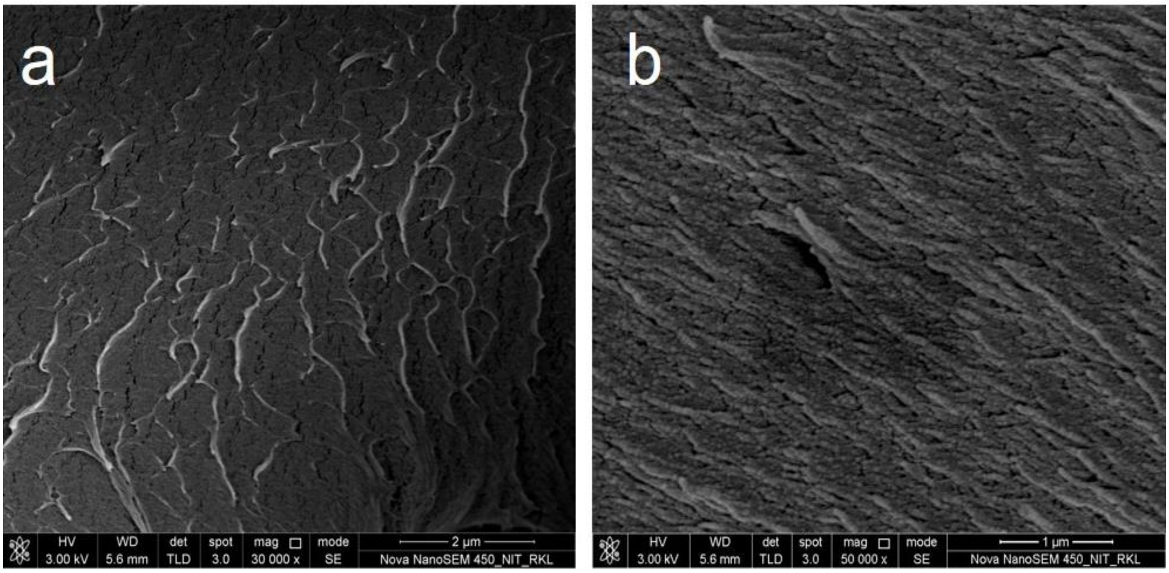

Figure 7.15. Morphology of representative PGT composites after tensile deformation; (a) nucleation of microvoids throughout the composite strip, (b) separation of the fillers from the matrix exhibiting fibrillar structures.

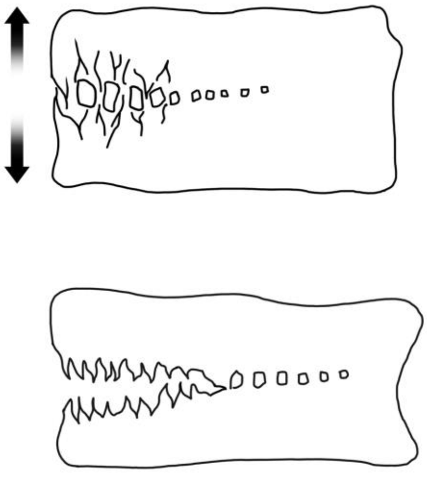

Figure 7.16. Schematic of the classical crazing process.

The majority of the known nanomechanics were observed in the deformation and fracture of the PGT sample, including debonding, plastic void growth, micro-shear bonding, and matrix deformation. Formation of micro-voids followed by the growth of these voids around the nanostructured fillers occurs leading to the detachment of fillers. However, plastic yielding of these voids relieves the triaxial stresses and makes the surrounding region more restricted to further debonding. The stress-strain traces of the composites can be reconciled with this.

Furthermore, the edge regions of the extensively deformed (broken samples after 200% strain) exhibited narrow protrusions. These protrusions may have formed by rolling up of the edges of the graphene sheets after deformation (Fig.7.17). These features were homogeneously distributed in the fractured domains indicating the uniform transfer of the load in tension; the presence of fillers was low for the PGT-0.4 (Fig.7.17a), whereas the number density of the fillers was high in the PGT-1 (Fig.7.17b). These micrographs represent some of the most direct evidence of the fracture process and clearly, corroborate the high ductility observed for these composites.

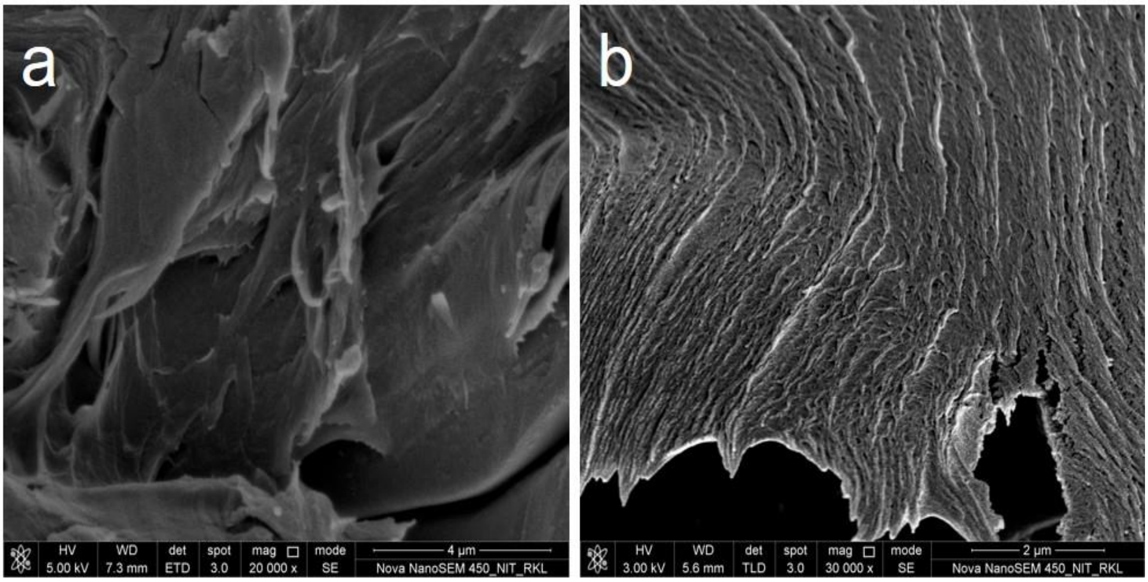

Figure 7.17 Scanning electron microscopy of fractured (a) PGT-0.4 (b) PGT-1 nanocomposites.

7.6 Chapter Summary.

Triethylamine functionalized graphene oxide reinforced PVA nanocomposites were found to have the following salient features:

- The novel method of using triethylamine as a reductant and functionalizing agent resulted in composites with the excellent homogeneity of the fillers.
- Progressive increase in the crystallinity of the polymeric phases was found to increase with filler loadings, which was corroborated by the scanning calorimetry studies.
- Exceptional improvements in tensile strength and elastic modulus was observed for the composites along with superior ductility.
- Strain-hardening was observed in the stress-strain patterns indicating a progressive strengthening of the composites.
- The microstructures of the composites as evidenced by HRTEM and HAADF-STEM imaging exhibited nematic liquid crystalline type ordered microdomains with excellent homogeneity.
- The covalent linkage of the triethylamine at the edges of homogeneously ordered dispersed fillers led to efficient load transfer exhibiting excellent mechanical properties.

Chapter 8

Ultra strong PVA nanocomposites with sequential treatment of triethylamine and hydrazine systems.

In this chapter, a novel dual stage *in-situ* treatment of graphene oxide reinforced PVA nanocomposites have been carried out.with the use of triethylamine followed by hydrazine. The physicochemical properties, structure, morphology, and microstructures have been discussed in the context of the resulting exceptional mechanical properties.

Many theoretical and experimental investigations have corroborated the excellent mechanical properties (tensile strength, elastic modulus) of graphene. However, these properties have not been as effectively harnessed in polymer nanocomposites with the carbon-based nanostructures as fillers. Property enhancement is possible when the applied load on the composites is efficiently transferred to the filler/filler networks. For this thing to happen effectively, many parameters cause influence, including morphology, microstructure, homogeneity of the fillers, and strong chemical interactions. Stacking of the fillers as has been the issue specifically for graphene-based two-dimensional fillers, for it reduces the effective filler/matrix interface area. Fully exfoliated fillers with homogeneous distribution throughout the polymer matrix creates more interfaces per unit volume of the composites. In such a microstructure, if chemical interactions strengthen these interfaces, effective load transfer can occur leading to enhancement in mechanical properties.

Therefore, in this chapter, a novel processing scheme is outlined to embody the above said microstructural features. In the earlier chapters, it was shown that triethylamine as a reductant and reducing agent that creates unique microstructures of the composites with exceptional mechanical properties. Likewise, the hydrazine reduced PGH system also has shown controlled as well as aligned morphology, without aggregation or restacking of the fillers. Thus, in the current method, both of the reductants were used sequentially. First, the aqueous blend of PVA and GO was treated with triethylamine, which was then further reduced by hydrazine. The nanocomposite films were cast by solvent casting and evaporation process, similar to the fabrication of all other composites in this work. The filler fractions were maintained at similar levels with 0.4, 08 and 1 wt% addition and produced composites which were named as PGTH-0.4, PGTH-0.8, and PGTH-1.

The fabricated films were smooth and dense black in appearance without any visible defects, such as pinholes, or laminations. The overall look is shown in the Fig.8.1.

Figure 8.1. Digital images of the PGTH composites.

8.1 Structural and thermal behavior.

The PGTH series of films showed a clear presence of the 19.6° peak with a progressive increase in the peak intensity with an increase in the filler content (Fig.8.2a). The PGTH-0.4 sample itself showed a discernible increase in the said peak intensity, indicating that there is the influence of crystallinity with the small volume fraction of fillers. This was much more pronounced in the PGHT-0.8 and PGTH-1 samples with the latter showing maximum intensity. Comparatively, the intensity of the PGTH films was highest amongst all of the samples tested in this work across all forms of functionalization. Thus it is quite clear that the TEA functionalization followed by hydrazine reduction process induces better crystallization of the polymeric chains. It is interesting to note that simple hydrazine reduction of the PVA and the GO fillers did not induce as much crystallization of the matrix polymers as a simple blending of the PVA and GO system did. (although, higher crystallization was observed only for the PGO- 1 samples). On the other hand, composites of PVA and GO formed with TEA functionalisation did improve the crystallinity (Fig.8.2b). The fact that TEA functionalization followed by hydrazine reduction process improved crystallization, can be reconciled as follows: functionalisation of the GO platelets with TEA results in the strong interaction of the functional groups at the edges of the filler and the PVA matrix chains leading to crystallization at the edges of the filler. This has been shown clearly by the XRD and transmission electron microscopy that the crystalline domains precipitate in the vicinity of the fillers. In the PGTH series of samples, similar behavior can also be expected. The hydrazine reduction removes the groups at the basal planes (epoxy). This presumably favors the growth of extended polymer chains throughout the basal plane regions.

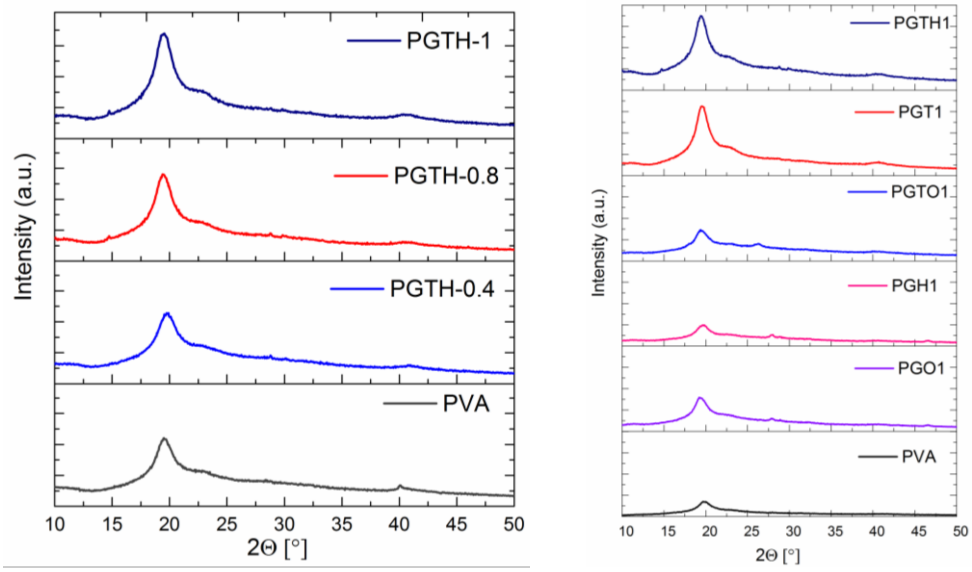

Figure 8.2 (a). X-ray diffractograms of the PGTH composites; PVA is added for reference and comparison. (b) X-ray diffratogram of 1% composites of all PVA based systems.

The thermal behavior of the PGTH composites was unique and different from most of the other composite fabricated in this work. To begin with, the shift in the glass transition temperature of the PGTH composites was high as can be seen in the Fig.8.3. The T_g for the PGTH sample was the highest for all of the composites considered here. T_g of PGTH-0.8 sample was 112℃, which was higher than the pure PVA, and comparable to the PGO series. These observations clearly indicate that amorphous regions of the polymer matrix are significantly influenced by the TEA/hydrazine process and that it moves with an increased amount of fillers.

Chemically, this evolution arises as a result of the complex functionalities introduced in the polymer chains. In a common phenomenon, the polymer chains containing hydroxyl groups on the edges interact with the edge groups of the filler through hydrogen bonding to form PGO composites. Functionalizing the PGO composites with TEA introduces functionality at the edges resulting in the formation of stable quaternary ammonium ions as discussed in the previous chapter, (PGT composites). Further reducing the PGT composite films with hydrazine results in the formation of strong, complex compounds called as hydrazimines $[R_3NNH_2]^+$. (Equations discussed later). Complex compounds of hydrazimines develop a strong network of interphase at the polymer- filler region, thus manifesting large increase in T_g. It may thus be inferred that the graphene-based fillers are also embedded uniformly in the polymer matrix.The strong network requires a large amount of energy to allow the mobility of the entangled amorphous chains requiring a higher temperature for transitions from glassy to a rubbery state.

Structurally, polymers are a combination of crystalline and some amorphous regions. The structures contain regions of lower and higher atomic density. Reduction of the fillers introduces bulky hydrazimines, a portion of which bond to the amorphous domains in the polymer. Thus the entangled polymer chains bonded to the fillers result in an increase in the glass transition temperature. Along with the increase in T_g, the PGTH composites exhibited a distinct increase in the melting temperature. The substantial increase in the melting temperature as much as 5℃ has not been observed in any other samples carried out in this work. Additionally, from the melting endotherm the percent crystallinity values were calculated that exhibited higher values than the pure PVA or any other PVA/graphene-based composite fabricated in this work. The X-ray diffractograms corroborate with these observations of enhanced crystallinity. This may have resulted from homogeneous nucleation of the polymer crystallites at the edges of the filler that may have spanned around the fillers. The composites in the PGTH type microstructure can be hypothesized to be a unique one with improved crystallinity as well as improved distribution of the fillers in the amorphous regions in the matrix. It is expected that the volume fraction of the amorphous domains may be considerably lower than pure PVA and most of the other composites, albeit stronger as evident by the higher T_g.

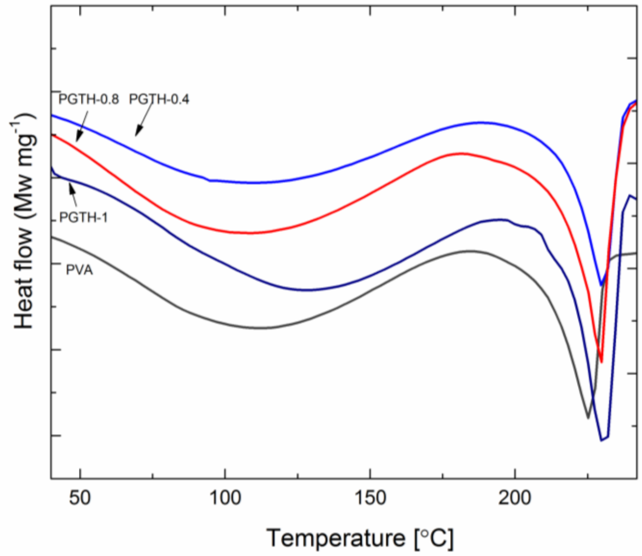

Figure 8.3. DSC thermograms of the PGTH composites.

Sample name	T_g (°C)	T_m (°C)	χ_c (%)
PVA	105	225	30
PGTH-0.4	106	229	32
PGTH-0.8	112	230	35
PGTH-1	121	230	37

Table 8.1. Thermal properties of the PGTH composites.

8.2 Infrared and Raman spectroscopy.

Strong interfacial interactions between the matrix and the fillers are attributed to small molecule functionalization of the reduced graphene sheets. The FTIR analysis can study qualitative analysis of the extent of such interactions (Fig. 8.3). This technique cites the hydrogen bonding between the matrix and the filler promoting large interfacial interactions. Reduction of GO fillers by TEA is described in chapter 4. Herein the interaction of TEA with the GO sheets intercalated in a polymer matrix, followed by the added effect of hydrazine on the system is discussed.

In the first step, GO filler interacts with the PVA chains through strong hydrogen bonding (Fig.8.4, step A). These bonds are reflected as strong alcoholic bonds (3200 cm^{-1}), vinyl stretch (2900-2930 cm^{-1}), C-OH bond (1428 cm^{-1}), crystalline zones of the polymer (1140 cm^{-1}) and amorphous zones at 1090 cm^{-1}. Apart from this GO interaction with PVA is reflected by the presence of few C=O stretch (1560 cm^{-1}) and some epoxy bonds that merge with the C-O bonds of PVA at 1090 cm^{-1} (depicted in Fig.8.5). However, the epoxy bonds of GO are not so prominent here as seen in the PGO spectrum (Fig.5.4).

In the next step, TEA molecule interacts with the PGO films, (Fig.8.4, step B). The interaction is previously confirmed by a set of peaks observed at 1556 cm^{-1} (C=O quats), C-N bonds (1231 cm^{-1}) at the edges and restoration of the C=C by the presence of C-H alkene stretch at 2916 cm^{-1}, (Fig.7.5).

Further treating the functionalized PGT system with hydrazine, produces no significant physical changes in the film, but reduces the intensity of C=O peaks for the quaternary salts at 1556 cm^{-1}. This interaction of hydrazine with the quaternary salts produces stable quaternized hydrazine complexes, also known as hydrazinium ions, (Fig.8.4, step C). Analogous to the quaternary ammonium salts, these salts are a new family of compounds which are water soluble and alkali stable. Represented as [$R_3N^+NR_2$], these cations are bonded to the side to reduced graphene sheets on the edges and another side to form hydrogen bonds with PVA chains.

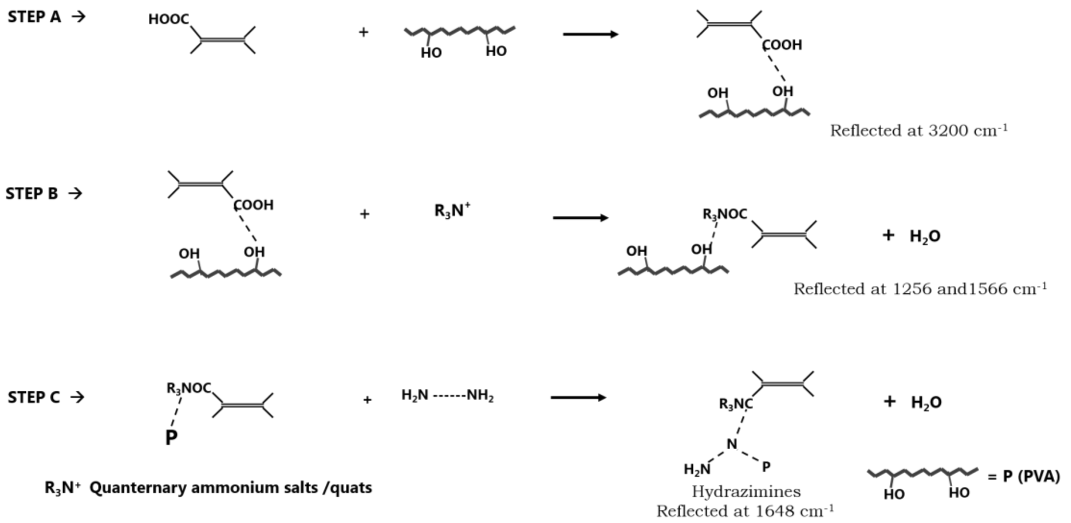

Figure 8.4. Reaction mechanism of TEA functionalized GO reinforced PVA with hydrazine treatment, P= PVA.

These compounds do not particularly reflect in the IR spectra. However, the presence of few NH bonds at 1600-1640 cm^{-1}, describe the interaction of hydrazine to the PVA polymer and the carboxylates of the graphene sheets (Fig.8.5).

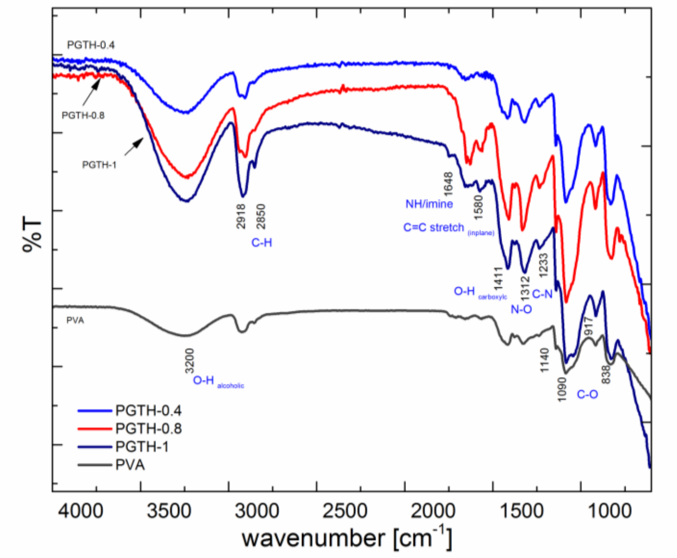

Figure 8.5. FTIR spectra for the PGO and corresponding PGTH films.

The schemata in the Fig.8.4 is an attempt to understand the reaction mechanisms at the edges of the GO sheets. Reduction of GO by TEA has already been discussed in the previous chapters. Herein, we have considered P (for PVA) and NH_2 as two R groups attached to N to form hydrazimines. These NH peaks arise only by the formation of hydrazimines by the reaction of TEA followed by hydrazine over the PVA molecule, no traces of the tertiary amine peaks are observed (Fig.8.6).

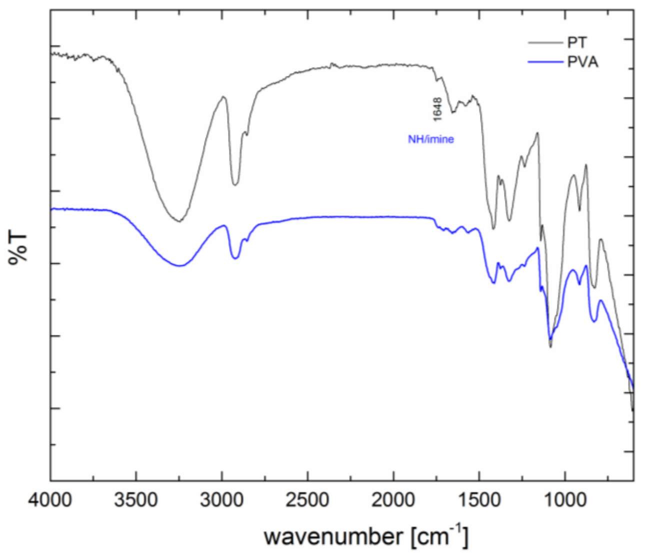

Figure 8.6. FTIR spectra of the PVA films treated with TEA followed by hydrazine.

As compared to the other systems utilizing quaternary amines at the edges induce much steric hindrance at the interface. Simultaneous development of NH bonds as a result of conjugation of quaternary amines with the OH of PVA matrix responsibly induces strong interactions between the PVA and fillers resulting in efficient load transfer to the fillers (Fig.8.7).

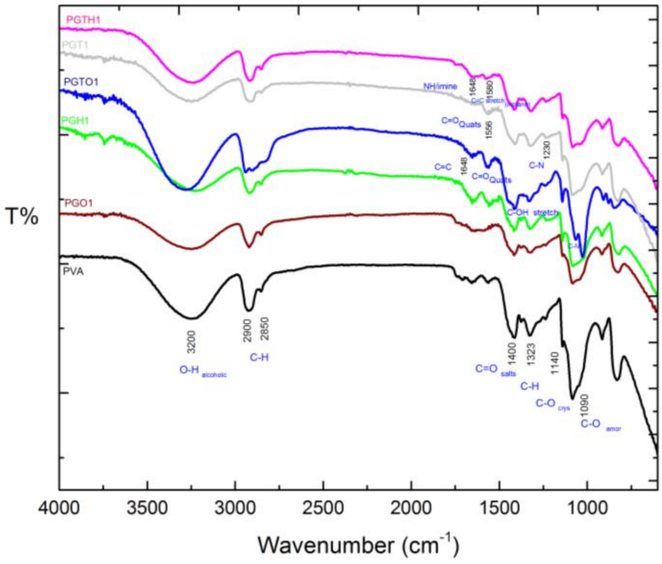

Fig.8.7. FTIR spectra of all 1% PVA- graphene based composite films.

The intensities of the amorphous and crystalline regions of the pristine PVA polymer are not much affected by the peak position, but there exists a substantial decrease in the intensity of the amorphous peak of PVA at 1090 cm^{-1}, symbolizing conversion of the amorphous regions to regular arrangements of the crystalline regions.

Wavenumber	Functional groups	PVA	PGO1	PGH1	PGT1	PGTH1
3384-3200	-OH alcoholic	✓	✓		✓	✓
2900-2930	CH_2 stretch	✓	✓		✓	✓
1650-1600	C=C stretch				✓ (medium)	N-H/imines (strong bonds)
1566	Carboxylate salts				✓	✓ (low intensity)
1428	Aliphatic CH_2	✓	✓		✓	✓
1325	CH bend	✓	✓		✓ shits to 1332 strong bond	✓ 1330 Strong bonds
1248,1060	C-N, aliphatic amines				✓	✓
1140	Bounded C-O crystalline zone	✓	✓		✓ (stronger)	✓ (strongest)
1090	Unbounded C-O amorphous zone	✓	✓		✓ weaker	✓ weakest
825	Liberation peak of PVA and water	✓	✓		✓	✓

Table 8.2. Approximate regions of various types of bonds present in the PGTH films.

The PVA composites with dual stage functionalized graphene oxide (by TEA and hydrazine) exhibited Raman polarized G band at 1593 cm^{-1} and the D band at ~1317cm^{-1} (Fig.8.8). The G band indicated restoration of carbon double bonds in the basal plane with a shift to lower wavenumbers; consistent with reduction as was seen for the PGH composites. The I_D/I_G ratio, however, was 1.59, which was comparatively higher for a reduced system. The fact that in-plane order existed in the graphene based fillers along with an increase in the I_D/I_G ratio indicates much higher proportion of edges/interfaces in the fillers. As will be discussed in the microstructure section, the rise in the ratio could be attributed to the formation of nanoribbons, thus creating additional edges of the carbon based fillers. Therefore, a higher interface area density (per unit volume) of the nanocomposites with the restored in-plane sp^2 character of the fillers in the PGTH composites can be deduced from the Raman spectrum.

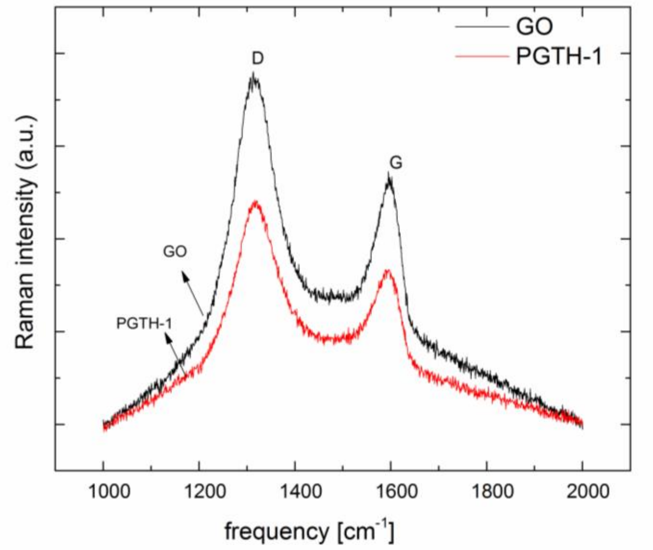

Figure 8.8 Raman spectra for the PGTH films.

8.3 Mechanical behavior.

Typical stress-strain curves of the PGTH films are depicted in Figure 8.9, with their corresponding mechanical values summarized in Table 8.3. The modulus of elasticity increased exceptionally from 0.34 GPa for the pristine PVA film to 2.5, 2.7 and 3 GPa for the PGTH-0.4, PGTH-0.8, and PGTH-1 films respectively. These values are much higher than the elastic modulus of the GO reinforced PVA (PGO) counterparts, and even comparatively higher than the PGT based films. The yield strength values also follow a similar trend with an excellent increase from 15.7 MPa for the PVA films to 114, 197 and 230 MPa for the PGTH-0.4, PGTH-0.8, and PGTH-1 samples respectively (Fig.8.9). Such an increase in the strength values to the author's knowledge has not been reported in the literature in the PVA system for such a lower loading of fillers. Another interesting feature is, like, in the PGT films, all of the PGTH films exhibited strain hardening after the elastic region. Prima facie it can be said that the graphene fillers strongly impede the plastic deformation/flow of the polymeric chains.

One can also observe that the strain hardening was subtle in the PGTH-0.4 films, but much more pronounced in the PGTH-0.8 and the PGTH-1 samples. The observation reconciles with the fact that the 0.8 and 1% filler loaded samples possess a number of the fillers per unit deformation volume, thus leading to enhanced toughness.

In a general trend, stiffer polymer composites exhibit lowered failure strain. However, the PGTH films show sufficiently high elongation at strain values additionally with the high strengths. This phenomenon is attributed to the modification of the surface chemistry of the developed composites, discussed later in the chapter. *In-situ* functionalization of GO by TEA, followed by hydrazine reduction which gets rid of the unmodified epoxy groups and strengthen the matrix and TEA molecules by conjugation. Reduction of the epoxy groups on the basal planes also restores the conjugation of carbon double bonds (sp^2 character), which can also be viewed as the disappearance of atomic defects on the plane. The intrinsic elastic modulus of the fillers, thus also increases due to a more ordered basal plane. As discussed in the previous chapters, the increased strengthening of the PGTH films is attributed to the strong edge to edge interactions of the fillers with the matrix. This results in a relatively large modulus values coupled with a large surface area of the reduced graphene sheets allowing most of the load taken up by the filler.

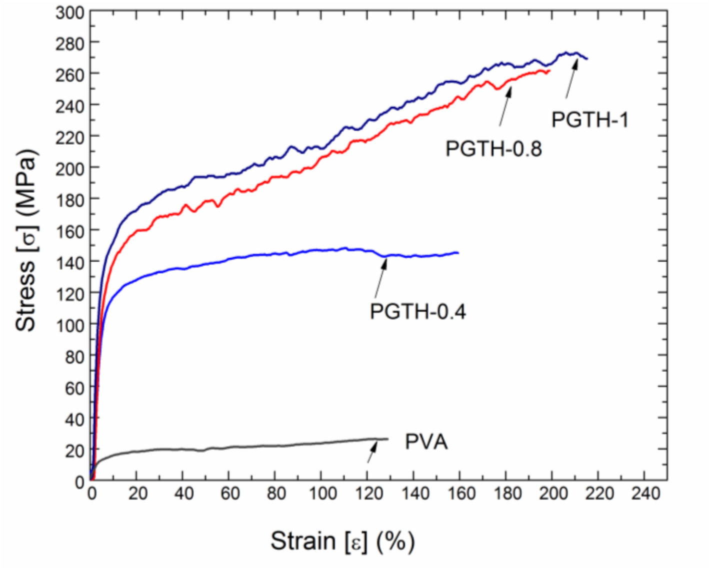

Figure 8.9. Representative stress-strain curves for PVA, PGTH-0.4, PGTH-0.8 and PGTH-1 composites.

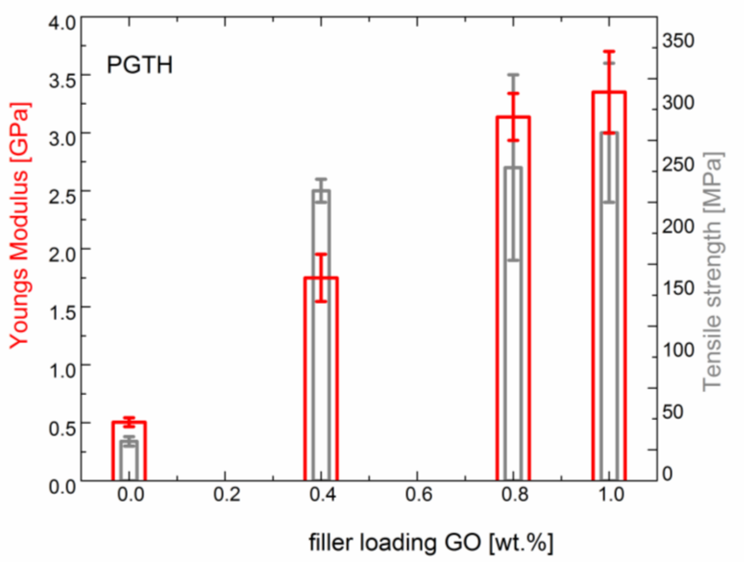

Figure 8.10. Mechanical properties of the PGTH composites.

Sample name	Youngs modulus (GPa)	Ultimate strength (MPa)	Elongation at break (%)	Yield strength (MPa)
PVA film	0.34± 0.04	22.45 ±3.66	125	15.72±3.06
PGTH-0.4	2.55±0.13	139±19.1	142	121.45±20.6
PGTH-0.8	2.74±0.85	269±18.9	197	165.45±22.08
PGTH- 1	3.06±0.67	289±33.1	230	178.84±14.67

Table 8.3. Tensile values corresponding the representative tensile graph.

The composite also exhibits exceptional ductility to the extent of 200%. This was similar to the PGT series of composites with such high values of tensile strength and failure strain; the materials can be counted as ultra-tough composites with excellent energy absorption capability.

8.4 Interfacial interactions.

The experimental values of tensile strength for the PGTH films are validated by the Pukanszky model (Fig.8.11). The model displayed values like 1.8, 2.5 and 2.57 for the PGTH-0.4, PGTH-0.8, and PGTH-1 composite films. These values are distinctly high as compared to the previous systems. These high values define the PGTH systems like a typical case of surface treated filler incorporated in the polymer matrix. Dual functionalisation of the PGO films produce very strong adhesive forces amongst the graphene sheets and the matrix, resulting in high interfacial strengths across the polymer- graphene interface.

The comparable values of B for the PGTH-0.8 and PGTH-1 indicate that the interfacial strengthening effect is maximizing in these level of filler loading, although the exact loading with respect to peak mechanical properties has not been worked out. This interfacial coefficient is an indicative numerical parameter which is a result of multiple effects including, chemical functionalization by TEA and hydrazine, the morphology of the fillers and their distribution, contributing to the enhancement of polymer crystallinity and the synergistic reinforcement effects by the two-dimensional fillers and *in-situ* formed one-dimensional nanoribbons.

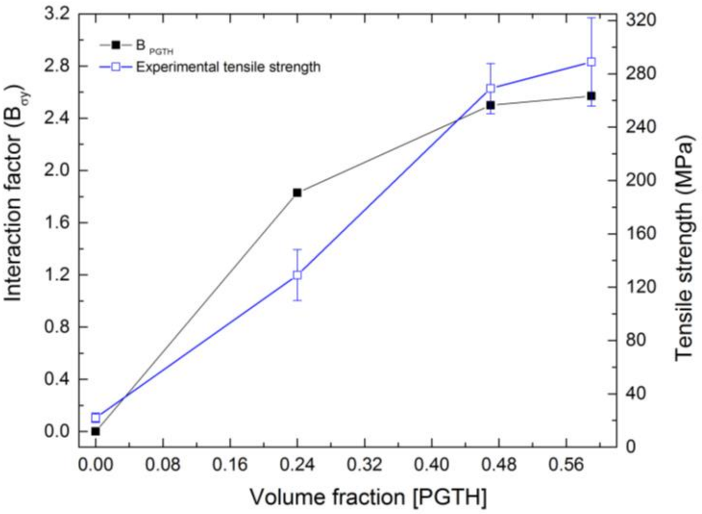

Figure 8.11. Dependence of Interaction factor B on the tensile strength of PGTH composites for their corresponding volume fractions.

8.5 Morphological and microstructural aspects.

An understanding of the structure-property relationship of the composites can be better acquired by observing the morphology and microstructure. Imaging of colloidal PGTH solution drop-cast on carbon coated TEM grid provide direct information regarding the dispersed state of the graphene sheets in the matrix. Bright field TEM images of the PGTH-1 composites exhibited a homogeneous distribution of the graphene-based fillers in the polymer matrix in addition to the platy type filler reinforced matrix. Additional features were observed where one-dimensional ribbon-shaped formations were homogeneously distributed in the matrix (Fig.8.12a). Higher magnification image of it (Fig.8.12b), showed the clear contrast of the ribbon structures in the polymer matrix. High-resolution imaging of various other regions in the composite interestingly exhibited such one-dimensional structures with various degrees of bent shapes, (Fig.8.12c &d). Some of the fillers even appeared to be looped. Furthermore, there were periodic contrasts in the one-dimensional bands, measurements of which led to believe these layered structures to be graphitic in nature. Such features have not been found in the literature in polymer systems. It is theorized that these one-dimensional ribbons may have resulted from the unzipping of the few layered graphene oxide fillers. Formation of one-dimensional carbon structures by the unzipping of graphene have been reported in the literature [320]. It is suspected that the wrinkled structures on the GO platelets may have been completely ripped off the surface tearing the whole layer, as well as forming such additional ribbons, although the exact mechanism for the formation is not known yet.

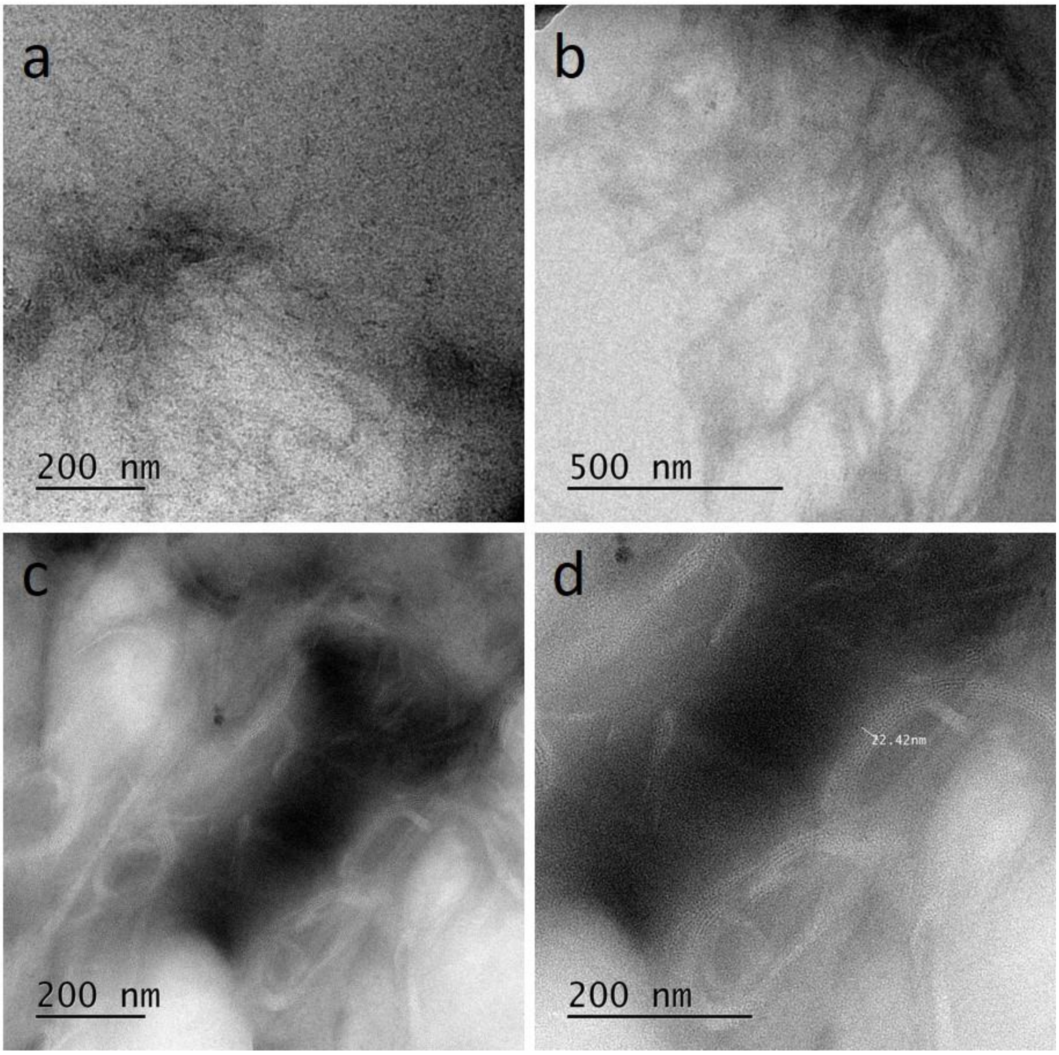

Figure 8.12. Transmission electron microscopy of PGTH composites; (a) bright field image (b) high-resolution bright field image showing the fibrillar reinforcements, (c) high-resolution micrographs showing graphene type order in the one-dimensional ribbons.

The exhibition of these microstructures and morphology proves multiple synergistic effects of strengthening to be operative in these composites. In addition to the typical two-dimensional morphology of the GO/CCG fillers in the polymer and associated strengthening mechanism, the existence of the one-dimensional fillers acts as additional reinforcements. Such synergistic effects can lead to strengthening in three dimensions.

Different regions of the composites were further explored with STEM imaging. The typical distribution of one or more multiple sheets of graphene was observed in many regions as can be seen from the HAADF-STEM images (Fig.8.13a & b). The one-dimensional ribbons can also be observed in high magnification STEM images (Fig.8.13c). These fibrous inclusions can aid effective load transfer from the matrix to reinforcements, causing improvement in elastic modulus. These features corroborate the exceptional improvement in elastic modulus of the composites (over an order of magnitude increase as compared to the pure polymer). Furthermore, in the plastic deformation region also, these reinforcements can aid failure by the crack bridging process. A classical crack bridging process was observed with these composites (Fig.8.13d), where a few of the formed carbon nanoribbons were found anchored on both of their ends to polymer matrices, clearly depicting a bridge, and resisting failure. The chemical aspect should also be considered wherein these one-dimensional ribbons are bonded to the matrices through the formation of hydrogen bonds between the oxygen containing functionalities on carbon ribbons and the polymer matrix. These features act as direct evidence for the exceptional ductility shown by the composites along with excellent elastic modulus. A synergistic effect of the two-dimensional fillers and the one-dimensional ribbons, thus improves the toughness of the composites, in a way similar to the CNT and graphene reinforced polymer composites.

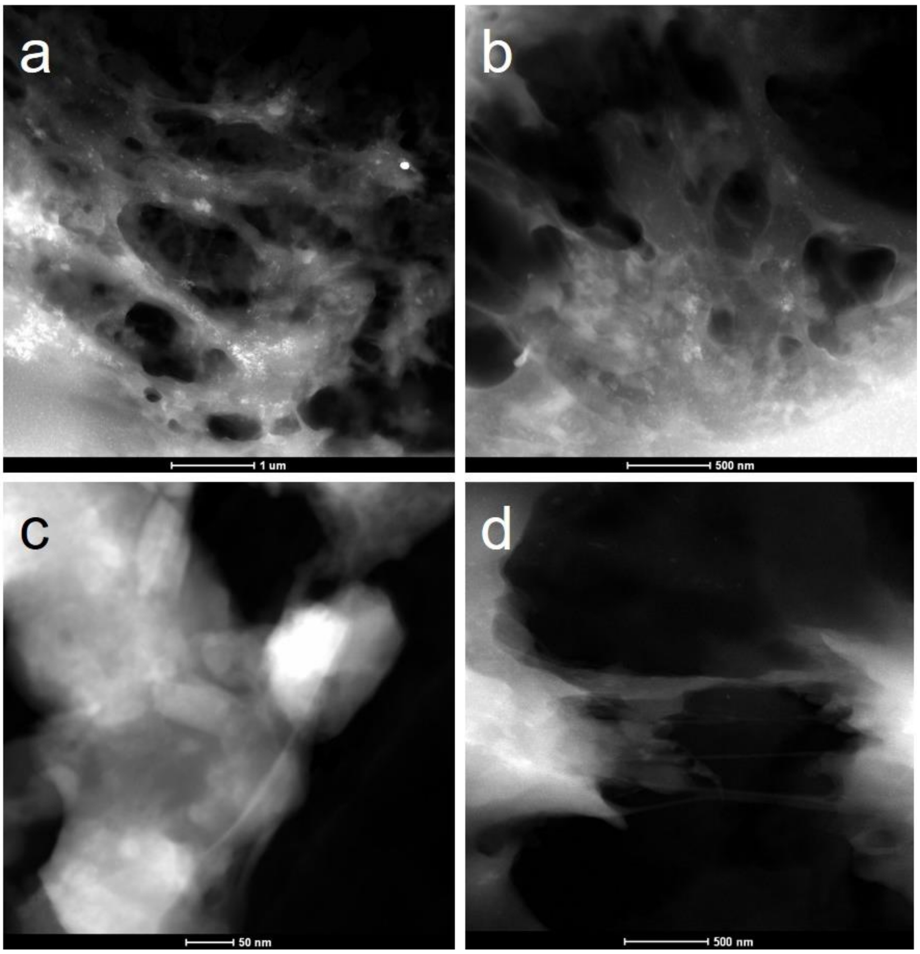

Figure 8.13. HAADF-STEM images of PGTH composites; (a & b) general distribution of graphene oxide in the polymer matrix, (c) high-resolution STEM image of a region indicating platy filler along with one-dimensional reinforcements, (d) direct evidence of the crack bridging process by the nanoribbons.

The cryo-fractured PGTH composites exhibited microstructures and morphology that were entirely different from the other composites discussed in here in this thesis. In addition to the roughened cross-section of the fractured specimens (as was seen for the PGT composites), nanostructured fibrillar protrusions were seen on the edges of the reinforcements (Fig8.14 a &b). From the images, it appeared that the entire edge sheet structure reinforcement (GO) is split up into multiple nanoribbons. The formation of these ribbons has been consistently observed in this work, from transmission electron microscopy, and also from scanning electron microscopy of fractured samples. These nanoribbons might add another level of strengthening mechanism with synergistic effects as has been obtained in both GO and CNT-reinforced polymer composites. These ribbons were found all over the edges of the graphene-based fillers. It did not appear that these ribbons were independently strewn around in the polymer matrix. The one end of the protrusion open and another attached to the matrix/filler and the pulled out morphology indicate that the moiety would have aided immensely in the strengthening and toughening process. The pulled out features (Fig.8.14c &d) exhibit coiled configurations to adopt a thermodynamically stable state. Even in these micrographs of the polymer coated two-dimensional fillers; the nanostructured ribbons can be observed. Thus, the synergistic strengthening by two-dimensional fillers and one-dimensional ribbons was confirmed by electron microscopy.

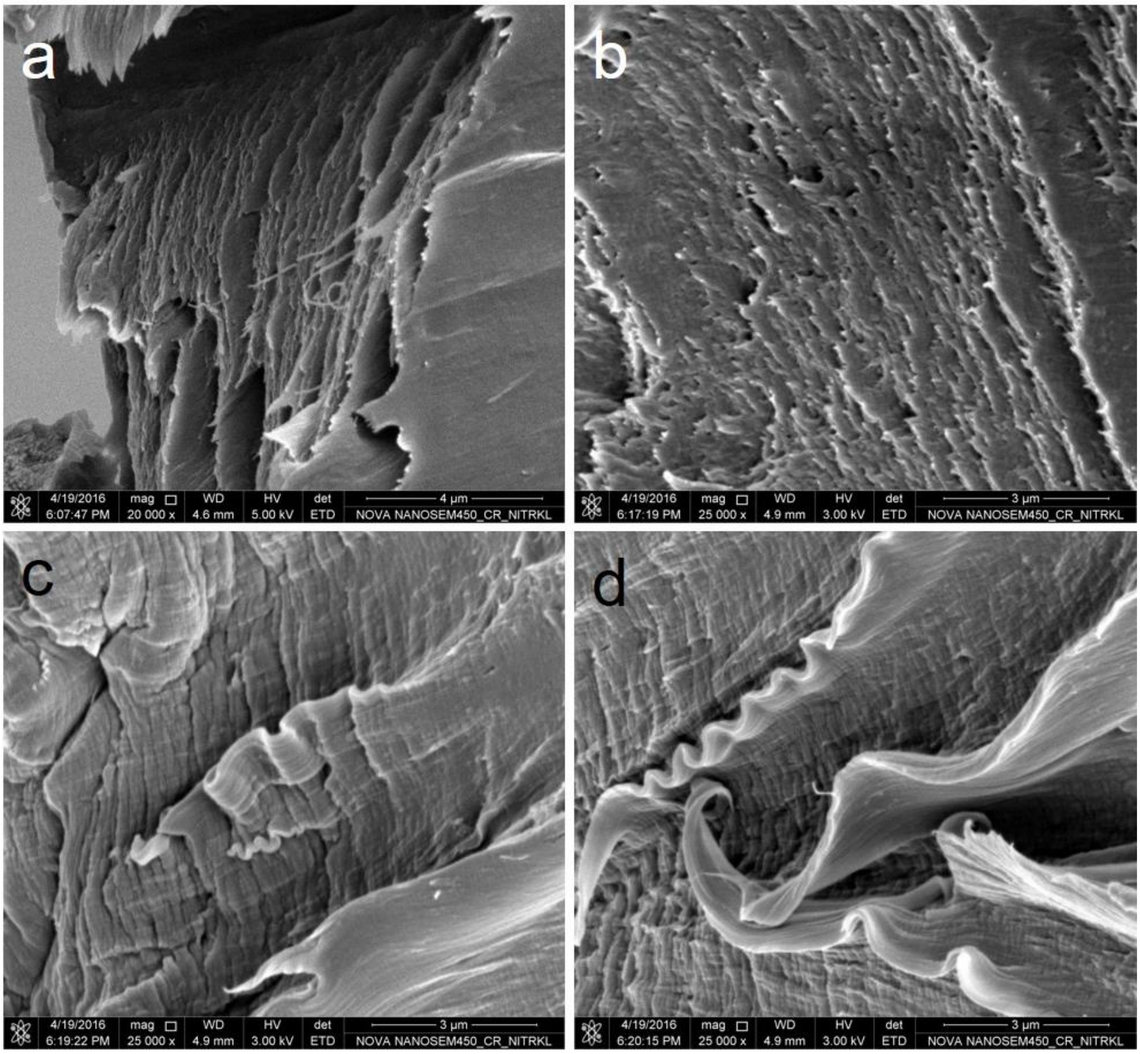

Figure 8.14. Cryo-fractured scanning electron micrographs of the PGTH composites.

8.6 Chapter Summary.

The important outcomes of this chapter can be summarized as follows:

- Dual stage functionalized graphene oxide fillers *in-situ,* with triethylamine followed by hydrazine, in the PVA matrix resulted in composites that showed improved crystallinity. The glass-transition, as well as melting temperatures, were found to be shifted to higher temperatures, indicating that the fillers impede the segmental mobility of the polymeric chains.

- Novel interpenetrating reinforcements were observed with the presence of sheet-like graphene and graphene nanoribbons. The synergistic effects of the two-dimensional and one-dimensional fillers resulted in exceptional improvement of mechanical properties.
- The elastic modulus and the tensile strength of the composites exhibited an order of improvement over the corresponding pure polymer properties. The specific strength of the developed composites was better than aluminum or magnesium based alloys.
- HRTEM and HAADF-STEM imaging revealed the interpenetrating microstructures as well the process of crack bridging.

Chapter 9

Concluding remarks

In the work embodied in this thesis, subtle variations in the processing of graphene oxide reinforced PVA nanocomposites have exhibited remarkable changes in the morphology, structure, microstructure and mechanical properties of the fabricated composites. Most of these parameters are co-operative and contribute to the achievement of improved material properties.

The basic premise of reinforcing nanostructured fillers in the polymer composites is the homogeneity of the filler dispersion. Herein, utilization of the processing steps including *in-situ* reduction, ensured homogeneous dispersion of the fillers in all of the composites, except for the triethanolamine functionalised (PGTO) system. The PGTO composite films exhibited some restaking of the reduced graphene sheets, leading to a reduced polymer- GO interfacial area and thus reduced structural properties. In addition, composite systems developed by *in-situ* reduction carried out by utilizing hydrazine, triethylamine, or the sequential functionalization by both yielded uniform dispersion of the reduced fillers in the polymer matrix. Such uniform dispersions motivate the formation of strengthened interfaces and hence better structure-property relationship.

Positron annihilation lifetime studies revealed that both graphene oxide and hydrazine reduced graphene oxide filler added to the PVA matrix, produced similar extents of the interfaces. Such uniformity in dispersion coupled with the interfacial interactions amongst the fillers and the polymer matrix led to improvement in the mechanical properties. This study was congruent with the further results obtained from the structural and thermal behavior of the composites systems.

A major outlook of the polymer composite system revolves around the contentious study of the filler-induced crystallinity in the polymer composites. Literature suggests both increases as well as a decrease in the polymer crystallinity on the addition of nanostructured carbon fillers. In this work, it is comprehensively shown that graphene oxide when added to the semi-crystalline polymer always improved the crystallinity of the overall composite system. Comparing the effect of crystallinity on different filler loading, and different reductants utilized, it was found that at a very low filler loading, as was the case for 0.4 wt% GO loading in the PGO or hydrazine reduced (PGH) system, the effect of crystallinity was not so pronounced. However, the Triethylamine functionalized GO fillers (with or without hydrazine) treatment exhibited improved crystallinity even at lower filler loadings. Consequently, these systems had the highest percent crystallinity with increasing filler content in the polymer to 1 wt% filler loading. The exceptional improvement in the crystalline nature of the polymer indicates well exfoliation, intercalation, and bonding of the fillers within the matrix. This is also congruent with the improvement in the glass transition and melting temperatures for the nanocomposites. It may be argued that the functionalized fillers act as heterogeneous nucleating sites for the growth of the polymer crystals, and homogeneity of filler dispersion influences the growth of the crystalline and amorphous domains in the polymer matrix. It can be suggested that interaction of the GO sheets in the amorphous domains of the polymer matrix led to an increase in the glass transition temperature, whereas nucleation and growth of the polymer crystals in and around the fillers led to an increase in the melting temperature. In the PGTH composite, the distribution of the fillers in the polymer was found to increase both the glass transition and the melting temperature of the composites.

This study reveals exceptional improvement in the mechanical properties of the composites, leading to almost an order of improvement in the elastic modulus as well as the tensile strength. The fact that such improvements have been achieved with only 0.7 volume% of the fillers lay a strong emphasis on the microstructure as well as the interfacial strengthening of the composites. The specific strengths of some of the studied systems in this work match with those of Al and Mg-based alloys, which is exciting. It is suggested that the covalent linkages formed through the TEA molecule at the filler edges result in the strengthening of the matrix- filler interface. The highly exfoliated filler morphology with large aspect ratio imparts efficient load transfer from the matrix to the filler. Moreover, restoration of the carbon double bonds in the basal planes of the fillers improves the elastic modulus of the filler itself. All of these features cooperatively enhance mechanical properties of the composites, especially in the PGT and PGTH system.

Microstructural and morphological features of some of the composites studied in this work reveal a few very important aspects. Use of transmission electron microscopy in studying polymer nanocomposite microstructure is less represented unlike its study of metals and ceramics. Conventional imaging, as well as HAADF-STEM based exploration, can be used to observe clear patterns in composite microstructures, despite the systems being of low atomic weight elements. One of the most important finds of this work is the formation of nematic ordered liquid crystalline type domains of the fillers in the polymer matrix. It was clearly observed with conventional as well as HAADF imaging. These macroscopically random, yet microscopically ordered filler domains, and the homogeneous distribution of such features are attributed to excellent improvement in mechanical properties. This type of ordering may allow tailoring of electronic/ electrical properties for functional applications. The development of this approach is partially in contrast to the generally proposed percolation network theory for change in electronic properties. In the current work, however, in the context of mechanical properties, the two-dimensional in-plane nematically ordered filler patches with highly crystalline polymer regions, cooperatively have led to much improved mechanical properties and fracture behavior.

Another unique aspect of the multistage treated (PGTH) composites was the synergistic reinforcement effect of two-dimensional graphene based fillers and the *in-situ* generated one-dimensional graphene based nanoribbons. The uniform observation of the said microstructures underscore the entangling effects of two different types of nanostructured fillers (with very different aspect ratio) clearly explain the exceptional improvement in the mechanical properties of the nanocomposites. While the formation of these nanoribbons is not entirely understood, it clearly warrants further investigation and applications of similar synthesis protocols in other polymeric systems for strength improvements. Th e impact of the said microstructures or electronic properties is also an interesting aspect of future work.

In summary, investigations on graphene oxide, and the same functionalized with different amines in a PVA polymer matrix indicated interesting structural, morphological, and microstructural variations along with distinctly different mechanical properties. Such improved mechanical properties as attributed to the strengthening of the polymer matrix and filler interface by utilizing novel solvents which act as both reductants and functionalizing agents. This work demonstrates these finds in a PVA model system for aqueous processable polymers. These concepts can be applied to other polymer systems of choice, and clearly, warrants further investigation on other systems.

REFERENCES

[1] U. Szeluga, B. Kumanek, and B. Trzebicka, “Synergy in hybrid polymer/nanocarbon composites. A review,” *Composites Part A: Applied Science and Manufacturing,* vol. 73, pp. 204-231, 2015.

[2] J.-F. Zou, Z.-Z. Yu, Y.-X. Pan, X.-P. Fang, and Y.-C. Ou, “Conductive mechanism of polymer/graphite conducting composites with low percolation threshold,” *Journal of Polymer Science Part B: Polymer Physics,* vol. 40, no. 10, pp. 954-963, 2002.

[3] G.-H. Chen, D.-J. Wu, W.-G. Weng, and W.-L. Yan, “Preparation of polymer/graphite conducting nanocomposite by intercalation polymerization,” *Journal of Applied Polymer Science,* vol. 82, no. 10, pp. 2506-2513, 2001.

[4] F. Hassouna, A. Laachachi, D. Chapron, Y. El Mouedden, V. Toniazzo, and D. Ruch, “Development of new approach based on Raman spectroscopy to study the dispersion of expanded graphite in poly(lactide),” *Polymer Degradation and Stability,* vol. 96, no. 12, pp. 2040-2047, 2011.

[5] Z. Spitalsky, D. Tasis, K. Papagelis, and C. Galiotis, “Carbon nanotube–polymer composites: Chemistry, processing, mechanical and electrical properties,” *Progress in Polymer Science,* vol. 35, no. 3, pp. 357-401, 2010.

[6] A. D. Winter, E. Larios, F. M. Alamgir, C. Jaye, D. A. Fischer, and E. M. Campo, "Polymer-carbon nanotube composites: electrospinning, alignment and interactions." p. 91700H.

[7] R. Blake, J. N. Coleman, M. T. Byrne, J. E. McCarthy, T. S. Perova, W. J. Blau, A. Fonseca, J. B. Nagy, and Y. K. Gun'ko, “Reinforcement of poly(vinyl chloride) and polystyrene using chlorinated polypropylene grafted carbon nanotubes,” *Journal of Materials Chemistry,* vol. 16, no. 43, pp. 4206-4213, 2006.

[8] C. Lee, X. Wei, J. W. Kysar, and J. Hone, “Measurement of the elastic properties and intrinsic strength of monolayer graphene,” *Science,* vol. 321, no. 5887, pp. 385-8, 2008.

[9] A. A. Balandin, S. Ghosh, W. Bao, I. Calizo, D. Teweldebrhan, F. Miao, and C. N. Lau, “Superior Thermal Conductivity of Single-Layer Graphene,” *Nano Lett,* vol. 8, no. 3, pp. 902-907, 2008.

[10] K. I. Bolotin, K. J. Sikes, Z. Jiang, M. Klima, G. Fudenberg, J. Hone, P. Kim, and H. L. Stormer, “Ultrahigh electron mobility in suspended graphene,” *Solid State Communications,* vol. 146, no. 9–10, pp. 351-355, 2008.

[11] J. L. Vickery, A. J. Patil, and S. Mann, “Fabrication of Graphene–Polymer Nanocomposites With Higher-Order Three-Dimensional Architectures,” *Advanced Materials,* vol. 21, no. 21, pp. 2180-2184, 2009.

[12] X. Wang, L. Zhi, and K. Mullen, “Transparent, conductive graphene electrodes for dye-sensitized solar cells,” *Nano Lett,* vol. 8, no. 1, pp. 323-7, 2008.

[13] J. D. Fowler, M. J. Allen, V. C. Tung, Y. Yang, R. B. Kaner, and B. H. Weiller, “Practical chemical sensors from chemically derived graphene,” *ACS Nano,* vol. 3, no. 2, pp. 301-6, 2009.

[14] L. R. Bunnell, "Method for producing thin graphite flakes with large aspect ratios," Google Patents, 1993.

[15] K. S. Novoselov, V. I. Fal'ko, L. Colombo, P. R. Gellert, M. G. Schwab, and K. Kim, “A roadmap for graphene,” *Nature,* vol. 490, no. 7419, pp. 192-200, 2012.

[16] C. K. Chua, and M. Pumera, “The reduction of graphene oxide with hydrazine: elucidating its reductive capability based on a reaction-model approach,” *Chem Commun (Camb),* vol. 52, no. 1, pp. 72-75, 2016.

[17] H. A. Becerril, J. Mao, Z. Liu, R. M. Stoltenberg, Z. Bao, and Y. Chen, “Evaluation of Solution-Processed Reduced Graphene Oxide Films as Transparent Conductors,” *ACS Nano,* vol. 2, no. 3, pp. 463-470, 2008.

[18] H. C. Schniepp, J. L. Li, M. J. McAllister, H. Sai, M. Herrera-Alonso, D. H. Adamson, R. K. Prud'homme, R. Car, D. A. Saville, and I. A. Aksay, “Functionalized single graphene sheets derived from splitting graphite oxide,” *J Phys Chem B,* vol. 110, no. 17, pp. 8535-9, 2006.

[19] P. Steurer, R. Wissert, R. Thomann, and R. Mülhaupt, “Functionalized Graphenes and Thermoplastic Nanocomposites Based upon Expanded Graphite Oxide,” *Macromolecular Rapid Communications,* vol. 30, no. 4-5, pp. 316-327, 2009.

[20] S. A. M. N. Muralidharan, “Thermally reduced graphene oxide/thermoplastic polyurethane nanocomposites as photomechanical actuators,” *Adv. Mat. Lett.,* vol. 4, no. 12, pp. 5, 2013.

[21] Y. Zhu, M. D. Stoller, W. Cai, A. Velamakanni, R. D. Piner, D. Chen, and R. S. Ruoff, “Exfoliation of graphite oxide in propylene carbonate and thermal reduction of the resulting graphene oxide platelets,” *ACS Nano,* vol. 4, no. 2, pp. 6, 2010.

[22] S. Stankovich, R. D. Piner, S. T. Nguyen, and R. S. Ruoff, “Synthesis and exfoliation of isocyanate-treated graphene oxide nanoplatelets,” *Carbon,* vol. 44, no. 15, pp. 3342-3347, 2006.

[23] M. Moazzami Gudarzi, “Enhancement of dispersion and bonding of graphene-polymer through wet transfer of functionalized graphene oxide,” *eXPRESS Polymer Letters,* vol. 6, no. 12, pp. 1017-1031, 2012.

[24] M. Fang, K. Wang, H. Lu, Y. Yang, and S. Nutt, “Covalent polymer functionalization of graphene nanosheets and mechanical properties of composites,” *Journal of Materials Chemistry,* vol. 19, no. 38, pp. 7098, 2009.

[25] S. R. L. B. Qi, X. E. Xiao, L. L. Pan, F. Z. Tan, J. H. Yu, “Enhanced thermal and mechanical properties of epoxy composites by mixing thermotropic liquid crystalline epoxy grafted graphene oxide,” *eXPRESS Polymer Letters,* vol. 8, no. 7, pp. 11, 2014.

[26] S. T. Clarke, Callahan *Building Green: A Complete How-to Guide to Alternative Building Methods-Earth Plaster, Straw Bale, Cordwood, Cob, Living Roofs*, p.^pp. 276: Sterling Publishing Company, Inc, 2009.

[27] G. W. Jeon, and Y. G. Jeong, “Electric heating films based on m-aramid nanocomposites containing hybrid fillers of graphene and carbon nanotube,” *Journal of Materials Science,* vol. 48, no. 11, pp. 4041-4049, 2013.

[28] L. Lapcik, P. Jindrova, B. Lapcikova, R. Tamblyn, R. Greenwood, and N. Rowson, “Effect of the talc filler content on the mechanical properties of polypropylene composites,” *Journal of Applied Polymer Science,* vol. 110, no. 5, pp. 2742-2747, 2008.

[29] M. R. Schutz, H. Kalo, T. Lunkenbein, A. H. Groschel, A. H. E. Muller, C. A. Wilkie, and J. Breu, “Shear stiff, surface modified, mica-like nanoplatelets: a novel filler for polymer nanocomposites,” *Journal of Materials Chemistry,* vol. 21, no. 32, pp. 12110-12116, 2011.

[30] D. Cai, and M. Song, “A simple route to enhance the interface between graphite oxide nanoplatelets and a semi-crystalline polymer for stress transfer,” *Nanotechnology,* vol. 20, no. 31, pp. 315708, 2009.

[31] Y. Matsuo, K. Tahara, and Y. Sugie, “Structure and thermal properties of poly(ethylene oxide)-intercalated graphite oxide,” *Carbon,* vol. 35, no. 1, pp. 113-120, 1997.

[32] H. Kim, A. A. Abdala, and C. W. Macosko, “Graphene/Polymer Nanocomposites,” *Macromolecules,* vol. 43, no. 16, pp. 6515-6530, 2010.

[33] Z. Xu, and C. Gao, “In situPolymerization Approach to Graphene-Reinforced Nylon-6 Composites,” *Macromolecules,* vol. 43, no. 16, pp. 6716-6723, 2010.

[34] R. K. Layek, S. Samanta, D. P. Chatterjee, and A. K. Nandi, “Physical and mechanical properties of poly(methyl methacrylate) -functionalized graphene/poly(vinylidine fluoride) nanocomposites: Piezoelectric β polymorph formation,” *Polymer,* vol. 51, no. 24, pp. 5846-5856, 2010.

[35] S. G. Miller, J. L. Bauer, M. J. Maryanski, P. J. Heimann, J. P. Barlow, J. M. Gosau, and R. E. Allred, “Characterization of epoxy functionalized graphite nanoparticles and the physical properties of epoxy matrix nanocomposites,” *Composites Science and Technology,* vol. 70, no. 7, pp. 1120-1125, 2010.

[36] J. Liang, Y. Huang, L. Zhang, Y. Wang, Y. Ma, T. Guo, and Y. Chen, “Molecular-Level Dispersion of Graphene into Poly(vinyl alcohol) and Effective Reinforcement of their Nanocomposites,” *Advanced Functional Materials,* vol. 19, no. 14, pp. 2297-2302, 2009.

[37] X. Zhao, Q. Zhang, D. Chen, and P. Lu, “Enhanced Mechanical Properties of Graphene-Based Poly(vinyl alcohol) Composites,” *Macromolecules,* vol. 43, no. 5, pp. 2357-2363, 2010.

[38] H.-L. Ma, Y. Zhang, Q.-H. Hu, S. He, X. Li, M. Zhai, and Z.-Z. Yu, “Enhanced mechanical properties of poly(vinyl alcohol) nanocomposites with glucose-reduced graphene oxide,” *Materials Letters,* vol. 102-103, pp. 15-18, 2013.

[39] R. K. Layek, S. Samanta, and A. K. Nandi, “The physical properties of sulfonated graphene/poly(vinyl alcohol) composites,” *Carbon,* vol. 50, no. 3, pp. 815-827, 2012.

[40] Q. Li, Z. Li, M. Chen, and Y. Fang, “Real-time study of graphene’s phase transition in polymer matrices,” *Nano Lett,* vol. 9, no. 5, pp. 2129-2132, 2009.

[41] O. Monticelli, S. Bocchini, A. Frache, E. S. Cozza, O. Cavalleri, and L. Prati, “Simple Method for the Preparation of Composites Based on PA6 and Partially Exfoliated Graphite,” *Journal of Nanomaterials,* vol. 2012, pp. 5, 2012.

[42] L. S. Schadler, L. C. Brinson, and W. G. Sawyer, “Polymer nanocomposites: A small part of the story,” *Jom,* vol. 59, no. 3, pp. 53-60, 2007.

[43] S. Stankovich, D. A. Dikin, G. H. Dommett, K. M. Kohlhaas, E. J. Zimney, E. A. Stach, R. D. Piner, S. T. Nguyen, and R. S. Ruoff, “Graphene-based composite materials,” *Nature,* vol. 442, no. 7100, pp. 282-6, Jul 20, 2006.

[44] S. J. Dillon, M. Tang, W. C. Carter, and M. P. Harmer, “Complexion: A new concept for kinetic engineering in materials science,” *Acta Materialia,* vol. 55, no. 18, pp. 6208-6218, 2007.

[45] R. Mahendran, D. Sridharan, K. Santhakumar, and G. Gnanasekaran, “Green Route Fabrication of Graphene Oxide Reinforced Polymer Composites with Enhanced Mechanical Properties,” *Journal of Nanoscience,* vol. 2016, pp. 8, 2016.

[46] A. Abdolmaleki, S. Mallakpour, and S. Borandeh, “Research Article,” *Polymer Composites,* vol. 37, no. 6, pp. 1924-1935, 5, 2016.

[47] Y. R. Lee, Raghu,Anjanapura V.,Jeong, Han Mo,Kim, Byung Kyu, “Properties of Waterborne Polyurethane/Functionalized Graphene Sheet Nanocomposites Prepared by an in situ Method,” *Macromolecular Chemistry and Physics,* vol. 210, no. 15, pp. 1247-1254, 2009.

[48] F. Wang, L. T. Drzal, Y. Qin, and Z. Huang, “Size effect of graphene nanoplatelets on the morphology and mechanical behavior of glass fiber/epoxy composites,” *Journal of Materials Science,* vol. 51, no. 7, pp. 3337-3348, 2016.

[49] S. H. Maruf, D. U. Ahn, J. Pellegrino, J. P. Killgore, A. R. Greenberg, and Y. Ding, “Correlation between barrier layer Tg and a thin-film composite polyamide membrane's performance: Effect of chlorine treatment,” *Journal of Membrane Science,* vol. 405–406, pp. 167-175, 2012.

[50] J. Holbery, and D. Houston, “Natural-fiber-reinforced polymer composites in automotive applications,” *The Journal of The Minerals, Metals & Materials Society (TMS),* vol. 58, no. 11, pp. 80-86, 2006.

[51] M. F. Maitz, “Applications of synthetic polymers in clinical medicine,” *Biosurface and Biotribology,* vol. 1, no. 3, pp. 161-176, 9, 2015.

[52] H.L.Wang, “Application of Fiber Reinforced Composites in Sports Equipment,” *Applied Mechanics and Materials,* vol. 416, pp. 3, 2013.

[53] L. Mishnaevsky, “Composite materials for wind energy applications: micromechanical modeling and future directions,” *Computational Mechanics,* vol. 50, no. 2, pp. 195-207, 2012.

[54] R. Talreja, "Manufacturing defects in composites and their effects on performance," *Polymer Composites in the Aerospace Industry,* pp. 99-113: Woodhead Publishing, 2015.

[55] A. A. Rahman, Ilias Al Zahrani, Saeed M. Eleithy, Rabeh H., “A review of the applications of nanocarbon polymer composites,” *Nano,* vol. 06, no. 03, pp. 185-203, 2011.

[56] L. V. Silva, C. C. Angrizani, J. R. Souza, S. C. Amico, and J. T. N. Medeiros, “Use of polyester/glass-fiber residues as fillers for composites,” *Journal of Applied Polymer Science,* vol. 124, no. 1, pp. 302-310, 2012.

[57] M. Usman, S. Adeosun, and G. Osifeso, “Optimum calcium carbonate filler concentration for flexible polyurethane foam composite,” *Journal of Minerals and Materials Characterization and Engineering,* vol. 11, no. 03, pp. 311, 2012.

[58] G. Motors, "The First 75 Years," E. o. A. Quarterly, ed., New York: Crown Publishers, Inc, 1983.

[59] H. v. Yoshitake, no. 9, , p. 124. 1996, *Plastics Age,* vol. 42, no. 9, 1996.

[60] D. Dowsan, “Swimming pools: Fiberglass resurfacing option extends useful lifeGRC Fiberglass Coatings ” *Composites technology*, 2006.

[61] W. D. Callister, and D. G. Rethwisch, *Materials science and engineering : an introduction*, 2014.

[62] R. W. Messler, *The Essence of Materials for Engineers*: Jones & Bartlett Learning, 2010.

[63] A. Varvani-Farahani, “Composite Materials: Characterization, Fabrication and Application-Research Challenges and Directions,” *Applied Composite Materials,* vol. 17, no. 2, pp. 4, 2010.

[64] R. J. Young, and M. Liu, “The microstructure of a graphene-reinforced tennis racquet,” *Journal of Materials Science,* vol. 51, no. 8, pp. 3861-3867, 2016, 2016.

[65] A. Kasgoz, D. Akın, A. İ. Ayten, and A. Durmus, “Effect of different types of carbon fillers on mechanical and rheological properties of cyclic olefin copolymer (COC) composites,” *Composites Part B: Engineering,* vol. 66, pp. 126-135, 11, 2014.

[66] K. O. U. P.E.Imoisilli, I.T.Adejugbe, D.Adgidzi, S.O.O.Olusunle, “Mechanical properties of rice husk/carbon black hybrid natural rubber composite ” *Chemistry and material research,* vol. 3, no. 8, pp. 6, 2013.

[67] K. Senthivel, K. Manikandan, and B. Prabu, “Studies on the Mechanical Properties of Carbon Black/Halloysite Nanotube Hybrid Fillers in Nitrile Rubber Nanocomposites,” *Materials Today: Proceedings,* vol. 2, no. 4-5, pp. 3627-3637, 2015.

[68] S. Praveen, P. K. Chattopadhyay, S. Jayendran, B. C. Chakraborty, and S. Chattopadhyay, “Effect of rubber matrix type on the morphology and reinforcement effects in carbon black-nanoclay hybrid composites—A comparative assessment,” *Polymer Composites,* vol. 31, no. 1, pp. 97-104, 2010.

[69] Y.-P. Wu, W. Zhao, and L.-Q. Zhang, “ Macromol. Mater. Eng. 8/2006,” *Macromolecular Materials and Engineering,* vol. 291, no. 8, pp. 905-905, 2006.

[70] W. Di, G. Zhang, Y. Peng, and Z. Zhao, “Two-step PTC effect in immiscible polymer blends filled with carbon black,” *Journal of Materials Science,* vol. 39, no. 2, pp. 695-697, 2004.

[71] R. Tlili, A. Boudenne, V. Cecen, L. Ibos, I. Krupa, and Y. Candau, “Thermophysical and Electrical Properties of Nanocomposites Based on Ethylene–Vinylacetate Copolymer (EVA) Filled with Expanded and Unexpanded Graphite,” *International Journal of Thermophysics,* vol. 31, no. 4, pp. 936-948, 2010.

[72] J. Kratochvíla, A. Boudenne, and I. Krupa, “Effect of filler size on thermophysical and electrical behavior of nanocomposites based on expanded graphite nanoparticles filled in low-density polyethylene matrix,” *Polymer Composites,* vol. 34, no. 2, pp. 149-155, 2013.

[73] A. J. C. Glover, Minzhen Overdeep, Kyle R. Kranbuehl, David E. Schniepp, Hannes C., “In situ reduction of Graphene Oxide in Polymers,” *Macromolecules,* vol. 44, no. 24, pp. 9821-9829, 2011.

[74] A. Yasmin, J.-J. Luo, and I. M. Daniel, “Processing of expanded graphite reinforced polymer nanocomposites,” *Composites Science and Technology,* vol. 66, no. 9, pp. 1182-1189, 7, 2006.

[75] W. Zheng, X. Lu, and S.-C. Wong, “Electrical and mechanical properties of expanded graphite-reinforced high-density polyethylene,” *Journal of Applied Polymer Science,* vol. 91, no. 5, pp. 2781-2788, 2004.

[76] A. J. Waddon, M. J. Hill, A. Keller, and D. J. Blundell, “On the crystal texture of linear polyaryls (PEEK, PEK and PPS),” *Journal of Materials Science,* vol. 22, no. 5, pp. 1773-1784, 1987, 1987.

[77] S. Kumar, Doshi, HaritSrinivasarao, Mohan,Park, Jung O,Schiraldi, David A., “Fibers from polypropylene/nano carbon fiber composites,” *Polymer,* vol. 43, no. 5, pp. 1701-1703, 3, 2002.

[78] B. S. Jijun Zeng, W.S.Johnson, David Schiraldi,Satish Kumar, “Processing and properties of poly(methyl methacrylate)/carbon nanofiber composites ” *Composites Part B: Engineering,* vol. 35, pp. 6, 2004.

[79] J. Xu, J. P. Donohoe, and C. U. Pittman Jr, “Preparation, electrical and mechanical properties of vapor grown carbon fiber (VGCF)/vinyl ester composites,” *Composites Part A: Applied Science and Manufacturing,* vol. 35, no. 6, pp. 693-701, 6, 2004.

[80] L. P. Joseph H. Koo, Andre Lee, *Nanocomposites for carbon fibre reinforced polymer matrix composites* 2004.

[81] R. Sadeghian, Gangirreddy,S., Minaaie, B., & Hsiao, K., “Manufacturing carbon nanofibres toughned polyster/glass fibre composites using vacuum assited resin tranfer molding for enhancing the mode-1 delamination resistance,,” *Composites Part A,* vol. 37, pp. 8, 2006.

[82] S. Vivekanandhan, M. Misra, and A. K. Mohanty, “Thermal, mechanical, and morphological investigation of injection molded poly(trimethylene terephthalate)/carbon fiber composites,” *Polymer Composites,* vol. 33, no. 11, pp. 1933-1940, 2012.

[83] D. Chen, F. Lu, and B. Jiang, “Tensile properties of a carbon fibre 2d woven reinforced polymer matrix composite in through-thickness direction,” *Journal of Composite Materials*, 2012.

[84] P. S. K. Jo B.W, Kim D.K,, “Mechanical properties of nano-MMT reinforced polymer composite and polymer concrete,” *Construction and building materials,* vol. 22, pp. 6, 2008.

[85] M. Bauer, Kahle, O.,Landeck,S.,Uhlig,C and Wurzel,R., “High performance composites using nanotechnology,” *Advanced Materials Research,* vol. 32, pp. 4, 2008.

[86] D. Y. C. Chen, & D. Raghvan., “Synthesis, characterization and mechanical properties evaluation of thermally stable apophyllite vinyl ester nanocomposite ” *Polymers for advanced technologies,* vol. 18, pp. 8, 2007a.

[87] J. Karger-Kocsis, Gryshuk, O.,Frohlich,J. & Muhaupt, R. , “Interpenetrating vinylester/epoxy resins modified with organophilic layered silicates,” *Composites Science and Technology,* vol. 63, pp. 9, 2003.

[88] D. A. A.Kasgoz, Ali Imran Ayten “Effect of different types of carbon fillers on mechanical and rheological properties of cyclic olefin copolymer (COC) composites ” *Composites Part B: Engineering,* vol. 66, pp. 10, 2012.

[89] A.J.Bedanokov, “Polymer nanocomposites,” 2011.

[90] J. K. Pandey, A. P. Kumar, M. Misra, A. K. Mohanty, L. T. Drzal, and R. Palsingh, “Recent advances in biodegradable nanocomposites,” *Journal of Nanoscience and Nanotechnology,* vol. 5, no. 4, pp. 497-526, 2005.

[91] M. Sternitzke, “Structural ceramic nanocomposites,” *Journal of the European Ceramic Society,* vol. 17, no. 9, pp. 1061-1082, 1997.

[92] M. Alexandre, and P. Dubois, “Polymer-layered silicate nanocomposites: preparation, properties and uses of a new class of materials,” *Materials Science and Engineering: R: Reports,* vol. 28, no. 1, pp. 1-63, 2000.

[93] R. Gangopadhyay, and A. De, “Conducting polymer nanocomposites: a brief overview,” *Chemistry of Materials,* vol. 12, no. 3, pp. 608-622, 2000.

[94] S. Anandan, “Viologen impregnated PVDF with TiO2 nanofiller as a solid polymer electrolyte for dye-sensitized solar cells,” *Current Applied Physics,* vol. 8, no. 1, pp. 99-103, 1, 2008.

[95] S. F. a. R. D. Mathad, "Effect of nanofiller on conducitvity in PEO-PMMA-LiClO$_4$ polymer electrolyte," *International Journal of Advanced science and techology,* vol. 81, pp. 3, 2015.

[96] S. Anandan, and R. Sivakumar, "Effect of loaded TiO2 nanofiller on heteropolyacid-impregnated PVDF polymer electrolyte for the performance of dye-sensitized solar cells," *physica status solidi (a),* vol. 206, no. 2, pp. 343-350, 2009.

[97] L. L. Xiaowu Fan, Philip B.Messersmith, "Surface-initiated polymerization from TiO2 nanoparticle surfaces through a biomimetic initiator: A new route toward polymer–matrix nanocomposites," *Compos. Sci. Technol.,* vol. 66, pp. 7, 2006.

[98] W. K. Chee, H. N. Lim, N. M. Huang, and I. Harrison, "Nanocomposites of graphene/polymers: a review," *RSC Advances,* vol. 5, no. 83, pp. 68014-68051, 2015.

[99] D. R. a. D. P. Sabu Thomas, *Spctroscopy of polymer nanocomposites* Cambridge Mathew deans, 2016.

[100] E. G. a. C. C.-J. Damien M. Marquis, *Properties of Nanofillers in Polymer, Nanocomposites and Polymers with Analytical Methods*: Intech, 2011.

[101] L. Ferroni, G. Pezzotti, T. Isshiki, and H.-J. Kleebe, "Determination of amorphous interfacial phases in Al 2 O 3/SiC nanocomposites by computer-aided high-resolution electron microscopy," *Acta Materialia,* vol. 49, no. 11, pp. 2109-2113, 2001.

[102] M. R. Johan, O. H. Shy, S. Ibrahim, S. M. Mohd Yassin, and T. Y. Hui, "Effects of Al$_2$O$_3$ nanofiller and EC plasticizer on the ionic conductivity enhancement of solid PEO–LiCF$_3$SO$_3$ solid polymer electrolyte," *Solid State Ionics,* vol. 196, no. 1, pp. 41-47, 2011.

[103] K. Sownthari, and S. Austin Suthanthiraraj, "Influence of Al2O3 nanofiller on the properties of polymer electrolyte based on poly-ε-caprolactone," *Polymer Bulletin,* vol. 72, no. 1, pp. 61-73, 2015.

[104] D. R. Paul, and L. M. Robeson, "Polymer nanotechnology: Nanocomposites," *Polymer,* vol. 49, no. 15, pp. 3187-3204, 2008.

[105] R. Merijs Meri, I. Bochkov, A. Grigalovca, J. Zicans, J. Grabis, R. Kotsilkova, and I. Borovanska, "Nanocomposites Based on ZnO Modified Polymer Blends," *Macromolecular Symposia,* vol. 321-322, no. 1, pp. 130-134, 2012.

[106] Y. Shin, D. Lee, K. Lee, K. H. Ahn, and B. Kim, "Surface properties of silica nanoparticles modified with polymers for polymer nanocomposite applications," *Journal of Industrial and Engineering Chemistry,* vol. 14, no. 4, pp. 515-519, 7, 2008.

[107] S. Z. Barus, Marco Lazzari, Massimo Costa, Luigi, "Preparation of polymeric hybrid nanocomposites based on PE and nanosilica," *Polymer,* vol. 50, no. 12, pp. 2595-2600, 2009.

[108] M. Conradi, "Nano silica-Reinforced Polymer composites " *Materials and technology,* vol. 47, pp. 9, 2013.

[109] S. e. Ajayan P, L.,& Braun, P, "Nanocomposite science and technolgy.," *Ed.Wiley*, 2003.

[110] O. Kamigaito, "What can be improved by nanometer composites?," *Journal of the Japan Society of Powder and Powder Metallurgy,* vol. 38, no. 3, pp. 315-321, 1991.

[111] S. Iijima, "Helical microtubules of graphitic carbon," *Nature,* vol. 354, no. 6348, pp. 56-58, 1991.

[112] K. Balasubramanian, and M. Burghard, "Chemically Functionalized Carbon Nanotubes," *Small,* vol. 1, no. 2, pp. 180-192, 2005.

[113] P. M. Ajayan, "Nanotubes from Carbon," *Chem Rev,* vol. 99, no. 7, pp. 1787-1800, 1999.

[114] M.-F. Yu, O. Lourie, M. J. Dyer, K. Moloni, T. F. Kelly, and R. S. Ruoff, "Strength and Breaking Mechanism of Multiwalled Carbon Nanotubes Under Tensile Load," *Science,* vol. 287, no. 5453, pp. 637-640, 2000.

[115] B. Peng, M. Locascio, P. Zapol, S. Li, S. L. Mielke, G. C. Schatz, and H. D. Espinosa, "Measurements of near-ultimate strength for multiwalled carbon nanotubes and irradiation-induced crosslinking improvements," *Nat Nano,* vol. 3, no. 10, pp. 626-631, 2008.

[116] T. Filleter, R. Bernal, S. Li, and H. D. Espinosa, "Ultrahigh Strength and Stiffness in Cross-Linked Hierarchical Carbon Nanotube Bundles," *Advanced Materials,* vol. 23, no. 25, pp. 2855-2860, 2011.

[117] L. P. Zanello, B. Zhao, H. Hu, and R. C. Haddon, "Bone Cell Proliferation on Carbon Nanotubes," *Nano Lett,* vol. 6, no. 3, pp. 562-567, 2006.

[118] K. Jensen, W. Mickelson, A. Kis, and A. Zettl, "Buckling and kinking force measurements on individual multiwalled carbon nanotubes," *Physical Review B,* vol. 76, no. 19, pp. 195436, 2007.

[119] L. Jin, C. Bower, and O. Zhou, "Alignment of carbon nanotubes in a polymer matrix by mechanical stretching," *Applied Physics Letters,* vol. 73, no. 9, pp. 1197-1199, 1998.

[120] O. S. P.M.Ajayan, C.Colliex and D.Trauth, "Alligned carbin nanotube arrays formed by cutting a polymer - resin nanotube composite," *Science and Engineering of Composite Materials,* vol. 265, no. 5176, pp. 4, 1994.

[121] W. A. de Heer, A. Châtelain, and D. Ugarte, "A Carbon Nanotube Field-Emission Electron Source," *Science,* vol. 270, no. 5239, pp. 1179-1180, 1995.

[122] W. Feng, X. D. Bai, Y. Q. Lian, J. Liang, X. G. Wang, and K. Yoshino, “Well-aligned polyaniline/carbon-nanotube composite films grown by in-situ aniline polymerization,” *Carbon,* vol. 41, no. 8, pp. 1551-1557, 2003.

[123] N. R. Raravikar, L. S. Schadler, A. Vijayaraghavan, Y. Zhao, B. Wei, and P. M. Ajayan, “Synthesis and Characterization of Thickness-Aligned Carbon Nanotube−Polymer Composite Films,” *Chemistry of Materials,* vol. 17, no. 5, pp. 9, 2005.

[124] J. Qian, P. He, and K. Nie, “Nonisothermal crystallization of PP/nano-SiO2 composites,” *Journal of Applied Polymer Science,* vol. 91, no. 2, pp. 1013-1019, 2004.

[125] R. E. Gorga, and R. E. Cohen, “Toughness enhancements in poly(methyl methacrylate) by addition of oriented multiwall carbon nanotubes,” *Journal of Polymer Science Part B: Polymer Physics,* vol. 42, no. 14, pp. 2690-2702, 2004.

[126] M. Lopez Manchado, L. Valentini, J. Biagiotti, and J. M. Kenny, “Thermal and mechanical properties of single-walled carbon nanotubes–polypropylene composites prepared by melt processing,” *Carbon,* vol. 43, pp. 1499-1505, 2005.

[127] W. Wang, P. Ciselli, E. Kuznetsov, T. Peijs, and A. H. Barber, “Effective reinforcement in carbon nanotube–polymer composites,” *Philosophical Transactions of the Royal Society of London A: Mathematical, Physical and Engineering Sciences,* vol. 366, no. 1870, pp. 1613-1626, 2008.

[128] J. Fritzsche, H. Lorenz, and M. Klüppel, “CNT Based Elastomer-Hybrid-Nanocomposites with Promising Mechanical and Electrical Properties,” *Macromolecular Materials and Engineering,* vol. 294, no. 9, pp. 551-560, 2009.

[129] S. U. Khan, J. R. Pothnis, and J.-K. Kim, “Effects of carbon nanotube alignment on electrical and mechanical properties of epoxy nanocomposites,” *Composites Part A: Applied Science and Manufacturing,* vol. 49, pp. 26-34, 6, 2013.

[130] A. K. Gupta, and S. P. Harsha, “Studies of Mechanical Properties of Multiwall Nanotube Based Polymer Composites,” *Journal of Nanotechnology in Engineering and Medicine,* vol. 5, no. 3, pp. 031006-031006, 2014.

[131] Y. C. Min le Wu, Liang Zhang, Hang Zhan,Lei Qiang and Jian Nong Wang “High performance Carbon Nanotube/Polymer composite fibre from Layer-by-layer deposition,” *ACS Appl Mater Interfaces,* vol. 8, pp. 8, 2016.

[132] E. W. S. Wong, P.E., “Nanobeam mechanics, Elasticity, Strength, and toughness of nanorods and nanotubes ” *Science and Engineering of Composite Materials,* vol. 277, pp. 5, 1997.

[133] M. Yu, Dyer .M.J.;Kelly,T.F,;Rouff, R.S., “Strength and breaking mechanism of multiwalled carbon nanotubes uner tensile load,” *Science and Engineering of Composite Materials,* vol. 287, pp. 4, 2000.

[134] J. W. Gilman, "Flame Retardant Mechanism of Polymer–Clay Nanocomposites," *Flame Retardant Polymer Nanocomposites,* pp. 67-87: John Wiley & Sons, Inc., 2006.

[135] B. Z. Z. Jang, A., *Process for producing dispersible nano graphene platelets from oxidized graphite,* US, Feb 14, 2012.

[136] K. S. Novoselov, A. K. Geim, S. V. Morozov, D. Jiang, Y. Zhang, S. V. Dubonos, I. V. Grigorieva, and A. A. Firsov, “Electric field effect in atomically thin carbon films,” *Science,* vol. 306, no. 5696, pp. 666-9, Oct 22, 2004.

[137] Z.-S. Wu, G. Zhou, L.-C. Yin, W. Ren, F. Li, and H.-M. Cheng, “Graphene/metal oxide composite electrode materials for energy storage,” *Nano Energy,* vol. 1, no. 1, pp. 107-131, 2012.

[138] O. C. Compton, S. W. Cranford, K. W. Putz, Z. An, L. C. Brinson, M. J. Buehler, and S. T. Nguyen, “Tuning the mechanical properties of graphene oxide paper and its associated polymer nanocomposites by controlling cooperative intersheet hydrogen bonding,” *ACS Nano,* vol. 6, no. 3, pp. 2008-2019, 2012.

[139] D. R. Bortz, E. G. Heras, and I. Martin-Gullon, “Impressive Fatigue Life and Fracture Toughness Improvements in Graphene Oxide/Epoxy Composites,” *Macromolecules,* vol. 45, no. 1, pp. 238-245, 2012.

[140] M.-Y. Shen, T.-Y. Chang, T.-H. Hsieh, Y.-L. Li, C.-L. Chiang, H. Yang, and M.-C. Yip, “Mechanical Properties and Tensile Fatigue of Graphene Nanoplatelets Reinforced Polymer Nanocomposites,” *Journal of Nanomaterials,* vol. 2013, pp. 9, 2013.

[141] K. I. Bolotin, K. J. Sikes, J. Hone, H. L. Stormer, and P. Kim, “Temperature-dependent transport in suspended graphene,” *Phys Rev Lett,* vol. 101, 2008, 2008.

[142] S. V. Morozov, K. S. Novoselov, M. I. Katsnelson, F. Schedin, D. C. Elias, J. A. Jaszczak, and A. K. Geim, “Giant Intrinsic Carrier Mobilities in Graphene and Its Bilayer,” *Phys Rev Lett,* vol. 100, no. 1, pp. 016602, 2008.

[143] H. Park, S. Chang, X. Zhou, J. Kong, T. Palacios, and S. Gradečak, “Flexible Graphene Electrode-Based Organic Photovoltaics with Record-High Efficiency,” *Nano Lett,* vol. 14, no. 9, pp. 5148-5154, 2014.

[144] K. D. sattler, *Graphene, Fullerenes ,Nanotubes and Nanodiamonds* University of Hawaii, Honolulu USA: CRC press ,Taylor and Francis Group.

[145] K. S. Novoselov, A. K. Geim, S. V. Morozov, D. Jiang, Y. Zhang, S. V. Dubonos, I. V. Grigorieva, and A. A. Firsov, "Electric Field Effect in Atomically Thin Carbon Films," *Science,* vol. 306, no. 5696, pp. 666-669, 2004.

[146] R. C. Croft, "Lamellar compounds of graphite," *Quarterly Reviews, Chemical Society,* vol. 14, no. 1, pp. 1-45, 1960.

[147] H. C. Schniepp, J.-L. Li, M. J. McAllister, H. Sai, M. Herrera-Alonso, D. H. Adamson, R. K. Prud'homme, R. Car, D. A. Saville, and I. A. Aksay, "Functionalized Single Graphene Sheets Derived from Splitting Graphite Oxide," *The Journal of Physical Chemistry B,* vol. 110, no. 17, pp. 8535-8539, 2006.

[148] K. V. Emtsev, F. Speck, T. Seyller, L. Ley, and J. D. Riley, "Interaction, growth, and ordering of epitaxial graphene on SiC{0001} surfaces: A comparative photoelectron spectroscopy study," *Physical Review B,* vol. 77, no. 15, pp. 155303, 2008.

[149] F. Varchon, R. Feng, J. Hass, X. Li, B. N. Nguyen, C. Naud, P. Mallet, J. Y. Veuillen, C. Berger, E. H. Conrad, and L. Magaud, "Electronic Structure of Epitaxial Graphene Layers on SiC: Effect of the Substrate," *Phys Rev Lett,* vol. 99, no. 12, pp. 126805, 2007.

[150] R. Ruoff, "Graphene: Calling all chemists," *Nat Nano,* vol. 3, no. 1, pp. 10-11, 2008.

[151] W. S. Hummers, and R. E. Offeman, "Preparation of graphitic oxide," *J Am Chem Soc,* vol. 80, 1958.

[152] Y. Fan, L. Wang, J. Li, J. Li, S. Sun, F. Chen, L. Chen, and W. Jiang, "Preparation and electrical properties of graphene nanosheet/Al2O3 composites," *Carbon,* vol. 48, no. 6, pp. 1743-1749, 2010.

[153] S.-H. Kang, T.-H. Fang, and Z.-H. Hong, "Electrical and mechanical properties of graphene oxide on flexible substrate," *Journal of Physics and Chemistry of Solids,* vol. 74, no. 12, pp. 1783-1793, 12, 2013.

[154] K. Yong-Jin, K. Yuna, N. Konstantin, and H. Byung Hee, "Engineering electrical properties of graphene: chemical approaches," *2D Materials,* vol. 2, no. 4, pp. 042001, 2015.

[155] J. Zhang, Y. Yu, and D. Huang, "Good electrical and mechanical properties induced by the multilayer graphene oxide sheets incorporated to amorphous carbon films," *Solid State Sciences,* vol. 12, no. 7, pp. 1183-1187, 2010.

[156] A. A. Balandin, "Thermal properties of graphene and nanostructured carbon materials," *Nat Mater,* vol. 10, no. 8, pp. 569-581, 2011.

[157] A. Yu, P. Ramesh, M. E. Itkis, E. Bekyarova, and R. C. Haddon, "Graphite Nanoplatelet−Epoxy Composite Thermal Interface Materials," *The Journal of Physical Chemistry C,* vol. 111, no. 21, pp. 7565-7569, 2007.

[158] L. A. Falkovsky, "Optical properties of graphene," *Journal of Physics: Conference Series,* vol. 129, no. 1, pp. 012004, 2008.

[159] J. Yang, Y. Zhou, L. Sun, N. Zhao, C. Zang, and X. Cheng, "Synthesis, characterization and optical property of graphene oxide films," *Applied Surface Science,* vol. 258, no. 12, pp. 5056-5060, 2012.

[160] S. Stankovich, D. A. Dikin, R. D. Piner, K. A. Kohlhaas, A. Kleinhammes, Y. Jia, Y. Wu, S. T. Nguyen, and R. S. Ruoff, "Synthesis of graphene-based nanosheets via chemical reduction of exfoliated graphite oxide," *Carbon,* vol. 45, no. 7, pp. 1558-1565, 2007.

[161] P. Anadao, "Polymer/ Clay Nanocomposites: Concepts, Researches, Applications and Trends for The Future," 2012.

[162] Z. Wang, S. Wu, J. Zhang, P. Chen, G. Yang, X. Zhou, Q. Zhang, Q. Yan, and H. Zhang, "Comparative studies on single-layer reduced graphene oxide films obtained by electrochemical reduction and hydrazine vapor reduction," *Nanoscale Res Lett,* vol. 7, pp. 161, 2012.

[163] N. Cao, and Y. Zhang, "Study of Reduced Graphene Oxide Preparation by Hummers Method and Related Characterization," *Journal of Nanomaterials,* vol. 2015, pp. 5, 2015.

[164] S. Pei, and H.-M. Cheng, "The reduction of graphene oxide," *Carbon,* vol. 50, no. 9, pp. 3210-3228, 2012.

[165] D. Yang, A. Velamakanni, G. Bozoklu, S. Park, M. Stoller, R. D. Piner, S. Stankovich, I. Jung, D. A. Field, C. A. Ventrice Jr, and R. S. Ruoff, "Chemical analysis of graphene oxide films after heat and chemical treatments by X-ray photoelectron and Micro-Raman spectroscopy," *Carbon,* vol. 47, no. 1, pp. 145-152, 2009.

[166] S. Stankovich, R. D. Piner, X. Chen, N. Wu, S. T. Nguyen, and R. S. Ruoff, "Stable aqueous dispersions of graphitic nanoplatelets via the reduction of exfoliated graphite oxide in the presence of poly(sodium 4-styrenesulfonate)," *J. Mater. Chem.,* vol. 16, no. 2, pp. 155-158, 2006.

[167] N. A. Kotov, I. Dékány, and J. H. Fendler, "Ultrathin graphite oxide–polyelectrolyte composites prepared by self-assembly: Transition between conductive and non-conductive states," *Advanced Materials,* vol. 8, no. 8, pp. 637-641, 1996.

[168] S. Pei, J. Zhao, J. Du, W. Ren, and H.-M. Cheng, “Direct reduction of graphene oxide films into highly conductive and flexible graphene films by hydrohalic acids,” *Carbon,* vol. 48, no. 15, pp. 4466-4474, 2010.

[169] W. Gao, L. B. Alemany, L. Ci, and P. M. Ajayan, “New insights into the structure and reduction of graphite oxide,” *Nat Chem,* vol. 1, no. 5, pp. 403-8, Aug, 2009.

[170] N. Mohanty, A. Nagaraja, J. Armesto, and V. Berry, “High-throughput, ultrafast synthesis of solution-dispersed graphene via a facile hydride chemistry,” *Small,* vol. 6, no. 2, pp. 226-231, 2010.

[171] D. Luo, G. Zhang, J. Liu, and X. Sun, “Evaluation criteria for reduced graphene oxide,” *The Journal of Physical Chemistry C,* vol. 115, no. 23, pp. 11327-11335, 2011.

[172] H.-J. Shin, K. K. Kim, A. Benayad, S.-M. Yoon, H. K. Park, I.-S. Jung, M. H. Jin, H.-K. Jeong, J. M. Kim, J.-Y. Choi, and Y. H. Lee, “Efficient Reduction of Graphite Oxide by Sodium Borohydride and Its Effect on Electrical Conductance,” *Advanced Functional Materials,* vol. 19, no. 12, pp. 1987-1992, 2009.

[173] Z. Lei, L. Lu, and X. S. Zhao, “The electrocapacitive properties of graphene oxide reduced by urea,” *Energy & Environmental Science,* vol. 5, no. 4, pp. 6391-6399, 2012.

[174] S. Kwon, J. H. Ko, K. J. Jeon, Y. H. Kim, and J. Y. Park, “Enhanced nanoscale friction on fluorinated graphene,” *Nano Lett,* vol. 12, no. 12, pp. 6043-8, 2012.

[175] S. Eigler, S. Grimm, M. Enzelberger-Heim, P. Muller, and A. Hirsch, “Graphene oxide: efficiency of reducing agents,” *Chem Commun (Camb),* vol. 49, no. 67, pp. 7391-7393, 2013.

[176] M. H. P. Alimard, “Graphene:Synthesis and Applications in Biotechnology - A Review,” *World Applied Programming,* vol. 2, no. 6, pp. 12, 2012.

[177] H. J. Shin, K. K. Kim, A. Benayad, S. M. Yoon, H. K. Park, I. S. Jung, M. H. Jin, H. K. Jeong, J. M. Kim, and J. Y. Choi, “Efficient reduction of graphite oxide by sodium borohydride and its effect on electrical conductance,” *Advanced Functional Materials,* vol. 19, no. 12, pp. 1987-1992, 2009.

[178] M. Periasamy, and M. Thirumalaikumar, “Methods of enhancement of reactivity and selectivity of sodium borohydride for applications in organic synthesis,” *Journal of Organometallic Chemistry,* vol. 609, no. 1–2, pp. 137-151, 2000.

[179] R. Verdejo, S. Lamoriniere, B. Cottam, A. Bismarck, and M. Shaffer, “ Removal of oxidation debris from multiwalled carbon nanotubes,,” *Chem. Commun.*, pp. 3, 2007.

[180] V. Singh, D. Joung, L. Zhai, S. Das, S. I. Khondaker, and S. Seal, “Graphene based materials: Past, present and future,” *Progress in Materials Science,* vol. 56, no. 8, pp. 1178-1271, 2011.

[181] V. M. Rasu Ramachandran, Shen-Ming Chen, Ramiah Saraswathi, Bih-Show Lou, “Recent Trends in Graphene based Electrode Materials for Energy Storage Devices and Sensors Applications,” *International Journal of electrochemical Science and Technology of Advanced Materials,* vol. 8, pp. 15, 2013.

[182] L. Kou, and C. Gao, “Bioinspired design and macroscopic assembly of poly(vinyl alcohol)-coated graphene into kilometers-long fibers,” *Nanoscale,* vol. 5, no. 10, pp. 4370-8, 2013.

[183] V. H. Pham, T. T. Dang, S. H. Hur, E. J. Kim, and J. S. Chung, “Highly conductive poly(methyl methacrylate) (PMMA)-reduced graphene oxide composite prepared by self-assembly of PMMA latex and graphene oxide through electrostatic interaction,” *ACS Appl Mater Interfaces,* vol. 4, no. 5, pp. 2630-6, 2012.

[184] G. Carotenuto, S. D. Nicola, G. Ausanio, D. Massarotti, L. Nicolais, and G. P. Pepe, “Synthesis and characterization of electrically conductive polyethylene-supported graphene films,” *Nanoscale Res Lett,* vol. 9, no. 1, pp. 1-7, 2014.

[185] P. A. Amnaya, C. L. Dimitris, and C. H. Daniel, “Modeling of graphene–polymer interfacial mechanical behavior using molecular dynamics,” *Modelling and Simulation in Materials Science and Engineering,* vol. 17, no. 1, pp. 015002, 2009.

[186] M. El Achaby, Arrakhiz, Fatima-Ezzahra,Vaudreuil, Sébastien, el Kacem Qaiss, Abou,Bousmina, Mostapha,Fassi-Fehri, Omar, “Mechanical, thermal, and rheological properties of graphene-based polypropylene nanocomposites prepared by melt mixing,” *Polymer Composites,* vol. 33, no. 5, pp. 11, 2012.

[187] H. T. Hu, X. B. Wang, J. C. Wang, L. Wan, F. M. Liu, H. Zheng, R. Chen, and C. H. Xu, “Preparation and properties of graphene nanosheets-polystyrene nanocomposites via in situ emulsion polymerization,” *Chemical Physics Letters,* vol. 484, no. 4-6, pp. 247-253, 2010.

[188] L. L. Z. X.Y.Yuan, C.C.Liao, J.W.Dai, “Improved properties of chemically modified graphene/poly(methyl methacrylate) nanocomposites via a facile in-situ bulk polymerization,” *eXPRESS Polymer Letters,* vol. 6, no. 10, pp. 12, 2012.

[189] J. Wang, H. Hu, X. Wang, C. Xu, M. Zhang, and X. Shang, “Preparation and mechanical and electrical properties of graphene nanosheets–poly(methyl methacrylate) nanocomposites via in situ

suspension polymerization," *Journal of Applied Polymer Science,* vol. 122, no. 3, pp. 1866-1871, 2011.

[190] K. W. Putz, O. C. Compton, M. J. Palmeri, S. T. Nguyen, and L. C. Brinson, "High-Nanofiller-Content Graphene Oxide–Polymer Nanocomposites via Vacuum-Assisted Self-Assembly," *Advanced Functional Materials,* vol. 20, no. 19, pp. 3322-3329, 2010.

[191] T. Ramanathan, A. A. Abdala, S. Stankovich, D. A. Dikin, M. Herrera-Alonso, R. D. Piner, D. H. Adamson, H. C. Schniepp, X. Chen, R. S. Ruoff, S. T. Nguyen, I. A. Aksay, R. K. Prud'Homme, and L. C. Brinson, "Functionalized graphene sheets for polymer nanocomposites," *Nat Nanotechnol,* vol. 3, no. 6, pp. 327-31, Jun, 2008.

[192] J. M. Gohil, A. Bhattacharya, and P. Ray, "Studies On The Crosslinking Of Poly (Vinyl Alcohol)," *Journal of Polymer Research,* vol. 13, no. 2, pp. 161-169, 2005.

[193] Y. An, Z. Tai, Y. Qi, X. Yan, B. Liu, Q. Xue, and J. Pei, "Friction and wear properties of graphene oxide/ultrahigh-molecular-weight polyethylene composites under the lubrication of deionized water and normal saline solution," *Journal of Applied Polymer Science,* vol. 131, no. 1, 2014.

[194] C. Dongyu, Y. Kamal, and S. Mo, "The mechanical properties and morphology of a graphite oxide nanoplatelet/polyurethane composite," *Nanotechnology,* vol. 20, no. 8, pp. 085712, 2009.

[195] H. D. Wagner, and R. A. Vaia, "Nanocomposites: Issues at the interface," *Materials Today,* vol. 7, no. 11, pp. 38-42, 2004.

[196] Q. Wu, Y. Xu, Z. Yao, A. Liu, and G. Shi, "Supercapacitors Based on Flexible Graphene/Polyaniline Nanofiber Composite Films," *ACS Nano,* vol. 4, no. 4, pp. 1963-1970, 2010.

[197] G. Goncalves, P. A. A. P. Marques, A. Barros-Timmons, I. Bdkin, M. K. Singh, N. Emami, and J. Gracio, "Graphene oxide modified with PMMA via ATRP as a reinforcement filler," *Journal of Materials Chemistry,* vol. 20, no. 44, pp. 9927-9934, 2010.

[198] H. Yang, C. Shan, F. Li, Q. Zhang, D. Han, and L. Niu, "Convenient preparation of tunably loaded chemically converted graphene oxide/epoxy resin nanocomposites from graphene oxide sheets through two-phase extraction," *Journal of Materials Chemistry,* vol. 19, no. 46, pp. 8856-8860, 2009.

[199] M. S. Dresselhaus, and G. Dresselhaus, "Intercalation compounds of graphite," *Advances in Physics,* vol. 30, no. 2, pp. 139-326, 1981.

[200] E. Tkalya, M. Ghislandi, A. Alekseev, C. Koning, and J. Loos, "Latex-based concept for the preparation of graphene-based polymer nanocomposites," *Journal of Materials Chemistry,* vol. 20, no. 15, pp. 3035-3039, 2010.

[201] J. Wang, and M. Ellsworth, "Graphene Aerogels," *ECS Transactions,* vol. 19, no. 5, pp. 241-247, 2009.

[202] H. D. a. B. F. Staples TL, *Chemistry of superadsorbent Polyacrylates In Modern Superadsorbent Polymer Technology*, New York: Wiley -VCH, 1998.

[203] Y. Li, G. Huang, X. Zhang, B. Li, Y. Chen, T. Lu, T. J. Lu, and F. Xu, "Magnetic Hydrogels and Their Potential Biomedical Applications," *Advanced Functional Materials,* vol. 23, no. 6, pp. 660-672, 2013.

[204] S. Kiatkamjornwrong, "Superadsorbent polymers and superadsorbent polymer composites " *Science Asia,* vol. 33, no. Suppliment 1, pp. 5, 2007.

[205] V.Buhler, *Polvinyl pyrrolidoen Excipients for pharmaceuticals* 1st ed., Berlin,Germany: Springer, 2005.

[206] R. L. Will, U.; Yokose, K *Synthetic water soluble polymers* 2016.

[207] G. Saunders, MacCreath, B, *Biodegradable polymer analysis of biodegradable polymers by GPC-SEC. Application Compendium*, Santa Clara CA, USA, 2010.

[208] L. Bromberg, "Polyether-Modified Poly(acrylic acid): Synthesis and Applications," *Industrial & Engineering Chemistry Research,* vol. 37, no. 11, pp. 4267-4274, 1998.

[209] S. A. R. Botto, P.J.Faramus,E.L.Nair C.H., *Removal of metabolic components from blood*, U.S. Patent number 7,066,900, 27 June, 2006.

[210] G. E. Puetz, J. , *Method of eliminating potentially toxic and /or Harmful substances* US WO 02081006, 17 October 2002.

[211] M. C. Z. Paiva, B.Fernando, K. A. S.Lin, Y.Kennedy, J. M.Sun, Y. P., "Mechanical and morphological characterization of polymer–carbon nanocomposites from functionalized carbon nanotubes," *Carbon,* vol. 42, no. 14, pp. 2849-2854, 2004.

[212] B. W. Wenjing Ni, Huaping Wang and Yumei Zhang, "Fabrication and properties of Carbon nanotubes and poly (vinyl alcohol) composites " *Journal of Macromolecular Science, part B: Physics,* vol. 45, pp. 5, 2006.

[213] C. Surawut, S. Anuvat, and S. Pitt, "Mechanical and electro-rheological properties of electrospun poly(vinyl alcohol) nanofibre mats filled with carbon black nanoparticles," *Nanotechnology,* vol. 18, no. 14, pp. 145705, 2007.

[214] Y. Hou, J. Tang, H. Zhang, C. Qian, Y. Feng, and J. Liu, “Functionalized Few-Walled Carbon Nanotubes for Mechanical Reinforcement of Polymeric Composites,” *ACS Nano,* vol. 3, no. 5, pp. 1057-1062, 2009.

[215] M. C. Cadek, J. N. Ryan, K. P. Nicolosi, V. Bister, G. Fonseca, A. Nagy, J. B.Szostak, K. Béguin, F.Blau, W. J., “Reinforcement of Polymers with Carbon Nanotubes: The Role of Nanotube Surface Area,” *Nano Lett,* vol. 4, no. 2, pp. 353-356, 2004.

[216] D. Q. Pei Zhang, Hongfei Chen, Jun Sun, Jiajun Wang, Chuanxiang Qin, and Lixing Dai, “Preparation of MWCNTs grafted with polyvinyl alcohol thorugh freidel-Craft alkylation and their composite fibres with enhanced mechanical properties.,” *Journal of Materials Chemistry A,* vol. 3, no. 4, pp. 9, 2015.

[217] Y. Xu, W. Hong, H. Bai, C. Li, and G. Shi, “Strong and ductile poly(vinyl alcohol)/graphene oxide composite films with a layered structure,” *Carbon,* vol. 47, no. 15, pp. 3538-3543, 2009.

[218] A. B. S. Tayser Sumer Gaaz , Majid Niaz Akhtar , Abdul Amir H. Kadhum, Abu Bakar Mohamad and Ahmed A. Al-Amiery “Properties and Applications of Polyvinyl Alcohol, Halloysite Nanotubes and Their Nanocomposites,” *MOLECULES,* vol. 20, pp. 15, 2015.

[219] I. Stoševski, J. Krstić, N. Vokić, M. Radosavljević, Z. K. Popović, and Š. Miljanić, “Improved Poly(vinyl alcohol) (PVA) based matrix as a potential solid electrolyte for electrochemical energy conversion devices, obtained by gamma irradiation,” *Energy,* vol. 90, Part 1, pp. 595-604, 2015.

[220] K. M. Khoo, and Y. P. Ting, “Polyvinyl alcohol as an immobilization matrix--a case of gold biosorption,” *Water Sci Technol,* vol. 43, no. 11, pp. 17-23, 2001.

[221] S.-K. Chae, C. H. Mun, D.-Y. Noh, E. Kang, and S.-H. Lee, “Simple Fabrication Method for a Porous Poly(vinyl alcohol) Matrix by Multisolvent Mixtures for an Air-Exposed Model of the Lung Epithelial System,” *Langmuir,* vol. 30, no. 41, pp. 12107-12113, 2014.

[222] C. C. Thong, D. C. L. Teo, and C. K. Ng, “Application of polyvinyl alcohol (PVA) in cement-based composite materials: A review of its engineering properties and microstructure behavior,” *Construction and building materials,* vol. 107, pp. 172-180, 2016.

[223] A. M. Youssef, S. M. El-Sayed, H. H. Salama, H. S. El-Sayed, and A. Dufresne, “Evaluation of bionanocomposites as packaging material on properties of soft white cheese during storage period,” *Carbohydr Polym,* vol. 132, pp. 274-85, 2015.

[224] M. S. Peresin, Y. Habibi, A.-H. Vesterinen, O. J. Rojas, J. J. Pawlak, and J. V. Seppälä, “Effect of Moisture on Electrospun Nanofiber Composites of Poly(vinyl alcohol) and Cellulose Nanocrystals,” *Biomacromolecules,* vol. 11, no. 9, pp. 2471-2477, 2010.

[225] N. C. K. EM. Amin, and B. Winther-Jensen,, “Polyvinyl-alcohol (pva)-based RF humidity sensor in microwave frequency,” *Progress In Electromagnetics Research B,* vol. 54, pp. 17, 2013.

[226] T. N. a. T. G. S.Morimune, "Graphene oxide reinforced poly(vinyl alcohol) nanocomposites." p. 5.

[227] L. Jiang, X. P. Shen, J. L. Wu, and K. C. Shen, “Preparation and characterization of graphene/poly(vinyl alcohol) nanocomposites,” *Journal of Applied Polymer Science,* vol. 118, no. 1, pp. 275-279, 2010.

[228] X. Yuan, “Enhanced interfacial interaction for effective reinforcement of poly(vinyl alcohol) nanocomposites at low loading of graphene,” *Polymer Bulletin,* vol. 67, no. 9, pp. 1785-1797, 2011.

[229] R. Surudžić, A. Janković, M. Mitrić, I. Matić, Z. D. Juranić, L. Živković, V. Mišković-Stanković, K. Y. Rhee, S. J. Park, and D. Hui, “The effect of graphene loading on mechanical, thermal and biological properties of poly(vinyl alcohol)/graphene nanocomposites,” *Journal of Industrial and Engineering Chemistry,* vol. 34, pp. 250-257, 2016.

[230] J. Wang, X. Wang, C. Xu, M. Zhang, and X. Shang, “Preparation of graphene/poly(vinyl alcohol) nanocomposites with enhanced mechanical properties and water resistance,” *Polymer International,* vol. 60, no. 5, pp. 816-822, 2011.

[231] C. Bao, Y. Guo, L. Song, and Y. Hu, “Poly(vinyl alcohol) nanocomposites based on graphene and graphite oxide: a comparative investigation of property and mechanism,” *Journal of Materials Chemistry,* vol. 21, no. 36, pp. 13942, 2011.

[232] Q. Bian, H. Tian, Y. Wang, Q. Liu, X. Ge, A. V. Rajulu, and A. Xiang, “Effect of graphene oxide on the structure and properties of poly(vinyl alcohol) composite films,” *Polymer Science Series A,* vol. 57, no. 6, pp. 836-844, 2015.

[233] H. J. G. m. Salavagione, Marián A,Martínez, Gerardo, “Polymeric Modification of Graphene through Esterification of Graphite Oxide and Poly(vinyl alcohol),” *Macromolecules,* vol. 42, no. 17, pp. 6331-6334, 2009.

[234] J. Guo, L. Ren, R. Wang, C. Zhang, Y. Yang, and T. Liu, “Water dispersible graphene noncovalently functionalized with tryptophan and its poly(vinyl alcohol) nanocomposite,” *Composites Part B: Engineering,* vol. 42, no. 8, pp. 2130-2135, 2011.

[235] H. K. Cheng, N. G. Sahoo, Y. P. Tan, Y. Pan, H. Bao, L. Li, S. H. Chan, and J. Zhao, “Poly(vinyl alcohol) nanocomposites filled with poly(vinyl alcohol)-grafted graphene oxide,” *ACS Appl Mater Interfaces,* vol. 4, no. 5, pp. 2387-94, 2012.

[236] M. Cano, U. Khan, T. Sainsbury, A. O’Neill, Z. Wang, I. T. McGovern, W. K. Maser, A. M. Benito, and J. N. Coleman, “Improving the mechanical properties of graphene oxide based materials by covalent attachment of polymer chains,” *Carbon,* vol. 52, pp. 363-371, 2013.

[237] S. Mo, L. Peng, C. Yuan, C. Zhao, W. Tang, C. Ma, J. Shen, W. Yang, Y. Yu, Y. Min, and A. J. Epstein, “Enhanced properties of poly(vinyl alcohol) composite films with functionalized graphene,” *RSC Advances,* vol. 5, no. 118, pp. 97738-97745, 2015.

[238] J. Chen, Y. Li, Y. Zhang, and Y. Zhu, “Preparation and characterization of graphene oxide reinforced PVA film with boric acid as crosslinker,” *Journal of Applied Polymer Science,* vol. 132, no. 22, pp. 8, 2015.

[239] L. Shao, J. Li, Y. Guang, Y. Zhang, H. Zhang, X. Che, and Y. Wang, “PVA/polyethyleneimine-functionalized graphene composites with optimized properties,” *Materials & Design,* vol. 99, pp. 235-242, 2016.

[240] C. Wan, and B. Chen, “Reinforcement and interphase of polymer/graphene oxide nanocomposites,” *Journal of Materials Chemistry,* vol. 22, no. 8, pp. 3637, 2012.

[241] M. Yang, V. Koutsos, and M. Zaiser, “Interactions between Polymers and Carbon Nanotubes: A Molecular Dynamics Study,” *The Journal of Physical Chemistry B,* vol. 109, no. 20, pp. 10009-10014, 2005.

[242] J. Hu, X. Jia, C. Li, Z. Ma, G. Zhang, W. Sheng, X. Zhang, and Z. Wei, “Effect of interfacial interaction between graphene oxide derivatives and poly(vinyl chloride) upon the mechanical properties of their nanocomposites,” *Journal of Materials Science,* vol. 49, no. 7, pp. 2943-2951, 2014.

[243] X. Yang, Y. Tu, L. Li, S. Shang, and X.-m. Tao, “Well-Dispersed Chitosan/Graphene Oxide Nanocomposites,” *ACS Appl Mater Interfaces,* vol. 2, no. 6, pp. 1707-1713, 2010.

[244] P. May, U. Khan, A. O'Neill, and J. N. Coleman, “Approaching the theoretical limit for reinforcing polymers with graphene,” *Journal of Materials Chemistry,* vol. 22, no. 4, pp. 1278-1282, 2012.

[245] I.A.Ovid'ko, “Enhanced mechanical properties of polymer-matrix nanocomposites reinforced by graphene inclusions: A review,” *Rev.adv.mater.Sci,* vol. 34, no. 1, pp. 7, 2013.

[246] T. Kuilla, S. Bhadra, D. Yao, N. H. Kim, S. Bose, and J. H. Lee, “Recent advances in graphene based polymer composites,” *Progress in Polymer Science,* vol. 35, no. 11, pp. 1350-1375, 2010.

[247] S. Sinha Ray, and M. Okamoto, “Polymer/layered silicate nanocomposites: A review from preparation to processing,” *Progress in Polymer Science (Oxford),* vol. 28, no. 11, pp. 1539-1641, 2003.

[248] S. W. Cranford, and M. J. Buehler, “Packing efficiency and accessible surface area of crumpled graphene,” *Physical Review B,* vol. 84, no. 20, 2011.

[249] J. Zhang, J. Xiao, X. Meng, C. Monroe, Y. Huang, and J.-M. Zuo, “Free Folding of Suspended Graphene Sheets by Random Mechanical Stimulation,” *Phys Rev Lett,* vol. 104, no. 16, pp. 166805, 2010.

[250] S. F. Braga, V. R. Coluci, S. B. Legoas, R. Giro, D. S. Galvão, and R. H. Baughman, “Structure and Dynamics of Carbon Nanoscrolls,” *Nano Lett,* vol. 4, no. 5, pp. 881-884, 2004.

[251] F. Niklaus, G. Stemme, J.-Q. Lu, and R. J. Gutmann, “Adhesive wafer bonding,” *Journal of Applied Physics,* vol. 99, no. 3, pp. 031101, 2006.

[252] D. Li, M. B. Müller, S. Gilje, R. B. Kaner, and G. G. Wallace, “Processable aqueous dispersions of graphene nanosheets,” *Nat Nanotechnol,* vol. 3, 2008.

[253] H. Vincent, B. Nedjma, R. Noël, E. Thomas, D. Cécile, and B. Vincent, “Large and flat graphene flakes produced by epoxy bonding and reverse exfoliation of highly oriented pyrolytic graphite,” *Nanotechnology,* vol. 19, no. 45, pp. 455601, 2008.

[254] Y. Takatoshi, K. Jaeho, I. Masatou, and H. Masataka, “Low-temperature graphene synthesis using microwave plasma CVD,” *Journal of Physics D: Applied Physics,* vol. 46, no. 6, pp. 063001, 2013.

[255] L. Gong, R. J. Young, I. A. Kinloch, S. J. Haigh, J. H. Warner, J. A. Hinks, Z. Xu, L. Li, F. Ding, I. Riaz, R. Jalil, and K. S. Novoselov, “Reversible Loss of Bernal Stacking during the Deformation of Few-Layer Graphene in Nanocomposites,” *ACS Nano,* vol. 7, no. 8, pp. 7287-7294, 2013.

[256] X. Fan, W. Peng, Y. Li, X. Li, S. Wang, G. Zhang, and F. Zhang, “Deoxygenation of Exfoliated Graphite Oxide under Alkaline Conditions: A Green Route to Graphene Preparation,” *Advanced Materials,* vol. 20, no. 23, pp. 4490-4493, 2008.

[257] Y. Lei, Z. Tang, R. Liao, and B. Guo, “Hydrolysable tannin as environmentally friendly reducer and stabilizer for graphene oxide,” *Green Chemistry,* vol. 13, no. 7, pp. 1655-1658, 2011.

[258] Y. Wang, Z. Shi, and J. Yin, “Facile synthesis of soluble graphene via a green reduction of graphene oxide in tea solution and its biocomposites,” *ACS Appl Mater Interfaces*, vol. 3, no. 4, pp. 1127-33, Apr, 2011.

[259] L. Q. Xu, W. J. Yang, K.-G. Neoh, E.-T. Kang, and G. D. Fu, “Dopamine-Induced Reduction and Functionalization of Graphene Oxide Nanosheets,” *Macromolecules*, vol. 43, no. 20, pp. 8336-8339, 2010.

[260] F. Hassouna, S. Kashyap, A. Laachachi, V. Ball, D. Chapron, V. Toniazzo, and D. Ruch, “Peculiar reduction of graphene oxide into graphene after diffusion in exponentially growing polyelectrolyte multilayers,” *J Colloid Interface Sci*, vol. 377, no. 1, pp. 489-96, 2012.

[261] M. Traina, and A. Pegoretti, “In situ reduction of graphene oxide dispersed in a polymer matrix,” *Journal of Nanoparticle Research*, vol. 14, no. 4, pp. 1-6, 2012.

[262] A. J. Glover, M. Cai, K. R. Overdeep, D. E. Kranbuehl, and H. C. Schniepp, “In Situ Reduction of Graphene Oxide in Polymers,” *Macromolecules*, vol. 44, no. 24, pp. 9821-9829, 2011.

[263] L. Liu, A. H. Barber, S. Nuriel, and H. D. Wagner, “Mechanical Properties of Functionalized Single-Walled Carbon-Nanotube/Poly(vinyl alcohol) Nanocomposites,” *Advanced Functional Materials*, vol. 15, no. 6, pp. 975-980, 2005.

[264] H. J. Salavagione, and G. Martínez, “Importance of Covalent Linkages in the Preparation of Effective Reduced Graphene Oxide−Poly(vinyl chloride) Nanocomposites,” *Macromolecules*, vol. 44, no. 8, pp. 2685-2692, 2011.

[265] S. K. Sharma, J. Prakash, and P. K. Pujari, “Effects of the molecular level dispersion of graphene oxide on the free volume characteristics of poly(vinyl alcohol) and its impact on the thermal and mechanical properties of their nanocomposites,” *Physical Chemistry Chemical Physics*, vol. 17, no. 43, pp. 29201-29209, 2015.

[266] V. Azmeera, P. Adhikary, and S. Krishnamoorthi, “Synthesis and Characterization of Graft Copolymer of Dextran and 2-Acrylamido-2-methylpropane Sulphonic Acid,” *International Journal of Carbohydrate Chemistry*, vol. 2012, pp. 7, 2012.

[267] S. Lee, J.-Y. Hong, and J. Jang, “The effect of graphene nanofiller on the crystallization behavior and mechanical properties of poly(vinyl alcohol),” *Polymer International*, vol. 62, no. 6, pp. 901-908, 2013.

[268] L. Gong, Kinloch, I. A,Young, R. J,Riaz, I,Jalil, R,Novoselov, K. S., “Interfacial stress transfer in a graphene monolayer nanocomposite,” *Adv Mater*, vol. 22, no. 24, pp. 2694-7, 2010.

[269] S. Morimune, T. Nishino, and T. Goto, “Poly(vinyl alcohol)/graphene oxide nanocomposites prepared by a simple eco-process,” *Polym J*, vol. 44, no. 10, pp. 1056-1063, 2012.

[270] J. C. H. Affdl, and J. L. Kardos, “The Halpin-Tsai equations: A review,” *Polymer Engineering & Science*, vol. 16, no. 5, pp. 344-352, 1976.

[271] B.Pukanzy, “Influence of interface interaction on the ultimate tensile properties of polymer composites,” *Composites*, vol. 21, no. 3, pp. 8, 1990.

[272] B. Pukánszky, “Influence of interface interaction on the ultimate tensile properties of polymer composites,” *Composites*, vol. 21, no. 3, pp. 255-262, 1990.

[273] Z. Demjén, B. Pukánszky, and J. Nagy, “Evaluation of interfacial interaction in polypropylene/surface treated CaCO3 composites,” *Composites Part A: Applied Science and Manufacturing*, vol. 29, no. 3, pp. 323-329, 1998.

[274] M. A. Rafiee, J. Rafiee, I. Srivastava, Z. Wang, H. Song, Z. Z. Yu, and N. Koratkar, “Fracture and fatigue in graphene nanocomposites,” *Small*, vol. 6, no. 2, pp. 4, 2010.

[275] M. A. Rafiee, J. Rafiee, Z. Wang, H. Song, Z.-Z. Yu, and N. Koratkar, “Enhanced Mechanical Properties of Nanocomposites at Low Graphene Content,” *ACS Nano*, vol. 3, no. 12, pp. 3884-3890, 2009.

[276] R. Rafiq, D. Cai, J. Jin, and M. Song, “Increasing the toughness of nylon 12 by the incorporation of functionalized graphene,” *Carbon*, vol. 48, no. 15, pp. 4309-4314, 2010.

[277] S. J. V. Frankland, A. Caglar, D. W. Brenner, and M. Griebel, “Molecular Simulation of the Influence of Chemical Cross-Links on the Shear Strength of Carbon Nanotube−Polymer Interfaces,” *The Journal of Physical Chemistry B*, vol. 106, no. 12, pp. 3046-3048, 2002.

[278] W. S. Hummers, and R. E. Offeman, “Preparation of Graphitic Oxide,” *J Am Chem Soc*, vol. 80, no. 6, pp. 1339-1339, 1958.

[279] N. A. Peppas, and E. W. Merrill, “Differential scanning calorimetry of crystallized PVA hydrogels,” *Journal of Applied Polymer Science*, vol. 20, no. 6, pp. 1457-1465, 1976.

[280] "Standard Test Method for Tensile Properties of Plastics," ASTM International, 2014.

[281] K. Liang, H. Hongkun, and G. Chao, “Click chemistry approach to functionalize two-dimensional macromolecules of graphene oxide nanosheets,” *Nano-Micro Letters*, vol. 2, no. 2, pp. 177-183, 2010.

[282] S. Deng, and V. Berry, “Wrinkled, rippled and crumpled graphene: an overview of formation mechanism, electronic properties, and applications,” *Materials Today,* vol. 19, no. 4, pp. 197-212, 2016.

[283] S. Li, X. Lu, Y. Xue, J. Lei, T. Zheng, and C. Wang, “Fabrication of Polypyrrole/Graphene Oxide Composite Nanosheets and Their Applications for Cr(VI) Removal in Aqueous Solution,” *PLoS One,* vol. 7, no. 8, pp. 43328, 2012.

[284] N. R. Wilson, P. A. Pandey, R. Beanland, R. J. Young, I. A. Kinloch, L. Gong, Z. Liu, K. Suenaga, J. P. Rourke, S. J. York, and J. Sloan, “Graphene oxide: structural analysis and application as a highly transparent support for electron microscopy,” *ACS Nano,* vol. 3, no. 9, pp. 2547-56, 2009.

[285] A. C. Ferrari, and D. M. Basko, “Raman spectroscopy as a versatile tool for studying the properties of graphene,” *Nat Nano,* vol. 8, no. 4, pp. 235-246, 2013.

[286] A. A. K. King, B. R. Davies, N. Noorbehesht, P. Newman, T. L. Church, A. T. Harris, J. M. Razal, and A. I. Minett, “A New Raman Metric for the Characterisation of Graphene oxide and its Derivatives,” *Scientific Reports,* vol. 6, pp. 19491, 2016.

[287] G. Sobon, J. Sotor, J. Jagiello, R. Kozinski, M. Zdrojek, M. Holdynski, P. Paletko, J. Boguslawski, L. Lipinska, and K. M. Abramski, “Graphene oxide vs. reduced graphene oxide as saturable absorbers for Er-doped passively mode-locked fiber laser,” *Opt Express,* vol. 20, no. 17, pp. 10, 2012.

[288] M. Pawlyta, J.-N. Rouzaud, and S. Duber, “Raman microspectroscopy characterization of carbon blacks: Spectral analysis and structural information,” *Carbon,* vol. 84, pp. 479-490, 2015.

[289] G. Yang, “One-pot Preparation of Reduced Graphene Oxide/Silver Nanocomposite and Its Application in the Electrochemical Determination of 4-Nitrophenol ” *International Journal of ELECTROCHEMICAL Science and Engineering of Composite Materials,* vol. 10, no. 11, pp. 8, 2015.

[290] S. Kashyap, S. Mishra, and S. K. Behera, “Aqueous Colloidal Stability of Graphene Oxide and Chemically Converted Graphene,” *Journal of Nanoparticles,* vol. 2014, pp. 1-6, 2014.

[291] F. Yang, Y. Liu, L. Gao, and J. Sun, “pH-Sensitive Highly Dispersed Reduced Graphene Oxide Solution Using Lysozyme via an in Situ Reduction Method,” *The Journal of Physical Chemistry C,* vol. 114, no. 50, pp. 22085-22091, 2010.

[292] R.J.Hunter, "Electro kinetics and zeta potential," *Foundations of Colloid Science* 2, R.J.Hunter, ed., Oxford University Press 2001, p. 2.

[293] T. Kuila, P. Khanra, N. H. Kim, J. K. Lim, and J. H. Lee, “Effects of sodium hydroxide on the yield and electrochemical performance of sulfonated poly(ether-ether-ketone) functionalized graphene,” *Journal of Materials Chemistry A,* vol. 1, no. 32, pp. 9294, 2013.

[294] D. Zhang, X. Zhang, Y. Chen, C. Wang, and Y. Ma, “An environment-friendly route to synthesize reduced graphene oxide as a supercapacitor electrode material,” *Electrochimica Acta,* vol. 69, pp. 364-370, 2012.

[295] Y. Zhu, S. Murali, M. D. Stoller, K. Ganesh, W. Cai, P. J. Ferreira, A. Pirkle, R. M. Wallace, K. A. Cychosz, and M. Thommes, “Carbon-based supercapacitors produced by activation of graphene,” *Science,* vol. 332, no. 6037, pp. 1537-1541, 2011.

[296] S. Dubin, S. Gilje, K. Wang, V. C. Tung, K. Cha, A. S. Hall, J. Farrar, R. Varshneya, Y. Yang, and R. B. Kaner, “A One-Step, Solvothermal Reduction Method for Producing Reduced Graphene Oxide Dispersions in Organic Solvents,” *ACS Nano,* vol. 4, no. 7, pp. 3845-3852, 2010.

[297] D. L. Pavia, *Introduction to Spectroscopy*: Brooks-Cole, 2008.

[298] B. Song, C. Sizemore, L. Li, X. Huang, Z. Lin, K.-s. Moon, and C.-P. Wong, “Triethanolamine functionalized graphene-based composites for high performance supercapacitors,” *Journal of Materials Chemistry A,* vol. 3, no. 43, pp. 21789-21796, 2015.

[299] P. Sepahi Rad, M. Montazer, and M. Karim Rahimi, “Simultaneous antimicrobial and dyeing of wool: A facial method,” *Journal of Applied Polymer Science,* vol. 122, no. 2, pp. 1405-1411, 2011.

[300] T. Soderberg, *Organic Chemistry with a Biological emphasis*, University of Minnesota, Morris, 2016.

[301] G. Liu, S. Gui, H. Zhou, F. Zeng, Y. Zhou, and H. Ye, “A strong adsorbent for Cu2+: graphene oxide modified with triethanolamine,” *Dalton Transactions,* vol. 43, no. 19, pp. 6977-6980, 2014.

[302] Y. Mingfa, W. Tao, Q. Na, H. Yongkai, and Q. Daping, “Controllable ring-opening polymerization of trimethylene carbonate catalyzed by aliphatic tertiary amines in the presence of benzyl alcohol or F127,” *Polymer International,* vol. 61, no. 10, pp. 1525-1531, 2012.

[303] H. L. Poh, F. Sanek, A. Ambrosi, G. Zhao, Z. Sofer, and M. Pumera, “Graphenes prepared by Staudenmaier, Hofmann and Hummers methods with consequent thermal exfoliation exhibit very different electrochemical properties,” *Nanoscale,* vol. 4, no. 11, pp. 3515-22, 2012.

[304] K. H. Kim, M. Yang, K. M. Cho, Y. S. Jun, S. B. Lee, and H. T. Jung, “High quality reduced graphene oxide through repairing with multi-layered graphene ball nanostructures,” *Sci Rep,* vol. 3, pp. 3251, 2013.

[305] I. Ostolska, and M. Wisniewska, “Application of the zeta potential measurements to explanation of colloidal CrO stability mechanism in the presence of the ionic polyamino acids,” *Colloid Polym Sci,* vol. 292, no. 10, pp. 2453-2464, 2014.

[306] P.-D. Hong, J.-H. Chen, and H.-L. Wu, “Solvent effect on structural change of poly(vinyl alcohol) physical gels,” *Journal of Applied Polymer Science,* vol. 69, no. 12, pp. 2477-2486, 1998.

[307] Y. Matsuo, K. Hatase, and Y. Sugie, “Preparation and Characterization of Poly(vinyl alcohol)- and Cu(OH)2−Poly(vinyl alcohol)-Intercalated Graphite Oxides,” *Chemistry of Materials,* vol. 10, no. 8, pp. 2266-2269, 1998.

[308] S. K. Mallapragada, N. A. Peppas, and P. Colombo, “Crystal dissolution-controlled release systems. II. Metronidazole release from semicrystalline poly(vinyl alcohol) systems,” *Journal of Biomedical Materials Research,* vol. 36, no. 1, pp. 125-130, 1997.

[309] D. Galpaya, M. Wang, M. Liu, N. Motta, E. Waclawik, and C. Yan, “Recent Advances in Fabrication and Characterization of Graphene-Polymer Nanocomposites,” *Graphene,* vol. 01, no. 02, pp. 30-49, 2012.

[310] S. Ansari, A. Kelarakis, L. Estevez, and E. P. Giannelis, “Oriented arrays of graphene in a polymer matrix by in situ reduction of graphite oxide nanosheets,” *Small,* vol. 6, no. 2, pp. 205-9, Jan, 2010.

[311] R. Imani, S. H. Emami, and S. Faghihi, “Synthesis and characterization of an octaarginine functionalized graphene oxide nano-carrier for gene delivery applications,” *Physical Chemistry Chemical Physics,* vol. 17, no. 9, pp. 6328-6339, 2015.

[312] D. R. Dreyer, S. Park, C. W. Bielawski, and R. S. Ruoff, “The chemistry of graphene oxide,” *Chem Soc Rev,* vol. 39, no. 1, pp. 228-40, 2010.

[313] S. L. Tymoczko JL, "Biochemistry," *Chemical Bonds in Biochemistry*, New York: W H Freeman, 2002.

[314] J. Scheirs, *Compositional and Failure Analysis of Polymers: A Practical Approach*: Wiley, 2000.

[315] D. L. P. gary Mlampmn, George S. Kriz and James R.VYvyan, *spectroscopy , 4e*, 4 ed.: Cengage Learning India Private Limited 2010.

[316] X. Zhao, Z. Xu, B. Zheng, and C. Gao, “Macroscopic assembled, ultrastrong and H2SO4-resistant fibres of polymer-grafted graphene oxide,” *Scientific Reports,* vol. 3, pp. 3164, 2013.

[317] B. Dan, N. Behabtu, A. Martinez, J. S. Evans, D. V. Kosynkin, J. M. Tour, M. Pasquali, and I. I. Smalyukh, “Liquid crystals of aqueous, giant graphene oxide flakes,” *Soft Matter,* vol. 7, no. 23, pp. 11154-11159, 2011.

[318] J. Yuan, A. Luna, W. Neri, C. Zakri, T. Schilling, A. Colin, and P. Poulin, “Graphene liquid crystal retarded percolation for new high-k materials,” *Nat Commun,* vol. 6, pp. 8700, 2015.

[319] A. Jakli, and A. Saupe, *One- and Two-Dimensional Fluids: Properties of Smectic, Lamellar and Columnar Liquid Crystals*: CRC Press, 2006.

[320] S. V. Rotkin, I. Zharov, K. Hess, H. Kuzmany, K. Atkinson, M. Mehring, and S. Roth, “Zipping of graphene edge as a mechanism for NT nucleation,” *AIP Conference Proceedings,* vol. 591, no. 1, pp. 454-457, 2001.

Curriculum Vitae

Name: Swarnima Kashyap
Address: D-103, Arpan darpan housing society,
Kanyapada, Near Maharaja Towers, Film city road,
Goregaon east, Mumbai.
Maharashtra 400063
Ph:+91-7077109746
E-mail: swarnimakashyap.ch@gmail.com
Date of Birth: 31st October, 1987

Academic Credentials

- Ph.D. Department of Ceramic Engineering from National Insitute of Technology Rourkela, 2012- till date.
- M.Tech in Nanotechnology 2011 from Amity University, Noida, Uttar Pradesh.
- B.Tech in Chemical Engineering 2009 from Dr. Ambedkar Institute of Technology, Kanpur, Uttar Pradesh.
- Senior secondary school 2005 from Guru Nanak Fifth Centenary School, Mussoorie, Uttaranchal.

Research interests-Graphene technology, polymer composites processing and fabrication.

Publications

1. Swarnima Kashyap, Swadesh K. Pratihar, Shantanu K. Behera, *Strong and ductile graphene oxide reinforced PVA nanocomposites*, Journal of Alloys and Compounds, Volume 684, 5 November 2016, Pages 254–260.
2. Swarnima Kashyap, Shashank Mishra, and Shantanu K. Behera, *Aqueous Colloidal Stability of Graphene Oxide and Chemically Converted Graphene*, Journal of Nanoparticles, Volume 2014, (2014), Article ID 640281, 6 pages.
3. F. Hassouna, S. Kashyap, A. Laachachi, V. Ball, D. Chapron, V. Toniazzo, D. Ruch, *Peculiar reduction of graphene oxide into graphene after diffusion in exponentially growing polyelectrolyte multilayers*, Journal of Colloid and Interface Science, Volume 377, Issue 1, 1 July 2012, Pages 489–496.
4. S. Kashyap et al., Liquid crystalline nematic ordered ultrastrong graphene based PVA nanocomposites, Submitted.
5. S. Kashyap et.al., Ultrastrong and ultratough triethylamine and hydrazine reduced graphene based PVA nanocomposites, Submitted.
6. S. Kashyap et al., Aqueous colloidal stability of triethylamine treated graphene oxide.
7. S. Kashyap et al., Triethanolamine functionalized graphene oxide reinforced PVA nanocomposites, Submitted.
8. S. Kashyap et al, Positron annihilation lifetime spectroscopy of graphene oxide and reduced graphene oxide reinforced PVA nanocomposites.

Seminars attended

1. Oral presentation on "*Tensile behavior of graphene-based PVA nanocomposites*" at 5th national symposium for material research scholars, MR-13, 2013, held at IIT-Bombay.
2. Poster presentation on "*Development of super flexible Graphene-based Polymer films",* at International Conference on Nanoscience and Nanotechnology, Aligarh Muslim University, Aligarh, 2014.